29 June 2012 | $10

Science

Plant Metabolism

AAAS

cell sciences®

cytokine center

Browse our web site of recombinant proteins, including cytokines, growth factors, chemokines and neurotrophins. Daily shipping and competitive pricing are offered. Bulk quantities of many proteins available. Cell Sciences also carries corresponding antibodies and ELISA kits.

www.cellsciences.com

LIST OF PROTEINS

4-1BBL
4-1BB Receptor
6 Ckine
ACAD8
ACAT2
gAcrp30/Adipolean
Activin A
ACY1
ADAT1
Adiponectin
ADRP
AITRL
Akt1
Alpha-Feto Protein (AFP)
Alpha-Galactosidase A
Angiopoietin-1 (Ang-1)
Angiopoietin-2 (Ang-2)
Angiostatin K1-3
Annexin-V
apo-SAA
Apoliprotein A-1
Apoliprotein E2
Apoliprotein E3
Apoliprotein E4
APRIL
Artemin
ATF2
Aurora A
Aurora B
BAFF
BAFF Receptor
BCA-1 / BLC / CXCL13
BCMA
BD-1
BD-2
BD-3
BDNF
Bivalirudin
BMP-2
BMP-4
BMP-7
BMP-13
sBMPR-1A
Brain Natriuretic Protein
BRAK
Breast Tumor Antigen
C5a
C5L2 Peptide
C-10
C-Reactive Protein
C-Src
Calbindin D-9K
Calbindin D-28K
Calbindin D-29K
Calmodulin
Calcitonin Acetate
Carbonic Anhydrase III
Carcino-embryonic Antigen
Cardiotrophin-1
Caspase-3
Caspase-6
CD4
CD14
CD22
CD40 Ligand / TRAP
CD95 / sFas Ligand
CD105 / Endoglin
CHIPS
CNTF
Collagen
CREB
CTACK/CCL27
CTGF
CTGFL/WISP-2
CTLA-4/Fc
CXCL16
Cytokeratin 8
DEP-1
Desmopressin
Disulfide Oxidoreductase
E-selectin
ECGF
EGF
Elafin/SKALP
EMAP-II
ENA-78
Endostatin
Enteropeptidase
Eotaxin
Eotaxin-2
Eotaxin-3 (TSC)
EPHB2
EPHB4
Eptifbatide
Erk-2
Erythropoietin (EPO)
Exodus-2
Fas Ligand
Fas Receptor
FGF-1 (acidic)
FGF-2 (basic)
FGF-4
FGF-5
FGF-6
FGF-7/ KGF
FGF-8
FGF-9
FGF-10
FGF-16
FGF-17
FGF-18
FGF-19
FGF-20
sFGFR-1 (IIIc) / Fc Chimera
sFGFR-2 (IIIc) / Fc Chimera
sFGFR-3 / Fc Chimera
sFGFR-4 / Fc Chimera
sFlt-1 (native)
sFlt-1 (D3)
sFlt-1 (D4)
sFlt-1 (D5)
sFlt-1 (D7)
Flt3-Ligand
sFlt-4
sFlt-4/ Fc Chimera
Follistatin
FSH
Fractalkine/ CX3C
G-CSF
α-Galactosidase A
Galectin-1
Galectin-3
Gastrointestinal CA
GCP-2
GDF-3
GDF-9
GDF-11
GDNF
GLP-1
Glucagon
Goserelin
GM-CSF
GPBB
GROα
GROβ
GROγ
GRO/MGSA
Growth Hormone
Growth Hormone BP
GST-p21/WAF-1
HB-EGF
HCC-1
HGF
Histdyl-tRNA synthetase
Histrelin
HRG1-β1
I-309
I-TAC
IFN-α
IFN-α A
IFN-α 2a
IFN-α 2b
IFN-β
IFN-γ
IFN-Omega
IGF-I
IGF-II
proIGF-II
IGFBP-1
IGFBP-2
IGFBP-3
IGFBP-4
IGFBP-4
IGFBP-5
IGFBP-6
IGFBP-7
IL-1α
IL-1β
IL-2
IL-3
IL-4
sIL-4 Receptor
IL-5
IL-6
sIL-6 Receptor
IL-7
IL-8 (72 a.a.)
IL-8 (77 a.a.)
IL-9
IL-10
IL-11
IL-12
IL-13
IL-13 analog
IL-15
IL-16 (121 a.a.)
IL-16 (130 a.a.)
IL-17
IL-17B
IL-17D
IL-17E
IL-17F
IL-19
IL-20
IL-22
IL-31
Insulin
IP-10
JE
JNK2a1
JNK2a2
KC / CXCL1
KGF
L-asparaginase
LAG-1
LALF Peptide
LAR-PTP
LC-1
LBP
LD-78β
LDH
LEC/NCC-4
Leptin
LIGHT
LIX
LKM
LL-37
Lymphotactin
sLYVE-1
M-CSF
MCP-1 (MCAF)
MCP-2
MCP-3
MCP-4
MCP-5
MDC (67 a.a.)
MDC (69 a.a.)
MDH
MEC
Mek-1
MIA
Midkine
MIG / CXCL9
MIP-1α / CCL3
MIP-1β / CCL4
MIP-3 / CCL23
MIP-3α / CCL20
MIP-3β / CCL19
MIP-4 (PARC) / CCL18
MIP-5 / CCL15
MMP-3
MMP-7
MMP-13
Myostatin
Nanog
NAP-2
Neurturin
NFAT-1
beta-NGF
NOGGIN
NOV
NP-1
NT-1/BCSF-3
NT-3
NT-4
Ocreotide
Oncostatin M
Osteoprotegerin (OPG)
OTOR
Oxytocin
p38-α
Parathyroid Hormone
PDGF-AA
PDGF-AB
PDGF-BB
Persephin
PF-4
PIGF-1
PIGF-2
PKA α-subunit
PKC-α
PKC-γ
Pleiotrophin
PLGF-1
Polymyxin B (PMB)
PRAS40
PRL-1
PRL-2
PRL-3
Prokineticin-2
Prolactin
Protirelin
PTHrP
PTP1B
PTP-IA2
PTP-MEG2
PTP-PEST
sRANK
sRANKL
RANTES
RELM-α
RELM-β
Resistin
RPTPβ
RPTPγ
RPTPμ
SCF
SCGF-α
SCGF-β
SDF-1α
SDF-1β
Secretin
SF20
SHP-2
STAT1
c-Src
TACI
TARC
TC-PTP
TECK
TFF2
TGF-α
TGF-β1
TGF-β2
TGF-β3
Thymosin α1
sTIE-1/Fc Chimera
sTIE-2/Fc Chimera
TL-1A
TNF-α
TNF-β
sTNFR1
sTNFR2
TPO
TRAIL/Apo2L
sTRAIL R-1 (DR4)
sTRAIL R-2 (DR5)
TSH
TSLP
TWEAK
TWEAK Receptor
Urokinase
VEGF121
VEGF145
VEGF165
VEGF-C
VEGF-C I525
EG-VEGF
VEGF-E
HB-VEGF-E
sVEGFR-1
sVEGFR-2
sVEGFR-3
WISP-1
WISP-2
WISP-3
WNT-1

CELL SCIENCES INC • 480 NEPONSET STREET, BUILDING 12A, CANTON, MA 02021 • INFO@CELLSCIENCES.COM

TOLL FREE: (888) 769-1246 • TEL: (781) 828-0610 • FAX: (781) 828-0542 • WEB: WWW.CELLSCIENCES.COM

SPECIAL SECTION

Plant Metabolism

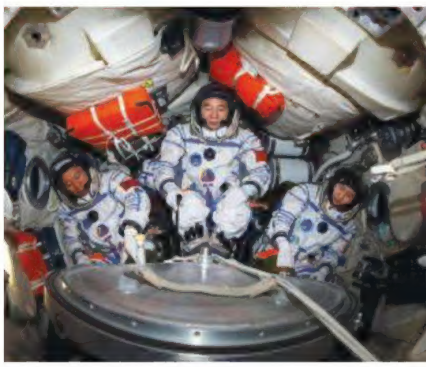

page 1630

CONTENTS continued >>

COVER

Wet bark of a Pacific yew tree (*Taxus brevifolia*) in Union, Washington, USA (vertical dimension ~15 centimeters). Wild Pacific yew thrives in the damp coastal forests of northwestern North America, with thin bark ranging in color from rose to auburn. The anticancer agent pactitaxel was originally derived from yew trees. Such complex and useful compounds are just one of the many outputs from plant metabolic networks, as analyzed in the special issue beginning on page 1657.

Photo: Don Paulson, www.donpaulson.com

DEPARTMENTS

Determining plant DNA content with the BD Accuri™ C6 flow cytometer

BD

Helping all people live healthy lives

Flow cytometry within reach.™

The BD Accuri™ C6 flow cytometer offers a capable yet simple tool to rapidly identify plant DNA. The affordable, benchtop cytometer can help characterize the DNA content of newly discovered plant species and the impact of environmental changes on genome.

Measuring just 11 x 14.75 x 16.5 inches and weighing just 30 pounds, the BD Accuri C6 flow cytometer gives you the power of flow cytometry when you need it. Best of all, you don't need to be a flow expert because the software's intuitive interface will guide you from sample collection to analysis. For faster throughput, the BD CSampler™ accessory offers reliable and easy-to-use automation with support for 48- and 96-well plates, and 24-tube racks for standard 12 x 75-mm tubes. Setup and maintenance are also simplified to increase availability and up time.

For more information about how you can more easily access the power of flow cytometry in your lab, visit **bdbiosciences.com/go/dna.**

Flow cytometry within reach.™

BD Biosciences
2350 Qume Drive
San Jose, CA 95131
bdbiosciences.com

SCIENCE PRIZE ESSAY

REVIEW

BREVIA

REPORTS

CONTENTS continued >>

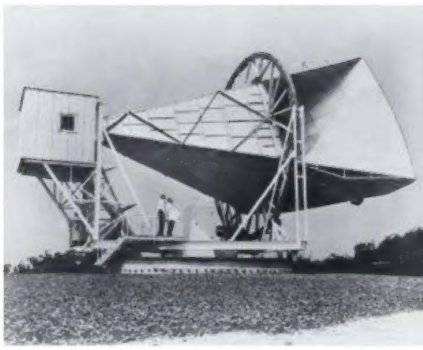

page 1640

pages 1644 & 1696

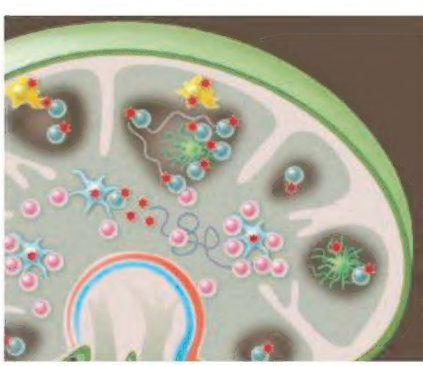

page 1676

Any sample, any application — no limits

Maximize success with QIAGEN sample technologies

- Innovative, room-temperature sample collection and stabilization
- DNA, RNA, and protein purification from any sample
- Hands-free automated sample preparation
- Reliable genetic, epigenetic, and gene expression analysis from FFPE samples
- Whole genome and transcriptome amplification to overcome sample limitations

Contact QIAGEN today or visit www.qiagen.com/sample-technologies

QIAGEN®

Sample & Assay Technologies

SCIENCEONLINE

SCIENCEXPRESS
www.sciencexpress.org

The Tides of Titan
L. Iess et al.
Gravity measurements by the Cassini spacecraft suggest that Saturn's moon Titan hosts a subsurface ocean.
10.1126/science.1219631
>> *News story p. 1629*

Synthesis and Structure of a Terminal Uranium Nitride Complex
D. M. King et al.
A uranium triple bond to nitrogen makes use of the heavy element's f orbitals.
10.1126/science.1223488

An Overlapping Protein-Coding Region in Influenza A Virus Segment 3 Modulates the Host Response
B. W. Jagger et al.
A previously unidentified influenza protein, partly old and partly new, turns off the expression of host genes.
10.1126/science.1222213

Landscape of Somatic Retrotransposition in Human Cancers
E. Lee et al.
Whole-genome sequencing provides evidence for somatic insertions in colorectal, prostate, and ovarian cancers.
10.1126/science.1222077

Regional Astrocyte Allocation Regulates CNS Synaptogenesis and Repair
H.-H. Tsai et al.
Astrocytes are not as interchangeable as previously thought.
10.1126/science.1222381

Programmable Dual-RNA–Guided DNA Endonuclease in Adaptive Bacterial Immunity
M. Jinek et al.
A prokaryotic RNA-directed targeting system can be designed to cleave any DNA sequence.
10.1126/science.1225829

TECHNICALCOMMENTS

Comment on "Global Correlations in Tropical Tree Species Richness and Abundance Reject Neutrality"
R. S. Etienne and J. Rosindell
Full text at www.sciencemag.org/cgi/content/full/336/6089/1639-b

Comment on "Global Correlations in Tropical Tree Species Richness and Abundance Reject Neutrality"
C. Mora
Full text at www.sciencemag.org/cgi/content/full/336/6089/1639-c

Comment on "Global Correlations in Tropical Tree Species Richness and Abundance Reject Neutrality"
A. Chen et al.
Full text at www.sciencemag.org/cgi/content/full/336/6089/1639-d

Comment on "Global Correlations in Tropical Tree Species Richness and Abundance Reject Neutrality"
F. Munoz et al.
Full text at www.sciencemag.org/cgi/content/full/336/6089/1639-e

Response to Comments on "Global Correlations in Tropical Tree Species Richness and Abundance Reject Neutrality"
R. E. Ricklefs and S. S. Renner
Full text at www.sciencemag.org/cgi/content/full/336/6089/1639-f

SCIENCENOW
www.sciencenow.org
Highlights From Our Daily News Coverage

Why Stress Makes You Miserable
Boosting a stress-related gene alleviates depression in rats.
http://scim.ag/Stress_Miserable

Who Controls Social Networks?
A Facebook study separates the leaders from the followers.
http://scim.ag/Social-Networks

The Elephant in the Womb
Ultrasounds reveal how elephants remain pregnant for 22 months.
http://scim.ag/Elephant_Womb

SCIENCESIGNALING
www.sciencesignaling.org
The Signal Transduction Knowledge Environment
26 June issue: http://scim.ag/ss062612

RESEARCH ARTICLE: Selective Effects of PD-1 on Akt and Ras Pathways Regulate Molecular Components of the Cell Cycle and Inhibit T Cell Proliferation
N. Patsoukis et al.

PODCAST
V. A. Boussiotis and A. M. VanHook
An inhibitory receptor blocks proliferation of autoreactive T cells.

PERSPECTIVE: How Plant Lysin Motif Receptors Get Activated—Lessons Learned from Structural Biology
R. Willmann and T. Nürnberger
A plant immune receptor is activated by chitin fragments that trigger receptor dimerization.

SCIENCETRANSLATIONAL MEDICINE
www.sciencetranslationalmedicine.org
Integrating Medicine and Science
27 June issue: http://scim.ag/stm062712

RESEARCH ARTICLE: Oxygen Gas–Filled Microparticles Provide Intravenous Oxygen Delivery
J. N. Kheir et al.

FOCUS: Boosting Oxygenation During Acute Respiratory Failure
R. C. Koehler
A foam containing oxygen gas–filled microparticles delivers oxygen during asphyxia.

STATE OF THE ART REVIEW: Fresh Approaches to Anti-Infective Therapies
C. Nathan
Characterization of resistant pathogens, new government policies, and creative discovery efforts are needed to maintain an effective antibacterial arsenal.

RESEARCH ARTICLE: Engineering a Prostate-Specific Membrane Antigen–Activated Tumor Endothelial Cell Prodrug for Cancer Therapy
S. R. Denmeade et al.
A prostate-specific membrane antigen–activated prodrug is being tested in patients with advanced cancer.

RESEARCH ARTICLE: AAV-Directed Persistent Expression of a Gene Encoding Anti-Nicotine Antibody for Smoking Cessation
M. J. Hicks et al.
Gene therapy with an anti-nicotine monoclonal antibody limits nicotine access to the brain in mice.

RESEARCH ARTICLE: Transplantation of Genetically Corrected Human iPSC-Derived Progenitors in Mice with Limb-Girdle Muscular Dystrophy
F. S. Tedesco et al.
Genetically corrected mesoangioblasts contribute to muscle in mice with limb-girdle muscular dystrophy.

SCIENCECAREERS
www.sciencecareers.org/career_magazine
Free Career Resources for Scientists

Experimental Error: Will That Be Trash or Credit?
A. Ruben
If scientists just want to make the world better, why do they expend energy clamoring for credit?
http://scim.ag/TrashOrCredit

New Technology Pollinates Plant Science
S. Webb
Advances in genetics and molecular biology are providing fresh tools for solving agricultural problems.
http://scim.ag/SWebb_PlantScience
>> *Plant Metabolism section p. 1657*

SCIENCEPODCAST
www.sciencemag.org/multimedia/podcast
Free Weekly Show
On the 29 June *Science* Podcast: mining plant biodiversity, vision in murky waters, China's space program, and more.

SCIENCE (ISSN 0036-8075) is published weekly on Friday, except the last week in December, by the American Association for the Advancement of Science, 1200 New York Avenue, NW, Washington, DC 20005. Periodicals Mail postage (publication No. 484460) paid at Washington, DC, and additional mailing offices. Domestic individual membership and subscription (51 issues): $149 ($74 allocated to subscription). Domestic institutional subscription (51 issues): $990; Foreign postage extra: Mexico, Caribbean (surface mail) $55; other countries (air assist delivery) $85. First class, airmail, student, and emeritus rates on request. Canadian rates with GST available upon request, GST #1254 88122. Publications Mail Agreement Number 1069624. **Printed in the U.S.A.**

Change of address: Allow 4 weeks, giving old and new addresses and 8-digit account number. **Postmaster:** Send change of address to AAAS, P.O. Box 96178, Washington, DC 20090–6178. **Single-copy sales:** $10.00 current issue, $15.00 back issue prepaid includes surface postage; bulk rates on request.

AAAS
ADVANCING SCIENCE, SERVING SOCIETY

EDITED BY STELLA HURTLEY

The Immune System in Three Dimensions

Immune cells must traffic within the tissues in which they reside and also through the bloodstream and lymphatic system in order to defend the host against infection. Until 10 years ago, immunologists had very little idea about how the immune response was coordinated in three dimensions. This all changed with the application of two-photon microscopy, applied intravitally or on tissue explants, to the immune system. **Germain *et al.*** (p. 1676) review how studies using this technology have informed our knowledge of immune system dynamics and discuss how to apply this technology in the future to gather further insights.

Go with the Flow

Effective absorption or filtration can be achieved by having a material with multiple levels of porosity, so that the main flow can occur in the larger channels, while smaller passageways can be used to sequester a secondary material. It can be difficult to make these materials because the pores need to be different sizes, but still fully connected to each other. **Zhang *et al.*** (p. 1684) show that a hierarchical zeolite can be made through a simple process using a single structure-directing agent that causes repetitive branching. This leads to a material with improved transport and catalytic properties.

The Sedimentary Life of Earthquakes

Estimating the hazards associated with possible large earthquakes depends largely on evidence of prior seismic activity. The relatively new global seismic networks installed to monitor earthquakes, however, have only captured the very recent history of fault zones that can remain active for thousands of years. To understand the recurrence of large earthquakes along the Alpine Fault in New Zealand, **Berryman *et al.*** (p. 1690) looked to the sediments near an old creek for evidence of surface ruptures and vertical offset. Along this fault segment, 24 large earthquakes seem to have occurred over the last 6000 years, resulting in a recurrence interval of ~329 years. The activity is more regular than other similar strike-slip faults, such as the San Andreas Fault in California.

Dating Wood Rot >>

Specific lineages within the basidiomycete fungi, white rot species, have evolved the ability to break up a major structural component of woody plants, lignin, relative to their non–lignin-decaying brown rot relatives. Through the deep phylogenetic sampling of fungal genomes, **Floudas *et al.*** (p. 1715; see the Perspective by **Hittinger**) mapped the detailed evolution of wood-degrading enzymes. A key peroxidase and other enzymes involved in lignin decay were present in the common ancestor of the Agaricomycetes. These genes then expanded through gene duplications in parallel, giving rise to white rot lineages.

Early Burrowers

Direct fossil evidence of animals from Ediacaran period—the time in Earth's history just before extensive animal diversification in the Cambrian—is scant. However, the remains of animal activity in sediment, which remain intact through geologic time can provide clues about animal behavior and evolution. **Pecoits *et al.*** (p. 1693; see the Perspective by **Droser and Gehling**) found a suite of fossil animal burrows in sedimentary rocks in Uruguay. Radiometric dating places the age of the structures at ~585 million years old, coinciding with the likely emergence of stem-group bilaterians. The complex morphologies of the fossil burrows suggest that these animals actively grazed and had the ability to burrow deep within sediments.

Spinning Backwards

When atoms and molecules collide, the energy embedded in the reaction products gets distributed among translations, vibrations, and rotations. Decades of meticulous experiments have mapped out the quantum mechanical rules underlying this distribution process, particularly in simple systems comprising just three light atoms. Now, **Jankunas *et al.*** (p. 1687; see the Perspective by **Yang *et al.***) describe a previously unappreciated wrinkle in the elementary reaction of an H atom with deuterium. Typically, products with low vibrational and rotational excitation tend to scatter backwards from the collision, whereas the spinning products scatter sideways. Above a certain vibrational threshold, however, spinning HD products were observed to scatter backwards.

Pots and Crocks

The invention of pottery allowed for more secure storage of food than was provided by baskets or hide pouches, and the vessels could also be used in cooking. The earliest pottery has been thought to have appeared in China and Japan ~18,000 years ago, several thousands of years before the advent of agriculture. **Wu *et al.*** (p. 1696); see the Perspective by **Shelach**) have now dated broken pieces of pottery from a cave in China, the earliest of which date to ~20,000 years ago, the time of the Last Glacial Maximum. Scorch marks on many pieces imply that the pottery was used in cooking.

Alkaloid Synthetic Pathway

Noscapine, a nonaddictive alkaloid found in the opium poppy, can be used as a cough suppressant and a tubulin-binding antitumor agent. **Winzer *et al.*** (p. 1704, published online 31 May; see the Perspective by **DellaPenna and O'Connor**) found that a cluster of 10 genes were key to the production of noscapine. Poppies homozygous for this gene cluster produced high levels of noscapine, heterozygous poppies produced low levels of noscapine, and those poppies lacking the gene cluster produced no noscapine. Silencing individual genes in turn and analyzing the accumulation of intermediate metabolites allowed the biosynthetic pathway of noscapine to be elucidated.

Plant Hormone Modulators

The activity and stability of several plant hormones is modulated by conjugation with various amino acids and their derivatives. **Westfall *et al.*** (p. 1708, published online 24 May) solved the crystal structures for two acyl acid amido synthetases from *Arabidopsis*. The findings suggest how the enzymes might discriminate between apolar and acidic amino acids and lend insight into the reaction chemistries that add functional diversity to hormone signaling pathways.

Pretty or Sweet

The grocery-store tomato that looks beautiful but tastes like tart cardboard arises from selection processes favoring phenotypes that make commercial production more reliable. Significant in that selection process was a mutation that reduced the mottled color variations of unripe green tomatoes, leaving them a uniform, pale, green. **Powell *et al.*** (p. 1711) analyzed the molecular biology of the mutation. The *uniform ripening* mutation turns out to disable a transcription factor called *Golden 2-like* (*GLK2*). *GLK2* expression increases the fruit's photosynthetic capacity, resulting in higher sugar content.

Seeing in the Dark

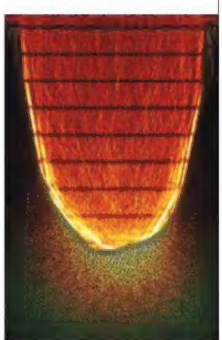

Elephantnose fish are known to use electrosensing to navigate their murky freshwater environment. However, unlike some other animals from dark environments, they have retained their eyes and some dependence on vision. While most vertebrate vision optimizes either photon catch (for increased light capture) or visual acuity, **Kreysing *et al.*** (p. 1700) show that the unique structures of the grouped retinae found in the eyes of this species matches rod and cone sensitivity, which allows for the simultaneous use of both types of photoreceptors over a large range of dim light intensities.

Noncanonical Pathway

The textbook view of translation of messenger RNA to protein is that it is always initiated from open reading frames (ORFs) that begin with an AUG codon (encodes methionine) by an initiator methionine-bound transfer RNA (tRNA). There is evidence, however, that some polypeptides are produced from non–AUG-initiated ORFs. **Starck *et al.*** (p. 1719; see the Perspective by **Dever**) used a variety of biochemical techniques to determine the underlying mechanism for such nontraditional translation initiation. Comparison of translation initiation from AUG-initiated ORFs with those beginning with leucine CUG-initiated ORFs revealed that cells can use an elongator Leu-tRNA to initiate translation at CUG codons. CUG-initiated peptides were presented by major histocompatibility class I molecules and could activate T cells.

Don't Terminate Me!

DNA transcription progresses through three phases—initiation, elongation, and termination—of messenger RNA chains. The transcribing enzyme, RNA polymerase (Pol) II, recruits factors that assist in each of these phases. **Mayer *et al.*** (p. 1723) now show that the C-terminal domain (CTD) of actively elongating Pol II is phosphorylated at conserved tyrosine residues. This modification impairs recruitment of termination factors. Factor exchange on the transcribing polymerase enzyme may be explained by an extended CTD code that is based on differential phosphorylation of the tyrosines and two well-characterized serine residues in the CTD.

Loading a Spring

To regulate cellular RNA levels, transcription must be balanced by RNA degradation. An important player is the exosome, which can unwind and degrade structured RNA. **Lee *et al.*** (p. 1726) used single-molecule fluorescence analysis to investigate how degradation and unwinding are coupled in the catalytic subunit of the yeast exosome complex, Rrp44. Rrp44 apparently digests several base pairs without unwinding, accumulates the energy, which it then uses to unwind four to five base pairs in a burst. Similar spring-like behavior has been proposed for conventional helicases, except that the stored energy comes from hydrolysis of adenosine triphosphate rather than the RNA polymer.

CREDIT: DR. MORITZ KREYSING/MUNICH UNIVERSITY

Thermo SCIENTIFIC

Quantify, verify,

In science there are always essential steps in any workflow. Accurate measurements of DNA, RNA and protein samples are critical for confidence in qPCR, sequencing, microarrays or bioproduction, but there's a better alternative to the time and complexity of conventional methods. Using minimal sample (0.5 – 2.0 µL), **Thermo Scientific NanoDrop** instruments make concentration and purity analysis so incredibly easy, and so much faster, you won't notice this step on the way to your ultimate discovery.

simplify

- Realize the difference.
Try any NanoDrop instrument for FREE.
www.thermoscientific.com/nanodrop

NanoDrop™ Lite
Basic microvolume measurements

NanoDrop™ 2000C
Full-spectrum microvolume and cuvette measurements in a single instrument

NanoDrop™ 2000
Full-spectrum microvolume measurements

NanoDrop 8000
Higher throughput, full-spectrum microvolume measurements

NanoDrop 3300
Full-spectrum microvolume fluorescence measurements

Máire Geoghegan-Quinn is the European Commissioner for Research, Innovation and Science.

Science Friction

AS EUROPEAN COMMISSIONER, I ENCOUNTER FANTASTIC SCIENCE EVERY DAY, MORE OFTEN THAN not while meeting the scientists who produce it. That is why I am particularly looking forward to the Euroscience Open Forum (ESOF) 2012 in Dublin (11 to 15 July). Scientists' passion for their work is infectious and has driven me to give them all the support I can. I am not a scientist, although I have gained a deeper appreciation for science in recent years. What I am is a politician. That means that what I understand well is the business of using scarce resources in the best way possible.

At the moment, budgets are very tight in Europe and elsewhere. It is clear to me and my colleagues in the European Commission (EC) that a greater portion of those scarce resources must be devoted to science. However, not everyone gets it, and as we meet in Dublin we are facing a battle to maintain the central place of science in European society. There is a real risk that science might be seen as a luxury as governments look for budget cuts. On a more fundamental level, scientific knowledge may even be at risk of losing its preeminent position in this modern information society.

Science is a necessity, not a luxury. The world is facing challenges on a scale not encountered before, including climate change, geopolitical upheaval, and demographic shifts. This has made policy-making more complex than ever, and informed decisions require the best evidence-based knowledge and advice we can produce. Science is also the key to our economic recovery. In Europe, countries that have invested in research are weathering the recent crisis much better. Innovative companies are more resilient, continuing to attract customers with the best products and services. So investment in science is investment in competitiveness and jobs.

But for me, scientific enquiry is important in itself. Curiosity-driven science defines and shapes human progress. The Large Hadron Collider may generate spinoffs and business opportunities, but it has a noble quest: to address some of the most fundamental questions of physics, advancing our understanding of the most fundamental laws of nature. I am very proud of the great work of the European Research Council, which in its first 5 years has already helped more than 2500 top researchers to follow their curiosity.

The EC recognizes the need for more science. That is why we have proposed an increase from €55 billion to €80 billion for our 7-year research budget, to fund our future research and innovation program Horizon 2020. Starting in 2014, Horizon 2020 will fund everything from the best frontier research to close-to-market applied science. It will be complemented with proposals to create better framework conditions for research and innovation. These include recommendations to complete the European Research Area, a true single market for ideas in Europe. We are also investing in research infrastructure through cohesion funds and meeting Innovation Union commitments, such as the unitary European patent, the setting of common standards, and facilitating access to venture capital.

The challenge now is to make sure we bring everyone along for the ride. The European project is based on progress, and science means progress. But the old models of doing science from on high are obsolete. We have to collaborate more widely across countries and across disciplines to meet our current challenges. We have to explain better what science is doing and why, in language that nonscientists can understand. We need to encourage more children to study science, not just so they can participate in the knowledge economy, but because a basic understanding of science is essential for living in an ever more complex and technological world. So when we meet in Dublin in July at ESOF, scientists have to stand up and be counted. They have to convince policy-makers to invest in science. And they have to convince the public to continue to believe in science. I will be with them all the way. Because science matters, now more than ever.

– Máire Geoghegan-Quinn

10.1126/science.1226098

EDITORS' CHOICE

EDITED BY KRISTEN MUELLER AND MARIA CRUZ

PLANETARY SCIENCE

Debating the Grandest Canyon

Valles Marineris is a prominent trough on Mars that extends for several thousands of kilometers and is 5 to 10 km deep, the longest, deepest canyon in the solar system (the Grand Canyon is less than 2 km deep). Although it lies on the edge of Mars' giant volcano Tharsis, the formation of Valles Marineris has been debated. Two recent papers provide a thorough discussion of previous models and approach the canyon's formation in different ways. Andrews-Hanna, in a final of three papers analyzing the feature, proposes that the trough formed as a direct result of Tharsis—the mass of this giant volcanic center is not fully supported by the underlying crust, and it formed in part over a preexisting tectonic boundary on Mars. Volcanism focused along this boundary could have weakened the crust, allowing localized subsidence and flow of the crust at depth, forming the trough. Yin mapped the geology along Valles Marineris in detail in several areas and argues that left-lateral strike-slip faulting along the trough, yielding displacement of more than 100 km, was important. Such faulting can enhance subsidence, as seen on Earth in places such as the Dead Sea Basin and Death Valley. Neither model requires large amounts of extension across the trough. — BH

J. Geophys. Res. **117**, 10.1029/2012JE004059 (2012); *Lithosphere* **4**, 10.1130/L192.1 (2012).

POLICY

Spend for a Cure?

Advocates for public spending on biomedical research proclaim the importance of such investments in developing treatments for disease. Government-funded research indeed affects aspects of commercial drug development. Yet many features of this relationship remain unclear. Blume-Kohout compiled longitudinal data from six sources, including a commercial database of pharmaceutical R&D, and National Institutes of Health (NIH) project descriptions and awards. She analyzed how changes in the way NIH allocated research funds targeting 67 different diseases affected the number of drugs being developed to treat those diseases. Consistent with prior research, analysis of grants awarded from 1975 through 2006 showed that a sustained 10% funding increase targeting a specific disease led to a 4.5% increase in the number of drugs targeting that disease entering Phase I clinical trials, with a lag of up to 12 years. In contrast, she found no evidence that changes in the allocation of funds across the NIH disease portfolio affect industry's decisions to invest in Phase III clinical trials for treatments for those diseases. Thus, NIH funding influences the early stages of drug discovery and testing but may not affect the later, more costly stages of drug development. — BW

J. Pol. Anal. Manag. **31**, 641 (2012).

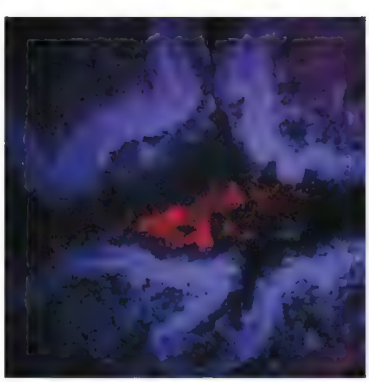

BIOMATERIALS

The Great Mucus Barrier

Mucus is often thought of as a nuisance when you have a bad cold or runny nose, but this is only one aspect of its broader use by the body to filter out foreign materials. Its tenacity in grabbing onto particulate matter also makes it difficult to deliver drugs to tissues that are protected by a mucus layer, such as the vaginal tissues, but delivery and sustained dosing to this region could aid in the prevention of sexually transmitted diseases or cervical cancer. Ensign *et al.* designed mucus-penetrating particles by coating either carboxylic acid–coated polystyrene nanoparticles or poly(lactic-co-glycolic acid) nanoparticles with a dense layer of polyethylene glycol. When administered in a hypotonic solution to mice, the regular particles got trapped in the cervicovaginal mucus layer, whereas the coated particles covered the entire vaginal epithelium, including that of the vaginal folds, in less than 10 min. In tests on the delivery of small molecules using the particles as part of a vaginal gel, the coated particles showed not only greater but also much more uniform coverage, and there was retention of the small molecules a full day after administration. In a final demonstration, modified acyclovir, a drug for treating herpes simplex 2, was loaded into the particles and compared with a soluble form of the drug. Whereas almost 90% of the mice became infected with HSV2 in the latter case, the drug-loaded coated particles provided protection for more than half the mice. — MSL

Sci. Transl. Med. **4**, 138ra79 (2012).

NEUROSCIENCE

Decoding Depression Circuits

Fluoxetine is a widely prescribed antidepressant that acts as a selective serotonin reuptake inhibitor. Schmidt *et al.* define a particular set of neurons in the mouse brain that can mediate the effects of this drug. They focused on a set of neurons in the cerebral cortex that extend to the striatum and express the adapter protein p11 (encoded by the *S100a10* gene). p11 is

CREDITS (TOP TO BOTTOM): NASA/JPL-CALTECH; L. M. ENSIGN *ET AL., SCI. TRANSL. MED.* **4**, 138RA79 (2012)

known to stabilize the expression of serotonin receptors at the cell surface, and the loss of p11 is associated with depressive behaviors. The authors used a translational profiling method to monitor a specific set of neurons in the cerebral cortex that express p11 and found that they specifically responded to fluoxetine. Depletion of p11 in the cortex showed that these neurons were required for the behavioral effects of the drug. Thus, changes in signaling through serotonin receptors in p11-expressing cells appear to account for the beneficial effect of fluoxetine. However, depletion of p11 was not sufficient to cause depression-like behavior. Thus, in this case, as might be expected for complex disorders such as depression, the cell types that mediate the therapeutic response apparently do not represent the anatomical location of the original genesis of the disease. — LBR

Cell **149**, 1152 (2012).

EVOLUTION

Ecology Splits Genomes

Evolutionary biologists wish to know how the environment and specialization of a species factor into the process of speciation. Nosil *et al.* present single-nucleotide polymorphism (SNP) data from eight populations of stick insects (*Timema cristinae*) that use two different plant species as their hosts, show slight phenotypic differences, and are in the process of speciation. Using a Bayesian model to estimate the differences between the expected and observed allele frequencies and to perform pairwise comparisons among the populations, the authors executed a genome-wide assessment of the genomic signatures related to the host-specific divergence and other ecological and evolutionary factors. As expected, the authors observed an excess of highly divergent polymorphisms between population pairs experiencing mating isolation. Isolation by distance, however, and a correlation between allele frequencies and climatic variables appear to also influence the genomic variation between populations. Thus, these analyses suggest that multiple ecological and evolutionary factors affect the speciation process, and it cannot be explained solely by the shift in plant host use. — LMZ

Proc. R. Soc. London. Ser. B **279**, 10.1098/rspb.2012.0813 (2012).

MATERIALS SCIENCE

Locating Lithium in Oxide Anodes

Lithium titanate anodes are finding use in applications such as electric vehicles, where high charging and discharging rates are needed. Lu *et al.* have studied a model material, the spinel $Li_4Ti_{55}O_{12}$, using a spherical-aberration–corrected scanning transmission electron microscopy technique. This method can locate lithium ions despite their inherent low contrast, given their low atomic number. The authors examined half-charged materials and could observe a sharp interface between the $Li_4Ti_{55}O_{12}$ and $Li_7Ti_{55}O_{12}$; the Ti and O columns are well aligned between these phases, but the Li ions shifted lattice sites, which is consistent with the lack of strain between these phases. They also show that the charge state of the Ti atoms is heterogeneous, and the presence of these local changes in valence is consistent with calculations that reveal strong lithium-electron interactions. — PDS

Adv. Mater. **24**, 3233 (2012).

IMMUNOLOGY

A One-Two Punch

It's well known that viral infection can leave you susceptible to bacterial infections—a bad cold or flu followed by pneumonia is a well-known and oft-experienced example. But why? Negishi *et al.* now reveal a potential mechanism. They find that triggering of RIG-I–like receptors (RLRs), which are most often triggered by viruses, can inhibit Toll-like receptor (TLR)

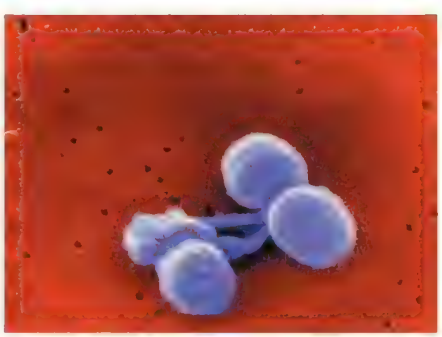

signaling, which is essential for some antibacterial responses. In particular, RLR signaling induces the transcription factor IRF3, which binds to and blocks the transcriptional activation of *Il12b*. *Il12b* encodes the p40 subunit of the cytokine interleukin-12—a molecule very important to the defense against bacterial infections. In mice, activation of RLRs led to attenuated TLR signaling and consequently, decreased T cell responses dependent on IL-12 and another cytokine that uses p40, IL-23. The consequence of such reduced immunity was that mice succumbed to sublethal doses of a bacterial infection if they were first infected with a virus. — KLM

Nat. Immunol. **13**, 659 (2012).

CREDIT: JANICE CARR/CDC

www.sciencemag.org

Science

1200 New York Avenue, NW
Washington, DC 20005
Editorial: 202-326-6550, FAX 202-289-7562
News: 202-326-6581, FAX 202-371-9227
Bateman House, 82-88 Hills Road
Cambridge, UK CB2 1LQ
+44 (0) 1223 326500, FAX +44 (0) 1223 326501

Subscription Services For change of address, missing issues, new orders and renewals, and payment questions: 866-434-AAAS (2227) or 202-326-6417, FAX 202-842-1065. Mailing addresses: AAAS, P.O. Box 96178, Washington, DC 20090-6178 or AAAS Member Services, 1200 New York Avenue, NW, Washington, DC 20005

Institutional Site Licenses please call 202-326-6755 for any questions or information

Reprints: Author Inquiries 800-635-7181
Commercial Inquiries 803-359-4578

Permissions 202-326-7074, FAX 202-682-0816

Member Benefits AAAS Travels: Betchart Expeditions 800-252-4910; Apple Store www.store.apple.com/us/go/eppstore/aaas; NASA Federal, 1-888-NASA-FCU (1-888-627-2328) or www.nasafcu.com; Cold Spring Harbor Laboratory Press Publications www.cshlpress.com/affiliates/aaas.htm; GEICO Auto Insurance www.geico.com/landingpage/go51.htm?logo=17624; Hertz 800-654-2200 CDP#343457; Office Depot https://bsd.officedepot.com/portalLogin.do; Seabury & Smith Life Insurance 800-424-9883; Subaru VIP Program 202-326-6417; VIP Moving Services www.vipmayflower.com/domestic/index.html; Other Benefits: AAAS Member Services 202-326-6417 or www.aaasmember.org.

science_editors@aaas.org	(for general editorial queries)
science_letters@aaas.org	(for queries about letters)
science_reviews@aaas.org	(for returning manuscript reviews)
science_bookrevs@aaas.org	(for book review queries)

Published by the American Association for the Advancement of Science (AAAS), *Science* serves its readers as a forum for the presentation and discussion of important issues related to the advancement of science, including the presentation of minority or conflicting points of view, rather than by publishing only material on which a consensus has been reached. Accordingly, all articles published in *Science*—including editorials, news and comment, and book reviews—are signed and reflect the individual views of the authors and not official points of view adopted by AAAS or the institutions with which the authors are affiliated.

AAAS was founded in 1848 and incorporated in 1874. Its mission is to advance science, engineering, and innovation throughout the world for the benefit of all people. The goals of the association are to: enhance communication among scientists, engineers, and the public; promote and defend the integrity of science and its use; strengthen support for the science and technology enterprise; provide a voice for science on societal issues; promote the responsible use of science in public policy; strengthen and diversify the science and technology workforce; foster education in science and technology for everyone; increase public engagement with science and technology; and advance international cooperation in science.

Information for Authors
See pages 752 and 753 of the 10 February 2012 issue or access www.sciencemag.org/about/authors

EDITOR-IN-CHIEF **Bruce Alberts**
EXECUTIVE EDITOR **Monica M. Bradford**
NEWS EDITOR **Colin Norman**
MANAGING EDITOR, RESEARCH JOURNALS **Katrina L. Kelner**
DEPUTY EDITORS **R. Brooks Hanson, Barbara R. Jasny, Andrew M. Sugden, Valda J. Vinson**

Editorial senior editors/commentary Lisa D. Chong, Brad Wible; **senior editors** Gilbert J. Chin, Pamela J. Hines, Paula A. Kiberstis (Boston), Marc S. Lavine (Toronto), Beverly A. Purnell, L. Bryan Ray, Guy Riddihough, H. Jesse Smith, Phillip D. Szuromi (Tennessee), Valda Vinson, Jake S. Yeston, Laura M. Zahn (San Diego); **associate editors** Kristen L. Mueller, Jelena Stajic, Sacha Vignieri, Nicholas S. Wigginton; **book review editor** Sherman J. Suter; **associate letters editor** Jennifer Sills; **editorial manager** Cara Tate; **senior copy editors** Jeffrey E. Cook, Cynthia Howe, Harry Jach, Lauren Kmec, Barbara P. Ordway, Trista Wagoner; **copy editor** Chris Filiatreau; **senior editorial coordinators** Carolyn Kyle, Beverly Shields; **editorial coordinators** Joi S. Granger, Anita Wynn; **publications assistants** Ramatoulaye Diop, Le-Toya Mayne Flood, Aneera Dobbins, Jeffrey Hearn, Lisa Johnson, Dona Mathieu, Scott Miller, Jerry Richardson, Teresa R. Sakon, Brian White; **editorial assistant** Patricia M. Moore; **executive editorial assistant** Yolanda O'Bannon (San Francisco); **executive assistant** Alison Crawford; **administrative support** Maryrose Madrid; **editorial fellow** Melissa R. McCartney

Editorial director, web and new media Stewart Wills; **senior web editor** Sarah Crespi; **web editor** Kerry Klein; **web development manager** Martyn Green; **web developers** Corinna Cohn, Andrew Whitesell

News deputy news editors Robert Coontz, David Grimm (Online), Eliot Marshall, Jeffrey Mervis, Leslie Roberts, John Travis; **contributing editors** Elizabeth Culotta, Polly Shulman; **news writers** Yudhijit Bhattacharjee, Adrian Cho, Jennifer Couzin-Frankel, Carolyn Gramling, Jocelyn Kaiser, Richard A. Kerr, David Malakoff, Greg Miller, Elizabeth Pennisi, Robert F. Service (Pacific NW), Erik Stokstad; **web developer** Daniel Berger; **interns** Jane J. Lee, Meghna Sachdev; **contributing correspondents** John Bohannon, Jon Cohen (San Diego, CA), Daniel Ferber, Ann Gibbons, Sam Kean, Eli Kinkisch, Andrew Lawler, Mitch Leslie, Charles C. Mann, Virginia Morell, Gary Taubes; **copy editors** Melissa Raimondi, Linda B. Felaco; **administrative support** Scherraine Mack; **bureaus** San Diego, CA: 760-942-3252, FAX 760-942-4979; Pacific Northwest: 503-963-1940

Production director Wendy K. Shank; **assistant managers** Rebecca Doshi, Lori Murphy; **senior specialists** Steve Forrester, Chris Redwood, Anthony Rosen; **Preflight director** David M. Tompkins; **manager** Marcus Spiegler; **specialists** Jason Hillman, Tara Kelly

Art director Yael Fitzpatrick; **associate art director** Laura Creveling; **senior illustrators** Chris Bickel, Katharine Sutliff; **illustrators** Yana Hammond, Bricelyn Strauch; **senior art associates** Holly Bishop, Preston Huey, Nayomi Kevitiyagala; **art associates** Kay Engman, Garvin Grullón; **photo editor** Leslie Blizard

***Science* International**

Europe (science@science-int.co.uk) **editorial: international managing editor** Andrew M. Sugden; **senior editor/commentary** Julia Fahrenkamp-Uppenbrink; **senior editors** Caroline Ash, Stella M. Hurtley, Ian S. Osborne, Peter Stern; **associate editor** Maria Cruz; **contributing editor** Helen Pickersgill; **editorial support** Samantha Hogg, Alice Whaley; **administrative support** Janet Clements, Nicola Morris, John Wood; **news: deputy news editor, u.k.** Daniel Clery; **contributing editor, europe** Martin Enserink; **contributing correspondents** Michael Balter (Paris), Kai Kupferschmidt (Berlin), Gretchen Vogel (Berlin)

Asia Japan Office: Asca Corporation, Tomoko Furusawa, Rustic Bldg. 7F, 77 Tenjin-cho, Shinjuku-ku, Tokyo 162-0808, Japan; +81 3 6802 4616, FAX +81 3 6802 4615, inquiry@sciencemag.jp; **asia news editor** Richard Stone (Beijing: rstone@aaas.org); **contributing correspondents** Dennis Normile [Japan: +81 (0) 3 3391 0630, FAX +81 (0) 3 5936 3531; dnormile@gol.com]; Hao Xin [China: cindyhao@gmail.com]; Mara Hvistendahl [China: mhvisten@aaas.org]; Pallava Bagla [South Asia: +91 (0) 11 2271 2896; pbagla@vsnl.com]

EXECUTIVE PUBLISHER **Alan I. Leshner**
PUBLISHER **Beth Rosner**

Fulfillment Systems and Operations (membership@aaas.org); **customer service supervisor** Pat Butler; **specialists** LaToya Casteel, Michelle Ofordire, April Marshall; **manager, data entry** Mickie Napoleoni; **data entry specialists** Tarrika Hill, JJ Regan, Eva Mae Campbell

Business Operations and Administration director Deborah Rivera-Wienhold; **business systems and financial analysis director** Randy Yi; **manager, fulfillment systems** Frits Buninghy; **systems analyst** Nicole Mehmedovich; **manager, business analysis** Eric Knott; **manager, business operations** Jessica Tierney; **business analysts** Cory Lipman, Celeste Troxler; Christine Wehrli; **financial analyst** Julia Nguyen; **rights and permissions: administrator** Emilie David; **associate** Elizabeth Sandler; **marketing director** Ian King; **marketing managers** Allison Pritchard, Alison Chandler, Julianne Wielga, Samantha Smith; **marketing associates** Aimee Aponte, Mary Ellen Crowley, Elizabeth Sattler, Rebecca Riffin; **senior marketing executive** Jennifer Reeves; **director, site licensing** Tom Ryan; **director, corporate relations** Eileen Bernadette Moran; **senior publisher relations specialist** Kiki Forsythe; **publisher relations manager** Catherine Holland; **publisher relations, eastern region** Phillip Smith; **publisher relations, western region** Ryan Rexroth; **customer relations manager** Iquo Edim; **marketing manager** Christina Schlecht; **marketing associates** Paulina Curto, Mitchell Edmund; **electronic media: director** Lizabeth Harman; **assistant manager** Lisa Stanford; **production specialists** Antoinette Hodal, Thomas Jaensch, Nichele Johnston, Kimberly Oster; **project manager** Trista Snyder; **computer specialists** Walter Jones, Kai Zhang; **program director, aaas membercentral** Peggy Mihelich

director, global collaboration, custom publications, advertising Bill Moran
commercial editor Sean Sanders: 202-326-6430
assistant commercial editor Tianna Hicklin 202-326-6463

Product (science_advertising@aaas.org); **midwest** Rick Bongiovanni: 330-405-7080, FAX 330-405-7081; **east coast/e. canada** Laurie Faraday: 508-747-9395, FAX 617-507-8189; **west coast/w. canada** Lynne Stickrod: 415-931-9782, FAX 415-520-6940; **uk/europe/asia** Roger Goncalves: TEL/FAX +41 43 243 1358; **japan**, Makiko Hara: +81 (0) 3 6802 4616, FAX +81 (0) 3 6802 4615; ads@sciencemag.jp; **china/taiwan** Ruolei Wu: +86 1367 1015 294 rwu@aaas.org

worldwide associate director of *Science* Careers Tracy Holmes: +44 (0) 1223 326525, FAX +44 (0) 1223 326532

Classified (advertise@sciencecareers.org); **u.s.: midwest/west coast/south central/canada** Tina Burks: 202-326-6577; **east coast/industry** Elizabeth Early: 202-326-6578; **sales administrator** Marci Gallun; **europe/row sales** Simone Jux, Lucy Nelson; **sales assistant** Kelly Grace; **japan** Yuri Kobayashi +81 (6) 6627-9250; careerads@sciencemag.jp; **china/taiwan** Ruolei Wu: +86 1367 1015 294 rwu@aaas.org; **advertising support manager** Karen Foote: 202-326-6740; **advertising production operations manager** Deborah Tompkins; **senior production specialist/graphic designer** Amy Hardcastle; **production specialist** Yuse Lajiminmuhip; **senior traffic associate** Christine Hall; **sales coordinator** Shirley Young

American Heart Association®

SCIENTIFIC SESSIONS 2012

Los Angeles, Calif.

Scientific Sessions and ReSS

Leading Discovery. Global Impact.

The Los Angeles spotlight is shining brightly on the latest scientific research, thanks to the American Heart Association's award-winning Scientific Sessions meeting. Join your colleagues in Southern California for the best scientific presentations, late-breaking clinical trials, continuing education credits, professional networking opportunities and more.

Housing and Registration Now Open:

Deadline to become an AHA/ASA Professional Member to receive registration discount	Sept. 26
Deadline for advance registration rates	Oct. 10
On-site rates apply	Oct. 11

Exhibits	Nov. 4–6
Scientific Sessions	Nov. 3–7
Resuscitation Science Symposium	Nov. 3–4
CVN Symposium	Nov. 6–7

scanlife.com

Register Now!

scientificsessions.org

AROUND THE WORLD

Washington, D.C. **1**

House Panel Set to Slash Climate, Environmental Research

The U.S. House of Representatives Appropriations Committee appears set this week to approve a 2013 spending bill that would impose deep cuts in climate and ecological research conducted by the Department of the Interior, the Environmental Protection Agency (EPA), and the U.S. Geological Survey (USGS).

A preliminary version of the Interior and Environment Appropriations Bill approved by a subcommittee on 19 June would cut funding for an array of climate research programs by 29%, or $101 million, from current levels. Spending at EPA would fall to $7 billion, or 17% below 2012 levels, while USGS would see a 9% cut to $967 million. The bill also seeks to block the Obama Administration from moving forward with some environmental regulations, including rules aimed at protecting streams and forests. If approved by the full committee, the bill still faces a vote in the full House and would have to be reconciled with a Senate version, which is likely to be very different. Final action is not expected until late this year.

Leeds, U.K. **2**

More Studies on Neglected Tropical Diseases

The investment surge in so-called neglected tropical diseases (NTDs) is paying off in research papers, according to a report by Thomson Reuters published last week. Between 1992 and 2011, the number of studies on NTDs—defined as diseases of the poor, but with HIV, tuberculosis, and malaria excluded—doubled to well over 5000 per year. Research on dengue, a painful viral disease that infects millions of poor city dwellers, grew particularly fast, and India and Brazil are catching up with traditional NTD strongholds like the United States, the United Kingdom, and France.

Despite that progress, the neglect is far from over, the report says. Although they affect billions, all of these diseases combined make up only 0.5% of the world's research literature, and coronary heart disease alone yields more than twice as many papers as the entire NTD field.

Washington, D.C. **3**

Senate Creates Foundation for Ag Research

U.S. agricultural research would gain a new fundraising tool under the $283 billion Farm Bill passed last week by the Senate. The bill charters the Foundation for Food and Agriculture Research (FFAR) and provides $100 million in matching funds to attract donors. The bill would also appropriate $200 million over 5 years for research on fruits, vegetables, and other "specialty crops"—13% less than what was provided by the 2008 Farm Bill. The bill also eliminates a $118 million biofuels research program.

The outlook is worse in the House of Representatives Agriculture Committee, which will begin marking up its version on 11 July. House lawmakers are looking for an additional $10 billion to cut from the bill, and the committee "flat out told us that they have zero interest in including FFAR in their farm bill," says Karl Glasener, director of science policy at the American Society of Agronomy, Crop Science Society of America, and Soil Science Society of America.

Rotterdam, The Netherlands **4**

Psychologist Resigns After Investigation of His Data

Statistical sleuthing by an anonymous fraud hunter in the United Sates led to the downfall of a marketing researcher at Erasmus University Rotterdam in the Netherlands. On 25 June, the university announced that social psychologist Dirk Smeesters, who specialized in consumer behavior, has resigned after an investigative panel found problems in some of his studies and concluded it had "no confidence in [their] scientific integrity." The university has asked for the retraction of two of Smeesters's papers.

Among Smeesters's research questions were the effects of messiness and whether death-related media stories might make consumers prefer domestic brands.

Smeesters conceded to "massaging" the data in some papers to "strengthen" outcomes, while defending his actions as common in his field, according to a report released by the university investigation com-

CREDITS (TOP TO BOTTOM): BRENDAN HOFFMAN/GETTY IMAGES; RAJESH KUMAR SINGH/AP PHOTO

mission. But the panel says it can't be sure some of his studies were actually carried out because Smeesters says he lost the raw data in a computer crash.

Using a new and unpublished statistical method to search for suspicious patterns, the whistleblower found that data in Smeesters's papers were "too good to be true," according to the panel, which agreed to keep his identity secret while he prepares a paper about his method. **http://scim.ag/smeesters**

THEY SAID IT

"Commission doesn't really do irony. Hope was to get young people onto site. That seems to be happening!"

—Michael Jennings, a spokesman for the European Commission, tweeting a response on 22 June to one suggestion that the commission's widely reviled video promoting its "Science: It's a Girl Thing!" campaign might have been an ironic ploy. **http://scim.ag/ECgirls**

Mountain View, California **5**

Privatizing the Hunt for Asteroids

Congress has told NASA to find any hill-sized asteroids before they hit Earth. President Barack Obama has directed NASA to send astronauts to a small asteroid the agency has yet to find. And entrepreneurs looking to mine asteroids must find their own mother lode.

The California-based B612 Foundation has a solution for everybody. The 10-year-old nonprofit organization has a preliminary design for a spacecraft bearing an infrared telescope. It would orbit the sun inside Earth's orbit for a glare-free view of the asteroids 140 meters in diameter and larger that are orbiting near—and possibly threatening—Earth. The mission closely resembles the search mission NASA came up with in 2003, says B612 Mission Director Harold Reitsema. But now the required technology has been demonstrated on successful NASA missions such as planet-hunting Kepler, he says, and a private organization like B612 should be able to cut NASA's mission cost in half. That does leave $100 million to $200 million to be raised from major donors and a "broad base" of more modest contributors.

Pinta Island, Ecuador **6**

A Galápagos Legend Dies

Lonesome George, a giant Galápagos tortoise thought to be the last member of his subspecies, has died. The tortoise was found dead by his keeper of 40 years, announced the director of the Galápagos National Park, Edwin Naula, on 24 June. His exact age wasn't known, but he was estimated to be about 100 years old. A primary draw for visitors to the Galápagos, he had become a symbol of the archipelago since he was found on Pinta Island by biologist Joseph Vagvolgyi in 1971.

Lonesome George was thought to be the last Pinta Island giant tortoise, or Chelonoidis nigra abingdoni. About 20,000 giant tortoises of other subspecies live on the Galápagos. Efforts to breed Lonesome George to females of close subspecies proved unsuccessful; although Lonesome George did mate with one female, the eggs were infertile.

Park officials are planning a postmortem to determine the cause of death; Lonesome George was not old for a giant tortoise, which can live for about 200 years.

University Presidents Commemorate Morrill Act

Clad in academic robes, the presidents of land-grant universities around the United States gathered in front of the Lincoln Memorial on 25 June to lay a wreath at the monument in commemoration of the 150th anniversary of the passing of the Morrill Act. The act allocated land to establish a system of industrial universities in each state based on the number of senators and representatives each had in Congress. The bill was signed into law by Abraham Lincoln on 2 July 1862.

The Association of Public and Land-Grant Universities (APLU) also held a convocation on 26 June, with Bill Gates as the keynote speaker. "The Morrill Act was the democratization of higher education at time when college was largely reserved for the children of the elite," APLU President Peter McPherson said in a statement 20 June.

CREDITS (TOP TO BOTTOM): PUTNEYMARK/WIKIPEDIA; ABBY BRACK LEWIS /LIBRARY OF CONGRESS

Random Sample

Olympics Take Medal for Most Over-Budget Megaproject

Seven years ago, when London won the honor of hosting the 2012 Summer Olympic Games, the city celebrated—but maybe it should have been groaning instead. A new economic study of the past 50 years of Olympics finds that the London Games are projected to cost twice as much as originally expected.

Public officials generally take estimated budgets for large and complex projects, from bridges to NASA space telescopes, with a grain of salt. But even among megaprojects, the Olympic Games hold a special honor: They are the most consistently over budget. In 50 years, none of the games has ever met its proposed budget, according to the study by Bent Flyvbjerg and Allison Stewart, economists at the University of Oxford's Saïd School of Business in the United Kingdom.

And the 2012 Summer Games in London take the cake, Flyvbjerg and Stewart say—they predict that these will be the most expensive Olympic Games in history, with a final price tag of $14.8 billion—101% higher than the originally proposed budget.

Flyvberg and Stewart may be in for a backlash, says Wladimir Andreff, an economist at Panthéon-Sorbonne University in Paris—a city that lost its bid to host the 2012 Games. "My own experience as a taxpayer is paying for the 1968 Grenoble Winter Games," he says, which took a decade to pay off. Andreff says that, in trying to discuss those costs, he has experienced media censorship during pro-Olympic campaigns. As for the London Games, this study's methodology was "cautious," he says, so the final costs are likely to be even larger than predicted.

NEWSMAKERS

SETI Head Steps Down

Astronomer **Jill Tarter**, who helped found the Search for Extraterrestrial Intelligence (SETI) Institute in 1984 and has served as its director for 35 years, is stepping down. She says she will instead focus on fundraising for the institute.

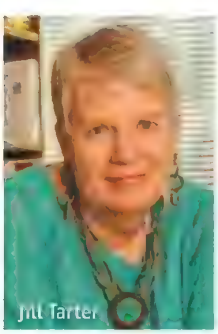

Tarter, 68, began her search for extraterrestrial life while a graduate student at Cornell University, where she worked on the SERENDIP project. She led NASA's High Resolution Microwave Survey in 1992 and 1993; that morphed into SETI's decade-long Project Phoenix, which searched 750 nearby star systems for extraterrestrial signals (the project ended in 2004, after finding no signals).

SETI and the University of California, Berkeley, began jointly operating the Allen Telescope Array in 2007, intended to increase the speed and the spectral range of the search for signals. But the project, which costs $3 million a year to operate, has been struggling financially.

Tarter was the inspiration for Jodie Foster's character in the 1997 movie *Contact*. At SETIcon, a gathering of astronomers, astronauts, and enthusiasts in Santa Clara, California, held a gala on 23 June honoring Tarter's work.

FINDINGS

Condors Suffer Lead Poisoning

A captive breeding program for the endangered California condor (*Gymnogyps californianus*) has increased the condors' numbers to almost 400. But a study published online 25 June in the *Proceedings of the National Academy of Sciences* finds that condors are still threatened by lead poisoning from scavenging the carcasses of animals shot with lead-based ammunition.

Condors feed on the remains of large animals—the most likely to have been shot. High levels of lead can shut down the condors' digestive system, causing the birds to starve. Research toxicologist Myra Finkelstein of the University of California, Santa Cruz, and colleagues checked more than 1000 blood samples from 150 condors between 1997 and 2010. About 70% of birds had signs of lead exposure; an analysis of lead isotopic ratios verified that bullets were the source.

The success of captive breeding programs may mask the danger of lead, Finkelstein says: Condors are caught twice a year, tested for lead, treated, and released. This will keep bird populations stable—but the researchers' models suggest that unless the lead ammunition is eliminated, the birds won't survive on their own. **http://scim.ag/condorlead**

BY THE NUMBERS

284,500 Number of people estimated to have died globally from 2009 pandemic influenza A (H1N1) in the first year the virus circulated in each country, according to *The Lancet*.

18 billion kilometers Distance of NASA's Voyager spacecraft from Earth. After a 35-year journey, an increase in cosmic rays hitting the spacecraft since 7 May could mean it's leaving the heliosphere and entering interstellar space.

CREDITS (TOP TO BOTTOM): GIDEON MENDEL/CORBIS; SETH SHOSTAK/SETI INSTITUTE

CREDIT: CHRIS MARCHAND/*THE DRYDEN OBSERVER*

Lake effect. Plans to defund Canada's Experimental Lakes Area research facility have sparked protests, such as this one in Kenora, Ontario.

CANADIAN SCIENCE

Environmental Science Feels Pinch in Canada's Budget

After Canada's Conservative government unveiled a sweeping $276 billion spending plan in March, many of the country's scientists breathed a sigh of relief. Although the budget—which is likely to win final approval from Canadian lawmakers this week—calls for cutting $5.2 billion in spending, eliminating 19,200 federal jobs, and shifting some funding from basic research to more applied projects, it leaves overall science budgets relatively unscathed. But as details have dribbled out on how the plan and accompanying policy changes will affect certain fields, relief has turned to unease—and even anger—for some Canadian researchers.

"Some organizations mistakenly thought this was a good plan," says Thomas Duck, an atmospheric scientist at Dalhousie University in Halifax, Nova Scotia. "But anyone who has been paying attention understands that this will have a devastating impact, … especially for the environmental and climate sciences."

Last week, such concerns made headlines as a quartet of former top fisheries officials from both ends of the political spectrum publicly slammed a government plan to defund a prominent ecological research station. Academic researchers, meanwhile, are assailing budget shifts that appear to have terminated two programs that paid for instruments and facilities for nonbiomedical basic research. Other scientists are warning that ongoing layoffs at federal environmental agencies—including a recently leaked plan to fire seven air-pollution researchers at Environment Canada—are crippling monitoring efforts. And they are decrying policy changes that will "streamline" environmental reviews of construction projects and remove protections for nongame fish.

The government is making the changes in order to channel funds to Canada's highest research priorities and fully develop oil sands and other natural resources that have the "huge potential to create even more jobs and growth," said Finance Minister John Flaherty when he released the plan. Critics, however, aren't persuaded. "This government isn't interested in science that is inconvenient for advancing its ideological and economic agenda," says Diane Orihel, an aquatic ecologist at the University of Alberta in Edmonton.

For Orihel, the government's controversial move to defund the Experimental Lakes Area (ELA) facility in northwestern Ontario is a prime example of its hostility to environmental science. Founded in 1968, ELA and the 58 lakes under its purview have hosted numerous international collaborations, including important studies of mercury pollution that have helped shape international controls (*Science*, 28 November 2008, p. 1316). In May, the Department of Fisheries and Oceans (DFO), which operates ELA with Environment Canada and the province of Ontario, announced that it would end funding in early 2013 and seek to transfer the facility to a university or nonprofit. Officials suggested that ELA's funding—less than $3 million annually—could be better spent studying the impact of oil development in western Canada.

It wasn't the first time the government had suggested closing ELA, but this time the backlash has been unusually ferocious, observers say. Within days, protests sprouted across Canada and letters from around the world began pouring in to Prime Minister Stephen Harper's office. "We are terribly worried" about ELA's "doom," wrote the Israel Oceanographic and Limnological Research institute. On 22 June, ELA advocates turned the public pressure up a notch, releasing a harsh letter to Harper from four former DFO senior officials. "We believe that you have been ill advised either by political staff … or by federal bureaucrats," they wrote. The letter also criticizes proposed changes to Canada's Fisheries Law, which will strip nongame fish of protection. "This is not about a few fish in drainage ditches," they wrote.

Whether such outrage will make a difference is unclear. Orihel says the ELA decision "is totally reversible" by the Harper government alone and holds out hope. Similarly, Dalhousie's Duck hopes public pressure will persuade officials to reverse the plan to lay off an Environment Canada team that monitors industrial air pollution.

Undoing the changes to the Fisheries Law, however, appears unlikely anytime soon, as the Canadian Senate is poised to approve the changes as part of a massive budget bill. That bill, known as C-38, also calls for a total of $45 million in cuts over the next few years to Canada's Natural Sciences and Engineering Research Council (NSERC), which pumps about $1 billion per year into academic science. To prepare, NSERC has already put on hold its Major Resources Support and Research Tools and Instruments programs. Both provided "crucial support for the kinds of research that industry is not inclined to fund," Duck says, such as an atmospheric research station in the high Arctic where he has worked. Now, he's hoping to find replacement funds for the station, because he believes the Harper government "doesn't have a history of backtracking on these kinds of things."

–DAVID MALAKOFF

ECOLOGY

Fences Make Good Nest Sites

KAENA POINT, HAWAII—Each week from November to July, ornithologist Eric VanderWerf drives from Honolulu to a sandy nature reserve here on Oahu Island's northwestern peninsula to count seabird chicks and check his rodent traps. Last year, the 20-hectare point was cut off from the rest of Oahu by a high-tech fence with a mesh so fine even baby mice can't get through it. Conservationists then removed all nest predators—such as rats that eat chicks and eggs—effectively returning the land to its prehuman state some 800 years ago, when the island had no land mammals and millions of seabirds flocked here to breed undisturbed.

VanderWerf's surveys show that this effort to provide nesting seabirds a safe haven seems to be working. The population of the point's colony of Laysan albatrosses has increased by 15%, to 400, since the fence was finished in March 2011, says VanderWerf, who co-owns Pacific Rim Conservation, based in Honolulu. And the number of wedge-tailed shearwater chicks that survived and flew off tripled to 1775 in 2 years.

This is good news for these oceangoing species, which, along with petrels, have been declining faster than any other category of birds. First put at risk by early Polynesian settlers and later by Europeans, these birds continue to be plagued not just when they visit land to breed but also while they are out at sea. A new, unpublished survey estimates that their numbers have dwindled by 25%—about 250 million seabirds—since 1950, says Michelle Paleczny, a fisheries biologist at the University of British Columbia, Vancouver.

Such numbers have helped spur more intensive efforts to protect seabird colonies, such as the fence-and-exterminate project in Hawaii. And they have been paying off, says Stuart Butchart, an ornithologist at Birdlife International in Cambridge, U.K. "The data show that eradications work," he says. "We know we can use them to reverse the decline of dozens of species, and that's why we need to expand them before more [species] are driven to extinction."

Seabirds' troubles date back to the expansion of Polynesian peoples across the Pacific 2 millennia ago. These birds have evolved to nest on the ground on islands free of mammals, some as large as Hawaii or New Zealand, others on mere rocks, and thus were easy prey to ocean explorers and the dogs and rats they introduced. Europeans also slaughtered millions of seabirds for the millinery trade and introduced cats, mongooses, and bigger rats to the islands the Polynesians had missed in the Pacific, as well as to islands in other oceans. A study published in the March 2012 issue of Birdlife International reported that 75% of the threatened pelagic-seabird species are affected by invasive predators where they nest.

More recently, industrial fishing has been taking a toll. Researchers estimate that 41% of seabird species suffer losses because the birds drown when they try to snatch baitfish from hooked lines set out by tuna boats. What's worse is that there are fewer fish for the birds to catch. Studies of stable-isotope values of carbon and nitrogen in seabird feathers and eggshells, some dating back to the 1980s, have suggested that many seabirds are eating smaller and less nutritious prey that require more energy to catch. Last year, researchers found that as the biomass of small fish such as anchovies shrinks from overfishing, so does the biomass of the seabird populations (*Science*, 23 December 2011, p. 1703). "A lot of seabirds are effectively being starved," says study leader Phillipe Cury, director of the Mediterranean and Tropical Fisheries Research Center in Sète, France.

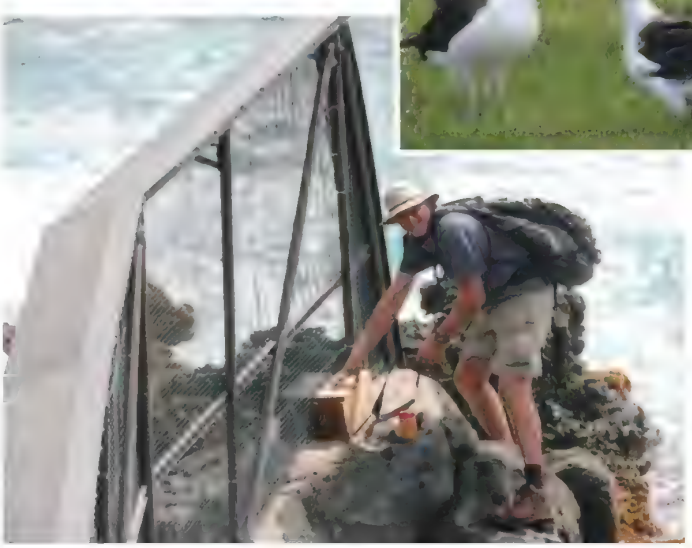

Fence me in. Eric VanderWerf checks a trap set to catch any predators that might get around the high-tech fence and eat the eggs of Laysan albatrosses (*inset*).

Predator-eradication programs are a bright spot for seabirds. In the past 35 years, conservationists have made about 300 islands pest-free with good results. The Pacific atoll of Midway is a case in point. When the American military started fortifying the island in 1940, more than 500,000 breeding Bonin petrels were showing up in the nesting season, says Elizabeth Flint of the U.S. Fish and Wildlife Service in Honolulu. But accidentally introduced rats reduced the petrel numbers to 5000 breeders. Less than 2 decades after the rats were eradicated, more than 300,000 petrels again fill the evening skies above Midway as they come and go from the burrows where they nest. Midway's albatross numbers, meanwhile, rebounded to 1.5 million birds, making the island's albatross colony the world's largest.

While some island-wide eradications continue—the U.S. Air Force killed tens of thousands of rats in early June in Wake Atoll, west of Hawaii—"most of the [islands] that are left and that have a lot of endangered species, like Gough and South Georgia in the Atlantic, are bigger, complicated, and will be more expensive," says conservation biologist Alex Wegmann of Island Conservation, an organization based in Santa Cruz, California, that specializes in eradications.

The alternative is to fence in parts of large islands like Fiji, Hawaii, or New Zealand. One advantage of fences on big islands is that they can be easier to fund than extermination projects on remote islands, says Tim Day of Xcluder, a Rotorua, New Zealand–based company that built the barrier at Hawaii's Kaena Point. Another is that they can be built near places where people live, creating an attraction that helps educate the public about seabird conservation. The Kaena Point fence, for instance, has helped create the world's only easily accessible and unsupervised albatross colony just 30 miles from a big city—Honolulu—and cost a relatively inexpensive $290,000 to set up. "Seabirds rebound much faster than other birds because immigration is added to reproduction," he points out. So keeping out exotic predators is "like taking the handbrake off when you're driving."

–CHRISTOPHER PALA

Christopher Pala is based in Washington, D.C., and often reports on marine issues.

CREDITS: CHRIS PALA

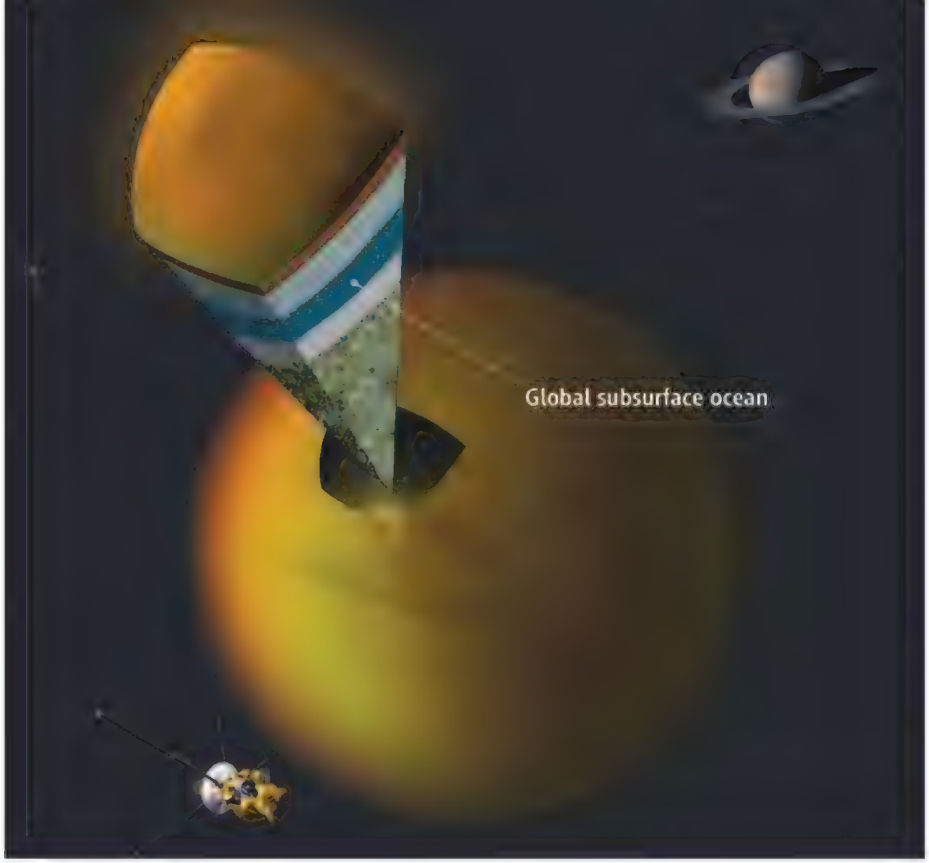

CREDIT: A. TAVANI/SAPIENZA UNIVERSITY OF ROME

PLANETARY SCIENCE

Cassini Spies an Ocean Inside Saturn's Icy, Gassy Moon Titan

To understand a planetary body, its origins and its history, it helps to look inside it. Planetary scientists have now done just that in the case of Saturn's big moon Titan, one of the solar system's most enigmatic bodies. Using only the subtly varying pitch of radio transmissions from the Cassini probe as it repeatedly flew by Titan, Cassini scientists have divined an ocean of water 100 kilometers beneath Titan's icy surface.

"It's an enormous technical achievement," says planetary physicist Francis Nimmo of the University of California, Santa Cruz. And it may help explain why the 5150-kilometer-diameter moon "confounds us at every turn," as Nimmo puts it. The only moon with more than a wisp of an atmosphere—Titan's is more dense than Earth's—and the only other solar system object with standing bodies of liquid, Titan may be steadily oozing the methane that sustains its dense cloaking haze and fills its lakes. The newly discovered ocean may have played a role in giving Titan's atmosphere its gas.

On Earth, it is seismologists who probe the interior, using seismic waves. But to peer inside Titan, Cassini scientists instead had to watch how the moon responded to incessant gravitational squeezing by Saturn. As Titan revolves around Saturn every 16 days in its slightly elliptical orbit, the giant planet rhythmically squeezes the moon, something like the way the sun and the moon raise tides in Earth's oceans. The squishier Titan's interior is, the more the moon deforms under the tidal massaging. The more Titan deforms, the more its own gravity field—which depends on the shape of Titan's mass—is distorted.

So the problem of inferring the physical state of Titan's interior became a problem of mapping out Titan's gravity field at different points in its orbit. For that, Cassini team members led by Luciano Iess of Sapienza University of Rome and Robert Jacobson of NASA's Jet Propulsion Laboratory in Pasadena, California, used the Doppler effect. Orbiting Saturn, Cassini beamed radio signals back to Earth during six flybys of Titan. As reported online this week in *Science*, the team measured the varying pitch of those signals precisely enough to gauge Cassini's changing speed with an accuracy of 10 micrometers per second (http://scim.ag/Iessl). That's 36 millimeters per hour for an object that is 1 billion or 2 billion kilometers away.

From Cassini's varying speed, a group led by Iess calculated Titan's varying gravity field, which enabled them to infer its interior state. The group found Titan to be as tidally pliable as if a liquid layer a couple of hundred kilometers thick—no doubt water—encircles the moon beneath 100 kilometers of ice. Another group within the team, led by Jacobson, got the same result using a different and independent method of analysis. "This tells us there must be a liquid layer beneath the surface," Iess says. Nimmo agrees: "I think there's an ocean there." But there seems to be more to Titan's surprisingly pliable interior. Its central region, beneath the ocean, may be solid but unusually soft; or, less likely, the ocean and overlying ice may be extra dense.

The discovery puts Titan in the inner-ocean club with Jupiter's moons Europa, Ganymede, and Callisto. And where there's an ocean, there might be life, right? Not so fast, says planetary physicist David Stevenson of the California Institute of Technology in Pasadena. Titan's ocean "doesn't have anything to do with life," he says. Inside Europa, planetary scientists believe hot springs on a rocky ocean floor may be belching all the nutrients and inorganic building blocks required by life. But other kinds of gravity studies show that Titan has a cold, icy ocean floor, so no hot water can be leaching life-giving chemicals into the ocean. "The interesting question," Stevenson says, "is to what extent is the interior ocean determining, or at least modifying, the geological history of Titan?"

Titan's ocean could conceivably be linked to surface geology as well as the atmosphere's methane, Stevenson says. The sun's ultraviolet radiation is continually cooking the atmosphere's large load of methane into complex organic molecules, the way it did on early Earth before life got started. But this prebiotic chemistry—lifeless but still of great interest to astrobiologists—destroys the atmosphere's methane so fast that it should have disappeared within a few tens of millions of years.

So either Titan got a big shot of methane in the geologically recent past, or methane is being resupplied from the interior. Either way, the ocean may have been involved. Changes in the ocean—perhaps by warming and thinning the overlying shell—may have freed up deep-seated methane. The methane and icy "lava" might then have erupted onto the surface. Some Titan geologists have said they can see the remains of ice volcano eruptions in Cassini radar images, but those claims have not gained much traction. After 8 years orbiting Saturn, Cassini has another 5 years to take quick looks at Titan, inside and out, but researchers would really like a new spacecraft that can linger in orbit about the still-mysterious moon.

–RICHARD A. KERR

In the hot seat. The crew of Shenzhou 9 prepares for China's first mission to dock spacecraft with astronauts aboard.

A New Dawn for China's Space Scientists

China's crewed space program has won admiration for the engineering prowess on display earlier this week in the Shenzhou 9 mission. Upcoming science missions hope to steal some of the spotlight

BEIJING—When Shenzhou 9 gently fired its thrusters to pull to within several centimeters of the orbiting Tiangong module on 24 June, mission managers were on edge. For a fleeting moment, a question hung in the air: Would the astronauts succeed in China's first attempt to manually dock the two spacecraft, circling Earth at 7.8 kilometers per second? They'd performed the maneuver on the ground, in a simulator, hundreds of times before. This was the real test. The slightest miscalculation could have spelled disaster for Shenzhou's three-person crew, including the country's first female astronaut. No country had lost someone in space—and China didn't want to be the first.

One person with a big stake in the mission says he was not sweating out that tense moment: Shenzhou's former chief designer, Qi Faren. "I wasn't nervous," he claims. Shenzhou's first flight in 1999, Qi says, was a far riskier roll of the dice. That landmark mission went well, as did the Shenzhou 9 docking maneuvers, completing a milestone on China's road to a sustained human presence in space. "It's a huge step," says Dean Cheng, an expert on China's space program with the Heritage Foundation in Washington, D.C. "Docking is essential to doing just about anything in space," he says, including China's plan to build a space station by 2020.

China's leaders had a lot riding on Shenzhou 9, too. The Communist Party, which is expected to begin a leadership transition this autumn, spent the first half of 2012 in damage-control mode over the fall of former governor Bo Xilai and the high-profile flight of blind activist Chen Guangcheng. For the party, the elegant pas de deux at 343 kilometers above Earth's surface was a timely propaganda triumph. "China's space program gives the party legitimacy," Cheng says. "The leaders can say, 'Look what we have done for the country.' "

The engineering feat is indisputable. "China is emerging as a world leader in space," says Mark Stokes, executive director of the Project 2049 Institute, a think tank in Arlington, Virginia, that produced an analysis of China's space program last April for the U.S.-China Economic and Security Review Commission.

Soon, China's basic researchers will take a star turn. Over the next several years, the country plans to launch five scientific missions, including a dark-matter probe and an attempt at long-distance quantum communication. Four more innovative missions are in the design stage, *Science* has learned: an

CREDITS: (TOP) QIN XIANAN/COLOR CHINA PHOTO/AP IMAGES; (BOTTOM LEFT TO RIGHT) BETTMANN/CORBIS/AP IMAGES; R. STONE/*SCIENCE*

MILESTONES OF CHINA'S SPACE PROGRAM

Space program founder Qian Xuesen returns home to a hero's welcome.

Debut satellite Dongfanghong 1 broadcasts "The East is Red."

x-ray telescope to study black holes, a solar imager that would swing high above and far below the line of sight between Earth and the sun, a space-based very-long-baseline interferometer (VLBI) tuned to long-millimeter wavelengths, and a four-satellite cluster to study coupling of the magnetosphere, ionosphere, and thermosphere. Scientific payloads are being assembled for Tiangong 1 and for two more Tiangong modules, including a crewed space laboratory, which China plans to launch in the next 3 years. And scientists are designing experiments for the future space station.

It's a new dawn for China's space scientists. For decades, they have been left in the shadows by the generals and engineers who run China's space program. China's sole dedicated science missions to date were Double Star, in which it teamed up with the European Space Agency (ESA) from 2003 to 2007 to study magnetic storms, and the ill-fated Mars probe Yinghuo-1, which failed to leave Earth orbit.

"When I look at astronomy textbooks, none of the discoveries were made by people working in China. I don't see a single photo taken by a Chinese telescope. It's very frustrating," says Zhang Shuang-Nan, an astrophysicist here at the Institute of High Energy Physics of the Chinese Academy of Sciences (CAS). "We feel more and more pressure, not just from the top, but also from the bottom, to produce knowledge," adds Wu Ji, director general of CAS's National Space Science Center (NSSC). With the raft of missions now in the works, they may end up not just revising but rewriting textbooks.

Rags to riches

The visionary who set China's sights on space also played a key role in the early days of the U.S. program. In the 1940s, Chinese-born aeronautical engineer Qian Xuesen was one of the founders of the Jet Propulsion Laboratory in Pasadena, California. Considered a genius by his peers, Qian, known in the United States by the older spelling of his name, Hsue-Shen Tsien, fell victim to the Red Scare and in 1950 was accused of being a Communist. The United States revoked his security clearance and—after 5 years of house arrest—exiled him to China. Qian returned home to a hero's welcome and soon proposed that the young nation start a missile program.

All systems go. Shenzhou 9 lifts off on 16 June.

A year after a small team set to work, the Soviet Union shocked the world on 4 October 1957 with the launch of Sputnik 1, the world's first artificial satellite. China wanted one, too. "However, we didn't even have a rocket at that time," says Qi, now a dean at Beijing University of Aeronautics and Astronautics. China turned to the Soviet Union for help; hundreds of engineers poured in. Key facilities were set up across the hinterlands to avoid offering fat targets. But several months after embarking on this vast enterprise, China, strapped for cash, aborted its space program to focus on guided missiles.

Qian bided his time working on weapons. Then, in a report to top leaders in 1965, Qian argued that China needed to reboot its space program because satellites were indispensable for military surveillance and communication. The government concurred and revived its space program. By then, though, the Sino-Soviet split meant that China had to go it alone. "They weren't talking to anyone, not the Soviets, certainly not the Americans," Cheng says. That's why, he says, "much of China's space program is domestically produced."

After a failed attempt in 1969, China on 24 April 1970 put its first satellite in orbit, becoming only the fifth country to do so. For 1 month, Dongfanghong 1 took readings of the ionosphere and transmitted data back to Earth. In a patriotic touch, it broadcast the song "The East is Red," for which it was named. "It was a simple satellite," says Qi, who served on the engineering team. But the 1-meter-wide debutante, heavier than the first satellites of the Soviet Union, United States, France, and Japan combined, made a powerful statement.

China then set its sights on a crewed program—but didn't get very far. "There were some key technical problems beyond our ability at that time," Qi says. In 1975, he recalls, "Premier Zhou Enlai convinced us to not try to match the Soviet Union and U.S., and first develop more satellites."

China hatched plans for a new crewed program in 1986. Work began in earnest in 1992, the year that Qi succeeded Qian as China's general spacecraft designer. Sanctions on

Shenzhou 1 marks the start of the crewed space program.

Yang Liwei orbits Earth for 21 hours aboard Shenzhou 5.

Double Star is the first bona fide space science mission.

Entangled Secret Messages From Space

SHANGHAI—Last summer, a stream of photons arced northwest across Qinghai Lake—China's biggest—traveling about 100 kilometers in the blink of an eye before impinging on a detector on the opposite shore. This was no ordinary beam of light: The photons were entangled, meaning they were produced in pairs with identical quantum states. At Qinghai, measuring the entangled pairs provided a key that could be used to unlock a coded message, decipherable to only those who know the photon pair's quantum state. The beauty is that any attempt to read the key alters it, making it theft-proof. The technology is expected to become the gold standard of cryptography. Several groups have tested quantum communications on Earth. But Qinghai was a proving ground for distributing quantum keys in the final frontier: space.

About 5 years from now, China plans to launch a spacecraft that will transmit entangled photon pairs to ground receivers. The European Space Agency may deploy a similar system on the International Space Station, and scientists in Canada and Singapore have proposed quantum microsatellites. China is moving faster. "We hope we will be the first real experiment in space," says the Chinese project's leader, Pan Jianwei, a physicist at the University of Science and Technology of China in Hefei. His team faces daunting challenges in sending quantum keys across great distances. But few scientists in China come more highly rated. "In quantum communication and multiphoton quantum optics, he's certainly in the top echelon," says quantum physicist Anton Zeilinger, whose group at the University of Vienna has distributed quantum keys by laser more than 144 kilometers in the Canary Islands and will participate in China's quantum-spacecraft project. The satellite, he says, will also be a platform for fundamental experiments probing the nature of entanglement, dismissed by Albert Einstein as "spooky action a distance," over unprecedented distances. If it succeeds, China intends to deploy a fleet of spacecraft that could make global quantum communication a reality. Potential users would include commercial banks and China's armed forces.

China's program is building on a steady stream of homegrown advances in generating entangled photons and quantum-key distribution over the past decade. In 2004, Pan's group transmitted entangled photons from a mountaintop to the ground near Hefei, demonstrating quantum-key distribution in the atmosphere. At that point, he says, "We started to think very seriously about doing this in space." The research is demanding. "We are working at the single-photon level. It's invisible to the eye," Pan says. In 2011, his team was the first to entangle eight photons at once. That feat "was really outstanding," Zeilinger says. "It required some elegant ideas."

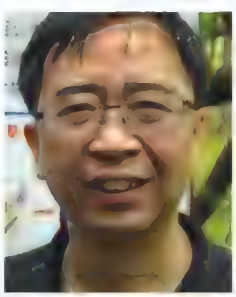

Crucial to the satellite effort, Pan's team is becoming defter at generating multiphoton entanglement. "The probability of creating a four-photon entanglement is small," Pan says. In 2004, they managed a few four-photon events per second. Now, he says, they churn out a few thousand per second. To devise their high-intensity entangled photon source, Pan says, "We had to develop some new technology and use some new tricks."

They put these tricks to work in a real-life setting in 2008. That year, Pan's

CREDITS: (TOP) ZHANG DONGDONG; (BOTTOM LEFT TO RIGHT): NASA IMAGES; IMAGINECHINA VIA AP IMAGES; SPACEBABE/WIKIMEDIA COMMONS

high-tech exports to China forced Qi's team to toil in isolation. As a result, he says, China "spent too much time and resources" developing the Shenzhou spacecraft, the workhorse of the crewed program. "On one hand, we felt uncomfortable about the restrictions. On the other hand, those restrictions helped us a lot," Qi says. "Although our spacecraft may not be the best, we successfully made it by ourselves." The second watershed event of China's space program came in 2003, when Shenzhou 5 carried astronaut Yang Liwei into orbit. China became the third country to independently send a person into space.

While other spacefaring nations have set up civilian agencies for peaceful exploration of space, in China the army has always run the show. For that reason, China's ultimate intentions are debated (see p. 1634). One concern is that China's space-industrial complex is bigger than any other country's. Two state-owned space enterprises together employ more than 267,000 people. Add in staff at space-related R&D institutes and university-based researchers, and the number of Chinese involved in the space program may top 300,000. This gargantuan ground force has propelled China into the upper echelon of spacefaring nations. China "is one of the elite," Cheng says.

China's space science community hasn't gotten there quite yet.

Rising from the ashes

On 9 November 2011, China thought it was on its way to the Red Planet. Early that morning, Russia launched the Fobos-Grunt spacecraft on a Proton rocket with the aim of landing on Mars and returning 200 grams of soil to Earth in 2014. China was hitching a ride. A small probe called Yinghuo-1, built by CAS's Center for Space Science and Applied Research, would separate from Fobos-Grunt before the spacecraft entered Mars orbit. Its aim was to take the most detailed measurements yet of the planet's magnetic field. "It really was our dream to go with the Russians," says Wu, who led the Yinghuo-1 design team.

Seconds after Fobos-Grunt had separated

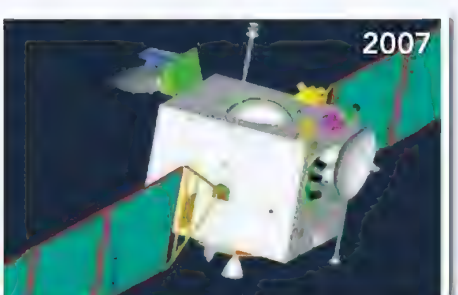

Lunar exploration program kicks off with Chang'e 1.

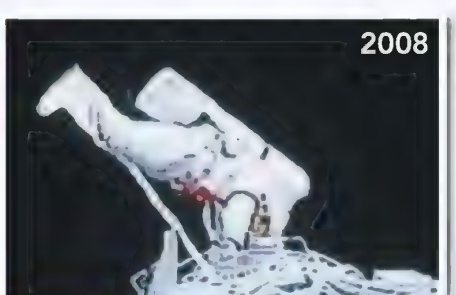

Zhai Zhigang goes for a 22-minute spacewalk outside of Shenzhou 7.

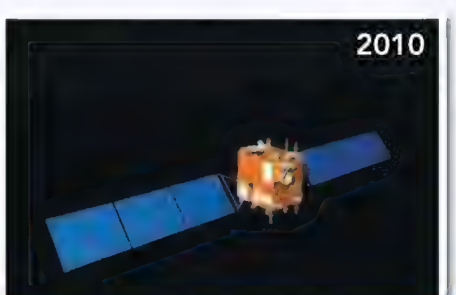

Chang'e 2 maps future lunar landing sites.

Cryptography's new frontier. In a trial run for a space-based experiment in quantum communication, a team led by Pan Jianwei (*left*) beamed entangled photons across Qinghai Lake in northwest China last summer.

CREDITS: (TOP) J. JIAN-WEI PAN; (BOTTOM LEFT TO RIGHT) MAGINECHINA VIA AP IMAGES; AP PHOTO/ RUSSIAN ROSCOSMOC SPACE AGENCY, HO; SUN ZIFA/COLOR CHINA PHOTO/AP IMAGES

group distributed quantum keys to three stations linked by 20 kilometers of fiber-optic cable. The keys were used to decipher encrypted phone conversations between the stations. That approach works fine for short distances, such as within a city, but the transmission efficiency by fiber optics diminishes with distance. "Beyond 100 kilometers, the loss is huge," Pan says. Quantum-key distribution between cities and continents will require exploiting the vacuum of space, where there is no photon loss.

Pan's achievements are all the more impressive considering that he started out as a theorist. After joining Zeilinger's lab to pursue his doctorate in 1996, Pan was intrigued by the group's hands-on work. "It took him a while to get used to the way we do experiments," Zeilinger recalls. "But he started coming up with his own ideas, and I realized this guy had talent." Thanks to his stellar work, Pan was elected to the Chinese Academy of Sciences last year at the tender age of 41, becoming one of the youngest academicians ever in China.

Pan will have to scale new heights to succeed in space. The quantum-mechanical principles themselves are straightforward—at least to the researchers. The key hurdle will be the exquisitely precise timing necessary to allow two ground receivers to measure the quantum state of entangled pairs at exactly the same moment. "That's very demanding," says Zeilinger, whose group will use receivers across Europe to tune in to China's spacecraft. For only a few minutes at a time, he says, stations in Europe and China can simultaneously view the satellite. "The satellite will be flying very fast. The distance is huge. We have to make sure the quantum signal can be transferred to the right point," adds Pan, whose team is devising the payload here at a new branch campus of his university.

If all goes well, Pan envisions a network of satellites that would function as repeater stations for global coverage. Although China's quantum spacecraft is a civilian project, military programs have a keen interest in unbreakable encrypted communications; U.S. efforts in satellite-based quantum communication appear to be classified. Even if a government agency ran the system, civilian information would be impervious to eavesdropping. "The satellite owner can only allow you or not allow you to communicate. Once they allow you, they cannot see the message. There is no way," Pan says. That may reassure Bank of America—but the Pentagon may not welcome a Chinese quantum-cryptography capability with open arms. **–R.S.**

from the rocket, the spacecraft's thrusters failed to execute a burn properly, stranding it and its piggybacked companion in low Earth orbit. Over the next several days, controllers at the Lavochkin Association in Moscow, which designed Fobos-Grunt, attempted to communicate with the spacecraft to set it back on course, but to no avail. Fobos-Grunt plunged back through the atmosphere on 15 January, broke apart, and disappeared over the Pacific Ocean. "It was very disappointing. A really big blow for our science," Wu says.

Wu's chagrin may prove short-lived. In the months before the Fobos-Grunt disaster, China had already begun drafting blueprints for a space science program that, it hopes, will make the country stand out not just for aeronautical engineering but for discoveries in space science, as well.

Until now, most other science missions have languished as mere proposals. Although the first two spacecraft launched under China's lunar exploration program—Chang'e 1 in 2007 and Chang'e 2 in 2010—carried scientific instruments, they "were more for prestige and engineering than for science," Wu says. After mapping future landing sites, Chang'e 2 is now en route for a flyby of 4179 Toutatis, a potentially hazardous asteroid that will whiz close to Earth at the end of the year. Chang'e 3, scheduled for launch in 2013, will be the first spacecraft to make a soft landing on the moon since the Soviet Union's Luna mission in 1976. It will roll out a rover that will analyze soil samples and set up an extreme ultraviolet telescope—the first astronomical observatory on the moon. Some officials have talked of a crewed lunar landing after 2020, but that adventure is not set in stone. The rationale for such a mission, Qi says, "is being hotly debated."

Heralding a new era for space science, on 3 May 2011, Wu announced that CAS will undertake five scientific missions in the coming years (*Science*, 20 May 2011, p. 904). CAS has budgeted $554 million over 5 years for the missions and established NSSC last year to oversee the burgeoning program.

Tiangong module is the first step toward the space station.

Yinghuo-1 is destroyed aboard the doomed Fobos-Grunt Mars probe (*pictured*).

Shenzhou 9 heralds an era of sustained presence in space.

Run by the Army for the Army?

BEIJING—Early in the morning on 11 January 2007, China fired a missile topped with a kinetic kill vehicle at a spacecraft in low Earth orbit, smashing it to smithereens. The shot did not ignite a conflict, as the target, an aging weather satellite, was China's own. But Fengyun-1C's obliteration sent a message. A few months earlier, the United States had unveiled a space policy pledging to "deny, if necessary, adversaries the use of space capabilities hostile to U.S. national interests." China's antisatellite (ASAT) test showed that two could play at that game.

Dual-use data. Last December, China launched its 10th Beidou navigation satellite, bringing the system online for commercial customers and giving its military a source of GPS information it can control.

Although the People's Liberation Army (PLA) runs China's space program, leaders here have long maintained that the nation's aspirations are benign. "China always adheres to the use of outer space for peaceful purposes, and opposes weaponization or any arms race in outer space," states a white paper released last December by China's State Council. A top diplomat reiterated that theme earlier this month at a conclave of the United Nations Committee on the Peaceful Uses of Outer Space. Helping to shape that perception are an ambitious slate of space science experiments planned over the next decade (see main text, p. 1630), and this month's Shenzhou 9 mission, which featured China's first docking of spacecraft with astronauts aboard.

But other aspects of China's space program keep the Pentagon's top brass up at night. Last year, in its annual report to Congress on China's military program, the U.S. Department of Defense asserted that "PLA strategists regard the ability to utilize space and deny adversaries access to space as central to enabling modern, informatized warfare." PLA writings, the report notes, "emphasize the necessity of 'destroying, damaging, and interfering with the enemy's reconnaissance … and communications satellites,' suggesting that such systems, as well as navigation and early warning satellites, could be among initial targets of attack to 'blind and deafen the enemy.' "

The direct-ascent ASAT test was a visible exercise in muscle-flexing. With much less fanfare, China is developing a number of other kinetic kill weapons and directed-energy technologies such as lasers and high-powered microwave beams to knock out spacecraft, the Pentagon says. China, it notes, can also jam common satellite communication bands and GPS receivers. "Barring effective countermeasures, the PLA's ability to complicate U.S. access to space assets is likely to grow over the next 10-15 years," states an April report from the U.S.-China Economic and Security Review Commission.

China's ultimate intention for its growing constellation of space-based sensors and transmitters is unclear. The network could be purely defensive, and it will have civilian applications in Earth observation and navigation. "A threat consists of both capabilities and intentions," says Mark Stokes, executive director of the Project 2049 Institute, a think tank in Arlington, Virginia, and author of the commission's report. "Beijing's intentions remain ambiguous."

Uncertainty is not surprising, considering that China from the start has blurred the lines between its military and civilian space activities. Soon after the Tiananmen Square crackdown in 1989, the United States imposed sanctions on the export of dual-use technologies to China. A decade later, the International Traffic in Arms Regulations effectively barred U.S. entities from using Chinese launch vehicles. Those were heavy blows for China's space program. "Space is 95% dual use," says Dean Cheng, a China space expert with the Heritage Foundation in Washington, D.C. "Any improvement in space technology can have military implications." In a report last April assessing U.S. space export policy, the U.S. Defense and State departments concluded that "China's civilian and military space industry are fused together such that reasonable regulators must consider the high likelihood that space-related items and technology will be diverted from a civil use and applied to military programs."

The U.S. government has compiled a lengthy dossier on attempts, some successful and others foiled, to acquire restricted technologies for China's space program. According to the space export report, recent cases include theft or diversion of space launch technical data, military-grade accelerometers, microwave amplifiers with radar applications, thermal insulation blankets for satellites, and carbon-fiber material for rockets and spacecraft. The report asserts that China's maturing space program "was often able to accomplish this progress by exploiting foreign technologies and items, especially those from the United States."

That conclusion may be too harsh. By most accounts, China's space program has depended on homegrown ingenuity far more than foreign technology. "We applied our own intelligence to solve our own problems," says Qi Faren, former chief designer of the Shenzhou spacecraft. "I'm not under the impression that they have relied on technology theft to advance their space program writ large," Cheng says.

Over the years, a once purely military effort has drawn more heavily on universities and civilian institutes. "The networks linking China's defense R&D community and traditionally civilian universities appear to be expanding significantly," the U.S.-China commission report states. It flags work in military optoelectronics R&D at Sichuan University in Chengdu, development of kinetic kill vehicle components at Zhejiang University in Hangzhou, and research on passive stealth coatings for reentry vehicles at Nanjing University.

With the 2007 ASAT test followed by a similar exercise in 2010, China raised the stakes in the Pacific. China paid a price for its 2007 use of firepower, which chilled relations between the Chinese and U.S. space programs and drew opprobrium over the roughly 3000 shards of Fengyun-1C that force the International Space Station to occasionally carry out evasive maneuvers. But other nations have been put on notice: In the future battlefield of space, China may speak softly, but it carries a big stick.

–R.S.

CREDIT: PHOTO BY SUN ZIFA/COLOR CHINA PHOTO/AP IMAGES

Astrophysics is set to take center stage. First off the blocks should be the Hard X-ray Modulation Telescope (HXMT), conceived nearly 20 years ago to observe black holes, neutron stars, and other objects based on their x-ray and gamma ray emissions. HXMT, China's first astronomy satellite, could be launched as early as 2014 and will be the first of three instruments in China's Black Hole Probe Program. Another mission incubating for years that now has a green light is KuaFu, a Sino-Canadian mission to study the sun's influence on space weather. Russia may join KuaFu, pegged for a 2015 launch along with Shijian 10, a spacecraft that will study the effects of strong radiation and microgravity on organisms and materials.

Work is also progressing on two later launches. One is the lead probe in China's Dark Matter Detection Program. The spacecraft, being designed by CAS's Purple Mountain Observatory in Nanjing, aims to register gamma rays generated when dark-matter particles annihilate each other. The fifth mission in the works, the Quantum Science Satellite, is designed to transmit entangled photons between a spacecraft and receiving stations on Earth (see p. 1632). Success would mark a first step in secure intercontinental quantum communication.

Four more missions that have passed preliminary reviews would considerably build up China's clout in spaceborne astrophysics. The goal is to get them launched in the next 5-year plan, beginning in 2016. One is the X-ray Timing and Polarization (XTP) telescope, conceived by CAS's Institute of High Energy Physics. As the lead facility in the planned Diagnostics of Astro-Oscillations Program, XTP would be "a much more powerful mission that goes far beyond HXMT," says Zhang, the project's leader. XTP would have a larger collection area and powerful mirrors to collect more photons—and thus observe fainter objects and scrutinize them in greater detail, he says. Astrophysicists around the world have been clamoring for just such a telescope, but early last year NASA and ESA canceled plans for an International X-ray Observatory, and a scaled-down version called Athena lost out to a Jupiter probe in an ESA competition which concluded last month.

XTP would study x-ray emissions from matter spiraling into a black hole, or x-ray signatures of frame-dragging generated, for instance, as a spinning black hole tugs at spacetime. "We'll look at the physics of extreme conditions," Zhang says. For now, XTP is a purely Chinese mission. But China is exploring teaming up with Germany, which is contemplating a scaled-down Athena called Gravitas. A big attraction for China is that Germany could equip a joint probe with a much more advanced mirror; restrictions on the sale of high-tech equipment to China would force Zhang's team to commission an inferior Chinese-made mirror.

"Although our spacecraft may not be the best, we successfully made it by ourselves."

—QI FAREN, SHENZHOU CHIEF DESIGNER

China's Space Astronomy Takes Flight

Black Hole Probe Program
- Hard X-ray Modulation Telescope (HXMT)
- Space Variable Objects Monitor satellite
- Gamma-ray Burst Polarization (POLAR) experiment (aboard Tiangong)

Diagnostics of Astro-Oscillations Program
- X-ray Timing and Polarization (XTP) satellite

Portraits of Astrophysical Objects Program
- Space Very Long Baseline Interferometer (VLBI) telescope array

Dark Matter Detection Program
- Dark Matter Detection Satellite
- High Energy Cosmic Radiation Detection Facility (aboard space station)

Solar Physics Program
- KuaFu
- Solar Polar Orbit Radio Telescope (SPORT)
- Space Solar Telescope

As the centerpiece of the Portraits of Astrophysical Objects Program, China intends to invest its long-standing expertise in VLBI in new space radio telescopes. Its current VLBI network consists of four large, ground-based dishes; three times a year, two of its dishes team up with the European VLBI Network for monthlong observation runs. China's plan calls for spacecraft that would operate in tandem or as arrays with ground dishes, mimicking a huge radio telescope whose effective diameter is the maximum distance between the instruments. They would follow in the footsteps of Japan, which operated a space-based array from 1997 to 2002, and Russia, which is now testing its Spektr-R radio telescope launched last year.

China's proposed array would initially consist of two long-millimeter-wavelength antennas, each 10 meters wide. Key challenges include getting the space antennas to work with high pointing accuracy and having enough bandwidth to transmit scientific data, says Hong Xiaoyu, director of the Shanghai Astronomical Observatory, which is designing the system and is open to international collaboration. The top priority would be to map the fine structure of supermassive black holes that inhabit the center of galaxies and their accretion disks, which are believed to be the power source for active galactic nuclei. Ten years after the first array, Hong says, his team hopes to launch millimeter-wave antennas. Longer baselines and shorter wavelengths produce a higher resolution of radio sources.

China also hopes to blaze a trail in interplanetary physics. NSSC is designing a solar probe that would receive a gravity assist from Jupiter, which would send it into a highly inclined orbit above and below the ecliptic plane, the line of sight between Earth and the sun. Only one previous satellite has followed a similar orbit: Ulysses, an ESA-U.S. probe launched in 1990 that measured a steady weakening of the solar wind and helped pinpoint sources of gamma ray bursts. NSSC's Solar Polar Orbit Radio Telescope (SPORT) would be the first to gaze down or up at coronal mass ejections streaming from the sun. Besides probing the properties of the solar wind and coronal mass ejections, Wu says, SPORT's spectacular bird's-eye view should improve forecasts of space weather.

The fourth new mission to pass mus-

"When I look at astronomy textbooks, none of the discoveries were made by people working in China."

—ZHANG SHUANG-NAN, INSTITUTE OF HIGH ENERGY PHYSICS, BEIJING

CREDIT: (TOP AND BOTTOM) ZHANG DONGDONG

ter is MIT, named for the magnetosphere, ionosphere, and thermosphere. The four-spacecraft cluster, another NSSC brainchild, would attempt to shed light on how electrons and other energetic particles flow between those regions of space.

To maintain the momentum of China's suddenly vibrant space science program, NSSC is about to call for proposals for another slate of missions—up to three more, Wu says—that would be funded after 2015. Unlike in Europe or the United States, the price tag won't be a showstopper. "In China, the decision process may be slow, but once a mission is approved, it will go," Zhang says. "We haven't had a mission canceled because of the budget."

They do face one big impediment: limited interactions with colleagues abroad, especially those from the United States. "If scientists from NASA come to China for a conference, they cannot talk with Chinese scientists one-to-one," Wu says. "It reminds me of our Cultural Revolution," he says, when science in China was largely suppressed. The NSSC and the U.S. National Academies are discussing ways to catalyze discussions between space scientists in the two countries. One tantalizing conversation starter may be China's long-term space astronomy plan, which envisions putting telescope arrays on the moon after 2035.

A lasting legacy

Shenzhou 9's success opens a new realm for Chinese scientists. The ability to perform docking maneuvers in space will allow China to ferry equipment to Tiangong 1 and add up to two more modules. Research on Tiangong involves closer coordination with the space program's military masters. Two years ago, CAS founded the Technology and Engineering Center for Space Utilization here to manage scientific payloads for Tiangong and the planned space station. The army-run China Manned Space Engineering Office has barred foreign correspondents from interviewing center staff. However, scientists elsewhere in CAS and at universities who are designing the experiments were able to speak with *Science*.

A bevy of experiments are now being readied for Tiangong, including an atomic clock, a materials science furnace, and a plant tissue culture apparatus. Astrophysicists also have reason to cheer. Among the approved projects, China and Switzerland are teaming up on POLAR, a gamma ray burst detector slated to fly on Tiangong 2 in 2014 as part of the Black Hole Probe Program. It will be the only dedicated instrument in space for measuring gamma ray polarization, which should help scientists determine the structure of a gamma ray jet's magnetic field, Zhang says. That, in turn, may shed light on the origin of gamma ray bursts. One hypothesis is that they are unleashed when a massive star collapses at the end of its life; another is that they are generated when neutron stars or black holes merge. "Each model predicts a different structure of the magnetic field," Zhang says.

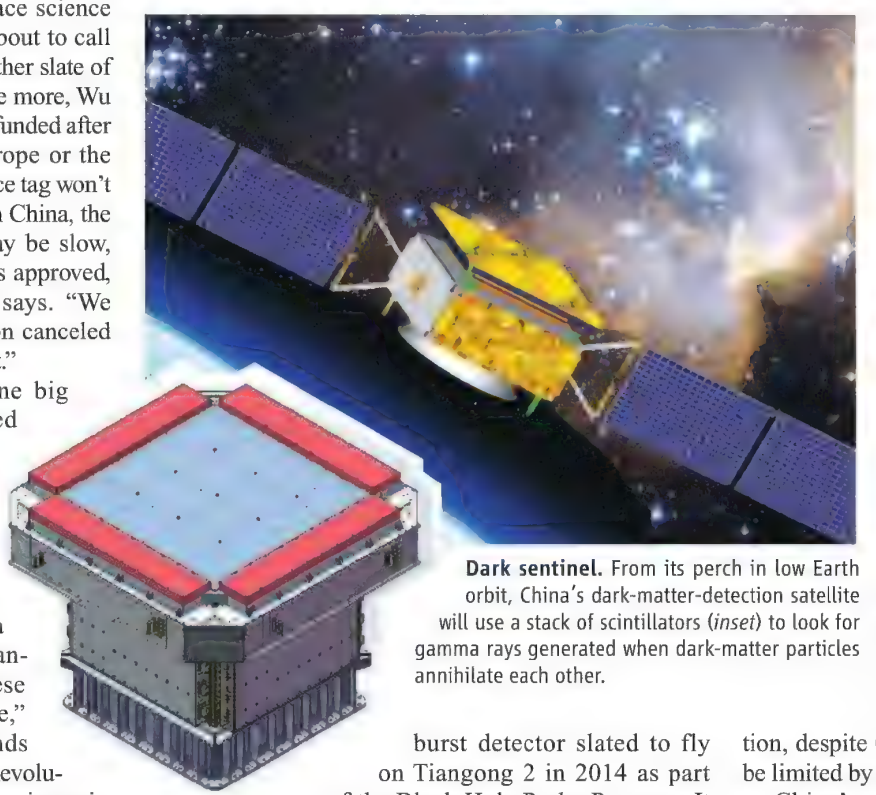

Dark sentinel. From its perch in low Earth orbit, China's dark-matter-detection satellite will use a stack of scintillators (*inset*) to look for gamma rays generated when dark-matter particles annihilate each other.

Online

sciencemag.org

Podcast interview with author Richard Stone (http://scim.ag/pod_6089).

Scientists here may never have had such a wealth of opportunities if China had been invited to join the 16-nation International Space Station. "China didn't have to make Tiangong if we could participate. But we were blocked out," Qi says. Tiangong is a steppingstone to a 60-ton space station that China announced last December that it would build by 2020.

Although a pipsqueak compared with the 450-ton International Space Station, China's space station should host high-powered science. China Manned Space Engineering Office is expected to approve the first payloads from among dozens of contenders early next year. Among those vying for space are a suite of astronomy experiments called the Cosmic Lighthouse Program. One of two proposed large instruments is the High Energy Cosmic Radiation Detection Facility to study dark matter and cosmic rays.

The other instrument would allow China to play a major role in the coming era of large-scale astronomical surveys—and possibly help unravel the nature of dark energy. China's wide-field optical telescope would complement planned instruments elsewhere, such as the Large Synoptic Survey Telescope (LSST), an 8.4-meter dish to be built in Chile that could see first light in 2018. But LSST will not be able to detect infrared or near-ultraviolet waves from cosmic sources, which are absorbed in the upper atmosphere, and its resolution, despite Chile's superb conditions, will be limited by atmospheric turbulence.

China's as-yet-unnamed mission also won't look in the infrared, as it is not possible to import astronomy-grade infrared detectors. Chinese industrial-grade detectors "don't have the needed performance," says team member Zhan Hu, a cosmologist here at the National Astronomical Observatory of China. But China's space station survey, he says, will complement other efforts with its high angular resolution and multiple bands covering optical and near-ultraviolet wavelengths. One challenge to mounting any telescope on a space station is that the station will rotate as it orbits. To keep a fixed gaze, the telescope must counterrotate. That job will be farmed out to optomechanical engineers. "They'll do the heavy lifting," Zhan says.

If the survey mission passes muster, Zhan is confident that Chinese scientists will have new knowledge to contribute to science. "With surveys, you always find something unexpected," he says. "Current physics cannot explain dark energy. We have an opportunity to discover some revolutionary physics."

–RICHARD STONE

With reporting by Bu Kai and Zhang Dongdong.

CREDITS: JIN CHANG

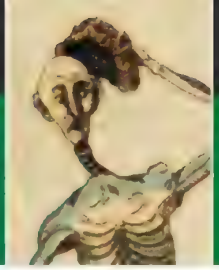

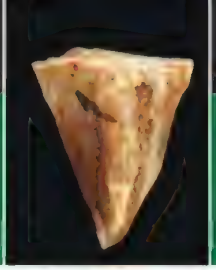

LETTERS

edited by Jennifer Sills

Postdocs: The Power of Unions

AS A POSTDOC AT THE UNIVERSITY OF CALIFORNIA–SANTA CRUZ AND PRESIDENT OF UAW LOCAL 5810, the union that represents over 6000 postdocs at the University of California, I read with interest A. I. Leshner's Editorial on the need for a broad-scale effort to standardize and improve the postdoc experience ("Standards for postdoc training," 20 April, p. 276). Leshner is right that many postdocs face numerous challenges, including limited job security, varying benefits, visa and immigration issues, and pay that fails to reflect our contributions.

To address these issues, Leshner unfortunately fails to recognize how the voice of postdocs themselves—through the democratic process of collective bargaining—can play a critical role. The contract that the UAW has negotiated with the University of California includes a minimum salary scale that matches the NIH/NRSA scale, a stable and comprehensive benefits plan, more job security, and the right to career development resources. With the increases we've won in paid time off, female postdocs no longer have to face uncertain maternity leave. And when work-related issues arise, there is an impartial process for resolving them.

Speaking with one voice. Postdoc unions can negotiate better benefits for their members.

In addition, being part of the UAW gives postdocs a more powerful voice and more political strength to advocate for issues such as science funding, progressive immigration reform, and gender equality in the academy.

When postdocs have an equal say in determining our working conditions, our quality of life improves, which in turn improves the quality of research. Our union welcomes the opportunity to work with the Committee on Science, Engineering, and Public Policy (COSEPUP) and all other interested parties for the good of postdocs and for the good of society.

NEAL SWEENEY

Department of Molecular, Cell and Developmental Biology, University of California-Santa Cruz, Santa Cruz, CA 95064, USA; UAW Local 5810, Berkeley, CA 94704, USA. E-mail: president@uaw5810.org

Postdocs: NPA's Success

THE NATIONAL POSTDOCTORAL ASSOCIATION (NPA) applauds the recent Editorial by A. I. Leshner calling for the scientific community to commit to providing quality postdoctoral experiences ("Standards for postdoc training," 20 April, p. 276). The NPA is ideally positioned to take up Leshner's call to action: In its first decade of existence, the NPA has laid the groundwork for the standards, norms, and expectations required to deliver an optimal postdoctoral experience.

The NPA's Recommendations for Postdoctoral Policies and Practices (*1*) have been adopted widely by research institutions and funding agencies. Due in large part to the NPA's efforts, the number of postdoc offices on record has increased from less than 25 in 2001 to more than 135 today. The NPA provides online toolkits and conducts site visits to help institutions establish postdoc offices as well as postdoc associations. In answer to Leshner's call to action, the NPA Board of Directors has undertaken an initiative to develop a national certification program to recognize institutions that are implementing best practices for supporting the postdoc experience. The NPA's track record, expertise in postdoctoral matters, and established support base place it years ahead of any alternative organization that might take on this challenge. We look forward to engaging the research community at all levels as we develop this program.

LORRAINE TRACEY,* MAHADEO SUKHAI, STACY L. GELHAUS, DAVID TAYLOR

NPA Board of Directors, National Postdoctoral Association, Washington, DC 20005, USA.

*To whom correspondence should be addressed. E-mail: Lorraine@nationalpostdoc.org

Reference

1. NPA, NPA Recommendations for Postdoctoral Policies and Practices (www.nationalpostdoc.org/recommendations).

Turing in Context

IN HIS PERSPECTIVE "BEYOND TURING'S machines" (13 April, p. 163), A. Hodges claims that in 1945 Turing "used his wartime technological knowledge to design a first digital computer." He also suggests that Turing's work of 1936 laid the foundation for encoding "all known processes," going "far beyond the vision of others at the time." These statements implicitly diminish the earlier work of Kurt Gödel and Konrad Zuse. In 1931, Gödel used the integers to design a universal language capable of encoding arbitrary computations and general algorithms that could prove theorems (*1*). This allowed him to identify the fundamental limits of math and provability. Turing and his adviser Alonzo Church later merely reformulated Gödel's work in an elegant way. Furthermore, Zuse's 1936 patent application Z23139/GMD Nr. 005/021 already described a concrete general computer, as opposed to a purely mathematical construct. By 1941, Zuse had physically built the first working universal digital machine, years ahead of anybody else [e.g., (*2*, *3*)]. Thus, unlike Turing, he not only had

a theoretical model but actual working hardware. Future hardware leader IBM was well aware of Zuse's breakthroughs and acquired an option on his patents at the earliest possible point after the war (*4*). The great computer science hero Turing surely deserves center stage on his centenary. But let's not exaggerate his achievements at the expense of others!

JÜRGEN SCHMIDHUBER

The Swiss AI Lab IDSIA, Galleria 1, 6928 Manno-Lugano, Switzerland. E-mail: juergen@idsia.ch

References

1. K. Gödel, *Monatsh. Math.* **38**, 173 (1931).
2. R. Rojas, *IEEE Ann. History Comput.* **19**, 5 (1997).
3. Konrad Zuse Internet Archive (www.zib.de/zuse/home.php).
4. IEEE Global History Network, Konrad Zuse: An Interview Conducted by Frederik Nebeker, IEEE Center for the History of Electrical Engineering (28 August 1994); www.ieeeghn.org/wiki/index.php/Oral-History:Konrad_Zuse.

Response

IN 1936, TURING DID FOLLOW GÖDEL'S 1931 revolution in logic. His first citation was to Gödel, and he described his mathematical argument as similar to Gödel's. But Turing successfully addressed Hilbert's question of decidability, a problem that Gödel's work had not settled. He did so based on an entirely original philosophical analysis of the concept of computing (which was in no way advised by Church).

Turing's 1936 work also introduced the concept of the universal machine, and this, rather than Gödel's work, provided the theoretical basis of the modern computer. In doing so, Turing introduced the concept that computation could act on general symbolic, not necessarily arithmetical, structures. In particular, he exploited the fact that a program is itself such a structure. It was on the basis of this deep understanding that in 1945 Turing could write the detailed plan and prospectus for what he called the practical version of his universal machine. It is a telling fact that in recent discussions of whether Zuse's machines (or indeed Babbage's Analytical Engine) were truly general-purpose, the criterion adopted is whether they can simulate any Turing machine (*1*). This is because Turing's definition of computability sets the definitive standard. In contrast, there is no need for such a discussion of how Turing's own plans embodied his theory.

Turing illustrated universality with examples from mathematical physics, algebra, and data processing, but also from non-numerical cryptology and chess-playing. Most strikingly, he emphasized that programs could be written in a user-friendly form, with the computer itself used to translate them into machine code. This all-encompassing and farsighted vision also led him into investigating the prospects for simulating the human brain by computable processes.

Many great figures—Gödel, Babbage, Church, von Neumann, and Shannon, to name just a few—populated the landscape in which Turing made his contributions. But Turing had a distinctive place connecting theory to practice and logic to physics.

ANDREW HODGES

Wadham College, University of Oxford, Oxford, OX1 3PN, UK. E-mail: andrew.hodges@wadh.ox.ac.uk

Reference

1. R. Rojas, "How to make Zuse's Z3 a universal computer" (www.zib.de/zuse/Inhalt/Kommentare/Html/0684/universal2.html).

TECHNICAL COMMENT ABSTRACTS

Comment on "Global Correlations in Tropical Tree Species Richness and Abundance Reject Neutrality"

Rampal S. Etienne and James Rosindell

Ricklefs and Renner (Reports, 27 January 2012, p. 464) showed correlations of species richness and individual abundance within families across continents and claimed that neutral theory predicts no such correlation. However, they did not substantiate this claim quantitatively with a neutral model. Here, we show that neutral theory can be consistent with these correlations and, consequently, that the correlations alone cannot reject neutrality.

Full text at www.sciencemag.org/cgi/content/full/336/6089/1639-b

Comment on "Global Correlations in Tropical Tree Species Richness and Abundance Reject Neutrality"

Camilo Mora

Ricklefs and Renner (Reports, 27 January 2012, p. 464) suggested that strong correlations in the diversity of shared families between isolated tree assemblages reject neutrality. Simulations of a neutral model indicate, however, that isolated assemblages under various configurations of random speciation and extinction do sustain strong correlations in the diversity of shared families. Thus, reported correlations support rather than reject neutral theory.

Full text at www.sciencemag.org/cgi/content/full/336/6089/1639-c

Comment on "Global Correlations in Tropical Tree Species Richness and Abundance Reject Neutrality"

Anping Chen, Shaopeng Wang, Stephen W. Pacala

Ricklefs and Renner (Reports, 27 January 2012, p. 464) found significant correlations for abundances and species diversities of families and orders of trees on different continents, which they suggested falsifies the neutral theory of biodiversity (NTB). We argue that the correlations among families and orders and the lack of correlations among genera can be explained by the NTB.

Full text at www.sciencemag.org/cgi/content/full/336/6089/1639-d

Comment on "Global Correlations in Tropical Tree Species Richness and Abundance Reject Neutrality"

François Munoz, Pierre Couteron, Stephen P. Hubbell

Ricklefs and Renner (Reports, 27 January 2012, p. 464) have argued that the neutral theory of biodiversity and biogeography cannot explain the correlations in family abundances and species richness found between tropical forests from distinct continents. However, we show that such patterns can arise from neutral processes of diversification, migration, and drift over large spatial and temporal scales.

Full text at www.sciencemag.org/cgi/content/full/336/6089/1639-e

Response to Comments on "Global Correlations in Tropical Tree Species Richness and Abundance Reject Neutrality"

Robert E. Ricklefs and Susanne S. Renner

The neutral models in the Technical Comments depend on the assumption of an initially homogeneous global tropical forest flora. Fossil data and phylogenetic reconstructions instead reveal a high degree of provincialism before the development of modern tropical forests with only occasional long-distance dispersal between continental regions, favoring parallel diversification of a small number of ancestral lineages that dispersed between regions at widely different times.

Full text at www.sciencemag.org/cgi/content/full/336/6089/1639-f

Letters to the Editor

Letters (~300 words) discuss material published in *Science* in the past 3 months or matters of general interest. Letters are not acknowledged upon receipt. Whether published in full or in part, Letters are subject to editing for clarity and space. Letters submitted, published, or posted elsewhere, in print or online, will be disqualified. To submit a Letter, go to www.submit2science.org.

TECHNOLOGY

Incubator of Innovations

Ann Johnson

American Telephone and Telegraph (AT&T) has a long tradition of introducing its newest technologies through carefully staged telephone calls. These exchanges were public relations stunts, and they were performed to demonstrate AT&T's ability to transmit the sound of the human voice through space. In 1876, Alexander Graham Bell famously summoned his assistant Thomas Watson by shouting into the mouthpiece of his invention, "Mr. Watson—come here—I want to see you." He repeated the stunt in 1915, this time sitting in New York and calling Watson in San Francisco, to demonstrate his company's new long-distance transmission capability. In a 1956 performance, Cleo Craig (AT&T chairman), seated in New York, rang up Charles Hill, Britain's postmaster general, in London to introduce a new transatlantic telephone cable. But the most impressive of these stunts was perhaps the 1962 call from Fred Kappel, AT&T president, to U.S. Vice President Lyndon B. Johnson. This transmission, from New Jersey to Washington, D.C., was not impressive for its spanning of geography, but because the signal was sent from New Jersey into space, then conveyed to Washington by the Telstar satellite. AT&T had entered the space age.

Jon Gertner's *The Idea Factory: Bell Labs and the Great Age of American Innovation* asks and answers the question of how Bell Laboratories, both as an institution and as a collection of personalities, made such innovations possible. In the case of Telstar, Gertner (a writer at the *New York Times Magazine*) details the challenges of developing an active satellite. He notes that it "was not one invention but rather a synchronous use of sixteen inventions patented at the Labs over the course of twenty-five years." Only a large firm like Bell Labs, with 13,000 employees at the time of Telstar, could yield so many new technologies, from the transistor to the solar cell, and figure out how to assemble them to interface with the most complex technological system in the world—the telephone system.

Bell Labs's life spanned the whole 20th century, and Gertner describes its beginning, middle, and end. The beginning is important for seeing AT&T's research and development wing as an innovation unto itself. Bell Laboratories was designed to bring cutting-edge science to make phone service better, cheaper, and ubiquitous. Early on, it developed important relationships with universities, and Bell Labs was able to hire some of the brightest young Ph.D. scientists. These academic connections were, in fact, personal. Frank Jewett, head of the Labs at its creation in 1925, had joined AT&T two decades earlier, fresh from physicist Robert Millikan's lab at the University of Chicago. Jewett was able to lure other Millikan students to the Labs, including future leader Mervin Kelly. After Millikan moved on to Caltech in 1921, Jewett recruited electrical engineer John Robinson Pierce and transistor coinventor William Shockley from Pasadena. Gertner is at his best in drawing vivid portraits of these characters, whose idiosyncracies were as notable as their scientific accomplishments.

Whereas the beginning period of Bell Labs focused on bringing scientists into industrial research, the Labs's move from Greenwich Village to Murray Hill, New Jersey, in 1942 generated new modes of interaction. The facilities at Murray Hill were designed to ensure chance encounters: "By intention, everyone would be in one another's way." Scientists, mathematicians, engineers, and technical assistants ran into each other in the hallways, worked in labs and offices together, and ate lunch at the same tables. Ideas were shared as a matter of daily conversation. To be sure, the sociocultural homogeneity of the Labs was a factor in its values; only during the war did AT&T acquiesce to hiring Jews. Women and African-Americans were rare at the Labs and are rarer still in Gertner's depiction. Nevertheless, what was most exceptional was the innovative productivity of the institution in its glory days, when Bell Labs, according to Gertner, "created the future." It is difficult not to share the author's nostalgia for the Labs when seen in light of the remarkable developments of the transistor, pulse code modulation, microwave transmission, the laser and maser, Telstar, fiber optics, and cellular transmission. Moreover, Gertner captures the fun the men he spotlights must have had working on these "wicked problems."

Gertner, like many others, laments the demise of Bell Labs. He asks where the innovations comparable to those it produced in the 20th century will come from in the 21st. The author gestures at the wicked problems in energy and calls for innovation on par with the Labs's telecommunications inventions. But he also shows the ways in which AT&T's monopoly was both unique and essential to the support of Bell Labs. AT&T was broken up because it stood outside of the logic of the free market. Gertner suggests, probably accurately, that market logic only spurs certain kinds of innovative processes—not "stupendous leaps" but rather progress characterized by "a continuous series of short sprints." However, there might be more hope for solving our wicked problems than Gertner implies. One of Kelly's dictums was to seek good problems, rather than good ideas. Creating an institution for innovation today that learns from but doesn't attempt to replicate Bell Labs seems like the problem at hand.

The Idea Factory
Bell Labs and the Great Age of American Innovation
by Jon Gertner
Penguin, New York, 2012. 446 pp. $29.95, £19.15. ISBN 9781594203282.

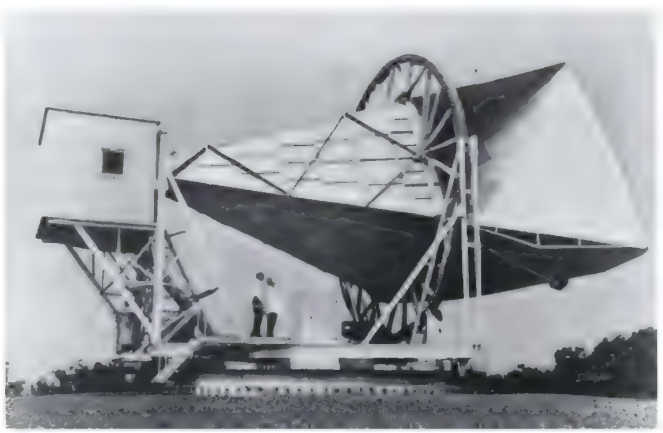

Crawford Hill horn. Built in 1959 for the ECHO satellite experiment, this reflector antenna was modified to work with Telstar. Using it in 1965, Bell Labs physicists Arno Penzias and Robert Woodrow Wilson discovered the cosmic microwave background radiation, work for which they shared a 1978 Nobel Prize.

CREDIT: NASA

The reviewer is at the Department of History, University of South Carolina, Columbia, SC 29208, USA. E-mail: ajohnson@mailbox.sc.edu

10.1126/science.1221909

EXHIBITIONS: MEDICINE

No Body Is As It Seems

Louise Whiteley

The cultural meanings of body size are constantly shifting, and the causes of bodily extremes are remarkably diverse. A very thin body might result from anorexia nervosa, from a sporting profession that demands asceticism, or from a political or religious fast. On the other hand, a very large body might speak of uncontrolled eating, a thyroid disorder, aesthetic preference, or simply genetic variation. The body is not always what it seems.

Ongoing controversy about using statistics such as body mass index to categorize people as under- or overweight emphasizes the difficulty with inferring health from body size alone. And wranglings over how eating disorders should be classified in the upcoming revision of the *Diagnostic and Statistical Manual of Mental Disorders* (*1*) reveal a lack of consensus about what a healthy relationship to food might look like in the first place.

The Weighty Body, an exhibition at Museum Boerhaave in Leiden, explores these conundrums and asks when our relationship to the body becomes dysfunctional. The exhibition doesn't attempt to answer this question though—instead gently fleshing out its knotty demand.

In four loosely themed sections, representations of thin and fat bodies offer glimpses into contemporary debates about their medical status. For instance, 19th-century images of Daniel Lambert's famously large, 50-stone (317-kg) body are accompanied by a bemused litany of evidence for his good health, and 17th-century etchings of fasting "wonder girls" are accompanied by stories of attempts to verify their abstinence and thus their unnatural ability to escape the body's needs. A collection of early dissertations on obesity and anorexia face each other across the room, and a selection of contemporary artworks highlight the contradictions of a culture in which advertisers use Photoshop to produce physiological impossibilities while artworks depicting extreme bodies are treated as dangerous. The exhibition poster features one of Ivonne Thein's (*2*) photographs of an impossibly thin, doll-like figure—when these images were taken up by "pro-anorexia" websites, the media criticism the artist received served to emphasize some of the issues she aimed to critique.

In dealing with these diverse materials, the curatorial stethoscope was applied lightly: the exhibition showcases symptoms rather than working toward a clear diagnosis. This could be frustrating for those with a clinical bent, and I would have liked to hear more about the development of the psychiatric debates. The light-touch interpretation also left the relationship between over- and undereating unclear, with the large body presented primarily as a flip side to the fasting, anorexic self. Especially in the context of contemporary controversy over the causes and consequences of obesity, it would have been interesting to give overeating as much attention as not eating.

But there is also something usefully subversive in telling medical history without an explicit framework of medical definitions and developments. It can leave space for the visitor to draw comparisons along social, cultural, or psychological lines, emphasizing the difficulty of extricating medical categories from their contexts. The restrained layout of the exhibition rooms, with dark partitions, open spaces, and simply hung pictures, provides a contemplative space that seems to support visitors in navigating their own course through this complex landscape. However, for those without a strong sense of direction, there's a risk that this openness could instead create a feeling of distance or fragmentation.

The Weighty Body
Fat or Thin, Vanity or Insanity

Museum Boerhaave, Leiden, Netherlands. 13 April to 9 September 2012. www.museumboerhaave.nl

The Weighty Body
Fat or Thin, Vanity or Insanity

Museum Dr. Guislain and Museum Boerhaave
Lannoo, Tielt, Belgium, 2010. Paper, 194 pp. £27.50, €29.95. ISBN 9789020992151.

The Weighty Body consists primarily of images, from illustrations of medical cases to newspaper reports, posters, advertisements, and artworks. This reflects the potent role of representations of the body in creating cultural meaning, affecting eating behavior, and disseminating scientific knowledge. In providing a historical view on this issue, the exhibition offers a soothing counterpoint to often-shrill arguments about the role of the media in eating disorders. But as with the question of psychiatric diagnosis, the exhibition resists a strong editorial line on media effects.

Instead, it is accompanied by a catalog that includes essays and commentaries and by a series of public events exploring food culture. For science communication, the increasingly popular combination of object-focused exhibitions with public engagement activities has the potential to exploit the best bits of both mediums: the visceral presence of the museum object feeding, and feeding off, debate and discussion.

The exhibition's entrance is flanked by two fairground mirrors, one concave, one convex. They shrink or expand the body instantly, bypassing the delay of consumption, invoking giggles and gasps. This Victorian parlor trick plays on the difficulty of reconciling the perceived body with its felt outlines, as also emphasized by recent research using body scanners to help patients with distorted body image come to terms with their size (*3*). Through a subtle, repeated insistence that the body is never quite what it seems, *The Weighty Body* has the potential to encourage caution, and compassion, in interpreting perceptions and representations of our embodied selves.

A very thin man. Claude Ambroise Seurat (19th century).

CREDIT: CLAUDE AMBROISE SEURAT/WELLCOME LIBRARY, LONDON

The reviewer is at the Medical Museion in the Faculty of Health Sciences, and the Novo Nordisk Center for Basic Metabolic Research, University of Copenhagen, 1310 Copenhagen K, Denmark. E-mail: louise.whiteley@sund.ku.dk

References
1. www.dsm5.org/ProposedRevision/Pages/FeedingandEatingDisorders.aspx.
2. www.ivonnethein.com/.
3. www.rgu.ac.uk/dmstaff/stewart-arthur.

10.1126/science.1222946

SCIENCE EDUCATION

European Teacher Training Reforms

The Bologna Process has contributed to a more academic and research-based orientation in European teacher education.

Johannes Bauer* and Manfred Prenzel

Preparing students for societal participation requires well-prepared science and mathematics teachers (*1*–*3*). There is increasing evidence that teacher education matters. Opportunities to learn in initial teacher education affect teachers' professional knowledge development (*4*–*6*). Such knowledge has been found to predict teaching quality and student achievement (*7*).

In many European countries, teacher education has recently undergone substantial transformations during the Bologna Process of higher-education reform (*2*, *8*, *9*). What trends these reforms have invoked and whether they are for better or for worse in terms of teacher education is unclear. There are two main reasons for this. First, "empirical evidence on the achievements so far in the ... signatory countries is thin" [p. 224 in (*10*)]. Second, recent international comparative studies on teacher education (*5*, *11*, *12*) provide no direct evidence of effects of the Bologna Process on account of study design and country selection. We argue that Bologna has contributed to increasing transparency in qualification requirements and making European teacher education more academic, competence-oriented, and research-based.

Teacher education meets Bologna

The aim of the Bologna Process is to address challenges of globalization in higher education (*13*). At the heart of this process are the evolving goals, structures, and tools for increasing international compatibility of higher education and addressing key problems, such as quality assurance (figs. S1 and S2) (*14*). Although the Bologna agenda is often perceived as concerned with structural issues, its focus on quality has implications for curricula (*8*). Bologna emphasizes the need for curricula and contents to be oriented around professionally relevant competences. This demands high transparency in learning outcomes in higher education (*10*).

The Bologna agenda is particularly challenging for teacher education, whose structure and length, providing institutions, and required qualifications have varied greatly across Europe (*2*). As teachers are employed in national educational systems, teacher education has become more embedded in national contexts than other professions (*8*). Its structure can vary widely within the same country because of regional differences or specific training programs according to educational level (*8*, *15*). Commitments of the Bologna Process have urged many countries to redesign their teacher education systems (*8*, *9*) and have provided a framework for implementation of existing national plans for teacher education reform (*10*).

Technische Universität München, TUM School of Education, Schellingstr. 33, D-80799 Munich, Germany.

*Author for correspondence. E-mail: jbauer@tum.de

Structural trends

Progress has been made in introducing a common structure of degrees in teacher education. About 89% of member countries and 68% of higher-education institutions have introduced the bachelor's-master's degree system in teacher education (*13*). Implementation of the tiered-degree structure in teacher education has been challenging, especially for countries that used a concurrent one-cycle model of teacher education (*16*). Considerable variation still exists concerning length of study and required entry qualifications for the teaching profession (table S1); so far, compatibility has only been achieved at the formal level of degrees. Whereas a joint-degree structure is a first step to enhancing international compatibility, it is not sufficient to bridge structural, curricular, cultural, and language differences across Europe (*8*). Even so, member countries today are in a better position to compare requirements and to learn from each other (*10*). These efforts have encouraged movement in existing systems, which has facilitated further reforms more directly related to quality.

Despite structural diversity, a stronger academic orientation in teacher education is visible in Bologna countries. In line with recommendations of the European Commission (*1*) and teacher unions (*17*), several countries have used the reforms to raise qualification requirements and to increase the length of studies (see the table). (See table S1 for qualification requirements in initial teacher education in the 47 Bologna member countries.)

With few exceptions, teacher education for all types of teachers is delivered in tertiary institutions, mostly universities (table S1). Compared with the pre-Bologna situation, countries like Denmark, Hungary, Italy, and Luxembourg have upgraded primary or lower-secondary teacher education to the university level. In Austria and Switzerland, former pedagogical academies have gained the status of universities of applied sciences in education. Of all the Bologna countries, 38% require a master's degree for at least all secondary teachers (table S1). Although the former diversity in degree systems makes comparison with the pre-Bologna situation difficult, the contrast with 1995 data on lower-secondary mathematics teachers (*18*) indicates that this requirement is new in at least seven countries (Hungary, Iceland, France, Portugal, Spain, Sweden, and Switzerland). Other countries plan to increase the number of teachers with master's degrees (Belgium, Georgia, and Norway) or already have a high percentage (Bulgaria and Poland) (*12*).

Percent of countries showing increased length of required teacher training post-Bologna:

- 46% for primary education teachers.
- 32% for lower-secondary education teachers.
- 46% for upper-secondary education teachers.

Lengthening teacher training. Percentages reflect 28 Bologna countries, of 47 total, for which pre- and post-Bologna data on required length of study are available (see table S1).

The movement to increase the length of studies is consistent with evidence on the role of extensive learning opportunities in the formation of future teachers' professional knowledge (*4*–*7*). This trend holds for primary education teachers, in line with growing appreciation of the importance of well-prepared teachers in the early years of education (*6*, *19*). Upgrading entry qualifications to the master's level and defining standards for teacher professionalism may further contribute to public perception of teachers as members of a high-level profession. This may make it a more attractive career choice for talented students (*2*, *20*). Such an effect, however, will also depend on competitive salaries within nations (*5*, *21*).

Curricular trends

Most Bologna countries have implemented the European Credit Transfer and Accumulation System (ECTS) in teacher education, organizing study contents into modules of

relevant learning outcomes that define competences (*8*). Competences are individual dispositions for meeting complex demands in a particular context (*22*). Use of competences as reference points can be seen as a transition from an input-driven curriculum design toward student-centered learning and assessment (*10*). Consensus-building on competence profiles for teachers is taking place at the national and European level.

At the European level, the Tuning project, a university initiative to develop competence profiles for various subject areas (*23*), has defined generic and profession-related competences for teacher education (*9*, *24*). Tuning highlights the role of orientation on learning outcomes to balance goals of convergence and compatibility, as well as appreciation of the diversity of European cultures, languages, and curricula. Competences serve as a "common language" [p. 18 in (*23*)] for describing the aims of curricula while maintaining individual countries' or universities' autonomy to emphasize specific interests.

Twenty countries are establishing national standards or guidelines for teacher education [see list in (*25*)]. Germany, for instance, has commissioned a system of nationwide guidelines that describe what teachers should know and be able to do. Mathematics teachers, for example, are to be able to apply research in mathematics education to analyze students' knowledge and learning processes and support individualized learning.

For most of these 20 countries, there is no detailed information regarding whether the standards were developed in negotiations among relevant stakeholders (e.g., in Germany, Netherlands, and Serbia) or top down (e.g., England) (*24*). Information is scarce regarding whether the primary function of standards lies in guiding teacher education or in assessment and accreditation. Such information would be required to better understand how they work in practice (*21*).

Policy and scientific debates around standards of teacher professionalism are increasingly based on understanding teaching as a research-based profession (*1*, *2*, *20*). The European Commission's communiqué on increasing the quality of teacher education (*1*) explicitly states the goal of equipping teachers with competencies and orientations required for evidence-based practice and lifelong learning. Alongside state-of-the-art knowledge in the subjects and education, teachers ought to acquire competencies to understand research on effective teaching and use this as a basis for their own practices (*2*, *20*). There are calls for teachers to be able to conduct their own classroom-based research to reflect upon and improve their teaching. The European Commission demands that, "As with members of any other profession, teachers have a responsibility to develop new knowledge about education and training" [p. 5 in (*1*)]. To attain these goals, many countries have followed the Finnish example (*2*): They have introduced training in research methods or student research projects in teacher education (*20*). It is unclear, however, whether this is a consistent trend within these countries.

Both the introduction of research skills and the use of standards in teacher education curricula will help encourage evidence-based practice in education (*26*). Standards provide a means to align study programs with evidence on quality teachers and effective teaching in mathematics and science (*5*). Methodological studies and research experiences support future teachers as they develop skills and attitudes needed for evidence-based practice (*2*, *20*). Although this does not guarantee improved student learning, evidence-based practice has gained acceptance in other professions (*26*).

Higher quality in teacher education?

Although teacher education reform has been an issue in Europe before, the Bologna Process has catalyzed structural and curricular transformations. The changes described will help achieve high-quality teacher education. Although the focus on outcomes and the use of standards have been subject to criticism in the context of teacher education (*21*, *27*), ongoing developments suggest a potential for improvement. In mathematics teacher education, for example, increased length of programs and use of standards offer chances to provide more extensive and higher-quality learning opportunities in the subject and subject education.

Evaluating benefits of these developments for attaining better-educated teachers will require establishment of a continuous international monitoring system similar to Trends in International Mathematics and Science Study (TIMSS) and Programme for International Student Assessment (PISA) in secondary education. Recent comparison studies on teacher education (*4*, *11*) took promising first steps and are ahead of other initiatives for international assessment in higher education (*28*). Existing approaches need to be extended in terms of participating countries and longitudinal designs for gathering evidence on changes in teacher education and their effects on professional knowledge, beliefs, and orientations of future teachers.

References and Notes

1. European Commission (EC), Improving the quality of teacher education (EC, Brussels, 2007); http://ec.europa.eu/education/com392_en.pdf.
2. Organization for Economic Cooperation and Development, *Teachers Matter* (OECD, Paris, 2005).
3. L. Darling-Hammond, J. Bransford, Eds., *Preparing Teachers for a Changing World* (Jossey-Bass, San Francisco, CA, 2005).
4. W. H. Schmidt, S. Blömeke, M. T. Tatto, *Teacher Education Matters* (Teachers College Press, New York, 2011).
5. W. H. Schmidt, R. Houang, L. S. Cogan, *Science* **332**, 1266 (2011).
6. S. Blömeke, U. Suhl, G. Kaiser, M. Döhrmann, *Teach. Teach. Educ.* **28**, 44 (2012).
7. J. Baumert *et al.*, *Am. Educ. Res. J.* **47**, 133 (2010).
8. J. Enders *et al.*, *The Extent and Impact of Higher Education Curricular Reform Across Europe* (Center for Higher Education Policy Studies, Enschede, Netherlands, 2006); http://ec.europa.eu/education/pdf/doc240_en.pdf.
9. P. Zgaga, Ed., *The Prospects of Teacher Education in South-East Europe* (Univ. of Ljubljana, Ljubljana, Slovenia, 2006).
10. J. Witte, J. Huisman, L. Purser, in *Higher Education to 2030* (OECD, Paris, 2009), vol. 2, pp. 205–229.
11. M. T. Tatto, S. Senk, *J. Teach. Educ.* **62**, 121 (2011).
12. OECD Secretary-General, *Creating Effective Teaching and Learning Environments* (OECD, Paris, 2009).
13. A. Sursock, H. Smidt, *Trends 2010: A Decade of Change in European Higher Education* (European Univ. Association, Brussels, 2010); www.eua.be/publications/.
14. P. L. Gaston, *The Challenge of Bologna* (Stylus, Sterling, VA, 2010).
15. J. Bauer *et al.*, *Z Erziehungswiss* **14**, 629 (2011).
16. Eurydice, *Key Data on Education in Europe 2009* (European Commission, Brussels, 2009).
17. European Trade Union Committee for Education (ETUCE), *Teacher Education in Europe* (ETUCE, Brussels, 2008); http://etuce.homestead.com/Publications2008/ETUCE_PolicyPaper_en_web.pdf.
18. OECD, *Education at a Glance: OECD Indicators* (OECD, Paris, 2000).
19. W. S. Barnett, *Science* **333**, 975 (2011).
20. H. Niemi, *Lifelong Learn. Europe* **2008**, 61 (2008).
21. R. Zuzovsky, Z. Libman, *Stud. Educ. Eval.* **32**, 37 (2006).
22. OECD, *The Definition and Selection of Key Competencies* (OECD, Paris, 2005); www.oecd.org/dataoecd/47/61/35070367.pdf.
23. J. Gonzáles, R. Wagenaar, *Universities' Contribution to the Bologna Process* (Univ. de Deusto, Bilbao, Spain, 2008).
24. N. Pantić, T. Wubbels, *Teach. Teach. Educ.* **26**, 694 (2010).
25. Austria, Bulgaria, Croatia, Czech Republic, Estonia, Finland, Germany, Iceland, Ireland, Italy, Liechtenstein, Lithuania, Moldova, Poland, Romania, Slovakia, Serbia, Switzerland, Netherlands, and UK. See refs. (*2*, *9*, *24*, *29*, *30*).
26. P. Davies, *Br. J. Educ. Stud.* **47**, 108 (1999).
27. M. Cochran-Smith, *Educ. Res.* **34**, 3 (2005).
28. H. Coates, S. Richardson, *High. Educ. Manag. Pol.* **23**, 51 (2011).
29. National education system descriptions available at the Eurypedia; http://eacea.ec.europa.eu/education/eurydice/eurybase_en.php.
30. D. Jorde, A. Olsen Moberg, M. Prenzel, S. Rönnebeck, M. Stadler, S-TEAM (Science–Teacher Education Advanced Methods) preliminary report: Work package 2/3, (Norwegian Univ. of Science and Technology (NNTU), Trondheim, Norway, 2010); https://www.ntnu.no/wiki/download/attachments/8324747/S-TEAMReport010210.doc?version=1&modification_Date=1265105177000.

Supplementary Materials

www.sciencemag.org/cgi/content/full/336/6089/1642/DC1

10.1126/science.1218387

ANTHROPOLOGY

On the Invention of Pottery

What was the function of early Asian pottery, which predates the invention of agriculture by about 10,000 years?

Gideon Shelach

On page 1696 of this issue, Wu *et al.* (*1*) report the latest of a series of exciting discoveries made over the past 20 years that have pushed back the earliest evidence for the invention of pottery by more than 10,000 years. Like their findings at the Xianrendong Cave (*1*), most of the earliest pottery has been discovered in south China (the Yangzi River basin and areas south of it), but evidence for early pottery is also known from the Yellow River basin, and indeed from a much larger area of East Asia that includes Japan and the Amur River basin (*2*–*4*). The early dating of East Asian ceramics refutes the idea that the beginning of pottery production was associated with the transition to agriculture. What was the societal context for its invention?

Socioeconomic changes before the invention of agriculture. Artifacts from Locality 1 of the Longwangchan site (the Yellow River basin) dated to ~25,000 calendar years before present (*8*): 1 to 4, microblade cores; 5 to 7, microlithic tools; 8, shell; 9, shovel; 10, grinding slab (quern). These and other technologies invented during the Last Glacial Maximum point to a time of socioeconomic development long before the invention of agriculture. Wu *et al.* contribute to this field by reporting pottery remains dated to ~20,000 years ago.

Documenting the invention and development of one of humankind's most fundamental technologies captures the imagination and is of great scientific importance. However, understanding the socioeconomic reasons for the development of pottery and the ways in which this new technology evolved and affected human adaptation and social norms is no less interesting or important. Research advances that address these issues have not been as dramatic.

The period around the Last Glacial Maximum (LGM), about 25,000 to 19,000 years ago, saw the advent of a new technological array that, in addition to pottery, included in many parts of China the production of small flake tools (or microliths) and grinding slab stones (*5*–*8*) (see the figure). It is widely held (*6*, *9*) that the artifacts produced by these new technologies enabled exploitation of a wider range of plants and animals and more efficient extraction of their nutritional elements through grinding and intensive cooking. The technological advances during the LGM predate agriculture by at least 10,000 years.

Department of East Asian Studies, Hebrew University, Jerusalem 91905, Israel. E-mail: msshe@huji.ac.il

It has long been suggested that broadening the spectrum of the human diet—including the consumption of foods that are hard to process and digest, of which cereals (rice and millet in China) are but one type—eventually led to the cultivation of wild plants and finally to their domestication (*10*). This remains a viable hypothesis about the initiation of a long-term process that resulted in one of humankind's most dramatic revolutions: the transition to food production, domestication of plants and animals, adoption of a sedentary way of life, and ultimately, the development of more complex societies.

However, the validity of this hypothesis should not be assumed. Rather, it should be tested using systematic research methods and scientific tools. For example, the diet of ancient human populations and the foods processed by prehistoric tools can be studied through chemical analysis of human bones and identification of plant starch and animal proteins extracted from potshards and grinding stones.

One of the issues most relevant to understanding socioeconomic change—not only in prehistoric societies but also in historic and even modern societies—is the context of technological innovations, or more specifically, the ways in which technologies are invented, developed, and adopted by society. The proverb "necessity is the mother of all invention" not only assumes a direct functional explanation, but also assumes that conditions of stress (caused by external forces, such as climate change, or by internal social tension) force people to change their old ways of doing things. Such assumptions are embedded in the idea that the scarcity of resources during the LGM forced people to develop better ways of collecting and processing food (*1*, *6*, *9*).

However, the archaeological data suggest that grinding stones only started to be widely used toward the end of the last glacial age, ~13,000 years ago; ceramic production on a larger scale may have commenced even later. It is thus likely that these technologies initially had a much more limited set of functions, and that their full socioeconomic potential remained dormant until ecological and social conditions provided opportunities for the realization of this potential.

This more complex trajectory allows for the possibility that the new technologies were initially developed for a different function from that which they ultimately served with greater economic and/or social effect. For example, contrary to the assumption that grinding stones were important because they facilitated the consumption of wild cereals, preliminary analysis of plant remains extracted from early slab querns and use-marks found on the querns suggest that the querns were used to process acorns or even nonfood materials such as pigments (*6*, *11*).

PHOTO CREDIT: WANG XIAOQING/INSTITUTE OF ARCHAEOLOGY, CHINESE ACADEMY OF SOCIAL SCIENCES

Similar trajectories for the development of grinding technologies are known from the Levant as well. Thus, technological change should not be conceived of as the consequence of one-off innovations, but rather as a long-term process that involves not only technological improvements but also the adaptation and change of economic habits and negotiations over cultural norms.

It is possible that pottery and other early technologies were invented independently in different places. However, the fact that early pottery is widely distributed in East Asia among different societies in many different environments, but not found among preagricultural societies elsewhere, suggests that it spread in East Asia through intersocietal interactions, perhaps along with other ideas and technologies.

Research endeavors such as those led by Wu *et al.* are fundamental for a better understanding of socioeconomic change during the LGM and the developments that led to the emergence of sedentary agricultural societies. However, anthropological perspectives on the context of pottery invention should help to broaden scientific attention from discovery and dating to the functions of early pottery and its social context. Research of this kind could elucidate the development of human societies in East Asia, as well as opening up new perspectives on the evolution of human societies and the origins of social complexity in general. More general issues awaiting serious consideration include, for example, whether the fact that in East Asia pottery predates agriculture by some 10 millennia, whereas in the Levant it postdates the transition to agriculture, signifies a fundamental difference in the socioeconomic development of the two regions.

References

1. X. Wu *et al.*, *Science* **336**, 1696 (2012).
2. E. Boaretto *et al.*, *Proc. Natl. Acad. Sci. U.S.A.* **106**, 9595 (2009).
3. Hebeisheng, *Acta Archaeol. Sin. Kaogu Xuabao* **3**, 361 (2010).
4. V. Y. Kuzmin, *Antiquity* **80**, 362 (2006).
5. T. Chung, *J. East Asian Archaeol.* **2**, 37 (2000).
6. R. G. Elston *et al.*, *Quat. Int.* **242**, 401 (2011).
7. B. D. Madsen, R. G. Elston, in *Late Quaternary Climate Change and Human Adaptation in Arid China*, D. B. Madsen, F. H. Chen, X. Gao, Eds. (Elsevier, Amsterdam, 2007), pp. 69–82.
8. J.-F. Zhang *et al.*, *J. Archaeol. Sci.* **38**, 1537 (2011).
9. O. Bar-Yosef, *Curr. Anthropol.* **52**, S175 (2011).
10. M. C. Stiner, *Proc. Natl. Acad. Sci. U.S.A.* **98**, 6993 (2001).
11. L. Liu *et al.*, *J. Archaeol. Sci.* **37**, 2630 (2010).

10.1126/science.1224119

MOLECULAR BIOLOGY

A New Start for Protein Synthesis

Protein synthesis that does not initiate with methionine is used by the mammalian immune system to process antigen.

Thomas E. Dever

Laboratory of Gene Regulation and Development, Eunice Kennedy Shriver National Institute of Child Health and Human Development, National Institutes of Health, Bethesda, MD 20892, USA. E-mail: tdever@nih.gov

Recent technical advances have led to the accumulation of vast amounts of DNA sequences, highlighting the importance of understanding how the information in DNA is translated into amino acids and proteins. To decipher this information, the cell first transcribes a "coding" segment of DNA into messenger RNA (mRNA). Next, the ribosome decodes the mRNA in blocks of three consecutive nucleotides, or codons, that each specify an amino acid. But, how does the ribosome know where to start reading on the mRNA? To ensure faithful translation, and thereby yield a functional protein, cells restrict translation initiation to AUG codons that specify the amino acid methionine (Met). In mammals and other eukaryotic cells, translation typically initiates at the AUG codon closest to the beginning of the mRNA. But on page 1719 of this issue, Starck *et al.* (*1*) show that in addition to the canonical AUG-methionine initiation pathway, CUG-leucine can also be used to initiate protein synthesis.

When decoding an mRNA, ribosomes rely on transfer RNA (tRNA) molecules, each of which is covalently attached to a specific amino acid at one end, while three nucleotides in the so-called anticodon loop at the other end pairs with a codon on the mRNA. Cells express two types of methionyl-tRNA: elongator $tRNA_e^{Met}$ decodes AUG codons within reading frames, whereas initiator $tRNA_i^{Met}$ is used exclusively to initiate translation. The eukaryotic translation ini-

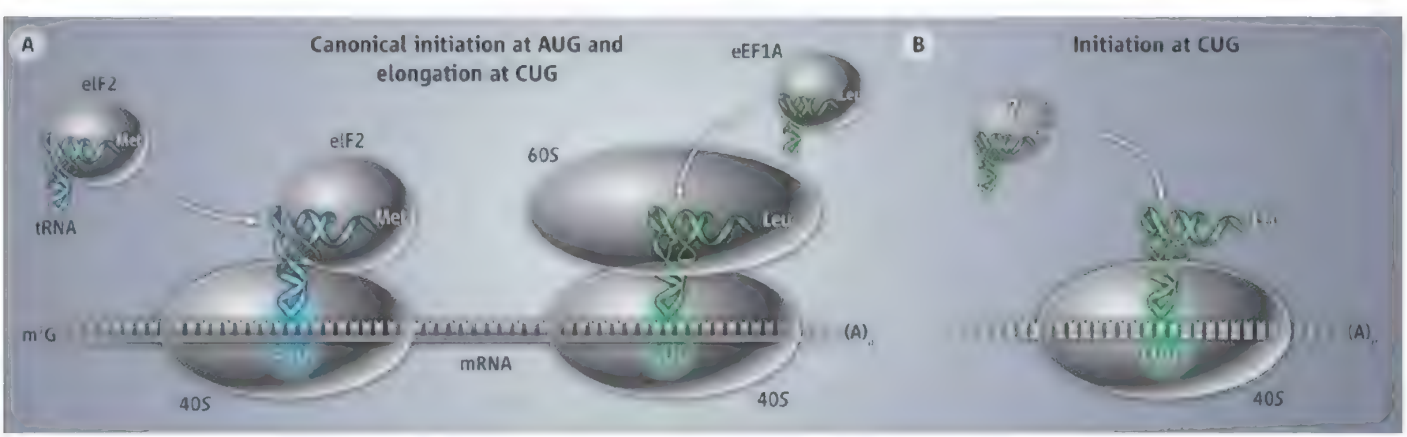

CREDIT: C. BICKEL/*SCIENCE*

How to begin? In the canonical initiation pathway (**A**), eIF2 delivers Met-$tRNA_i^{Met}$ to the ribosome. Base-pairing between $tRNA_i^{Met}$ and the mRNA directs protein synthesis to start at an AUG codon. During translation elongation, the translation elongation factor eEF1A delivers Leu-$tRNA^{Leu}$-CAG to decode CUG codons. Starck *et al.* show (**B**) that Leu-$tRNA^{Leu}$-CAG can also direct protein synthesis to start at a CUG codon.

tiation factor 2 (eIF2) binds Met-tRNA$_i^{Met}$ to the small (40*S*) ribosome in the first step of translation initiation (*2*) (see the figure). This complex then binds near the 5′ end of an mRNA and scans the mRNA sequence to identify a start site. Base-pairing interactions between the anticodon loop of the Met-tRNA$_i^{Met}$ bound to the ribosome and an AUG codon in the mRNA cause the ribosome to stop scanning and set the reading frame for protein synthesis (*3*). Typically the ribosome initiates protein synthesis at the AUG codon closest to the 5′ end of the mRNA, though context nucleotides flanking the start codon can influence the efficiency of translation initiation (*4*).

Exceptions to the rules limiting translation initiation to an AUG codon and to methionine have been reported. Naturally occurring non-AUG start codons have been reported for some cellular mRNAs (*5*); and seven out of the nine possible single-nucleotide substitutions at the AUG start codon of dihydrofolate reductase were functional as translation start sites in mammalian cells (*6*). In all of the cases in which it was examined, the amino-terminal residue of these proteins was methionine (*6*), suggesting that translation initiation relied on mis-pairing between the anticodon of Met-tRNA$_i^{Met}$ and the non-AUG start codon in the mRNA. In an alternate approach, proteins beginning with valine or glutamine were synthesized by expressing anticodon mutants of initiator tRNA$_i^{Met}$ that were mis-acylated in vivo (*7*). Notably, in both of these studies, translation initiation depended on tRNA$_i^{Met}$. Starck *et al.* reveal that in addition to the canonical Met-tRNA$_i^{Met}$ and AUG codon pathway, mammalian cells can initiate translation with leucine using a specific leucyl-tRNA that decodes the codon CUG.

Immune surveillance in vertebrates depends on the presentation of endogenously synthesized peptides on the cell surface by the major histocompatibility complex (MHC) (*8*). These peptides are encoded in conventional open reading frames, but also in alternate reading frames, in mRNA sequences 5′ or 3′ to the main protein coding reading frame, and in reading frames lacking an AUG start codon (*9*). CUG codons initiating these cryptic open reading frames can be decoded as leucine (*10*), and other Leu codons (CUC, CUA, UUG) cannot substitute (*11*). Moreover, the synthesis of these leucine-initiated peptides is enhanced under conditions that cause phosphorylation and inactivation of eIF2. These results indicate a mechanism of translation initiation for these cryptic antigenic peptides that relies neither on eIF2 nor on tRNA$_i^{Met}$. Starck *et al.* demonstrate that tRNA^{Leu} with the anticodon CAG (Leu-tRNA^{Leu}-CAG) participates in translation initiation at CUG start codons (tRNA base pairs with mRNA in antiparallel format with the C of the tRNA anticodon pairing with the G of the codon). The authors found that ribosomal initiation complexes assembled in vitro on mRNAs with an AUG start codon primarily contain tRNA$_i^{Met}$, whereas initiation complexes assembled on mRNAs with a CUG start codon contained both tRNA$_i^{Met}$ and tRNA^{Leu}-CAG. Further, mutating the anticodon of tRNA^{Leu}-CAG to CUA enabled translation of antigenic peptides in antigen-presenting cells to initiate in vivo at a UAG codon that normally functions as a termination codon.

The findings of Starck *et al.* raise interesting questions. How is Leu-tRNA^{Leu}-CAG delivered to the initiating ribosome? Does initiation at a CUG codon rely on any of the initiation factors that function in the AUG initiation pathway? Although the authors found that inhibiting expression of the factor eIF2A impaired initiation by Leu-tRNA^{Leu}-CAG, the involvement of other initiation factors in this pathway is not known. Perhaps there is something special about tRNA^{Leu}-CAG that enables it to initiate translation, or maybe other tRNAs also function in noncanonical initiation pathways. Does the Leu-tRNA^{Leu}-CAG initiation pathway contribute to the synthesis of cellular proteins other than antigenic peptides? Ribosomal profiling studies of mammalian cells have identified widespread use of CUG and other non-AUG initiation sites (*12*). Starck *et al.* demonstrated association of Leu-tRNA^{Leu}-CAG with initiation complexes assembled at the CUG start codon of the *Myc* oncogene, and a CUG start codon of human trypsinogen 4 is decoded as leucine (*13*). These results suggest that the Leu-tRNA^{Leu}-CAG initiation pathway may play an important role in cellular protein synthesis, and it will be interesting to learn how cells maintain the fidelity of protein synthesis in the face of this alternate initiation pathway.

References

1. S. R. Starck *et al.*, *Science* **336**, 1719 (2012).
2. J. R. Lorsch, T. E. Dever, *J. Biol. Chem.* **285**, 21203 (2010).
3. A. M. Cigan *et al.*, *Science* **242**, 93 (1988).
4. M. Kozak, *Gene* **234**, 187 (1999).
5. I. P. Ivanov *et al.*, *Nucleic Acids Res.* **39**, 4220 (2011).
6. D. S. Peabody, *J. Biol. Chem.* **264**, 5031 (1989).
7. H. J. Drabkin, U. L. RajBhandary, *Mol. Cell. Biol.* **18**, 5140 (1998).
8. B. P. Dolan *et al.*, *Cell. Mol. Life Sci.* **68**, 1481 (2011).
9. S. R. Starck, N. Shastri, *Cell. Mol. Life Sci.* **68**, 1471 (2011).
10. S. Malarkannan *et al.*, *Immunity* **10**, 681 (1999).
11. S. R. Schwab, K. C. Li, C. Kang, N. Shastri, *Science* **301**, 1367 (2003).
12. N. T. Ingolia *et al.*, *Cell* **147**, 789 (2011).
13. A. L. Németh *et al.*, *FEBS J.* **274**, 1610 (2007).

10.1126/science.1224439

PALEONTOLOGY

Old and Groovy

Mary L. Droser[1] and James G. Gehling[2]

The discovery of furrowed and backfilled trace fossils, claimed to be at least 585 million years old, raises questions about their origins.

Since Darwin's time, paleontologists and biologists have searched for evidence for the first bilaterian animals, which have a front and a back end as well as an upper and a lower side. Bilateral symmetry alone does not define this group, and confident interpretation of fossil embryos has proven difficult. On the other hand, evidence of sediment furrowing over extended distances has been widely accepted as evidence of bilaterian life: Flatworms may glide along a surface (*1*) and deep-sea protists can produce short furrowed surface traces (*2*), but making a long furrowed trace fossil with evidence of backfill requires a bilaterian body plan. On page 1693 of this issue, Pecoits *et al.* (*3*) describe furrowed, backfilled trace fossils dated to over 585 million years, which they interpret as the oldest bilaterian trace fossils and thus the oldest evidence of bilaterians.

Before this report, the oldest widely accepted evidence of bilaterians comes from simple furrow trace fossils of millimeter-scale width dated to 558 million years ago (*4*); similar trace fossils are known from several locations worldwide dated to ~560 to 542 million years ago, at the end of the Ediacaran period. They occur in rock units that preserve elements of the macroscopic soft-bodied animal fossil assemblages called the Ediacaran biota; however, trace fossils are found at far

[1]Department of Earth Sciences, University of California, Riverside, Riverside, CA 92521, USA. [2]South Australian Museum, Adelaide, South Australia 5000, Australia. E-mail: mary.droser@ucr.edu; jim.gehling@samuseum.sa.gov.au

fewer sites than body fossils (*5*). The body fossil *Kimberella*, occurring with associated fanned sets of scratch marks, is the oldest known body fossil regarded as a bilaterian, and perhaps a stem group mollusk (*6*). Most recently, sediment mixing through animal movement (bioturbation) has been described from ~555-million-year-old rocks (*7*). However, although found in some abundance when present, trace fossils are rare in rocks of this age and require the right combination of conditions for preservation and interpretation (see the figure).

Ancient sedimentary rocks can be very difficult to date, especially when body fossils are absent. In the best-case scenario, sedimentary rocks alternate with datable ash beds. In the absence of ash beds, Pecoits *et al.* present age databased on a granite intrusion associated with the succession, with an unusually limited contact zone and only minor alteration of the trace fossil-bearing sedimentary rocks. If we accept the age determination in their paper, the trace fossils reported by Pecoits *et al.* are the oldest definitive bilaterian trace fossils to date by nearly 30 million years.

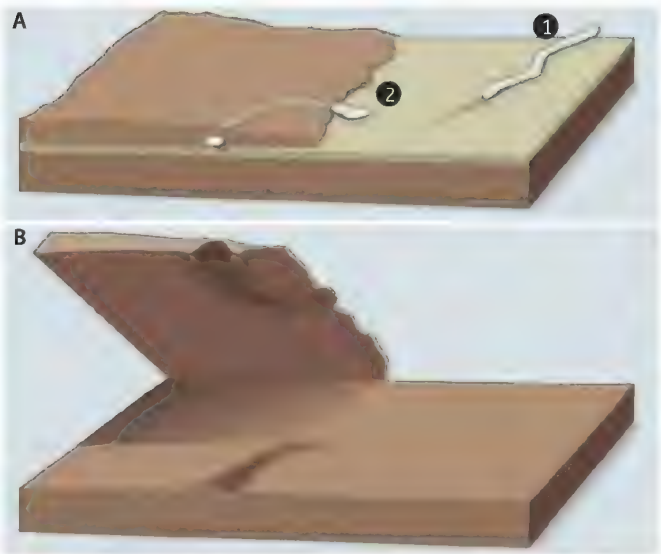

How worm burrows are preserved. **(A)** At time 1, worm 1 is moving along in the microbial mat; the furrow behind it closes a bit after the worm moves on. The sediment surface is not penetrated. Meanwhile, worm 2 has just entered underneath a discontinuous sand body. As this worm mines the microbial mat beneath the discontinuous sand, the sediment is impacted. The worm is (in this case) on the upper part of the mat surface and so leaves a furrow on the upper side, or negative groove on the base of the overlying sand. **(B)** Sandstone rocks at time 2 show the base of the overlying sand (now sandstone) and the top of the underlying sand (also now sandstone). The burrow of worm 1 is not preserved because the sand was never impacted. The burrow of worm 2 is preserved as a negative with furrows on the base of the bed, and a positive "cast" on the top of the underlying bed. Pecoits *et al.* now report evidence for such worm burrows from 585 million years ago.

Interpreting trace fossils, particularly morphologically simple ones, is not always clearcut. Trace fossils can superficially resemble physically and chemically induced sedimentary structures. Mud cracks, water escape structures, tubular fossils, algal fossils, and surface structures resulting from the presence of microbial mats can look remarkably like trace fossils. Thus, identification of trace fossils requires application of strict criteria, such as the presence of raised ridges and a consistent diameter, which Pecoits *et al.* consider carefully.

If bilaterians were present so early, why do we not recover associated body fossils? This question turns out to be relatively easy to answer. The trace fossils described by Pecoits *et al.*—and other similar burrows 555 million years in age (*7*)—were made by animals that were less than 1 cm long and had diameters of 1 or 2 mm, about the same diameter as the casting sand grains. Both the preservation of such an organism and its identification as the trace fossil progenitor are strokes of luck rather than the predictable outcomes of a targeted search; locomotive or feeding traces rarely occur together with the body fossil of the maker in strata of any age.

But why do we not see more trace fossils? The answer involves both ecology and preservation. From ~560 to 542 million years ago, before the advent of deep burrowing, the sea floor of the marine shelf was covered with microbial mats made up of accumulated organic debris and bacterial communities. Textured organic surfaces found with the fossils of the Ediacaran biota suggest that mat surfaces were diverse and likely included eukaryotes in the later Ediacaran (*8*). Today, animals effectively burrow most of the sea floor, except in extreme environments where metazoans are limited; in those settings, microbial mats still accumulate (*9*).

A mat-covered sea floor has several implications. The burrows of millimeter-scale Ediacaran animals moving horizontally while mining the microbial mat but not impacting the sediment below were very unlikely to be preserved. As the animal moves forward through the mat, the burrow will tend to close behind it because of the soft nature of the substrate. But imagine a sea floor with episodic sedimentation or discontinuous layers of sand formed by waning storms. An animal following the microbial mat under a thin sheet of sand impacts the sand both above and below, and it is that sand which can preserve the burrow (see the figure). The resulting trace fossils are found on both surfaces—parts and counterparts are preserved, as described by Pecoits *et al.*

The principal argument in their paper—that bilaterian traces are preserved in sediments demonstrably older than 580 million years—is at odds with previous suggestions that bilaterian traces first appear at the same time as putative bilaterian body fossils of motile organisms (*10*). It is unlikely that the bilaterian record predates that of organisms like sponges and soft corals, as well as developed microbial mats. Sponge biomarkers are recorded in 630-million-year-old rocks (*11*), and the oldest known large body fossils like *Charnia* occur in rocks dated at 575 million years. However, that is still at least 15 million years older than body fossils of probable bilaterian animals, such as *Kimberella* (*12*).

Given that all other Ediacaran trace fossils occur with well-developed mats and body fossils, the report by Pecoits *et al.* sets up the hypothesis that textured organic surfaces resulting from mats, if not Ediacaran body fossils, will be discovered accompanying these >585-million-year-old trace fossils. The work forces us to recognize the importance of understanding the conditions for preservation in interpreting the fossil record. Studies like the one by Pecoits *et al.* inspire us to continue to explore both the origins of animals and how the record of these early animals has been transmitted to us.

References

1. A. G. Collins, J. H. Lipps, J. W. Valentine, *Paleobiology* **26**, 47 (2000).
2. M. V. Matz, T. M. Frank, N. J. Marshall, E. A. Widder, S. Johnsen, *Curr. Biol.* **18**, 1849 (2008).
3. E. Pecoits *et al.*, *Science* **336**, 1693 (2012).
4. M. W. Martin *et al.*, *Science* **288**, 841 (2000).
5. M. L. Droser, J. G. Gehling, S. R. Jensen, *Palaeogeogr. Palaeoclimatol. Palaeoecol.* **232**, 131 (2006).
6. A. Seilacher, *Palaios* **14**, 86 (1999).
7. V. Rogov *et al.*, *Geology* **40**, 395 (2012).
8. J. G. Gehling, M. L. Droser, *Earth Sci. Rev.* **96**, 196 (2009).
9. N. Noffke, *Geobiology—Microbial Mats in Sandy Deposits from the Archean to Today* (Springer, Berlin, London, 2010).
10. G. E. Budd, S. Jensen, *Biol. Rev. Camb. Philos. Soc.* **75**, 253 (2000).
11. G. D. Love *et al.*, *Nature* **457**, 718 (2009).
12. G. M. Narbonne, J. G. Gehling, *Geology* **31**, 27 (2003).

10.1126/science.1223848

PLANT SCIENCE

Plant Gene Clusters and Opiates

A variety of poppy that produces high amounts of an alkaloid opiate requires a cluster of genes that encode key biosynthetic enzymes.

Dean DellaPenna[1] and Sarah E. O'Connor[2,3]

Plant natural products have a profound impact on human health and are prime targets for drug development, but full realization of their clinical potential is often curtailed because these compounds are typically produced in small amounts in slow-growing plant species. Improving production levels is essential for bringing new plant compounds into the drug development pipeline, but such improvements demand an understanding of the fundamental biological processes underlying complex natural product synthesis in plants. On page 1704 of this issue, Winzer *et al.* (*1*) define genes encoding the biosynthetic pathway for noscapine, a medicinal alkaloid produced by opium poppy.

Plants synthesize hundreds of thousands of diverse natural products that play key roles in their development and responses to environmental stress. Many of these metabolites also exhibit potent bioactivity or toxicity against insects and herbivores and provide plants with a selective advantage in these interactions. Although substantial metabolic cost is associated with the production of specialized plant metabolites, their biosynthetic pathways are strongly favored and maintained by natural selection. This continuous selection process has generated plant compounds with a range of pharmaceutical uses. Indeed, two-thirds of compounds now in clinical use originated from discoveries related to specialized plant metabolites (*2*). However, with few exceptions, a specific medicinally important compound is produced by only a handful of the estimated 400,000 plant species. Moreover, most medicinal species are poorly studied and are largely intractable to standard biochemical and genetic approaches. Recent advances in high-throughput sequencing, metabolomics, bioinformatics, and viral-based plant gene silencing have provided new avenues for rapidly advancing our understanding of biosynthetic pathways for such taxonomically restricted plant natural products (*3*).

Noscapine is a nonaddictive alkaloid that has been safely used for decades as an orally administered antitussive and has recently shown promising anticancer activity as a tubulin polymerization inhibitor and inducer of apoptosis (*4*). As an alkaloid, it is one of a group of more than 12,000 specialized plant metabolites present in about 20% of plant species and characterized by the presence of a nitrogen-containing heterocyclic ring. There is enormous chemical diversity among the alkaloids, with more than 20 biochemically and structurally distinct classes recognized. This chemical complexity makes characterizing the biosynthesis of individual alkaloids particularly difficult.

Plant species	Compound produced	Compound class	Likely function in host plant
Lotus japonicus	Linamarin	Cyanogenic glycoside	Herbivore defense
Manihot esculenta	Linamarin	Cyanogenic glycoside	Herbivore defense
Sorghum bicolor	Dhurrin	Cyanogenic glycoside	Herbivore defense
Zea mays	DIMBOA	Cyclic hydroxamic acid	Insect and microbial defense
Avena sativa	Avenacin A-1	Triterpene saponin	Antifungal
Oryza sativa	Phytocassane A	Diterpene phytoalexin	Antifungal
Oryza sativa	Momilactone A	Diterpene phytoalexin	Antifungal
Arabidopsis thaliana	Thalianol	Triterpene	Unknown
Arabidopsis thaliana	Marneral	Triterpene	Unknown
Papaver somniferum	Noscapine	Alkaloid	Unknown

Specialized metabolites. The biosynthetic pathways of the metabolites listed are partially or fully encoded in clusters in the genomes of the indicated plant species (*1*, *5*–*11*).

The elucidation of the noscapine pathway reported by Winzer *et al.* was greatly accelerated by their discovery that the biosynthetic genes are physically clustered in the poppy genome. By crossing poppy varieties containing high levels of morphine (a highly addictive alkaloid in the opium poppy) or noscapine, the authors show that the biochemically complex noscapine trait segregates as a single Mendelian locus. By comparing the transcriptomes (all of the messenger RNA molecules produced), metabolite profiles, and genomes of varieties that produce high morphine, high thebaine (another opiate alkaloid), and high noscapine, they identified 10 genes that are highly expressed in tissues of the high-noscapine variety but absent from the tissues and genomes of the high-morphine and high-thebaine varieties. By contrast, known genes for morphine synthesis were present and similarly expressed in all three varieties. A 401-kb genomic interval specific to the noscapine variety was found to contain all 10 genes, six of which were shown—by virus-induced gene silencing followed by metabolomics analysis of poppy, or by gene expression and biochemical assays in yeast—to encode specific steps of the noscapine pathway. Although some members of the noscapine biosynthetic cluster appear to have arisen by recent gene duplication, the majority of genes encode unrelated proteins that catalyze distinct reactions in the pathway (e.g., divergent cytochrome P450s and methyltransferases). The noscapine biosynthetic cluster adds to a growing body of knowledge about the involvement of gene clusters in the synthesis of specialized plant metabolites (see the figure).

Since the first identification of a tightly linked genetic cluster for the biosynthesis of cyclic hydroxamic acid in maize in 1997 (*5*), 10 additional instances of gene clusters for specialized metabolism in plants have been reported from seven other plant species (*1*, *6*–*11*). Specialized plant metabolism gene clusters occur relatively infrequently on a genome-wide basis, but as more are characterized, they will become easier to identify. Although we still do not understand the

CREDIT: Y. HAMMOND/*SCIENCE*

[1]Department of Biochemistry & Molecular Biology, Michigan State University, East Lansing, MI 48824, USA. [2]Department of Biological Chemistry, John Innes Centre, Norwich Research Park, Norwich, NR4 7UH, UK. [3]School of Chemistry, University of East Anglia, Norwich Research Park, Norwich NR4 7TJ, UK. E-mail: dellapen@msu.edu

forces that generate and maintain gene clusters for specialized plant metabolism (*12*), such clusters, once identified, are invaluable for decoding of complex, taxonomically restricted pathways in plants. One need only compare the pace of dissecting noscapine synthesis to the nearly two decades required to fully decipher the pathway for morphine to fully appreciate the power of such metabolic Rosetta stones. Low-cost, high-throughput sequencing has increasingly driven biosynthetic gene cluster identification in plants; as our ability to apply molecular genetic tools (such as virus-induced gene silencing) expands to more nonmodel plant species with unique biochemistries, we can anticipate that even more dark recesses of specialized plant metabolism will be illuminated.

References

1. T. Winzer *et al.*, *Science* **336**, 1704 (2012); 10.1126/science.1220757.
2. G. M. Cragg, D. J. Newman, *J. Ethnopharmacol.* **100**, 72 (2005).
3. D. K. Liscombe, S. E. O'Connor, *Phytochemistry* **72**, 1969 (2011).
4. M. Mahmoudian, P. Rahimi-Moghaddam, *Anti-Cancer Drug Discov.* **4**, 92 (2009).
5. M. Frey *et al.*, *Science* **277**, 696 (1997).
6. A. M. Takos *et al.*, *Plant J.* **68**, 273 (2011).
7. S. Swaminathan *et al.*, *Plant Cell* **21**, 3315 (2009).
8. B. Field *et al.*, *Proc. Natl. Acad. Sci. U.S.A.* **108**, 16116 (2011).
9. B. Field, A. E. Osbourn, *Science* **320**, 543 (2008).
10. K. Shimura *et al.*, *J. Biol. Chem.* **282**, 34013 (2007).
11. X. Qi *et al.*, *Proc. Natl. Acad. Sci. U.S.A.* **101**, 8233 (2004).
12. H. Y. Chu, E. Wegel, A. Osbourn, *Plant J.* **66**, 66 (2011).

10.1126/science.1225473

EVOLUTION

Endless Rots Most Beautiful

Deep phylogenetic sampling of 31 fungal genomes, including 12 new ones, reveals how wood-decaying enzymes evolved in white rot.

Chris Todd Hittinger

Fungal rots that decay wood were not prominent among the "endless forms most beautiful" that Darwin chronicled, but if he had known of the biochemical and evolutionary processes at work, they might have been. Woody plants fix an extraordinary amount of carbon during their lifetimes, building towering trees of decay-resistant lignocellulose. On page 1715 of this issue, Floudas *et al.* performed deep phylogenetic sampling of fungal genomes to describe how white rot Agaricomycetes fungi have evolved an arsenal of enzymes to degrade lignin and unlock its stored carbon (*1*).

As plants invaded land, lignin provided the rigidity necessary for vascular plants to grow above their rivals and move water and nutrients over long distances (*2*). Lignin is a dizzying web of polymerized phenylalanine derivatives with dozens of combinations of modifications and cross-links that make wood structurally sound and render it inaccessible to all but the most persistent chemical and biological assaults (*2*–*5*). The success of lignin-rich plants in the swamp forests of the Carboniferous Period created many of the coal-rich deposits that fueled the Industrial Revolution. But little carbon is buried today, in part because of white rot fungi. Floudas *et al.*'s analysis of 12 newly sequenced species of Agaricomycotina provides a treasure trove of wood-decaying enzymes to test and industrialize (*5*, *6*) as well as remarkable insights into the genomics of adaptive shifts, gene duplication and diversification, and parallel evolution.

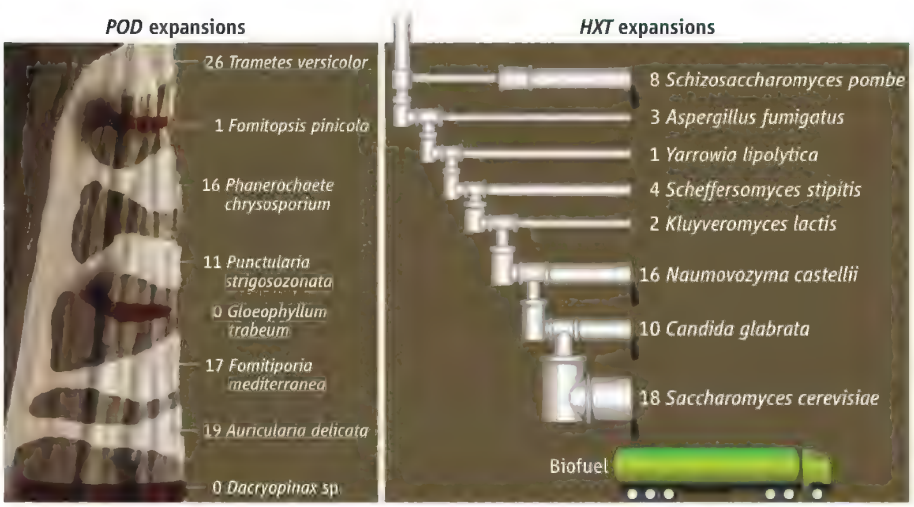

Parallel gene family expansions in fungi. (Left) Approximate evolutionary relationships (left to right, 300 million years ago to the present) and numbers of *POD* genes (also represented by width) in white and brown rot basidiomycetes. **(Right)** Relationships and numbers of *HXT* genes in ascomycetes; ethanol drops indicate taxa that ferment aerobically, including *S. cerevisiae*, the main producer of liquid biofuels.

Broad taxonomic and ecological sampling of rots allowed Floudas *et al.* to use state-of-the-art phylogenomic and ancestral state inference to trace the history of the Agaricomycetes and their myriad lignocellulolytic enzymes. Fifteen gene families deviate from the null expectation of a random birth-death process of gene duplication and loss, and instead exhibit significant lineage-specific expansions and contractions. For example, glycoside hydrolases, multicopper oxidases, and dye-decolorizing peroxidases expanded during the evolution of the lignin-degrading life-style of white rots, while contractions occurred in brown rot lineages that do not appreciably degrade lignin.

The most striking expansions and contractions are apparent in the fungal class II peroxidases (PODs), which are the primary lignin-degrading enzymes in white rots (*7*). The common ancestor of Agaricomycetes is inferred to have been a white rot with a modest repertoire of manganese peroxidase PODs. Indeed, nearly all modern white rot fungi possess several manganese peroxidases, whereas only a few species possess lignin peroxidases and versatile peroxidases capable of directly oxidizing aromatic rings. The branching pattern of the Agaricomycetes suggests that PODs independently expanded along multiple white rot lineages through gene duplication and independently contracted to zero or one *POD* genes in at least three brown rot lineages (see the figure). The few PODs found in non–white rot fungi all lack key sequences associated with lignolytic

Laboratory of Genetics, Wisconsin Bioenergy Initiative, Great Lakes Bioenergy Research Center, University of Wisconsin, Madison, WI 53706, USA. E-mail: cthittinger@wisc.edu

activity (*4*, *8*). Thus, the aggressive decay of lignin by white rots requires a diverse, refined suite of PODs and other enzymes.

The *POD* gene family expansions and contractions provide clear examples of genome content evolving in concert with the white or brown rot niches, but the parallel changes observed in some of the most lignolytic PODs are even more conspicuous. In both the lignin peroxidases (non–manganese-binding) and the versatile peroxidases (manganese-binding), natural selection repeatedly found the same solution to direct oxidation of lignin by changing a key external residue to tryptophan, enabling long-range electron transfer (*4*, *9*). Parallel alterations of the manganese-binding residues were also observed in several PODs, although it is unclear whether these are losses of function or trade-offs that enable new enzymatic properties. Adjusting specific residues is reminiscent of the spectral tuning that has occurred repeatedly in opsins to enable animals to see various light wavelengths (*10*).

As the white rots became experts in degrading the complex carbon stored in wood by duplicating and diversifying their *POD* gene families, *Saccharomyces* yeasts mastered fermenting simple sugars in sap and fruit, in part by duplicating and diversifying their hexose transporters (HXTs; see the figure). Most yeasts (and filamentous ascomycetes) have one to five *HXT* genes, but species that have evolved to ferment glucose in the presence of oxygen have extensively duplicated and diversified this gene family (*11*). The champion fermenter *S. cerevisiae* has 18 *HXT* genes that encode various specificities, capacities, and fine-tuned differential regulation (*12*, *13*). *HXT* expansions occurred independently in *Schizosaccharomyces pombe*, another yeast that ferments aerobically. The secondary or promiscuous activities exhibited by PODs and HXTs probably facilitated specialization after gene duplication (*14*, *15*).

The gene family expansions of white rots and fermentative yeasts complement both their ecologies and their potential uses in biofuel production. Current lignocellulosic biorefinery designs call for chemical and enzymatic deconstruction of biomass by enzymes modified from white rots and other decay specialists, followed by conversion of the hexoses and pentoses to ethanol by yeast (*6*). Although these complex genomic systems took hundreds of millions of years to evolve, we are beginning to understand them only just in time to exploit them to meet our energy needs.

References

1. D. Floudas, *Science* **336**, 1715 (2012).
2. J. K. Weng, C. Chapple, *New Phytol.* **187**, 273 (2010).
3. W. Boerjan *et al.*, *Annu. Rev. Plant Biol.* **54**, 519 (2003).
4. K. E. Hammel, D. Cullen, *Curr. Opin. Plant Biol.* **11**, 349 (2008).
5. A. T. Martínez *et al.*, *Curr. Opin. Biotechnol.* **20**, 348 (2009).
6. M. E. Himmel *et al.*, *Science* **315**, 804 (2007).
7. M. Tien, C. P. Tu, *Nature* **326**, 520 (1987).
8. L. F. Larrondo *et al.*, *Biophys. Chem.* **116**, 167 (2005).
9. W. A. Doyle *et al.*, *Biochemistry* **37**, 15097 (1998).
10. S. Yokoyama, *Prog. Retin. Eye Res.* **19**, 385 (2000).
11. Z. Lin, W.-H. Li, *Mol. Biol. Evol.* **28**, 131 (2011).
12. S. Ozcan, M. Johnston, *Microbiol. Mol. Biol. Rev.* **63**, 554 (1999).
13. R. Wieczorke *et al.*, *FEBS Lett.* **464**, 123 (1999).
14. R. A. Jensen, *Annu. Rev. Microbiol.* **30**, 409 (1976).
15. J. Piatigorsky, G. Wistow, *Science* **252**, 1078 (1991).

10.1126/science.1224682

CHEMISTRY

Rethinking Chemical Reactions at Hyperthermal Energies

Changes in the scattering direction of products for reactions at energies far above the transition-state barrier are driven by angular momentum effects.

Xueming Yang,[1,2] Timothy K. Minton,[1,3] Dong Hui Zhang[1]

A chemical reaction usually involves the breaking of old chemical bonds and the formation of new bonds. Internal vibrational energy or translational energy of the reacting molecules could affect the dynamics of chemical bond breaking and formation processes in an major way. The effects of vibrational excitation on chemical reactivity have been extensively investigated for decades (*1*, *2*), especially for highly vibrationally excited molecules. Studies of the translational effects on chemical dynamics have mainly focused on energies near the reaction barriers; reaction dynamics at hyperthermal translational energies (far above the barriers) has received much less attention. On page 1687 of this issue, Jankunas *et al.* (*3*) report that the dynamics of the simplest chemical reaction, $H + D_2 \rightarrow HD + D$, change in unexpected ways at hyperthermal translational energies and they provide a theoretical explanation for this unusual behavior.

At translational energies slightly above the reaction threshold, reaction trajectories normally follow the minimum energy path (MEP) (see the figure, panel A). As the energy increases, deviations from the MEP are possible and often change the dynamics in predictable ways. For example, in $H + D_2 \rightarrow HD + D$, reactive collisions along the collinear (MEP) pathway cause the HD products to rebound in the backward direction relative to the initial direction of the H

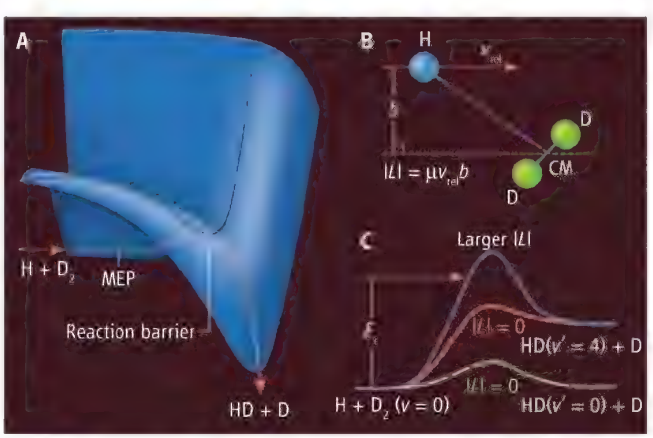

A matter of momentum. (**A**) The potential energy surface and the MEP are shown for the $H + D_2 \rightarrow HD + D$ reaction ($|L| = 0$). (**B**) Reaction geometry for the $H + D_2$ reaction with impact parameter b (CM is center of mass); the angular momentum of the collision is $L = \mu v_{rel} b$, where μ is the reduced mass of the collision partners and v_{rel} is the relative velocity. (**C**) Energy diagram along the reaction coordinate for the $H + D_2$ reaction with zero and larger L, where a larger L collision that has a high centrifugal barrier will inhibit the reaction at collision energy E_c below this barrier.

CREDIT: P. HUEY/*SCIENCE*

[1]State Key Laboratory of Molecular Reaction Dynamics, Dalian Institute of Chemical Physics, Chinese Academy of Sciences (CAS), Dalian 116023, China. [2]Department of Chemical Physics, University of Science and Technology of China, Hefei 230026, China. [3]Montana State University, Bozeman, MT 59717, USA. E-mail: xmyang@dicp.ac.cn (X.Y.); tminton@montana.edu (T.K.M.); zhangdh@dicp.ac.cn (D.H.Z.)

atom. As the collision energy increases, more reactive collisions with larger impact parameters b or higher orbital angular momentum L occur (see the figure, panel B). These events are expected to produce HD products that are scattered sideways and shift the distribution toward the forward direction.

Jankunas *et al.* used a three-dimensional ion imaging apparatus that employs the "photoloc" technique to measure the reaction probabilities for different product quantum states. These differential cross sections for the different rotational (j') and vibrational (v') states of the HD product were obtained at a collision energy of 1.97 eV (~11,000 K). The rotational state distributions for HD shift to higher j' values, as expected, when HD($v' = 1, 3$) products scatter increasingly into the forward direction. However, the HD($v' = 4$) products exhibit the opposite behavior, with a preference for more highly rotationally excited products to scatter toward the backward direction.

Accurate quantum dynamics calculations also show the same trend, in essential agreement with the experimental results. This turnaround in the rotational state distribution is counterintuitive based on the expected scattering behavior of "head-on" versus "grazing" collisions. The seemingly anomalous angular distributions have been attributed to the effect of a "centrifugal barrier" for high-impact parameter collisions. This angular momentum barrier occurs because the overall process must conserve L; if the reacting complex forms with large L (large b), the HD and H product complex can only separate if they maintain high L states.

As collision energy increases, reactive collisions with larger L become more important, and should produce rotationally excited HD products in more forward scattering directions. However, when the vibrational energy of the product is high, as for the HD($v' = 4$) product, the excess energy to overcome the centrifugal barrier needed for high L states is limited (see the figure, panel C). The increase in rotational excitation of HD($v' = 4$) will reduce this excess energy even further, and the rotationally excited HD($v' = 4$) product is suppressed in the forward scattering direction, making the angular distribution appear more backward scattered. This anomalous behavior was seen in the HD($v' = 4, j'$) products at a collision energy of 1.97 eV. This phenomenon can only occur at sufficiently high collision energies where a large centrifugal barrier limits the energy available for product rotation and the reaction deviates from the collinear MEP.

This anomalous result may explain the unexpected dynamics of a more complicated reaction, $O(^3P) + CH_4 \rightarrow OH + CH_3$, at hyperthermal energies (*4*). This reaction also has a collinear, O·····H–CH_3 MEP. At 3 eV, OH was vibrationally cold and rotationally excited, and CH_3 was vibrationally cold and also fairly rotationally cold. There was more product internal excitation when OH scattered backward. As most of the internal excitation went into OH rotation, it was concluded that backward-scattered OH was rotationally hotter than sideways/forward-scattered OH. A centrifugal barrier could suppress rotational excitation for forward-scattered OH products.

Additional studies are revealing the peculiar dynamics that may result from reactions beyond the MEP. A recent crossed-beams experiment on the H + CD_4 reaction showed that the total reaction probability initially increased with collision energy and then dropped quickly as the collision energy increased further (*5*). Theory showed that at energies far above the barrier, the incoming H atom moved so quickly that the heavier D atom on CD_4 could not keep up with the H atom to form the HD product. The MEP was actually suppressed at hyperthermal energies. Another interesting case of unusual hyperthermal chemistry is the $O(^3P)$ + HCl $\rightarrow$ ClO + H reaction (*6*). A non-MEP mechanism dominated at high collision energies, in which the H atom in the HCl molecule was oriented toward the O atom and produced forward-scattered ClO products.

These examples show that bimolecular chemical reactions at hyperthermal energies can occur along pathways that deviate far from the MEP, as in the case of unimolecular decomposition of formaldehyde (*7*). Rich chemical reaction dynamics can occur at hyperthermal energies and cannot simply be intuited from studies at lower energies.

References

1. R. N. Zare, *Science* **279**, 1875 (1998).
2. F. F. Crim, *Proc. Natl. Acad. Sci. U.S.A.* **105**, 12654 (2008).
3. J. Jankunas *et al.*, *Science* **336**, 1687 (2012).
4. J. Zhang *et al.*, *J. Phys. Chem. A* **115**, 10894 (2011).
5. W. Zhang *et al.*, *Proc. Natl. Acad. Sci. U.S.A.* **107**, 12782 (2010).
6. J. Zhang *et al.*, *J. Am. Chem. Soc.* **130**, 8896 (2008).
7. D. Townsend *et al.*, *Science* **306**, 1158 (2004).

Acknowledgments: X.Y. and D.H.Z. acknowledge support from National Natural Science Foundation of China and the Ministry of Science and Technology of China. T.K.M. acknowledges a CAS distinguished visiting fellowship.

10.1126/science.1223680

PHYSIOLOGY

De-Meaning of Metabolism

Mitchell A. Lazar and Morris J. Birnbaum

Implications of metabolic mechanisms in disease inspires reflection on the definition of metabolism.

Metabolism is a hot topic in science, from the epidemic of "metabolic diseases" such as obesity and diabetes to the rediscovery of altered "cancer metabolism" as a defining characteristic of malignant cells. As is often the case, once a topic has become in vogue, its name ceases to have meaning as researchers try to identify their work as relevant to the latest fashion. Thus, it is opportune to reconsider not only the meaning of "metabolism" but also whether the rebirth of metabolic research is incorporating many of the lessons learned through years of study in the last century.

Metabolism can be defined as "the chemical processes that occur within a living organism in order to maintain life" (*1*). This definition makes metabolism the primary subject of biochemistry, which is "the branch of science concerned with the chemical and physico-chemical processes and substances which occur within living organisms" (*2*). Thus, the definitions of biochemistry and metabolism clearly overlap. One conceptual distinction is that biochemistry is the study of the metabolites themselves, while metabolism refers to the conversion of nutrients to metabolites as well as the interconversion of metabolites within the body. In that context, biochemistry is more centered on steady-state amounts, whereas metabolism is more focused on flux, although flux is determined in part by mass action. The physiological implication is that metabolism is essentially the science of molecular transformation, which incorporates biological chemistry and energetics into a context necessarily constrained by physiology. By definition, metabolism is a process largely concerned

Division of Endocrinology, Diabetes, and Metabolism, Department of Medicine, and The Institute for Diabetes, Obesity, and Metabolism, Perelman School of Medicine at the University of Pennsylvania, Philadelphia, PA 19104, USA. E-mail: lazar@mail.med.upenn.edu; birnbaum@mail.med.upenn.edu

with the generation of energy by catabolism and the anabolic manufacture of cellular and extracellular constituents. Metabolism represents the essence of how organisms interact with their environment and, in doing so, overcome the thermodynamic mandate to "feed upon negative entropy" (*3*).

The field of signal transduction emerged from the desire to understand the effects of hormones on metabolism (*4*). Ironically, though modern signal transduction research is built upon principles developed through years of metabolism research, we are in danger of ignoring these lessons in the rebirth of metabolic research in the 21st century. In part, this is likely due to recent dominance of cancer metabolism, which represents a specialized situation in terms of its consideration of the tumor as an isolated entity, the cancer's intrinsic pathological state, and the unique influence on metabolism of somatic mutation followed by selection for autonomous growth and survival (*5*).

It follows that the most important distinction between how the term "metabolism" relates to cancer versus normal physiology and other pathological processes such as obesity and diabetes has to do with the dialogue between the single cell and the rest of the organism. A fundamental concept in molecular oncogenesis is that mutation of genes encoding intermediates in signaling pathways renders the cancer cell independent of, and unresponsive to, the normal control exerted by growth and survival factors (*6*). Uncontrolled growth requires fuel in the form of metabolites for which the cancer cell competes with normal cells; a cancer cell often requires more energy than the maintenance of normal cells, and the cancer cell is not programmed to adjust its fuel utilization based on the needs of the rest of the body.

Historically, a key aspect of "metabolism" is its link to "metabolic rate," which is the amount of energy used by an organism at rest (*7*). The metabolic rate concept was initially related to whole-body metabolism, and particularly the consumption of oxygen in the burning of biochemical fuels to create energy. Although basal metabolic rate reflects the sum of biological processes in single cells, the interaction between cells is essential to its regulation. Though host conditions such as hypoxia and blood supply might limit the metabolic capacity of the tumor cell, there is little exchange of information between the cancer and its host organism and the tumor rarely acts as a supplier of energetically useful metabolites. In fact, the opposite is more likely, as cancer cells may deplete their host of nutrients by their own rapid fuel consumption and stimulation of a cachectic response. On the other hand, caloric restriction of the host may reduce the growth of cancer by limiting nutrient availability as well as by reducing endocrine growth factors such as insulin.

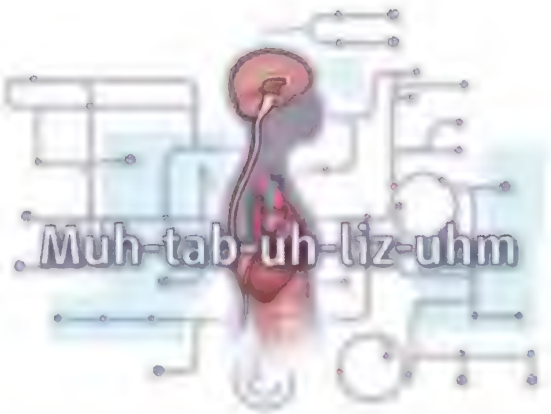

Muh-tab-uh-liz-uhm. It is important to clarify the definition of metabolism as it becomes increasingly recognized as an underlying mechanism in a range of diseases.

By contrast, metabolic control in professional metabolic cells such as fat cells (adipocytes), liver cells (hepatocytes), and muscle cells (myocytes) is unlike that in tumor cells, as the biological functions of these cells involve the coordinated partitioning of nutrients throughout the body. Indeed, obesity can be thought of as a pathological increase in the storage of lipid in adipocytes, and the elevated blood glucose concentrations that define diabetes result from inadequate partitioning of glucose between tissues and the blood compartment of the body. Hormone-producing endocrine cells and their metabolic tissue targets provide homeostatic control of energy metabolism at an organismal level, whereas the growth of cancer is dependent upon the cell-autonomous acquisition of fuel that is, in general, insensitive to hormonal signals that evolved to regulate metabolism in a more balanced manner. A major discovery of recent metabolic research has been that endocrine glands are not the only organs sending out directives to classic metabolic tissues, but in fact muscle, adipose tissue and liver are engaged in constant, active conversations with each other. Nonetheless, whether the relationship between a cell and the organism in which it resides is strictly parasitic as in cancer, mutually beneficial as in the classical insulin target tissues mentioned above, or maladaptive as in obesity and diabetes, metabolism of the cell is dependent upon its environment.

Increasingly, it is becoming clear that the exquisite specificity and fine-tuning of signal transduction cannot be explained by viewing the process as composed of linear pathways of varying strength operating in parallel (*8*). In retrospect, this should have been abundantly clear from the lessons of intermediary metabolism—that a multitude of pathways are inextricably interconnected, and the importance of any one depends on the conditions of the moment (*9*). Yet there is a real danger that the renaissance of metabolism will revert to archaic generalizations about "rate-limiting steps," often based on no more evidence than flux measurements under a single condition or, worse, quantitation of mRNA or protein concentrations of individual enzymes.

Thus, despite increased interest in metabolism, it is critical to recognize that although the cancer cell and normal cells use the same metabolic pathways, their metabolite selection and utilization rate are highly contextual. Regulating the response to available nutrients is largely cell-autonomous for the cancer cell, and adaptations frequently require a time scale dictated by somatic mutation and selection. By contrast, cells involved in classical metabolic homeostasis are highly responsive to nutritional, neural, and hormonal cues and are constantly engaged in a two-way dialogue with the organs producing such signals. Moreover, metabolism can refer to the entire sum of biological processes essential to life of a cell or organism, or to the synthesis, degradation, or redistribution of organic compounds as well as minerals that are important for life. As the scientific community continues to probe the role of metabolism in disease, it is essential that we remember which definition is most appropriate to the question at hand.

References and Notes

1. "Metabolism." *Oxford Dictionary of English* (Oxford Univ. Press, Oxford, UK, 2010).
2. "Biochemistry." *Oxford Dictionary of English* (Oxford Univ. Press, Oxford, UK, 2010).
3. E. Schrödinger, *What Is Life? The Physical Aspect of the Living Cell* (Cambridge Univ. Press, Cambridge, 1944).
4. M. Rodbell, *Nature* **284**, 17 (1980).
5. R. A. Cairns *et al.*, *Nat. Rev. Cancer* **11**, 85 (2011).
6. D. Hanahan, R. A. Weinberg, *Cell* **144**, 646 (2011).
7. D. F. Rolfe, G. C. Brown, *Physiol. Rev.* **77**, 731 (1997).
8. G. Weng *et al.*, *Science* **284**, 92 (1999).
9. D. A. Fell, *Biochem. J.* **286**, 313 (1992).

Acknowledgments: Supported by P01 DK49210; We thank Arthur Rubenstein for helpful discussions.

10.1126/science.1221834

RETROSPECTIVE

Norman L. Letvin (1949–2012)

A world leader in HIV/AIDS research was a dedicated mentor, influential international adviser, and a remarkable musician.

Gary J. Nabel,[1] Steven M. Wolinsky,[2] Barton F. Haynes[3]

He stood in thought, attentive to every detail, ready for his delivery. Well known for his clear and insightful presentations, Norman Letvin strode onstage with a different agenda this time. Clarinet in hand, he graced us, his scientific colleagues, with a world-class musical performance. Most did not even know that he played a musical instrument. But Norm was a remarkable talent who broke new ground, not only in the laboratory but also in music. He once played Mozart's clarinet quintet accompanied by Yo-Yo Ma. Sadly, his enthralling performances will be heard no more. After a long and valiant struggle with pancreatic cancer, Norman Letvin passed away on 28 May in Boston, Massachusetts. He fought this disease bravely for almost 5 years and, despite overwhelming medical challenges, maintained his commitment to the search for an AIDS vaccine and continued working until a week before he died.

CREDIT: GRAHAM RAMSAY

Norman Letvin's achievements were remarkable. He was born and raised in Detroit, Michigan, where his family recognized and nurtured his talent in music from a young age. As a 5-year-old, he taught himself to play the recorder, and he soon became proficient on the oboe and clarinet. He excelled as a scholarship student on the clarinet at the National Music Camp at Interlochen, Michigan, and performed professionally during his high school years. Offered scholarships at both the Juilliard School and the Curtis Institute of Music, he chose instead to attend Harvard College, where he continued his musical education but applied his prodigious intellectual energy to the social sciences and to medicine, graduating summa cum laude and with Phi Beta Kappa honors. After receiving his M.D. degree at Harvard Medical School in 1975, he completed his internal medicine residency at the University of Pennsylvania and the Massachusetts General Hospital. His postdoctoral fellowship with Baruch Benacerraf, Nobel laureate for discovery of the major histocompatibility complex, set the stage for Norm's lifelong interest in viral immunology and immunopathogenesis. These interests became the hallmark of his scientific career and his luminary achievements in the field of AIDS vaccine research.

Norm's accomplishments were exemplary in every sense. Among his professional achievements, he defined the first nonhuman primate models of AIDS by isolating the simian immunodeficiency virus and showing that it caused immune defects and fatal disease in Indian rhesus macaques. His scientific career was further highlighted by discoveries on the immunopathogenesis of lentiviral infection, the development of novel approaches for the vaccine stimulation of virus-specific cytotoxic T lymphocyte responses, and the identification of immune correlates of vaccine protection. Not surprisingly, he rose rapidly to the rank of professor at Harvard Medical School and served as chief of the division of viral pathogenesis at the Beth Israel Deaconess Medical Center. At the same time, Norm became a valuable and highly respected member of the AIDS vaccine community. A member of the National Institutes of Health (NIH) AIDS Vaccine Advisory Committee from its inception, he was a constant source of sound advice to the NIH and to HIV research scientists throughout the world. He was instrumental in establishing the Vaccine Research Center (VRC) at the National Institute of Allergy and Infectious Diseases, supporting its creation, selecting its scientific investigators, defining its mission and goals, and advancing the scientific agenda through advice and by experimentation. He was also a cofounder of the Center for HIV/AIDS Vaccine Immunology (CHAVI) consortium, and he was both a grantee and adviser to the Collaboration for AIDS Vaccine Discovery of the Bill and Melinda Gates Foundation.

Norm was always ready to give support and advice on the many challenging issues the AIDS vaccine development field faced. Moreover, he was a trusted and dedicated mentor to all who worked with him—students, fellows, and colleagues. He could also be counted on to provide honest and balanced perspective on any topic. Widely recognized as an international authority, he advised diverse international public health organizations on prevention and treatment of a wide spectrum of diseases with high human health impact, including tuberculosis, measles, and malaria, and helped to shape policy and strategic planning for deadly infectious diseases that plague the developing world. He was also an invaluable adviser for *Science*, where he served as a reviewing editor for 13 years.

Aside from his superlative professional successes, Norm was a renaissance man in its truest sense. He was a voracious reader, rehearsed regularly for decades with the Weston Wind Quintet, and graced both VRC and CHAVI retreats with his talented performances. His love for opera was no less than that for his beloved Boston sports teams: the Celtics, Red Sox, and New England Patriots. Finally, nothing was closer to his heart than his loving wife, Marion, and their four children, Andrea, Adam, Rebecca, and Elizabeth, who surrounded and comforted him in his final days.

Norm's passing is a loss to those who knew him personally but also deprives the AIDS vaccine research field of his wisdom, perspective, and impeccable judgment. There will be formal celebrations of his life and his accomplishments in the coming months. His many close colleagues hope to honor Norm by redoubling their commitment to finding an AIDS vaccine and holding to the high standards of scholarship and commitment that he exemplified.

[1]Vaccine Research Center, NIAID, National Institutes of Health, Bethesda, MD 20892, USA. [2]Northwestern University Feinberg School of Medicine, Chicago, IL 60611, USA. [3]Duke University Medical Center, Durham, NC 27705, USA. E-mail: gnabel@nih.gov

10.1126/science.1225947

IBI* SERIES WINNER

Engaging Students in Earthquakes via Real-Time Data and Decisions

Seismicity and Relative Risk, the IBI Prize–winning module, utilizes freely available earthquake data to help students apply their knowledge to risk-related decision-making.

Anne E. Egger

The topic of earthquakes appears in virtually all introductory undergraduate geoscience courses. Most students entering these courses already have some knowledge of earthquakes and why they occur, but that knowledge often derives from the most recent event in the news and can therefore be biased toward the most destructive earthquakes (*1*). In addition, students arrive at college with misconceptions (*2*, *3*), perhaps picked up from erroneous or poorly presented media coverage. These misconceptions can go unchecked or even be reinforced by introductory textbooks, most of which contain errors and oversimplifications about earthquake processes (*3*, *4*).

But we need not rely on the news media and textbooks in teaching. Earthquakes happen every day, and an exciting thing about earthquake science is near-instantaneous access to data collected by a global network of seismometers. The U.S. Geological Survey's (USGS) Earthquake Hazards Program hosts a Web site that serves data from that network in real time (http://earthquake.usgs.gov). Anyone can access and explore the data, which are available in both raw and interpreted form with supporting information. During 9 years of teaching introductory geoscience courses, I developed and refined an inquiry-based module called "Seismicity and Relative Risk" to take advantage of this reliable resource to engage students in learning more about earthquakes.

The refining part was instructive. Initially, I asked students to explore a static map of earthquakes (such as shown in the map) and then to write an essay that related earthquakes to plate boundaries. The results were disappointing. Students did not know how to describe patterns in the distribution of earthquakes or even seem to understand what "relate earthquakes to plate boundaries" meant. I realized that I was not giving them all of the tools they needed. Recent research shows that students often do not recognize that these static maps consist of data collected and analyzed by scientists; instead, they see them simply as "pictures" (*5*). In addition, about half of the students in introductory geoscience courses are not prepared for the level of abstract thinking that this assignment required (*6*). There are many learning benefits to be gained from incorporating data into classroom teaching (*7*); I needed my students to get their hands on these data so that they would become real for them.

Over the next few years, I tried different ways of incorporating data from the USGS site in class. In one version, pairs of students examined different regions and presented what they found in a few slides. This helped with describing patterns, but was tedious and repetitive for both me and the students, and it never got them beyond their descriptions. In the next version, students answered a series of questions that guided them through the USGS site. This was better, but students worked at very different paces; it was hard to

Central Washington University, 400 East University Way, Ellensburg, WA 98926, USA. E-mail: annegger@geology.cwu.edu

*IBI, Science Prize for Inquiry-Based Instruction; www.sciencemag.org/site/feature/data/prizes/inquiry/.

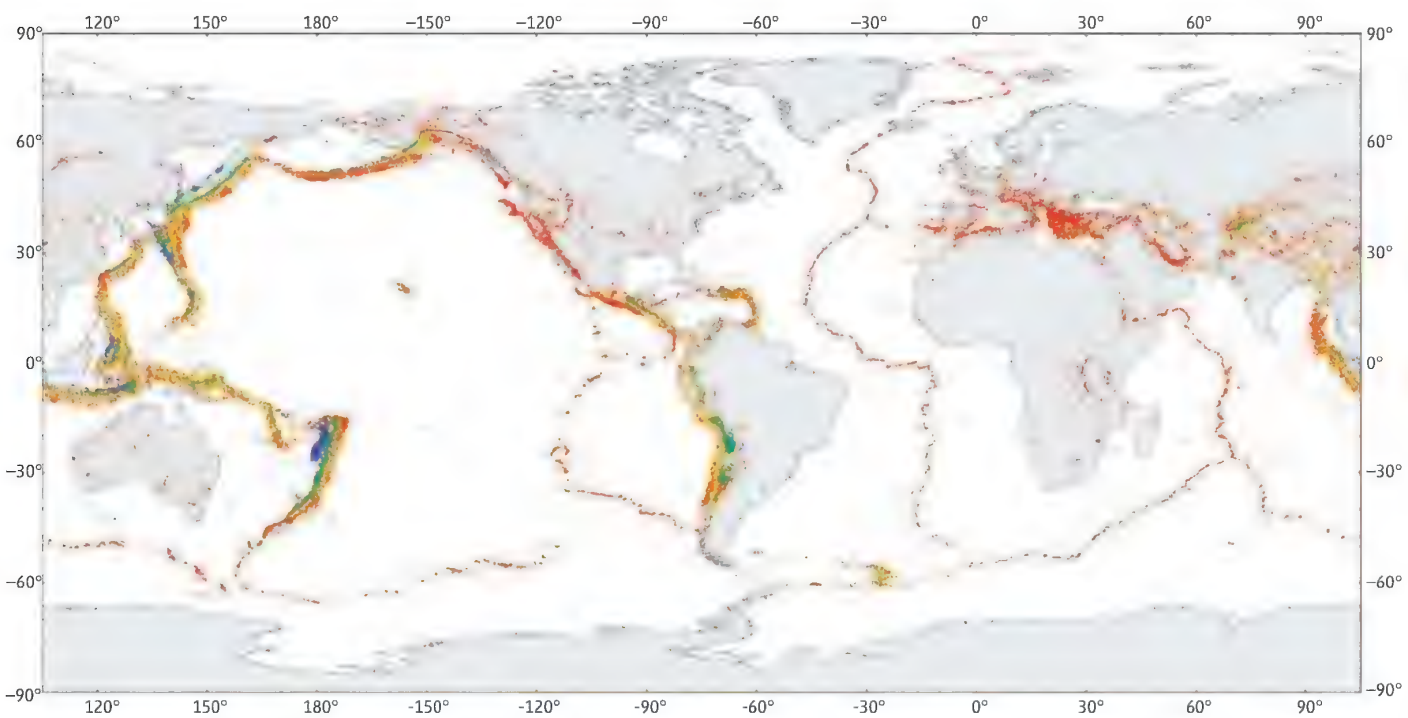

Earthquakes displayed. Global distribution of earthquakes greater than magnitude 3 from 2002 to 2011. Color represents the depth of the earthquake origin: red, 0–33 km; yellow, 33–100 km; green, 100–400 km; blue, >400 km.

PHOTO CREDIT: ANNE E. EGGER

finish class on time, and the questions were a challenge to grade fairly and boring to read.

Finally, I realized that having students navigate the USGS site was not my goal. Instead, I wanted them to be able to use and apply the information they found. The module's current three-part form leads from learning how to interpret the site to an in-depth exploration in which students have personal interest (*8*).

In the first part, students work in pairs on computers in class in highly structured inquiry (see the photo). After recalling that most earthquakes have occurred along the boundaries between the Earth's tectonic plates (see the map), students describe the distribution of recent seismicity around the world. They note that most, but not all, earthquakes fall into that familiar pattern. The class (35 to 80 students) is lively: Students exclaim when they see how many earthquakes have happened nearby, or how many occur in unexpected areas, and they ask a lot of questions. In class discussion, they volunteer interpretations for these "unexpected" earthquakes, and I provide feedback and a brief lecture about the causes (*8*).

Then the students drill deeper into one of those dots on the map. Each pair chooses a recent earthquake to look at in detail and to describe exactly which data were collected—and how. In discussion, they define the difference between earthquake magnitude (a measure of the energy released in the earthquake) and intensity (the extent to which it is felt at a particular place, which depends on several factors such as the earthquake magnitude, distance to the earthquake, and surface geology). They analyze the individual earthquake in the context of its location and tectonic setting. The first part of the exercise fosters the transition from an individual earthquake to the more abstract idea of how earthquakes relate to plate tectonics, providing them with the skills and understanding for simple analysis and interpretation.

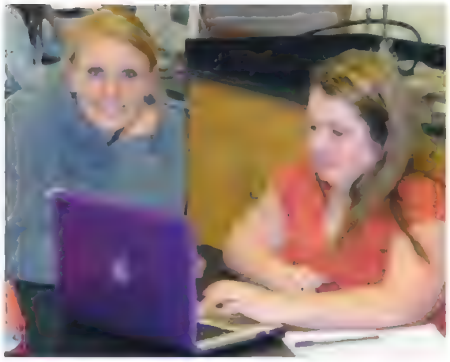

Exploring the USGS earthquake site.

They use these new skills in the second part of the module, which demands more abstract and open-ended inquiry. I ask students to write a brief paper summarizing the seismic activity of three different cities where they might move after graduating, in which they compare the risks associated with living in each location and choose which city they will live in (*8*). For a complete answer, students must determine which data about earthquakes are most relevant to a discussion of risk, formulate the appropriate questions to ask about those data, and assess the data to make a decision. There is no right answer, but students must justify their decisions.

This requires students to ask fundamental questions that may affect their lives. Is it riskier to live in a place with large, very deep earthquakes, or smaller-magnitude but shallower earthquakes? What about the tsunami danger? How prepared is the municipality to deal with a disaster? By personalizing the topic of earthquakes, I hope to provide situational interest in the topic, which has been shown effective in promoting learning (*9*). Although students sometimes express frustration that I do not tell them exactly what data they need, all of the information is easily accessible on the Web, and the exercise of using the USGS Web site provides them with the skills to search and access it.

A major advantage to this writing assignment is that each paper is unique, making them far more fun and interesting to grade than earlier versions of the assignment. I use a rubric for grading that emphasizes content, analysis, and coherence of the argument (*8*).

The final part of the module takes place in class after I have read their papers. I compile their decisions and show them the results. One location is never chosen unanimously, and the choices are often quite evenly spread, which prompts a discussion about which factors students weighed differently and why. Students gain a new appreciation for how different people interpret and weigh risk, as well as the inherently incomplete nature of the geologic record. I use this as an opportunity to lecture briefly on the complex role that science plays in policy and decision-making and about ongoing research on earthquakes and how students can get involved if they are interested.

One of my goals for this module is to empower students to use data to satisfy their own scientific curiosity, so they may be engaged in the scientific process beyond this introductory course. Many students have contacted me after the end of course to tell me that they looked up an earthquake that they felt, or pointed someone else to the Web site to see just how many earthquakes occur in the Bay Area every day; sometimes they have pointed out errors that they have heard in the news reports about earthquakes. By allowing students to work with real data in real time, they develop a personal connection and positive affect that motivates their future learning.

About the author

Anne E. Egger is an assistant professor at Central Washington University, jointly appointed in Geological Sciences and Science Education. The development and refining of this module took place while she was teaching at Stanford University, where she was a lecturer and the undergraduate program coordinator in the School of Earth Sciences. At Stanford, she extensively revised the introductory geoscience course to include more hands-on and inquiry-based activities such as this one. Egger's research involves combining the tools and techniques of geology and geophysics to better understand the geologic history of tectonically active regions. She is the codirector of Visionlearning (www.visionlearning.com), where she has authored modules for students in introductory science courses and coauthored a book titled *The Process of Science.*

PHOTO CREDITS: (TOP) ANNE E. EGGER; (BOTTOM) RICH VILLACRES/CENTRAL WASHINGTON UNIVERSITY

References and Notes

1. L. Barrow, S. Haskins, *J. Coll. Sci. Teach.* **26**, 143 (1996).
2. J. C. Libarkin, S. W. Anderson, *J. Geosci. Educ.* **53**, 394 (2005).
3. C. J. H. King, *Int. J. Sci. Educ.* **32**, 565 (2010).
4. J. M. Wampler, *J. Geosci. Educ.* **50**, 620 (2002).
5. S. Swenson, K. Kastens, *Spec. Pap. Geol. Soc. Am.* **474**, 189 (2011).
6. D. A. McConnell *et al., J. Geosci. Educ.* **53**, 462 (2005).
7. C. A. Manduca, D. W. Mogk, *Using Data in the Undergraduate Science Classroom: Final Report of an Interdisciplinary Workshop held at Carleton College, April 2002* [Science Education Resource Center (SERC), Carleton College, Northfield, MN, 2002].
8. A complete description of the module, including learning outcomes, guided exploration questions, slide presentations, writing prompts, and rubrics is available in the supplementary materials.
9. M. Ainley *et al., J. Educ. Psychol.* **94**, 545 (2002).

Acknowledgments: The module described in this article was developed while the author was employed at Stanford University and involved no additional funding. The module is fully documented assessments at SERC's Starting Point portal for teaching introductory level geoscience (http://serc.carleton.edu/introgeo/teachingwdata/examples/20816.html). I gratefully acknowledge the entire SERC staff and C. A. Manduca in particular.

Supplementary Materials

www.sciencemag.org/cgi/content/full/336/6089/1564/DC1

10.1126/science.1214293

INTERNATIONAL

Ambition, Challenges Shape S&T in Middle East, Northern Africa

Across the Middle East and North Africa, nations are embracing science as a way to drive economic development and improve the lives of their citizens. Some are investing heavily in universities and research centers, and several have space programs. Others are making strong commitments to science diplomacy.

But the region's researchers say they still face substantial challenges as they work to expand scientific capacity and pursue international partnerships. In a recent series of workshops cosponsored by AAAS and held in Jordan, Kuwait, Tunisia, and Dubai in the United Arab Emirates, the scientists said that young researchers in particular need better access to mentors, more opportunities to work with regional colleagues, and in some cases more funding and equipment. At the same time, they suggested, researchers must work closely with policy-makers to develop national scientific priorities.

"We can already see that governments and leaders in this part of the world are realizing that one of their best investments is to get younger people into science and technology," said Hayfaa Almudhaf, senior adviser to the director general of the Kuwait Institute for Scientific Research.

The workshops, organized by the AAAS Center for Science, Technology and Security Policy with institutions in the four host countries, focused on best practices in international bioscience. Gwenaële Coat, a senior program associate at the AAAS center, said some participants attended all the meetings to encourage region-wide representation in these research fields and ensure "the impact of the meetings will last for many years."

At the first meeting in October 2010 in Jordan, the participants realized that the workshops also were an excellent place to discuss broader challenges for the region's scientists. Two months later, however, popular protests in Tunisia marked the start of the Arab Spring movement. Revolutionary demonstrations spread throughout the region, and by the time the second workshop was held in Kuwait in March 2011, the upheaval had added a new layer of uncertainty to the region's prospects in science and technology.

The researchers were hopeful that new governments would support a higher profile for science. But their discussions had a different focus: Apart from any political change, how should scientists become more active in aligning research goals with national priorities? "Scientists keep discussing [these] issues in their own communities," Almudhaf said, "and think that the decision-makers will approach them first."

The workshops were especially valuable in highlighting some of these priorities, from clean water to infectious disease, which would benefit from stronger regional ties among researchers. "I think that there are a lot of learning opportunities between countries that have similar socioeconomic backgrounds and similar challenges," said Ayesha Abdullah, the managing director of Dubai Healthcare City. "But we don't yet have enough conferences and opportunities for networking."

Early career scientists who attended the last two workshops, held in Tunisia in November 2011 and in Dubai last March, spoke passionately about the need for more networking and mentorship.

"With young researchers, collaboration is easy to establish by Internet, but it's often limited to exchanging information," said Amel Benammar-Elgaaied, head of the genetics laboratory at the Faculty of Sciences of Tunis. Younger scientists, she said, need new ways to build relationships with established researchers in the region who are more likely to have financial and administrative support.

The researchers also have different needs depending on which country in the diverse area they come from, said Almudhaf. "The oil-rich countries in the Gulf might need more human resources" like mentors, she explained, "while in other parts of the region, funding is a critical factor."

These differences make it difficult to predict the Arab Spring's impact on young scientists, said Mona Mostafa Mohamed, the head of Cairo University's Cancer Biology Research Laboratory. In the North African countries at the epicenter of the uprising, she suggested, researchers who study abroad "for the time being might prefer to go and not to come back. They don't know how it's going to be yet."

Despite the uncertainties, the workshop participants pledged at the close of the Dubai workshop to write a collaborative article about their experiences and hold another regional conference in 2013. "I think with time, people will understand the importance of science and technology as a growth engine in developing countries," Abdullah said. "Science could be an answer to a lot of the challenges that the region faces." *–Becky Ham*

CREDIT: SESAME

Future vision. SESAME—Synchrotron-light for Experimental Science and Applications in the Middle East—represents the potential future of science and technology in the region. Now under construction in Jordan, the particle accelerator will foster ambitious, multidisciplinary research and build relationships across borders.

INTRODUCTION

Green Pathways

PLANTS USE COMPLEX METABOLIC PATHWAYS TO FEND OFF PATHOGENS, TO COORdinate reproduction with changes in day length, to accommodate environmental changes, and to select developmental pathways most suited to a given place and time. For these and other physiological processes, metabolism integrates inputs from both genome and environment. The process often involves the production and use of unusual chemicals that function for the plant as signals or defenses. Some of these chemicals are exploited by humans as pharmaceuticals, insecticides, spices, and nutritional supplements. This week, *Science* explores plant metabolism with a series of Reviews, Perspectives, and research Reports.

De Luca *et al.* (p. 1658) examine the diversity of plant chemical compounds used in medical settings and propose that we have the technology to discover even more useful compounds. Baxter and Dilkes (p. 1661) discuss the interplay between metabolic pathways and mineral elements available from the environment. Milo and Last (p. 1663) look for design principles that govern how metabolic pathways have arisen, insights that may help inform how we can in future tune metabolic pathways to our needs. Weng *et al.* (p. 1667) consider how the diversity of secondary metabolites may have arisen through permissive mutations, with core conserved proteins reserved for primary metabolism, where there is less room for error. And von Caemmerer *et al.* (p. 1671) discuss efforts to change photosynthesis in rice from the C_3 to the more efficient C_4 pathway, which would increase grain yield while reducing water and nitrogen needs. Finally, Gutiérrez (p. 1673) analyzes nitrogen metabolism, which lies at the core of agricultural productivity and is embedded in complex pathways of uptake and utilization.

In *Science* Careers (online), Sarah Webb explores career options in plant metabolism and uncovers work that is highly interdisciplinary, involving chemistry, biology, and computer science. Webb sees parallels between the field and translational work in biomedicine, in both the tools employed (molecular biology, analytical chemistry, and informatics) and in efforts to apply basic understanding to the solution of real-world problems.

In related research, Winzer *et al.* (p. 1704) identify a cluster of genes encoding several of the enzymes responsible for synthesis of the antitussive and anticancer alkaloid noscapine. Powell *et al.* (p. 1711) identify the transcription factor that, when mutated, led to nicely uniform tomatoes, only to discover that this same transcription factor, in normal form, promotes photosynthesis that elaborates the sugar content of the ripening fruit. Westfall *et al.* (p. 1708) present the crystal structures of enzymes that add tags to certain plant hormones, modulating their function. These examples highlight the diversity in metabolic pathways. Pathways pull components from various genetic tool kits; some of those components evolve independently and others do not. A push in one place can produce unexpected responses in other pathways. And metabolic pathways multiply with modifications, tweaks, and twinges every step of the way.

The 21st century brings new agricultural challenges as populations rise and land quality declines. Improved understanding of metabolic pathways can guide development of the crops and cultivation strategies that will form the foundation of a sustainable and plentiful harvest.

– PAMELA J. HINES AND LAURA M. ZAHN

Plant Metabolism

CONTENTS

Reviews

Perspectives

See also Perspective p. 1648; Reports pp. 1704, 1708, and 1711; and Science *Careers at http://scim.ag/PlantSci and* Science *Podcast at http://scim.ag/PlantPod*

Science

REVIEW

Mining the Biodiversity of Plants: A Revolution in the Making

Vincenzo De Luca,* Vonny Salim, Sayaka Masada Atsumi, Fang Yu

Only a small fraction of the immense diversity of plant metabolism has been explored for the production of new medicines and other products important to human well-being. The availability of inexpensive high-throughput sequencing is rapidly expanding the number of species that can be investigated for the speedy discovery of previously unknown enzymes and pathways. Exploitation of these resources is being carried out through interdisciplinary synthetic and chemical biology to engineer pathways in plant and microbial systems for improving the production of existing medicines and to create libraries of biologically active products that can be screened for new drug applications.

The vast chemical biodiversity of the plant world has been exploited for thousands of years by human cultures to prevent pain, to produce pleasure, for use in religious ceremony, and to cure various human diseases. The chemical entities responsible for this biological activity are small organic molecules that are often made in a limited number of plant species, a genus, a single family, or a few families. The fact that most individual molecules are restricted in their distribution to a particular taxonomic group has led to their traditional classification as "secondary" or more recently "special" (*1*) metabolites to differentiate them from "primary" metabolites present in all living plants. The traditional delivery of such remedies is through the consumption of therapeutic plants as food or as botanical formulations that are components of traditional pharmacopeias around the world. In contrast, scientific developments in industrialized countries have led to the identification of the individual active plant components involved and to the production of single-ingredient drugs via chemical synthesis. Today, nearly 25% of modern medicines are derived from nature, many of which were derived from traditional uses. Throughout the 20th century, single defined-ingredient drugs from natural extracts were increasingly replaced with synthetic molecules, which now are predominantly used in wealthy scientifically advanced nations; developing countries, comprising 80% of the world's population, rely primarily on ethnobotanical remedies. The most important commercially relevant pharmaceuticals to be derived from plants (Table 1) (*2*) are valued at over $25 billion (U.S.) per year. They include antineoplastic lignans (*Podophylum peltatum*); alkaloids or their synthetic derivatives with antineoplastic activity (*Catharanthus roseus* and *Camptotheca acuminata*); antigout agents (*Colchicum autumnale*); antitussive agents (*Papaver somniferum*); antiamoebic agents (*Psychotria ipecacuanha*); antimalarial agents (*Cinchona ledgeriana*); antihypertensive agents (*Rauvolfia serpentina*); cholinergic agents (*Physostigma venenosum*); emetics (*Psychotria ipecacuanha*); analgesic agents (*Papaver somniferum*); and terpenes and steroids with antineoplastic (*Taxus baccata*), antimalarial (*Artemisia annua*), adaptogenic (*Gingko biloba* and *Panax ginseng*), oral contraceptive (*Dioscorea mexicana*), and hormonal (*Dioscorea floribunda*) drug activities.

In spite of their biodiversity and value as ultimate sources of novel medicines, plant research in this area has declined as major pharmaceutical companies redeployed resources to combinatorial chemistry and computer-assisted design approaches for new drug discovery. The perceived disadvantages of traditional medicinal chemistry included low rates of lead compound discovery, slow and costly conversion of lead compounds to therapeutically useful forms, difficult and costly chemical syntheses, and difficulties with patent protection of products derived from nature. As new genomic, proteomic, and metabolomic tools were rapidly identifying molecular targets, together with the crystal structures of proteins responsible for different human diseases, industry switched to combinatorial chemistry and computer-assisted design of millions of virtual molecules together with high-throughput screening to produce new drugs. These efforts, accompanied by large increases in R&D spending, have not improved the rate of new drug discovery throughout the past decade (*3*). These trends, combined with our need to improve the supply of modern medicines and/or ethnobotanicals to the developing world, suggest that it is time to return to investigating plants as sources of new drugs. Highlighting this need is the fact that most of the developing world does not have access to opioids for the management of pain [the Pain Project (*4*)]. The main reason for the unavailability of painkillers may be the efforts to quell their illegal use and export to industrialized countries. However, safe precursors have been developed, such as opium poppy mutants grown in Tasmania (by the company Tasmanian Alkaloids) that accumulate thebaine, a safer precursor for the production of opioid drugs than codeine or morphine (*5*). If this innovation were applied to the cultivation of medicinal poppies around the world, it could decrease illicit poppy use.

Until recently, the elucidation of medicinally important plant biosynthetic pathways involved stepwise protein purification, protein sequencing, and use of the protein sequence to clone desired genes, followed by verification of gene function by recombinant protein expression in an appropriate host. A number of genes involved in the biosynthesis of the monoterpenoid indole alkaloids (MIAs) vindoline, catharanthine, ajmaline, and camptothecin have been identified, and most of the steps involved in morphine and taxol biosynthesis have been elucidated. Although this approach is slow and tedious, homology-based cloning approaches use sequence similarity to the newly discovered gene product to facilitate and speed up the cloning and functional identification of other gene family members. Unfortunately, this requires random testing of many members of the gene family, together with substrate availability, to determine whether a candidate gene is involved in the target pathway.

RNA interference (RNAi) is a general biological mechanism of living organisms to eliminate targeted mRNAs by a process known as homology-dependent gene silencing that controls many biological processes and pathways. The transformation of plants using RNAi involves the permanent introduction of short double-stranded RNA that interferes with the expression of the targeted gene. RNAi has been used to create transgenic poppies that accumulate the benzylisoquinoline alkaloid reticuline rather than the narcotic morphine (*6*). Because most medicinal plant species remain difficult to transform, target RNAi sequences associated with the surface of microscopic gold particles have been delivered as high-velocity projectiles into cells in order to trigger transient expression of RNAi. Many examples of successful transient RNAi have been reported to suppress or redirect the production of several metabolites. Similarly, virus-induced gene silencing (VIGS) technology exploits the ability of plant cells to mount an RNA-based defense that targets the genome of the invading virus (*7*). VIGS technology has many advantages, including its relatively low cost; it appears to be useful for an increasing number of plant hosts; and it is particularly useful for plants that are difficult to transform. Its disadvantages include the difficulty of achieving complete loss of function that may be required to display the required phenotype, the possibility that nontargeted

Department of Biological Sciences, Brock University, 500 Glenridge Avenue, St. Catharines, Ontario L2S 3A1, Canada.

*To whom correspondence should be adddressed. E-mail: vdeluca@brocku.ca

genes might also be suppressed, or the possibility that the phenotype produced by the suppression may produce toxic metabolites. Typically, the effectiveness of VIGS in suppressing host genes in any plant can be tested with virus vectors carrying components of carotenoid or chlorophyll biosynthesis to produce a white or photobleaching phenotype in the silenced sector. Successful VIGS has been used in Solanaceae species across a range of viral vectors (*8*) and has also been successfully applied to plants such as opium [*Papaver somniferum* (*9*)] and California poppy [*Eschscholtzia californica* (*10*)]. VIGS technology has identified genes involved in benzylisoquinoline alkaloid (BIA) biosynthesis and has helped identify the two reactions involved in the consecutive *O*-demethylation of thebaine to codeine and codeine to morphine in opium poppy (*11*). These demethylases provide the genetic tools necessary for generating thebaine- or codeine-accumulating poppy crops.

Furthermore, although tropane alkaloids (scopolamine, hyoscyamine, and atropine) have well-known human medical uses (Table 1) and their biosynthetic pathways have been well characterized, several key steps in their biosynthesis remain to be elucidated. Testing candidate genes encoding cytochrome P450s (CYP P450) of *Hyoscyamus niger*, representing tropane alkaloid pathway–enriched transcripts, with VIGS technology (*12*) identified a *CYP80F1* family member that when silenced showed preferential accumulation of littorine at the expense of hyoscyamine. Recombinant yeast lines expressing this gene converted littorine to hyoscyamine aldehyde and validated the results from the VIGS experiment (*12*). Although numerous MIA pathway genes from *Catharanthus roseus* have been well characterized at the biochemical and molecular levels, many more genes need to be characterized to complete these pathways (*13*, *14*). The successful VIGS-mediated suppression of 16-methoxy-2,3-dihydro-3-hydroxytabersonine *N*-methyltransferase (NMT) in *Catharanthus roseus* and targeted metabolic profiling of NMT-VIGS–silenced plants showed that they preferentially accumulated the NMT substrate 16-methoxy-2,3-dihydro-3-hydroxytabersonine rather than the downstream MIA vindoline (*15*). Validation of VIGS as a gene discovery tool in *Catharanthus roseus* should greatly speed up the discovery of the remaining MIA pathway genes required for making antineoplastic dimeric MIAs.

VIGS also may yield the substrates required to perform enzyme assays when confirming the biochemical functions of candidate genes, by expressing them in recombinant organisms. For example, demethylase-silenced opium poppies accumulated enough BIA intermediates that they were able to be purified with thin-layer chromatography (*11*) and used in functional expression studies in recombinant organisms. In contrast to thebaine and codeine, most of the substrates required to identify biochemical steps are involved in exotic pathways and are not commercially available. In many cases, chemical synthesis of such substrates has never been attempted or is extremely difficult to achieve. Thus the ability to produce required test substrates with VIGS provides an important tool for the functional characterization of candidate genes.

Recent improvements in RNA isolation from specialized plant cells have also allowed the speedy identification of entire biosynthetic pathways. For example, menthol and polymethylated flavone biosynthesis pathways (*16*) were identified by random sequencing of complementary DNA libraries of specialized glandular trichome cells of mint (*Mentha piperita*). This approach has identified a number of specialized pathways for the biosynthesis of a variety of glandular trichome–specific secondary metabolites (*1*). The assembly of the dimeric anticancer MIAs vinblastine and vincristine requires the biosynthesis of vindoline and catharanthine monomers in *Catharanthus roseus*. Random sequencing of RNA transcripts isolated from epidermal cells of *Catharanthus roseus* leaves (*13*) showed that most of the pathway for the assembly of anticancer MIAs is preferentially expressed in this specialized cell type (*14*). The biosynthesis of catharanthine in leaf epidermal cells was followed by its secretion to the leaf surface, whereas other vindoline pathway MIAs were transported to specialized internal mesophyl cells in the leaf to complete their conversion to vindoline (*13*, *14*) and thus were not represented in the leaf epidermis enriched transcript database (*13*). Four separate species of *Catharanthus* (*14*) exclusively accumulated catharanthine in leaf wax exudates, whereas vindoline was found within leaf cells, which explains why *Catharanthus* accumulates such low levels of the dimeric anticancer drugs.

The development of inexpensive large-scale sequencing tools, together with advances in obtaining proteomic and metabolomic information, is revolutionizing our ability to identify candidate genes involved in the biosynthesis of biologically

Table 1. Plant drugs of most economic value [modified from (*2*)]: codeine and morphine (*Papaver somniferum*); capsaicin (*Capsicum annuum, chinense*, and *fruitscens*); emetine (*Psychotria ipecacuanha*); atropine, hyoscyamine, and scopolamine (*Atropa belladonna, Datura stramonium*, and *Hysocyamus niger*); reserpine (*Rauvolfia serpentina*); artemisinin (*Artemisia annua*); quinine and quinoline (*Cinchona ledgeriana*); camptothecin (*Camptotheca acuminata*); vinblastine and vincristine (*Catharanthus roseus*); taxol (*Taxus baccata*); podophyllotoxin (*Podophylum peltatum*); yohimbine (*Rauvolfia serpentina*); quinidine (*Cinchona ledgeriana*); digoxin and digitoxin (*Digitalis purpurea*); galanthamine (*Narcissus pseudonarcissus*); physostigmin (*Physostigma venenosum*); pilocarpine (*Pilocarpus jaborandi*); diosgenin (*Dioscorea mexicana*); hecogenin (*Agave sisalana*); stigmasterol (*Glycine max*); ipecac (*Psychotria ipecacuanha*); sennenoside A and B (*Senna alexandrina*); cocaine (*Erythroxylon coca*); tubocurarine (*Chondrodendron tomentosum*); and nicotine (*Nicotiana tabaccum*)

Plant drugs of most economic value [modified from (2)]

analgesic **antitussive** codeine morphine capsaicin	**antiamoebic** emetine	**anticholinergic** atropine hyoscyamine scopolamine	**antihypertensive** reserpine	**antigout** colchicine
antimalarial artemisinin quinine quinoline	**antineoplastic** camptothecin vinblastine vincristine taxol podophyllotoxin	**aphrodisiac** yohimbine	**cardiac depressant** quinidine	**cardiotronic** digoxin digitoxin
cholinesterase inhibitor galanthamine	**cholinergic** physostigmin pilocarpine	**contraceptives hormonal drugs** diosgenin hecogenin stigmasterol	**emetic** ipecac	**laxative** sennoside A & B
local anesthetic cocaine	**muscle relaxant** tubocurarine	**smoking cessation** nicotine		

active metabolites. Large-scale transcriptome projects such as Phytometasyn (*17*, *18*), the Medicinal Plant Genomics Consortium (*19*), the Medicinal Plant Transcriptome Project (*20*), the Monocot Tree of Life Project (*21*), the 1000 Green Plant Transcriptome Project (*22*), and the Ancestral Angiosperm Genome Project (*23*) will aid in elucidating biosynthetic pathways and their evolution in plants. Having these transcriptomes in hand, combined with metabolic profiling, functional genomics, and systems biology approaches, is likely to reveal entire pathways for medicinal products. Candidate genes from large sequenced transcriptomes are now being used in VIGS projects, and when combined with metabolite profiling, will speed up the rate of discovery of genes involved in complex plant secondary metabolite pathways. These databases may be especially useful for new pathway discovery if a number of them are found as operon-like gene clusters, as was recently described for pathways leading to the biosynthesis of several defense compounds in *Arabidopsis*, barley, rice, and corn (*24*); and in opium poppy, where a 10-gene cluster involved in the biosynthesis of the antitumor alkaloid noscapine was located over 401 kb of genomic sequence (*25*).

Efforts are now under way to use recombinant technology to transfer medicinal production processes identified in plants to microorganisms or to other plant species. Recent successes (Fig. 1) include the production of resveratrol (*26*) and its improvement (*27*) in yeast and bacteria (*28*); artemisinic acid (*29*) and vanillin (*30*) in yeast; reticuline in bacteria (*31*) and in yeast (*32*); magnoflorine and scoulerine in yeast when fed with bacterially produced (*S*)-reticuline (*31*); taxadiene in yeast (*33*); and indoleglucosinolates in yeast (*34*). In most cases, however, the accumulation levels of these metabolites in microorganisms have remained low. In transgenic plants, the 3-step pathway for dhurrin biosynthesis was stably expressed in *Arabidopsis* (*35*), and the 13-step pathway for glucoraphanin biosynthesis was transiently expressed in tobacco (*Nicotiana bethamiana*) by using agroinfiltration (*36*). Transgenic *Arabidopsis* accumulating up to 4% dry weight of cyanogenic glucoside (*35*), using genes isolated from *Sorghum bicolor*, was highly resistant to flea beetles without significant transcriptomic and metabolomic effects on other endogenous activities. The successes of transient and stable expression approaches reflect the remarkable plasticity and potential of metabolic pathway engineering in plants.

An increasing number of genes involved in the biosynthesis of plant medicinal products have been crystallized. Using information obtained from the crystal structure of strictosidine synthase, mutants with expanded catalytic activity for a broader array of substrates were expressed in *Catharanthus* hairy roots together with soil bacteria halogenases. Transformed roots made chlorinated tryptophan, which was converted via tryptophan decarboxylase into chlorotryptamine derivatives and into chlorinated monoterpenoid indole alkaloids, including 10-chlorocatharanthine and 15-chlorotabersonine (*37*) (Fig. 1). This study showed that plants can serve as chemical factories by combining enzyme engineering, genes from microorganisms, and plant genetic engineering to produce non-natural MIAs that can be used to produce new MIA-based drugs that may cure disease while attenuating the side effects often associated with them. The majority of small molecules produced by plants remain to be tested for their possible biological activity and drug potential, because their levels in plants often remain below thresholds useful for testing purposes.

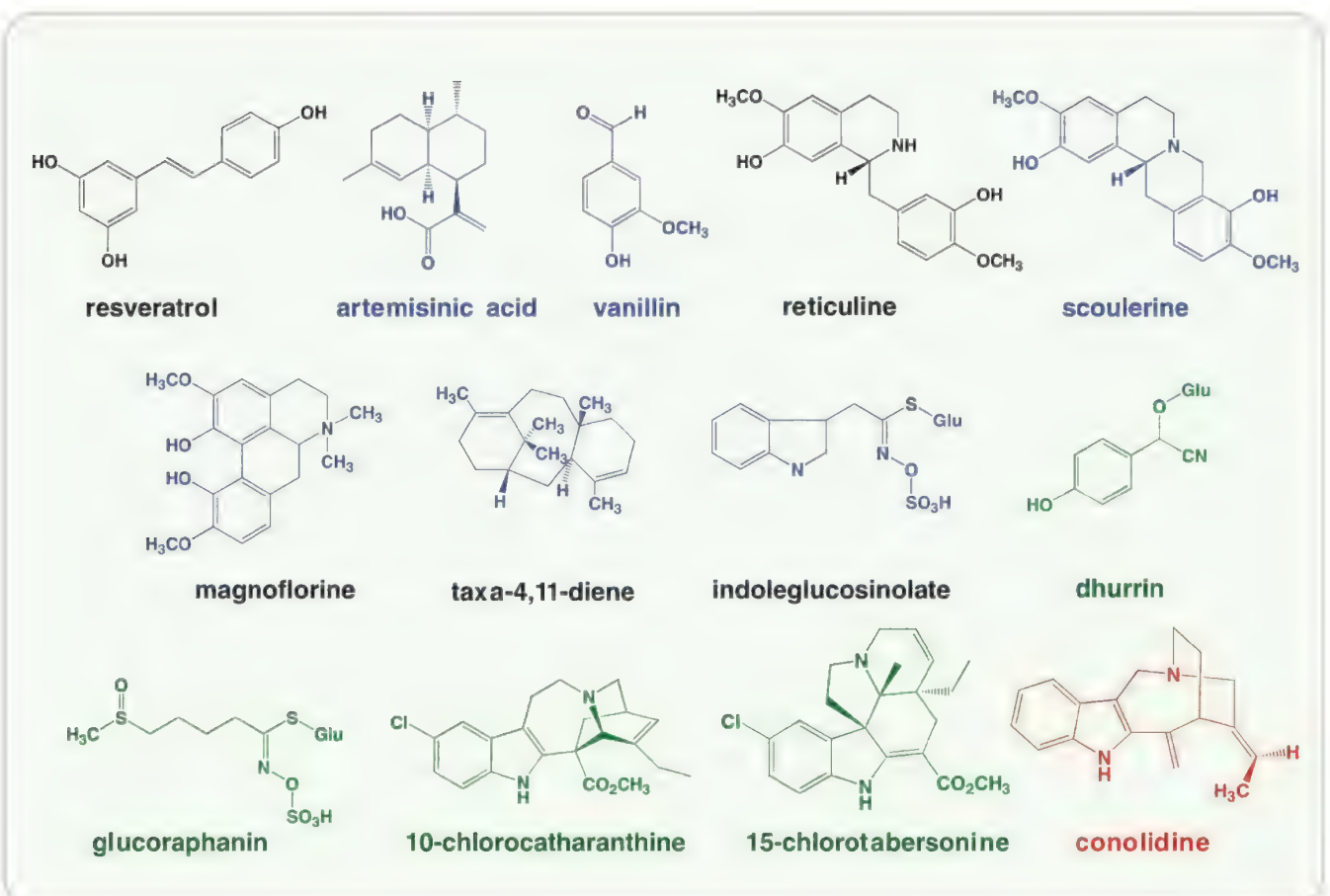

Fig. 1. Valuable secondary metabolites from plants that have been objects of pathway engineering in bacteria and yeast (black), in yeast (blue), and in plants (green). Conolodine (red) would be highly desirable to produce by pathway engineering in microorganisms or in plants.

Conolidine (Fig. 1) is an alkaloid first isolated from *Tabernamontana divaricata* together with a number of other MIAs with opioid analgesic properties. The rarity of this alkaloid (0.00014% yield from stem bark) precluded its testing for biological activity, and its de novo synthesis in sufficient quantities has shown that it is an effective nonopioid analgesic (*38*). Strictosidine is a central precursor of over 2000 different biologically active MIAs. Expression of the strictosidine pathway in a heterologous plant system such as tobacco or in microorganisms could be used as a scaffold for producing rare alkaloids such as conolidine by metabolic engineering of the remaining few steps.

Approximately two-thirds of new drugs in the past 25 years have originated from the discovery of particular secondary metabolites derived from natural biodiversity. This success has been attributed to the structural complexity of molecules found in living organisms, which have an average of 6.2 chiral centers per molecule as compared to an average of 0.4 chiral centers found in combinatorial libraries (*39*). Such chemically complex molecules are very difficult and costly to produce efficiently by chemical synthesis. A chiral center is defined as a carbon atom associated with four different atoms, so that their mirror images cannot be superimposed. The creation of new pathways in microorganisms and plants (Fig. 1) and the introduction of new reactions (*37*) or suppression of existing ones (*11*, *15*) in plants can be very effective for randomly generating previously unknown molecules. These could be biosynthetic intermediates from an existing pathway, or totally novel products could be produced from these intermediates (*18*). This should remove the bottleneck limiting the production of sufficient quantities of thousands of previously unknown metabolites with numerous chiral centers for testing and drug discovery. The affordability of genome sequencing adds a component to pathway discovery that can be combined with expression studies, functional analyses, and engineered plants to identify gene function across plant species. Such studies promise to reveal new biologically active secondary metabolites, making use of vast aspects of plant biodiversity for new drug discovery.

References and Notes

1. A. L. Schilmiller, R. L. Last, E. Pichersky, *Plant J.* **54**, 702 (2008).
2. I. Raskin *et al.*, *Trends Biotechnol.* **20**, 522 (2002).
3. www.imap.com/imap/media/resources/IMAP_PharmaReport_8_272B8752E0FB3.pdf.
4. www.internationalreporting.org/.
5. A. G. Millgate *et al.*, *Nature* **431**, 413 (2004).
6. R. S. Allen *et al.*, *Nat. Biotechnol.* **22**, 1559 (2004).
7. F. G. Ratcliff, S. A. MacFarlane, D. C. Baulcombe, *Plant Cell* **11**, 1207 (1999).
8. M. Senthil-Kumar, K. S. Mysore, *Trends Plant Sci.* **16**, 656 (2011).
9. L. C. Hileman, S. Drea, G. Martino, A. Litt, V. F. Irish, *Plant J.* **44**, 334 (2005).
10. S. Wege, A. Scholz, S. Gleissberg, A. Becker, *Ann. Bot. (London)* **100**, 641 (2007).
11. J. M. Hagel, P. J. Facchini, *Nat. Chem. Biol.* **6**, 273 (2010).
12. R. Li *et al.*, *Chem. Biol.* **13**, 513 (2006).
13. J. Murata, J. Roepke, H. Gordon, V. De Luca, *Plant Cell* **38**, 131 (2008).
14. J. Roepke *et al.*, *Proc. Natl. Acad. Sci. U.S.A.* **107**, 15287 (2010).
15. D. K. Liscombe, S. E. O'Connor, *Phytochemistry* **72**, 1969 (2011).
16. B. M. Lange *et al.*, *Proc. Natl. Acad. Sci. U.S.A.* **97**, 2934 (2000).
17. www.phytometasyn.com/
18. P. J. Facchini *et al.*, *Trends Biotechnol.* **30**, 127 (2012).
19. http://medicinalplantgenomics.msu.edu/
20. http://uic.edu/pharmacy/MedPlTranscriptome/index.html
21. www.botany.wisc.edu/givnish/monocotatol.htm
22. www.onekp.com
23. http://ancangio.uga.edu
24. H. Y. Chu, E. Wegel, A. Osbourn, *Plant J.* **66**, 66 (2011).
25. T. Winzer *et al.*, *Science* **336**, 1704 (2012); 10.1126/science.1220757.
26. J. V. W. Becker *et al.*, *FEMS Yeast Res.* **4**, 79 (2003).
27. Y. Wang *et al.*, *Metab. Eng.* **11**, 310 (2011).
28. C. G. Lim, Z. L. Fowler, T. Hueller, S. Schaffer, M. A. Koffas, *Appl. Environ. Microbiol.* **77**, 3451 (2011).
29. D. K. Ro *et al.*, *Nature* **440**, 940 (2006).
30. E. H. Hansen *et al.*, *Appl. Environ. Microbiol.* **75**, 2765 (2009).
31. H. Minami *et al.*, *Proc. Natl. Acad. Sci. U.S.A.* **105**, 7393 (2008).
32. K. M. Hawkins, C. D. Smolke, *Nat. Chem. Biol.* **4**, 564 (2008).
33. B. Engels, P. Dahm, S. Jennewein, *Metab. Eng.* **10**, 201 (2008).
34. M. D. Mikkelsen *et al.*, *Metab. Eng.* **14**, 104 (2012).
35. D. B. Tattersall *et al.*, *Science* **293**, 1826 (2001).
36. M. D. Mikkelsen, C. E. Olsen, B. A. Halkier, *Mol. Plant* **3**, 751 (2010).
37. W. Runguphan, X. Qu, S. E. O'Connor, *Nature* **468**, 461 (2010).
38. M. A. Tarselli *et al.*, *Nat. Chem.* **3**, 449 (2011).
39. M. Feher, J. M. Schmidt, *J. Chem. Inf. Comput. Sci.* **43**, 218 (2003).

Acknowledgments: This work was supported by a Natural Sciences and Engineering Research Council of Canada Discovery Grant (V.D.L.), Canada Research Chairs (V.D.L.), and a Genome Canada Team Grant.

10.1126/science.1217410

PERSPECTIVE

Elemental Profiles Reflect Plant Adaptations to the Environment

Ivan Baxter[1]* and Brian P. Dilkes[2]*

Most mineral elements found in plant tissues come exclusively from the soil, necessitating that plants adapt to highly variable soil compositions to survive and thrive. Profiling element concentrations in genetically diverse plant populations is providing insights into the plant-environment interactions that control elemental accumulation, as well as identifying the underlying genes. The resulting molecular understanding of plant adaptation to the environment both demonstrates how soils can shape genetic diversity and provides solutions to important agricultural challenges.

The majority of the elements that make up a plant, with the exception of carbon and oxygen, are obtained from soil through the roots. These soil-derived elements are required for plant structure, metabolism, protein function, signaling, and proper osmotic and electrochemical potential. Elemental accumulation requires the integration of processes across biological scales, including interactions with the soil matrix and biota, subcellular localization, metabolism, and gas exchange. Thus, the elemental composition of tissues [the "ionome" (*1*)] is a consequence of complex plant processes and plant-environment interactions.

[1]U.S. Department of Agriculture–Agricultural Research Service (USDA-ARS), Plant Genetics Research Unit, Donald Danforth Plant Science Center, St. Louis, MO 63132, USA. [2]Purdue University, West Lafayette, IN 47907, USA.

*To whom correspondence should be addressed. E-mail: ivan.baxter@ars.usda.gov (I.B.); bdilkes@purdue.edu (B.P.D.)

"Soil" is not a homogeneous entity at any scale. To adapt to element availability differences, which can vary across distances as small as a few meters (see Fig. 1), plants must alter their uptake and storage of both nutrients and toxic elements. Ionomic phenotyping of genetically distinct plants can identify alleles that alter element concentrations in tissues (*2*). The distribution of these alleles in plant populations can be related back to the soil characteristics of each plant's position on the landscape. This ecological genomics approach, comparing the spatial distribution of genetic polymorphisms affecting the ionome to soil composition, has begun to identify the genetic determinants of plant adaptation to the soils in which they grow (*3*, *4*).

The concentrations of distinct elements are interdependent and covary between genetic backgrounds and environmental conditions. Elemental species and compounds that are sufficiently similar in size and charge can be bound, metabolized, and transported by some of the same proteins, chelators, and pathways. This results in the coordinated accumulation of these chemically similar elemental species when the shared membrane transport proteins or chelating metabolites are up- or down-regulated. Examples include transport

of both Fe^{2+} and Zn^{2+} by an iron transporter (*5*), AsO_4^{3-} and PO_4^{3-} by phosphate transporters (*6*), and arsenite and silicic acid by silicic acid transporters (*7*). Similarly, the nonspecific chelator nicotianamine affects both iron and zinc accumulation in shoot vacuoles (*8*), and iron limitation increases leaf concentrations of zinc in *Arabidopsis thaliana* (*9*). Iron limitation also alters levels of molybdenum, which indicates that this covariation can include chemically dissimilar elements. Analyzing the ionome of recombinant inbred populations in several species (*10*–*13*) revealed multielement covariation networks that include many nonsimilar element pairs. The connections between elements in the covariation networks differed between genotypes, species, and environments. Plant responses to element limitation can affect nonintuitive sets of elements, which indicates that we have much to learn about how element accumulation is regulated. A future goal of ionomics research is to identify the molecular causes of this variation and to use genome sequences to identify orthologous processes across species.

Ionomic profiling of mutant populations is also identifying genes responsible for plant processes beyond membrane transport. In *A. thaliana*, the loss of either the *Enhanced Suberin 1* gene (*ESB1*) or the sphingolipid biosynthetic gene *TSC10A* increases suberin in the endodermis in roots (*14*, *15*). Both mutants accumulate more potassium, calcium, and iron in shoots. These multielement phenotypes were only observable by using the ionomics approach and provide genetic confirmation that the Casparian strip forms a barrier to transport for some elements, as hypothesized from histological evidence 147 years ago (*16*).

For traits that are responsive to the environment, extrapolating findings from a few environments or a few alleles will not be sufficient to explain the distribution of extant wild individuals or to predict the effects of changes in climate or land use. Multivariate differences in genotypes, soil types, climatic factors, and nutrients prohibit testing every combination. Alternatively, association mapping and population genetics use genetic markers and recombinant genotypes in extant populations to detect alleles of phenotypic consequence. The gene-level resolution of these approaches is an ideal complement to ionomics and other high-throughput phenotyping data. If the collection sites (wild) or preferred growth sites (domesticated) of the members of the population are known, environmental descriptors can be estimated for each accession. These environmental variables can be tested for correlation with allelic data to identify candidate genes as the molecular determinants of adaptation. For example, when 200,000 single-nucleotide polymorphisms (SNPs) were used to scan for signs of past selection in 1307 *A. thaliana* accessions, SNPs associated with laboratory-generated ionomic phenotypes (in 93 accessions) were overrepresented in regions that had undergone complete or nearly complete selective sweeps (*4*). This suggests that soil-driven selection plays a substantial role in patterns of diversity in *A. thaliana* and that ionomic profiling detects alleles with adaptive consequences across a wide range of environments.

The explanatory power of combining ionomics, association mapping, and environmental data is illustrated by studies of polymorphism in the Na^+ transporter HKT1. In *A. thaliana*, HKT1 knockouts exhibit altered sodium accumulation and sensitivity to salinity stress (*17*). Quantitative trait loci (QTLs) for sodium accumulation mapped to HKT1, and association mapping of sodium levels identified alleles of HKT1 that modulate leaf sodium accumulation (*3*, *18*). Colocalization of accessions with these alleles and high predicted soil sodium concentration implicate HKT1 in adaptation to sodic soils (*3*). The strength of this correlation is partly derived from the proximity of collection sites to the ocean, not exclusively from observed soil profiles. The resolution of current soil maps (at best ~10,000 m^2) and collection location metadata are likely insufficient to support most tests of soil-mediated selection; additional joint soil and accession collections may be required to obtain growth location environmental data.

Many questions regarding plant interactions with soil are best addressed in nonmodel plant species. For example, ionomic profiling of locally adapted plant species could help explain how certain species thrive on soils with radically different chemistries, such as serpentines (low calcium/magnesium ratio; low nitrogen, phosphorus, and potassium; and high heavy metals) (*19*). Such extreme conditions impose selective pressures on plants that result in fitness trade-offs such that sister taxa [e.g., *Lasthenia* (*20*)] can be found growing on either side of serpentine soil borders (Fig. 1) and even restricted to ionically distinct regions within a serpentine outcrop. Ionomic study of these forms of adaptation has the potential to uncover molecular mechanisms of adaptation and speciation. Identification of the genes responsible for adaptation to the environment, the role of soil-driven selection in patterns of genetic diversity, and the consequences and constraints imposed by plant physiology is now within our reach and could yield the necessary knowledge to make agriculture resilient to abiotic stress.

Production on most agricultural land is limited by soil elemental content (*21*). Adapting crops to overcome this constraint through improved genetics is an essential component of the effort to improve the human condition. Deficiencies of essential nutrients such as nitrogen, phosphorus, and potassium and excesses of toxic elements such as sodium and aluminum limit production in large parts of the developed and developing world. In addition to limiting yield, poor food quality—such as deficiencies in the essential nutrients iron, zinc, and calcium or excesses of the toxic elements arsenic and cadmium—can negatively impact human health. It is predicted that human population growth, soil nutrient depletion, and salinization by irrigation of fields will increase agricultural utilization of compromised soils. Fertilizer costs, already prohibitive for most farmers, will rise as the cost of producing nitrogen fertilizer rises and known reserves of phosphorus and potassium are depleted (*22*).

Fig. 1. Local soil variation can determine plant communities and performance. (**Left**) Soils surrounding serpentine outcrops have highly varied soil chemistries and plant species distinct from the surrounding environment inhabit them. (**Right**) Spatial variation in wheat plant performance due to saline soil. [Photos: (left) Nishanta Rajakaruna, (right) International Maize and Wheat Improvement Center (CIMMYT)]

However, substantial progress has been made in both ameliorating important elemental limits to crop production and improving food safety by utilizing a molecular understanding of elemental accumulation (*23*, *24*).

As an example of the former, analysis of wheat lines with an introgressed QTL for sodium tolerance identified an HKT1 allele that can extract Na^+ from xylem sap and thereby prevent sodium translocation to the shoots (*25*). Although a difference in leaf sodium was evident in all environments tested, yield gains were only evident where concentrations of sodium in the soil were highest. This confirms that, in the absence of meter-scale environmental information, heritable ionomic phenotypes are more informative for the adaptation of crop genotypes to high-sodium environment than yield and other complex traits that integrate many biological processes.

The shared transport of compounds containing arsenic and chemically similar molecules containing the nutrients silicon and phosphorus underlies both a global food safety crisis and its solution. In rice, silicic acid and phosphate transporters can also move arsenite and AsO_4^{3-}, respectively. Particularly in regions of Southeast Asia with high arsenic concentrations in groundwater, the promiscuity of these transporters is responsible for acute toxicity, disease, and shortened life spans because of dietary intake of arsenic via consumption of rice. Even in the United States, arsenic intake from rice increases breast cancer risk (*26*). Because we have a molecular understanding of arsenic uptake, breeding (*27*) and transgenic modification of crops with a transporter that sequesters arsenic in the root (*28*) have the potential to improve food safety and the health of hundreds of millions of people.

The prediction of tolerance to sodium stress by element accumulation measurements demonstrates that ionomics can accelerate crop improvement. This is complicated by the many agroecological challenges that limit yield and our insufficient understanding of the trade-offs that result from adaptation to particular soil conditions. Fortunately, the problem of local adaptation has been solved by evolution many times over. Ionomics and genetic association studies in model organisms and crops will directly identify alleles that promote element uptake or exclusion by plants. Using precise quantitative phenotyping of the ionome to characterize variation in plant-soil interactions, we are on the cusp of adding a new dimension to our understanding of why and how particular plants occupy their positions in the landscape and adapting agriculture to marginal soils.

References and Notes

1. D. E. Salt, I. Baxter, B. Lahner, *Annu. Rev. Plant Biol.* **59**, 709 (2008).
2. I. Baxter, *Briefings Funct. Genomics* **9**, 149 (2010).
3. I. Baxter *et al.*, *PLoS Genet.* **6**, e1001193 (2010).
4. M. W. Horton *et al.*, *Nat. Genet.* **44**, 212 (2012).
5. C. M. Palmer, M. L. Guerinot, *Nat. Chem. Biol.* **5**, 333 (2009).
6. F. J. Zhao, J. F. Ma, A. A. Meharg, S. P. McGrath, *New Phytol.* **181**, 777 (2009).
7. N. Mitani-Ueno, N. Yamaji, F. J. Zhao, J. F. Ma, *J. Exp. Bot.* **62**, 4391 (2011).
8. M. J. Haydon *et al.*, *Plant Cell* **24**, 724 (2012).
9. I. R. Baxter *et al.*, *Proc. Natl. Acad. Sci. U.S.A.* **105**, 12081 (2008).
10. E. Buescher *et al.*, *PLoS ONE* **5**, e11081 (2010).
11. A. Ghandilyan *et al.*, *J. Exp. Bot.* **60**, 1409 (2009).
12. M. A. Klein, M. A. Grusak, *Genome* **52**, 677 (2009).
13. R. P. Sankaran, T. Huguet, M. A. Grusak, *Theor. Appl. Genet.* **119**, 241 (2009).
14. I. Baxter *et al.*, *PLoS Genet.* **5**, e1000492 (2009).
15. D. Y. Chao *et al.*, *Plant Cell* **23**, 1061 (2011).
16. R. Caspary, *Jahrb. wissensc. Botanik* **4**, 101 (1865).
17. R. Munns, M. Tester, *Annu. Rev. Plant Biol.* **59**, 651 (2008).
18. A. Rus *et al.*, *PLoS Genet.* **2**, e210 (2006).
19. K. U. Brady, A. R. Kruckeberg, H. D. Bradshaw Jr., *Annu. Rev. Ecol. Evol. Syst.* **36**, 243 (2005).
20. J. M. Yost, T. Barry, K. M. Kay, N. Rajakaruna, *Am. J. Bot.* **99**, 890 (2012).
21. S. Wood, K. Sebastian, S. Scherr, *Pilot Analysis of Global Ecosystems: Agroecosystems* (International Food Policy Research Institute and the World Resources Institute, Washington, DC, 2000), pp. 45–54.
22. C. P. Vance, *Plant Physiol.* **127**, 390 (2001).
23. P. R. Ryan *et al.*, *J. Exp. Bot.* **62**, 9 (2011).
24. T. Sutton *et al.*, *Science* **318**, 1446 (2007).
25. R. Munns *et al.*, *Nat. Biotechnol.* **30**, 360 (2012).
26. D. Gilbert-Diamond *et al.*, *Proc. Natl. Acad. Sci. U.S.A.* **108**, 20656 (2011).
27. G. J. Norton *et al.*, *New Phytol.* **193**, 650 (2012).
28. G. Duan, T. Kamiya, S. Ishikawa, T. Arao, T. Fujiwara, *Plant Cell Physiol.* **53**, 154 (2012).

Acknowledgments: The authors acknowledge NSF (IOS-1126950), U.S. Department of Energy (DE-EE0003046), and USDA-ARS intramural funds.

10.1126/science.1219992

REVIEW

Achieving Diversity in the Face of Constraints: Lessons from Metabolism

Ron Milo[1] and Robert L. Last[2]*

Metabolic engineering of plants can reduce the cost and environmental impact of agriculture while providing for the needs of a growing population. Although our understanding of plant metabolism continues to increase at a rapid pace, relatively few plant metabolic engineering projects with commercial potential have emerged, in part because of a lack of principles for the rational manipulation of plant phenotype. One underexplored approach to identifying such design principles derives from analysis of the dominant constraints on plant fitness, and the evolutionary innovations in response to those constraints, that gave rise to the enormous diversity of natural plant metabolic pathways.

Metabolism meets two seemingly conflicting needs: responding dynamically to developmental and environmental changes while maintaining the homeostasis required by a living cell, organ, or whole organism. This challenge is especially acute for plants, which are sessile organisms that endure constantly changing environmental conditions over life spans ranging from weeks to hundreds of years. For example, carbon fixation and allocation in leaves responds dynamically to unpredictable changes in environment, with time scales ranging from minutes to months. Consistent with a need for rapid response, the turnover time of most key metabolites of central carbon metabolism is on the order of 1 s (*1*, *2*).

[1]Department of Plant Sciences, Weizmann Institute of Science, Rehovot 76100, Israel. [2]Department of Biochemistry and Molecular Biology and Department of Plant Biology, Michigan State University, East Lansing, MI 48824, USA.

*To whom correspondence should be addressed. E-mail: lastr@msu.edu

Plant metabolic phenotypes are the result of hundreds of millions of years of evolutionary history, during which some ancestral metabolic networks were restructured to meet the demands of changing environments while others remained close to their evolutionary ancient forms. For example, changes in temperature and aridity led to dozens of independently evolved variants of C4 metabolism for carbon fixation, even as the core process of the Calvin-Benson-Bassham pathway—which uses ribulose-1,5-bisphosphate carboxylase-oxygenase (RuBisCO) for carbon fixation—remained conserved (*3*–*5*). A current challenge in metabolism is to understand the physicochemical constraints on the structure and function of the metabolic network, and thereby gain insight into how evolution worked within these restrictions to shape the characteristics of extant plants.

Beyond Tinkering: The Utility of Design Principles for Plant Metabolic Engineering

Metabolic engineering promises opportunities to increase yield in agriculture and produce chemicals at lower economic and environmental cost. Despite progress, the rate of success in moving from concept to agricultural production or microbial fermentor has fallen short of expectations. For example, tens to hundreds of millions of dollars were spent in the public and private sector in

efforts to increase RuBisCO carboxylase activity and thus improve photosynthetic productivity of C3 plants. These studies yielded information about the structure and function of the enzyme but did not achieve the desired improvement in its kinetic properties (*6*). RuBisCO's kinetic properties seem already to be optimized by evolution (*7*, *8*). Thus, efforts in metabolic engineering have been limited by existing physicochemical constraints.

Metabolic engineering of a medically important plant metabolite, the antimalarial artemisinin (*9*), is said to have required an investment of more than $25 million and 150 person-years (*10*). One reason for the cost and complexity of the project is that it required the balanced expression of a large number of biosynthetic enzymes (*11*) to ensure a high production rate of the final product without leading to accumulation of deleterious reactive or toxic metabolic intermediates. Future metabolic engineering and synthetic biology projects demand better tools to predict which enzymes are key targets for adjusting expression and throughput.

To improve the efficiency and fulfill the promise of metabolic engineering, we must better understand the design and regulation principles governing metabolism. Understanding how evolution has led to designs that work well for the seemingly conflicting needs of stability and dynamic physiological responses might provide important clues.

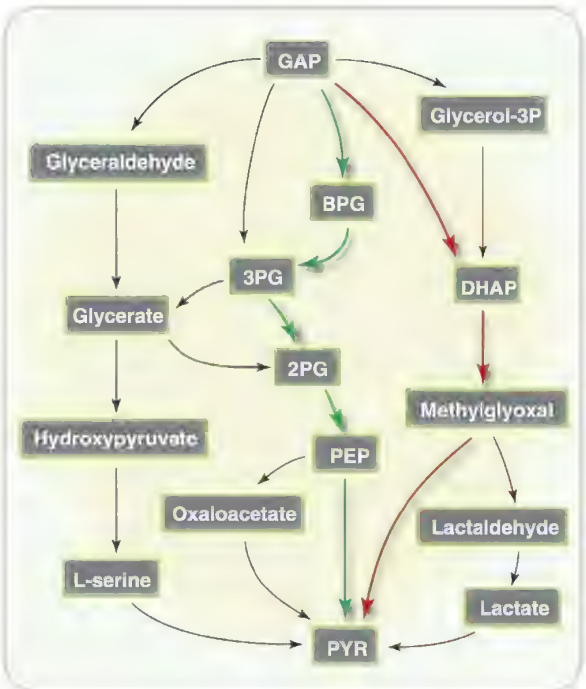

Fig. 1. The large number of alternative possibilities for metabolic transformations. Results from an analysis of the possible pathways for transforming glyceraldehyde-3-phosphate (GAP) into pyruvate (PYR), using the set of characterized enzymes from all organisms, are shown. The number of possibilities quickly increases as the number of steps becomes larger. The shortest theoretical path is denoted in red. The path used by Embden-Meyerhof-Parnas glycolysis is shown in green. 2PG, 2-phosphoglycerate; 3PG, 3-phosphoglycerate; PEP, phosphoenolpyruvate; DHAP, dihydroxyacetone phosphate.

Identification of Dominant Constraints Through Optimality Models

Using the concept of optimality (*12*), a fitness function is defined—for example, the production of a metabolite in the minimum number of steps—and the landscape of possible solutions is analyzed. The goal is to find the solution with the highest fitness given defined constraints. A constraint might be avoidance of highly reactive intermediates. The metabolic pathway derived is compared to the natural solution; a close correspondence would suggest that the constraints and fitness function analyzed might indeed be relevant. In contrast, if no correspondence is seen, the analysis would indicate that this is not the dominant constraint or fitness objective shaping the system. Although most work on optimality models was done in microbes, this approach is being extended to plant metabolism.

The space of possible paths for transforming an initial compound into a product is theoretically immense. Even with the limitation of using known enzymes with their canonical set of transformations encapsulated in the Enzyme Commission classes (oxidoreductases, transferases, hydrolases, lyases, isomerases, and ligases), there is still a combinatorial explosion of possible paths. However, the set of pathways found in nature, while showing biochemical diversity, is much smaller.

As an example, Fig. 1 illustrates the conversion of the key glycolytic metabolite glyceraldehyde-3-phosphate (GAP) to pyruvate. This can be achieved in numerous ways with known enzymes; there are seven options that each make use of five enzymes (the number of steps in Embden-Meyerhof-Parnas glycolysis, shown in green in Fig. 1) and more than 70 when allowing seven enzymatic steps. Some of these options are shown in Fig. 1, with the shortest path, which uses the highly reactive intermediate methylglyoxal, highlighted in red. The different paths vary in terms of their adenosine triphosphate (ATP) yield; number of steps; reactivity, stability, and toxicity of the metabolic intermediates (e.g., methylglyoxal); and thermodynamic feasibility.

These are only some of the possible constraints for a successful metabolic pathway (*13*). Uncovering the importance of these constraints is central to understanding the structure of metabolism and a key element in designing novel biosynthetic pathways. Examples of additional constraints are flux kinetics, investment in enzymes (protein cost), affinity and specificity, and whether intermediates are confined within subcellular compartments.

Analysis of the pentose phosphate pathway (PPP) (*14*) is an informative example of the application of optimality models to metabolism. In this analysis, the question was posed: How can five six-carbon sugars be converted into six five-carbon sugars with the minimal number of enzymatic steps? By choosing to constrain the possible reaction mechanisms to those catalyzed by known enzymes, the authors showed that the solution with the minimal number of steps is identical to the one arrived at by evolution. This analysis was recently extended to the central carbon metabolic network of *Escherichia coli* (*15*), in which the observed reaction network was found to connect the 13 precursor metabolites required to build biomass through the shortest paths. It remains to be seen whether optimality models can inform our understanding of pathways beyond central carbon metabolism, and whether these lessons can be tested and used in metabolic engineering.

In a very different approach, a flux balance analysis framework was used to predict the maximal possible yield of biomass per oxygen uptake rate on different carbon sources (*16*). This parameter was measured experimentally, leading to the conclusion that *E. coli* has close to the optimum predicted value for growth on glucose but is suboptimal for growth on glycerol. Lab evolution by propagation on glycerol for ~700 generations resulted in progressively improved growth, finally reaching the predicted optimum on glycerol.

The *E. coli* lac operon–encoded lactose utilization system is also being used to study factors contributing to optimality. One study investigated the impacts of altered expression of *lacZ*, the gene encoding the β-galactosidase enzyme, under varying concentrations of lactose (*17*). The protein cost is a quantification of the decrease in growth rate as a result of the expression of lacZ product; this could arise, for example, from ribosomes not being available for producing other proteins or because solvent capacity limits the total capacity of a cell to harbor proteins. The benefit measured is the increase in growth rate due to enhanced capacity to use lactose. Computationally maximizing the net difference between the cost and benefit gave predictions of optimal expression levels that varied according to the lactose concentration in the environment. These predictions were tested experimentally: After several hundred generations, *lacZ* expression levels adapted by mutation to achieve values close to those predicted. A recently published cost/benefit analysis of the lac operon presented evidence that activity, rather than expression, of the lacY lactose permease is the major physiological cost to the cell (*18*).

In addition to considering constraints and optimality principles of pathways and gene expression, it is informative to look at constraints on optimizing the building blocks of metabolism, enzymes. Some enzymes are considered optimal because they are able to perform catalysis at rates approaching the limit of diffusion; that is, the maximal turnover rate (k_{cat}) divided by the substrate affinity (K_M) is ~10^8 to 10^9 s^{-1} M^{-1}. However, very few metabolic enzymes are even close to this kinetic paragon status (*19*). A comprehensive analysis of nearly 2000 measured enzymes shows a distribution of turnover rates divided by affinities that peaks at ~10^5 s^{-1} M^{-1}, three orders of magnitude below the diffusion limit constraint (Fig. 2). In fact, the median maximal turnover rate value over all measured enzymes is ~10 s^{-1}—nowhere near the rates of 10^4 to 10^5 s^{-1} achieved by often-quoted record holders such as carbonic anhydrase and superoxide dismutase.

What limits typical enzymes from being better catalysts? The observed distributions suggest constraints other than the diffusion limit—for example, limitations on the affinity toward metabolites of low molecular weight as a consequence of maintaining specificity and to discriminate between compounds of similar structure. The trends in parameter values also suggest that the required flux might be an important determinant: Enzymes involved in central carbon metabolism are on average ~30 times faster than those involved in specialized metabolism (defined below and historically referred to as "secondary" metabolism; Fig. 2) (*20*). This might result from lower selective pressure for optimizing the kinetic parameters for maximal flux in specialized versus central metabolism.

Optimality model approaches aim to identify the forces that shape and constrain biological systems, rather than to ask whether biology is optimal. These studies sharpen our insight into likely important influences in the evolution of metabolic systems, yet the solutions might be different when driving forces vary. For example, even the fundamental process of carbon fixation, typically performed by the Calvin-Benson-Bassham pathway, is carried out in at least six alternative ways in various organisms (*21*). Similarly, there are a number of variants of glycolysis including the Entner-Doudoroff pathway. Such diversity is often suggested to be related to selective pressures from the organism's current or past ecological niche. Nowhere is this theme of metabolic diversity in the service of ecological adaptation more evident than in the realm of specialized metabolism.

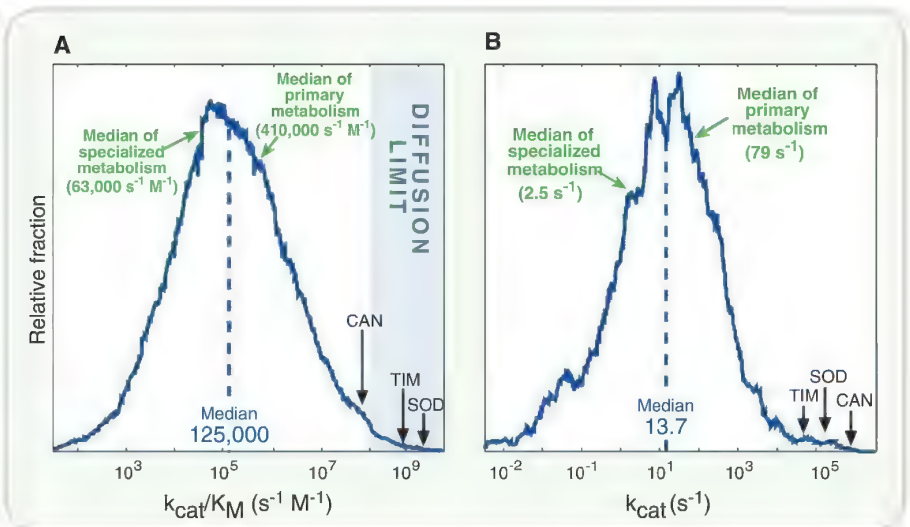

Fig. 2. Distributions of kinetic parameters compiled from published enzyme data. Only values obtained with natural substrates were included in the distributions. (**A**) Enzyme specificity constant (k_{cat}/K_M) values; N = 1882. (**B**) Enzyme turnover rate (k_{cat}) values; N = 1942. Enzymes operating within primary and specialized metabolism show markedly different k_{cat} and k_{cat}/K_M values. Numbers in parentheses represent the median values for each group. Locations of several well-studied and often quoted rapid enzymes are highlighted: CAN, carbonic anhydrase; SOD, superoxide dismutase; TIM, triosephosphate isomerase. [Adapted from (*19*)]

Constraints in the Land of Diversity: Evolving the Specialized Metabolism Buffet

In contrast to the products of central metabolism, specialized metabolites are diverse small molecules, each class of which is generally found in a subset of taxa. They are far more varied in structure than central metabolites, numbering in the hundreds of thousands of structures in the plant kingdom (*22*). Because of this complexity and their typical restriction to specific groups of plants, many enzymes of specialized metabolism are yet to be discovered. There is an increasing appreciation that these compounds serve a wide variety of physiological and ecological roles. For example, various roles for the taxonomically widespread and structurally diverse aromatic specialized metabolites have been documented, including the housekeeping function of protection against solar ultraviolet-B and specific signaling between legume roots and bacteria early in the establishment of symbiotic nitrogen fixation (*23*, *24*). Specialized

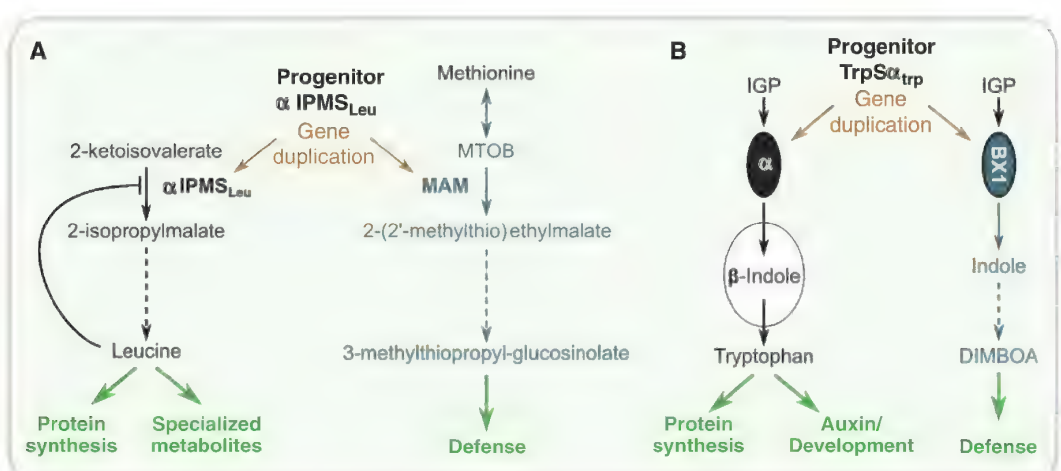

Fig. 3. Evolution of two enzymes of specialized metabolism by gene duplication and neofunctionalization. Enzymes and products of specialized metabolism are shown in blue, primary metabolism in black. Dashed lines indicate multiple enzymatic steps. (**A**) The committing enzyme of glucosinolate biosynthesis, MAM, evolved by duplication of a progenitor α-isopropylmalate synthase gene ($\alpha IPMS_{Leu}$). MTOB, 4-methylthio-2-oxobutanoate. (**B**) The maize BX1 indole synthase activity evolved from a progenitor TrpSα subunit. DIMBOA, 2,4-dihydroxy-7-methoxy-1,4-benzoxazin-3-one.

metabolites fulfill a diversity of adaptive roles for plants (*25*–*27*) and also serve as a source of many of the most important therapeutic agents in traditional and modern medicine.

We have a better understanding of the range of constraints and possible solutions for primary metabolism than for specialized metabolism. Nonetheless, it is instructive to attempt to infer some major constraints and design principles, inspired by the approaches in microbes and plant central metabolism. We propose that this strategy will lead to a better fundamental understanding of these fascinating and diverse metabolic networks, while improving our ability to engineer stress tolerance and synthesis of products useful to humankind.

One constraint is that the antimicrobial or antiherbivory functions of many characterized plant specialized metabolites are often associated with toxicity and chemical reactivity. How can such highly reactive compounds be safely produced and stored for a time of need? Strategies used by plants for alleviating the constraint of producing these toxic compounds include sequestration in subcellular compartments (such as the vacuole) and production or transport to specialized organs or cell types. For example, the pungent taste of mustard and horseradish is the result of glucosinolates; defensive compounds containing a reactive SCN group are kept in an inactive form via a glucose moiety (*28*, *29*). Tissue disruption by animal feeding unleashes the defensive activity of these compounds when glucosinolates come in contact with the enzyme myrosinase, and the combination rapidly produces nitriles, isothiocyanates, and other reactive and potentially noxious compounds. Thus, the plant avoids the toxic effects of glucosinolate degradation by sequestering the substrate metabolite and the enzyme in different cells or subcellular compartments until consumption by an herbivore. Another strategy used by many plants is storage of compounds in specialized structures. For example, epidermal hairs called glandular trichomes produce and store the metabolites that make basil and mint aromatic, whereas laticifers in opium poppy are the site of morphine accumulation.

Strong themes are emerging regarding the evolutionary and metabolic mechanisms for the synthesis of structurally diverse specialized metabolites. One is the recruitment of primary metabolic enzymes and pathways by gene duplication and acquisition of new enzymatic activities and biochemical regulatory mechanisms (e.g., altered allostery and protein-protein interaction, as discussed below). Another involves balancing the expression of central metabolic pathways with specialized metabolic pathway enzymes. For example, the regulation of amino acid biosynthetic pathways in plants is highly responsive to varied conditions that cause production of specialized metabolites from amino acids or their precursors (*30*).

Basing the production of specialized metabolites on the diversion of flux from central metabolism provides a source of abundant precursors but requires regulation at the branch point. One approach employed by evolution is duplication of a primary metabolic enzyme gene followed by alteration of enzyme activity and loss of regulation imposed by end-product feedback regulation on one of the resultant enzymes. An example is the evolution of methylthioalkylmalate synthase (MAM) in *Arabidopsis thaliana* and other mustard family plants, which leads to the protective glucosinolates (Fig. 3A) discussed above. This enzyme evolved from the committing enzyme of leucine biosynthesis: In addition to loss of feedback inhibition by leucine, the substrate specificity of the MAM enzyme has changed to catalyze the synthesis of glucosinolates (*31*). Together, these changes converted an enzyme of amino acid biosynthesis, which stringently regulates leucine production, into one that synthesizes a variety of alkyl glucosinolates. This example illustrates how relatively simple changes in protein structure and function can convert enzymes of central metabolism into those that divert flux for the production of specialized metabolites.

Indole synthase of maize (Bx1; benzoxazineless1), derived from the tryptophan synthase α (TrpSα) subunit, is an example of a gene duplication event leading to evolution of an enzyme with an unexpected activity (Fig. 3B) (*32*). The ancestral amino acid biosynthetic TrpSα enzyme requires interaction with a partner subunit (tryptophan synthase β; TrpSβ) for catalytic activity in organisms as diverse as bacteria and plants (*33*). In fact, the TrpSα product, indole, is channeled to the TrpSβ active site without being released from the complex. In contrast, indole synthase is a variant form of TrpSα that no longer interacts with the partner TrpSβ and converts the tryptophan pathway intermediate indole-3-glycerolphosphate (IGP) to indole in the committing step of synthesis of insecticidal and fungicidal cyclic hydroxamic acids. Thus, the evolution of chemical defenses in maize and other grasses accomplished a feat of protein engineering by eliminating the requirement for interaction between TrpSα and TrpSβ to produce indole for use as a precursor in specialized metabolism.

As is the case for carbon fixation and C4 metabolism described above, production of the same or functionally related metabolites is often achieved through different biosynthetic routes (*22*). Can optimality analysis identify constraints on specialized metabolic pathways by analysis of the alternative routes?

Monoterpenes and sesquiterpenes (hydrocarbons with carbon chain lengths of 10 and 15, respectively) are widespread in nature. Each class is produced by two enzymatic steps from the same five-carbon substrates: isopentenyl diphosphate and dimethylallyl diphosphate. Despite the use of common intermediates, the pathways are found in different compartments, and as a result, sesquiterpenes are typically derived from the cytosolic mevalonate pathway and monoterpenes from the plastidic deoxyxylulose 5-phosphate pathway. Glandular trichomes of cultivated tomato and a wild relative (*Solanum habrochaites* accession LA1777) produce and store large amounts of defensive monoterpenes or sesquiterpenes by analogous two-step pathways that are different from those of other organisms (*34*, *35*). Both enzymes arose from proteins that do not normally participate in these pathways: *cis*-polyprenyldiphosphate synthase and diterpene synthase. An outcome of this novel approach to specialized metabolism is that the synthesis of trichome sesquiterpenes in the wild tomato takes place in the plastid and uses substrates from the plastidic deoxyxylulose 5-phosphate pathway, rather than the cytosolic mevalonate pathway.

Two testable hypotheses come from comparing the evolutionarily reengineered pathways in trichomes to conventional terpene biosynthesis: (i) Moving sesquiterpene biosynthesis to the plastid allows higher flux production of these defensive compounds; (ii) freeing trichome metabolism from the canonical terpene biosynthetic pathway could reduce constraints on diversification, allowing faster evolution of novel chemistries in response to changing predator and pathogen populations.

Although the discovery of new plant metabolic enzymes and pathways is still labor-intensive, modern technologies allow this process to advance at an increasingly rapid pace. Rational engineering of plant function requires going beyond documenting the parts of the broad metabolic network toward developing a deep understanding of the fundamental principles that govern metabolic regulation. We suggest that there is value in uniting the diverse approaches discussed in this review, including the use of varied computational methods to generate hypotheses. In addition to providing new insights into metabolic networks, such efforts are essential for predictive metabolic and synthetic engineering that will help meet the looming crisis in providing food, energy, and materials for the rapidly growing world population.

References and Notes

1. M. Stitt, W. Wirtz, H. W. Heldt, *Biochim. Biophys. Acta* **593**, 85 (1980).
2. S. Arrivault *et al.*, *Plant J.* **59**, 826 (2009).
3. R. F. Sage, X. G. Zhu, *J. Exp. Bot.* **62**, 2989 (2011).
4. S. Weissmann, T. P. Brutnell, *Curr. Opin. Biotechnol.* **23**, 298 (2012).
5. S. von Caemmerer, W. P. Quick, R. T. Furbank, *Science* **336**, 1671 (2012).
6. S. M. Whitney, R. L. Houtz, H. Alonso, *Plant Physiol.* **155**, 27 (2011).
7. Y. Savir, E. Noor, R. Milo, T. Tlusty, *Proc. Natl. Acad. Sci. U.S.A.* **107**, 3475 (2010).
8. G. G. Tcherkez, G. D. Farquhar, T. J. Andrews, *Proc. Natl. Acad. Sci. U.S.A.* **103**, 7246 (2006).
9. D.-K. Ro *et al.*, *Nature* **440**, 940 (2006).
10. C. D. Smolke, P. A. Silver, *Cell* **144**, 855 (2011).
11. D. J. Pitera, C. J. Paddon, J. D. Newman, J. D. Keasling, *Metab. Eng.* **9**, 193 (2007).

12. G. A. Parker, J. Maynard Smith, *Nature* **348**, 27 (1990).
13. A. Bar-Even, A. Flamholz, E. Noor, R. Milo, *Nat. Chem. Biol.* **8**, 509 (2012).
14. E. Meléndez-Hevia, A. Isidoro, *J. Theor. Biol.* **117**, 251 (1985).
15. E. Noor, E. Eden, R. Milo, U. Alon, *Mol. Cell* **39**, 809 (2010).
16. R. U. Ibarra, J. S. Edwards, B. O. Palsson, *Nature* **420**, 186 (2002).
17. E. Dekel, U. Alon, *Nature* **436**, 588 (2005).
18. M. Eames, T. Kortemme, *Science* **336**, 911 (2012).
19. A. Bar-Even *et al.*, *Biochemistry* **50**, 4402 (2011).
20. J.-K. Weng, R. N. Philippe, J. P. Noel, *Science* **336**, 1667 (2012).
21. A. Bar-Even, E. Noor, R. Milo, *J. Exp. Bot.* **63**, 2325 (2012).
22. E. Pichersky, E. Lewinsohn, *Annu. Rev. Plant Biol.* **62**, 549 (2011).
23. L. G. Landry, C. C. Chapple, R. L. Last, *Plant Physiol.* **109**, 1159 (1995).
24. S. R. Long, *Plant Physiol.* **125**, 69 (2001).
25. N. K. Clay, A. M. Adio, C. Denoux, G. Jander, F. M. Ausubel, *Science* **323**, 95 (2009).
26. A. Weinhold, I. T. Baldwin, *Proc. Natl. Acad. Sci. U.S.A.* **108**, 7855 (2011).
27. P. Bednarek *et al.*, *Science* **323**, 101 (2009).
28. R. J. Hopkins, N. M. van Dam, J. J. van Loon, *Annu. Rev. Entomol.* **54**, 57 (2009).
29. B. A. Halkier, J. Gershenzon, *Annu. Rev. Plant Biol.* **57**, 303 (2006).
30. J. Zhao, C. C. Williams, R. L. Last, *Plant Cell* **10**, 359 (1998).
31. J. W. de Kraker, J. Gershenzon, *Plant Cell* **23**, 38 (2011).
32. M. Frey *et al.*, *Science* **277**, 696 (1997).
33. E. R. Radwanski, J. Zhao, R. L. Last, *Mol. Gen. Genet.* **248**, 657 (1995).
34. C. Sallaud *et al.*, *Plant Cell* **21**, 301 (2009).
35. A. L. Schilmiller *et al.*, *Proc. Natl. Acad. Sci. U.S.A.* **106**, 10865 (2009).

Acknowledgments: We thank A. Bar Even, A. Flamholz, A. D. Jones, E. Noor, A. Schilmiller, and T. Skaipe for input on the manuscript. Research in R.L.L.'s group is funded by NSF grants DBI-1025636 and MCB-1119778. Research in R.M.'s lab is funded by the European Research Council (grant 260392) and by the Israel Science Foundation (grant 750/09). R.M. is the incumbent of the Anna and Maurice Boukstein career development chair.

10.1126/science.1217665

REVIEW

The Rise of Chemodiversity in Plants

Jing-Ke Weng, Ryan N. Philippe, Joseph P. Noel*

Plants possess multifunctional and rapidly evolving specialized metabolic enzymes. Many metabolites do not appear to be immediately required for survival; nonetheless, many may contribute to maintaining population fitness in fluctuating and geographically dispersed environments. Others may serve no contemporary function but are produced inevitably as minor products by single enzymes with varying levels of catalytic promiscuity. The dominance of the terrestrial realm by plants likely mirrored expansion of specialized metabolism originating from primary metabolic pathways. Compared with their evolutionarily constrained counterparts in primary metabolism, specialized metabolic enzymes may be more tolerant to mutations normally considered destabilizing to protein structure and function. If this is true, permissiveness may partially explain the pronounced chemodiversity of terrestrial plants.

Plants produce a repository of structurally diverse chemicals, which are traditionally known as secondary metabolites, because many of them are not directly involved in central metabolism (*1*). The expansion of chemodiversity associated with secondary metabolites mirrors the tremendous adaptability of terrestrial plants. For instance, phytohormones regulate various aspects of plant growth and development in response to environmental cues, whereas phenolics and waxy cuticles act as ultraviolet sunscreens and prevent desiccation. Plant polymers such as lignin, sporopollenin, and rubber provide mechanical support, gamete protection, and wound healing. A variety of compounds, from pigments and flavors to volatile scents and antimicrobials, mediate an array of interspecies interactions that seduce pollinators and seed dispersers or deter pathogens and herbivores. Unlike primary metabolites required for central metabolism, specialized compounds are often biosynthesized in response to environmental cues or as a consequence of growth and development. In short, it is likely that these phytochemicals shape the interdependencies and diversity of plant ecosystems forming the base of the global food chain.

To date, genome comparisons across the green plant lineage suggest that the expansion of plant-specialized metabolism occurred concurrently with the colonization of land by plants approximately 500 million years ago (*2*). Necessary metabolic processes (for instance, the biosynthesis of phenylpropanoids and sporopollenin, likely prerequisites for the colonization of terrestrial habitats) became established during that period (*3*). New metabolic branches continuously arose throughout land-plant evolution, resulting in a contemporary repertoire of specialized metabolites, some of which are shared across various taxonomic groups, whereas others exist only in a single species (*4*, *5*).

The Emergence of Metabolism

Primordial metabolism is postulated to have consisted of chemical intermediates interconnected by a smaller number of multifunctional catalytic proteins, peptides, and/or RNAs (Fig. 1A) (*6*). Since its origin as a fundamental property of the cell, metabolism is generally regarded as having evolved toward increasing order and catalytic efficiency (Fig. 1A). Presently, enzymes belong to a handful of protein families, possess catalytic precision and kinetic speed, employ a limited repertoire of substrates, and produce a correspondingly narrow range of products (*6*).

Although the number of specialized metabolites and the enzymes required for their biosynthesis continues to expand, the number of protein folds associated with these enzymes is relatively restricted. In contrast to primary metabolism, in which selection constrained mutations to maintain the most stable and functional enzyme forms, we hypothesize that specialized metabolic enzymes may have emerged through early gene duplication, followed by mutations that broadened substrate selection and flattened activation barriers of their catalyzed reactions. The resulting mechanistic elasticity allowed single enzymes to catalyze multiple reactions and biosynthesize multiple products (Fig. 1A). This scenario is consistent with directed evolution focused on enzyme promiscuity (*7*, *8*) and the biochemical characterization of mutant libraries derived from phylogenetic relationships in several plant-specialized metabolic enzyme families (*9*–*11*).

Phylogenetic analyses suggest that catalytic expansion among many plant-specialized metabolic enzyme families arose once, suggesting that the initial event(s) separating primary and specialized metabolism were either very rare or rarely not deleterious and able to be maintained and eventually fixed within the population and/or species. However, following events such as gene duplication, alleles may occasionally function under relaxed selection such that at least one copy is able to accumulate mutations leading to greater mechanistic elasticity and, ultimately, neofunctionalization before the emergence of inactivating mutations. Expanded substrate recognition, flattened catalytic landscapes, and, consequentially, multiple products from a single enzyme are common in specialized metabolism (Fig. 1B). This contemporary observation hints that genetic drift and gene flow across populations can contribute to chemodiversity in the absence of toxicity or compromised organismal fitness due to a subset of minor products. In other cases, selection could favor specific functions or bias the emergence of multifunctional enzymes due to the advantageous use of multiple substrates and/or the formation of a set of ecologically beneficial products from a single enzyme or metabolic pathway.

Once a duplication-derived progenitor emerged, mutations may have loosened the energetic interdependencies of residues within the protein

Howard Hughes Medical Institute, Jack H. Skirball Center for Chemical Biology and Proteomics, The Salk Institute for Biological Studies, La Jolla, CA 92037, USA.

*To whom correspondence should be addressed. E-mail: noel@salk.edu

fold, which were previously fixed in the absence of a paralog (*12*). Even deleterious changes appearing in one paralog may be tolerated and not eliminated by selection, when the other paralog contributes to fitness. In such cases, the evolution of advantageous activities can now be favored in new environments. Neutral or deleterious allelic variations may also be retained due to genetic hitchhiking when the affected genes reside near loci under positive selection. The process of attenuating energetic interdependencies within an ancestral protein fold in subsequent generations may occur over a sufficiently short period of time to prevent nonfunctionalization. This, in turn, reshapes protein stability and dynamics as well as the enzyme catalytic properties, resulting in divergence of specialized enzymes from their origin in primary metabolism (Fig. 1B).

The chemically constrained catalytic landscapes of specialized enzymes that correlate sequence variation with catalytic properties bear little resemblance to those of primary metabolic enzymes. In primary metabolism, reactions are often catalyzed with high specificity accompanied by low levels of mechanistic elasticity; in short, the opposite of many specialized enzymes (Fig. 1B). Although protein structure is conserved in primary and secondary metabolism, increased catalytic promiscuity likely molded the evolution of specialized enzymes.

Supporting this view, a number of current specialized metabolic enzymes exhibit, on average, a greater ability to accept a broader range of substrates and to employ multiple energetically similar reaction mechanisms than related primary metabolic enzymes (*8*, *13*–*15*). Moreover, these enzymes seem to traverse functional space more easily than their structurally related cousins in primary metabolism to evolve new and often several metabolic products while retaining a modicum of their original function (*8*, *10*, *11*). Minimally, paralogs sporadically escaped nonfunctionalization to traverse functional space. Furthermore, specialized metabolic enzymes are ~30-fold less active than those of primary metabolism (*16*).

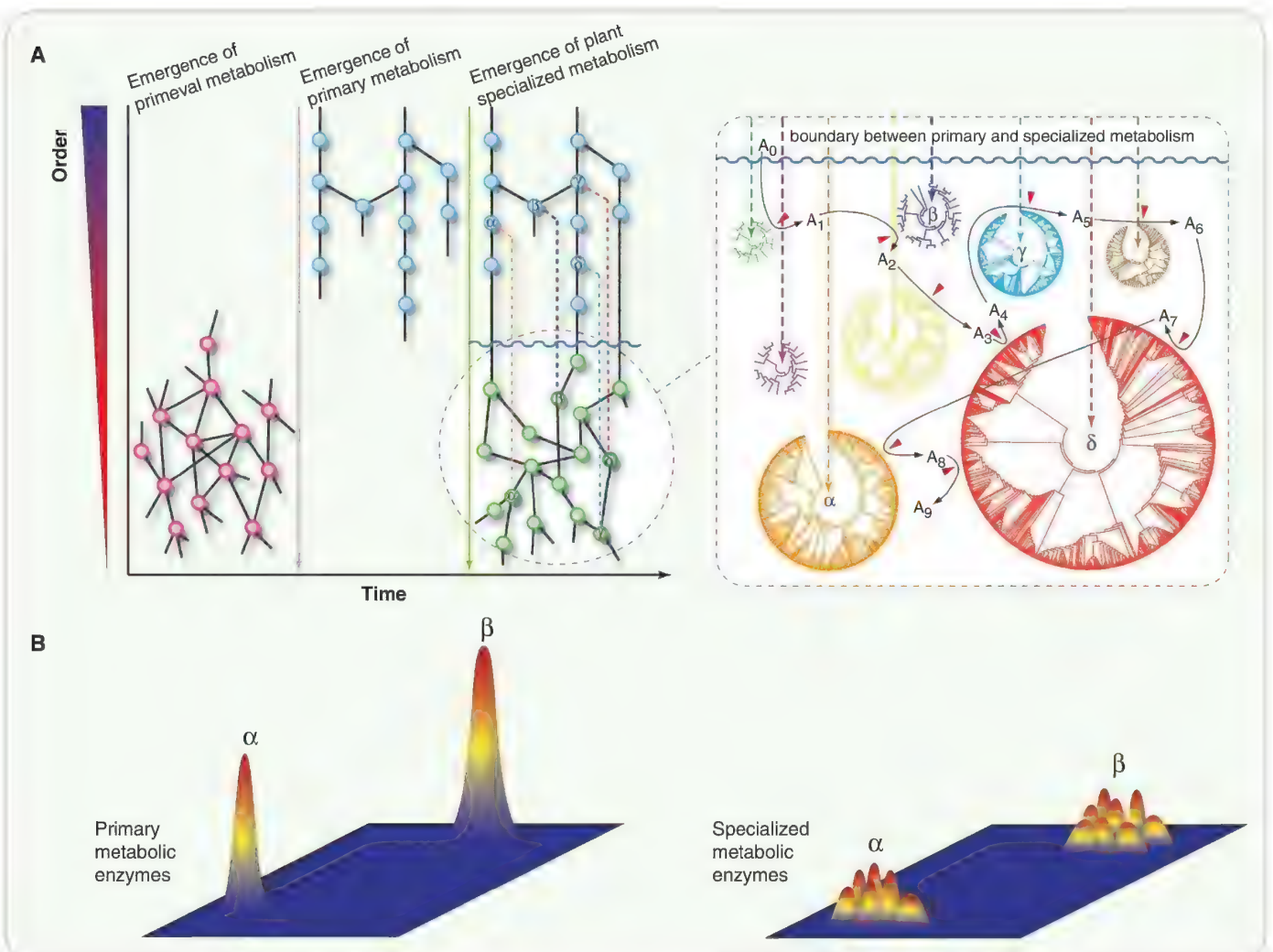

Fig. 1. Patterns of emergence and evolution of primary and specialized metabolism. (**A**) Primary metabolism likely arose from promiscuous primeval metabolic reactions and evolved toward greater catalytic precision and efficiency. Specialized metabolism likely emerged from primary metabolism. Due to early gene-duplication events, the functional constraints acquired by primary metabolic enzymes were released, allowing the mutational exploration of new areas of enzyme chemistry. Enzymes and reactions are represented by nodes (pink, blue, and green spheres) and links (black lines), respectively. The right panel illustrates the stepwise assembly of a specialized metabolic pathway using descendents from enzyme folds rooted in primary metabolism (indicated by circular phylogenetic trees and highlighted with Greek letters). Products of one reaction serve as substrates for another. Red arrowheads indicate the recruitment of single enzymes from protein families. (**B**) Hypothetical catalytic landscapes of primary and specialized metabolic enzymes relating sequence variation (horizontal plane) to the breadth of disparate enzymatic activities of stable protein folds (vertical axis). Catalytic specificity and efficiency for primary metabolic enzymes are maintained by natural selection, constraining their chemical mechanisms. Specialized metabolic enzymes often produce additional products from a single enzyme due to expanded substrate recognition and/or multiple chemical transformations within a single enzyme.

Diminished catalytic efficiency of multifunctional metabolic enzymes probably coincided with greater substrate permissiveness and the occurrence of several mechanistic routes to multiple products with little cost to the fitness of the host population. As long as the enzyme that must produce multiple products by virtue of its chemical mechanism yields at least one conferring a fitness advantage, the enzyme can be retained, barring issues of by-product toxicity. An enzyme does not have to evolve to perfection or absolute product specificity; it merely has to produce enough of the desired compound for the gene to be maintained in the population. As populations experience fluctuating abiotic and biotic ecological changes, one of the minor metabolites may also assume an advantageous function, thus resulting in fixation of the multifunctional paralog.

Molecular Exploitation of New Catalytic Space

Observed features of specialized metabolism include new catalysts emerging from progenitor enzymes catalyzing alternative reactions, or even from noncatalytic proteins. Positing that protein functional promiscuity serves as the starting point for functional innovation through natural selection (*7*, *11*), this property of specialized metabolic enzymes may be key to the rapid expansion of these systems. In some cases, the ancestral promiscuous activity can be inferred using a combination of biochemical and phylogenetic information. For instance, the evolution of rosmarinic acid biosynthesis in Lamiaceae herbs arose from gene duplication of a BAHD acyltransferase, where the progenitor enzyme probably exhibited low but measurable activity against a noncanonical substrate. After a gene-duplication event, one gene copy likely was selected for increased activity toward this substrate, resulting in the emergence of a new metabolic step (Fig. 2A) (*17*, *18*).

Refinement of a generalist ancestral enzyme into a catalytic specialist may also shape a metabolic trait. During anthocyanin biosynthesis in the *Iochroma* genus, dihydroflavonol reductase (DFR) catalyzes reduction of both dihydrokaempferol and its hydroxylated derivative dihydromyricetin. Thus, DFR serves two catalytic roles in parallel pathways resulting in red and blue pigments in flowers, respectively. In *I. gesnerioides*, DFR substrate recognition narrows substantially so that dihydrokaempferol is the preferred substrate, resulting in a derived red flower trait, deviating from the ancestral blue flower trait in the genus (Fig. 2B).

Moreover, enzyme families such as terpene synthases (TPSs) and type III polyketide synthases (PKS IIIs) exhibit a catalytic propensity to biosynthesize a multitude of products from a single enzyme (Fig. 2C) (*9*, *10*). The ability of TPSs and PKS IIIs to produce numerous products correlates with the nature of their bond-forming reactions, shaped by the facile reactivity of their catalytic intermediates (*19*).

Recurring Patterns of Metabolic Evolution

The phenotypic outcome of an evolving plant-specialized metabolic system relies on the recruitment of multifunctional enzymes from several radiating enzyme families into new pathways (Fig. 1A). Recent technological advances allow us to view the breadth of specialized metabolic

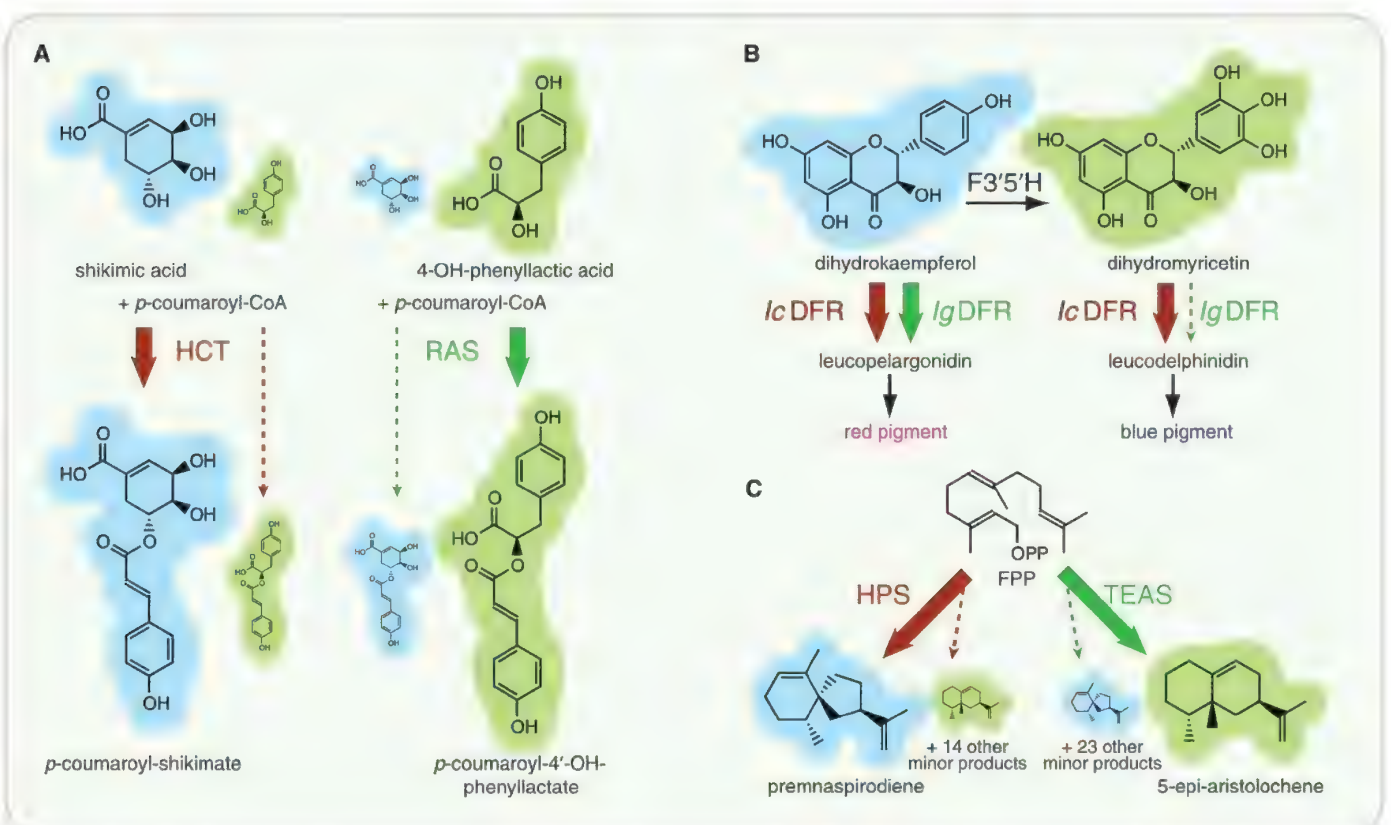

Fig. 2. Enzyme catalytic breadth underlies the expansion of chemodiversity in plant-specialized metabolism. (**A**) The emergence of rosmarinic acid synthase (RAS) in Lamiaceae likely followed substrate permissiveness of its evolutionary progenitor HCT, a more conserved enzyme ubiquitous in land plants. (**B**) By exploiting the broader substrate recognition of ancestral DFR, *I. gesnerioides* evolved a red flower color, deviating from the blue color common in the *Iochroma* genus. F3′5′H, flavonoid 3′5′ hydroxylase. (**C**) *Hyocyamus muticus* premnaspirodiene synthase (HPS) and *Nicotiana tabacum* 5-epiaristolochene synthase (TEAS) produce a multitude of products intrinsic to the elevated reactivity of multiple chemical intermediates in the TPS family. In the TEAS/HPS subfamily, this relaxed specificity leads to a diversity of minor products and distinct major products that provide antimicrobial defense in the *Solanaceae*. OPP, pyrophosphate; FPP, farnesyl pyrophosphate.

networks (*20*) and recognize recurring patterns of relaxed substrate recognition and energetically similar chemical mechanisms in individual enzymes affording incorporation into emerging metabolic pathways.

Typically, a handful of metabolites are co-opted by functionally diverse enzymes and serve as chemical "hubs" from which new metabolic paths often emerge in both primary and specialized metabolism. For example, acyl–coenzyme As (acyl-CoAs) serve as substrates for at least three enzyme families in primary and specialized metabolism. These include acyltransferases, NADH/NADPH-dependent reductases (NADH, the reduced form of nicotinamide adenine dinucleotide; NADPH, the reduced form of nicotinamide adenine dinucleotide phosphate), and ketoacyl synthases encompassing specialized PKS IIIs. In plant-specialized metabolism, the acyl-CoA, *p*-coumaroyl-CoA is a hub metabolite used by enzymes drawn from all three of these enzyme families, yielding structurally and functionally diverse phenylpropanoids. Moreover, metabolic pathways branching from these hubs are often taxonomically distributed, suggesting that at least some of these branches emerged after the initial chemical hubs were fixed in most organisms.

In addition to the recruitment of individual enzymes into emerging pathways, enzymes with expanded substrate recognition that act consecutively in a particular pathway can reappear, operating on disparate metabolites. For example, three catalytically sequential enzymes of the lignin biosynthetic pathway—hydroxycinnamoyl-CoA:shikimate hydroxycinnamoyl transferase (HCT), *p*-coumaroyl shikimic acid 3′-hydroxylase, and caffeoyl CoA 3-*O*-methyltransferase—duplicated and underwent neofunctionalization in the Brassicaceae family such that they function in hydroxycinammoyl-spermidine biosynthesis (*18*). Similar recruitment of a segment of the lignin biosynthetic pathway also occurred independently in the Lamiaceae, resulting in rosmarinic acid biosynthesis (*21*).

In some cases, specialized metabolic pathways are encoded as gene clusters in plant genomes as seen in maize (*22*), rice (*23*), *Arabidopsis* (*24*), oat (*25*), and *Selaginella* (*26*), suggesting that the evolution of gene clustering of some metabolic pathways provides a selective advantage. Indeed, the clustering of metabolic genes in plants probably facilitates efficient inheritance, as these genes are less likely to be broken up by recombination. Moreover, the physical proximity of genes can coordinate transcription through additional genomic and epigenetic mechanisms.

Future Directions

Although a few studies have interrogated the minimum set of mutations that dictate the emergence of specific functions in divergent plant-specialized metabolic enzymes (*9*, *10*), no particular study has addressed all viable mutational paths in these metabolic systems. This limits our ability to postulate evolutionary scenarios consistent with the stepwise assembly of mechanistically divergent metabolic pathways within the framework of Darwinian evolution and to quantify the incremental emergence of new activities with each mutational step. Could specialized metabolic enzymes and their pathways evolve along a wider set of evolutionary trajectories than their cousins in primary metabolism?

The lineage-specific birth of new metabolic pathways often involves neofunctionalization after gene duplication. Statistical coupling analysis (SCA), which measures covariation between pairs of amino acids on the basis of protein multiple-sequence alignments, can point to probable biophysical traits underpinning the emergence, expansion, and neofunctionalization of specialized metabolic enzyme families (*27*). The interconnected sets of covarying residues often form three-dimensional sector(s) that correlate with specific functionalities of a given protein family (*27*). The outcome of these analyses of primary and specialized metabolic enzymes sharing a common fold may provide biophysical hints to adaptive changes relating to substrate recognition, mechanistic elasticity, and protein structure and dynamics. Ultimately, covariation shapes an ensemble of dynamically accessible enzyme conformations in solution. These motions are undoubtedly linked with varying levels of relaxed catalytic trajectories often separating specialized metabolic enzyme families from their functionally constrained cousins in primary metabolism (*28*).

Ancestral sequence reconstructions, potentially guided by SCA, may offer additional insights into the evolutionary lineages of extant specialized metabolic enzymes (*11*, *29*). The reconstructed ancestral sequences are unlikely to represent exact alleles that were fixed in the ancestral population. Nevertheless, if one chooses species with sound phenotypic relationships such as time of divergence, overlapping chemical repertoires, and comparable developmental programs, a collection of calculated sequences should reasonably approximate ancestral sequences. Given that the biochemical functions of many specialized enzymes are typically influenced by a small fraction of their total residues, the ancestral reconstructions may then serve as useful approximations of what might have functionally occurred during the emergence and expansion of particular specialized enzyme families.

Given the widespread occurrence of catalytic promiscuity in specialized metabolism, it is also important to consider that enzymes possessing mechanistic elasticity use varied substrates and produce diverse products to create pools of chemicals that may not be directly selected against. In essence, certain (currently) nonuseful chemicals can be found in a plant due to catalytic linkage, as the enzyme producing a beneficial compound inevitably synthesizes by-products due to the high intrinsic reactivity of chemical intermediates accompanying its catalytic mechanism.

The remarkable chemodiversity in plants and its underlying metabolic diversity are reached via exploration of sequence space restrained by enzyme catalysis, protein stability, emerging and extant metabolic pathways, and, ultimately, organismal fitness. The ability to bridge the fields of evolutionary biology, chemistry, biophysics, and mechanistic enzymology to cooperatively tackle the complexity of specialized metabolism will provide a more informed understanding of the amazing tapestry of plant-specialized metabolites that are so essential to the sessile lifestyle of plants.

References and Notes

1. G. S. Fraenkel, *Science* **129**, 1466 (1959).
2. J. A. Banks *et al.*, *Science* **332**, 960 (2011).
3. J. K. Weng, C. Chapple, *New Phytol.* **187**, 273 (2010).
4. S. E. O'Connor, J. J. Maresh, *Nat. Prod. Rep.* **23**, 532 (2006).
5. R. Croteau, R. E. Ketchum, R. M. Long, R. Kaspera, M. R. Wildung, *Phytochem. Rev.* **5**, 75 (2006).
6. R. Fani, M. Fondi, *Phys. Life Rev.* **6**, 23 (2009).
7. A. Aharoni *et al.*, *Nat. Genet.* **37**, 73 (2005).
8. Y. Yoshikuni, T. E. Ferrin, J. D. Keasling, *Nature* **440**, 1078 (2006).
9. M. B. Austin, M. E. Bowman, J. L. Ferrer, J. Schröder, J. P. Noel, *Chem. Biol.* **11**, 1179 (2004).
10. P. E. O'Maille *et al.*, *Nat. Chem. Biol.* **4**, 617 (2008).
11. R. Huang *et al.*, *Proc. Natl. Acad. Sci. U.S.A.* **109**, 2966 (2012).
12. E. A. Ortlund, J. T. Bridgham, M. R. Redinbo, J. W. Thornton, *Science* **317**, 1544 (2007).
13. E. K. Lim *et al.*, *J. Biol. Chem.* **276**, 4344 (2001).
14. L. Kienow *et al.*, *J. Exp. Bot.* **59**, 403 (2008).
15. J. G. Kopycki *et al.*, *J. Mol. Biol.* **378**, 154 (2008).
16. A. Bar-Even *et al.*, *Biochemistry* **50**, 4402 (2011).
17. C. Landmann *et al.*, *Planta* **234**, 305 (2011).
18. M. Matsuno *et al.*, *Science* **325**, 1688 (2009).
19. M. B. Austin, P. E. O'Maille, J. P. Noel, *Nat. Chem. Biol.* **4**, 217 (2008).
20. A. L. Schilmiller, E. Pichersky, R. L. Last, *Curr. Opin. Plant Biol.* **15**, 338 (2012).
21. M. Petersen *et al.*, *Phytochemistry* **70**, 1663 (2009).
22. M. Frey *et al.*, *Science* **277**, 696 (1997).
23. K. Shimura *et al.*, *J. Biol. Chem.* **282**, 34013 (2007).
24. B. Field, A. E. Osbourn, *Science* **320**, 543 (2008).
25. X. Qi *et al.*, *Proc. Natl. Acad. Sci. U.S.A.* **101**, 8233 (2004).
26. J. K. Weng, T. Akiyama, J. Ralph, C. Chapple, *Plant Cell* **23**, 2708 (2011).
27. N. Halabi, O. Rivoire, S. Leibler, R. Ranganathan, *Cell* **138**, 774 (2009).
28. N. Tokuriki, D. S. Tawfik, *Science* **324**, 203 (2009).
29. P. D. Williams, D. D. Pollock, B. P. Blackburne, R. A. Goldstein, *PLOS Comput. Biol.* **2**, e69 (2006).

Acknowledgments: This work was supported by grants from the NSF. J.-K.W. is supported by a postdoctoral fellowship from the Pioneer Fund; R.N.P. is supported by a postdoctoral fellowship from the Natural Sciences and Engineering Research Council of Canada; and J.P.N. is an investigator with the Howard Hughes Medical Institute.

10.1126/science.1217411

PERSPECTIVE

The Development of C_4 Rice: Current Progress and Future Challenges

Susanne von Caemmerer,[1]* W. Paul Quick,[2] Robert T. Furbank[3]

Another "green revolution" is needed for crop yields to meet demands for food. The international C_4 Rice Consortium is working toward introducing a higher-capacity photosynthetic mechanism—the C_4 pathway—into rice to increase yield. The goal is to identify the genes necessary to install C_4 photosynthesis in rice through different approaches, including genomic and transcriptional sequence comparisons and mutant screening.

As the world population races toward 10 billion, agricultural scientists are realizing that another "green revolution" is needed for crop yields to meet demands for food. In rice, yield potential is limited by the photosynthetic capacity of leaves that, as carbohydrate factories, are unable to fill the larger number of florets of modern rice plants. One potential solution is to introduce a higher-capacity photosynthetic mechanism—the C_4 pathway—into rice. This is the goal of researchers in the international C_4 Rice Consortium: to identify and engineer the genes necessary to install C_4 photosynthesis in rice (*1*).

Rubisco, the primary CO_2-fixing enzyme in rice, is a poor catalyst of CO_2 at current atmospheric conditions. It has a tendency of confusing its substrate CO_2 with the more abundant O_2 as well as being a very slow catalyst of CO_2, turning over only once or twice per second. Rubisco's oxygenase activity requires the recycling of phosphoglycolate in the photorespiratory pathway, resulting in an energy cost and loss of previously fixed CO_2. Many photosynthetic organisms, including cyanobacteria, algae, and land plants, have developed active CO_2-concentrating mechanisms to overcome Rubisco's inefficiencies (*2*). Among land plants, this led to the development of C_4 photosynthesis, a biochemical CO_2-concentrating mechanism. C_4 photosynthesis arose multiple times in the past 60 million years in warm semi-arid regions, with early occurrences coinciding with low atmospheric CO_2 in the late Oligocene (*3*). During C_4 photosynthesis, CO_2 is fixed within specialized leaf tissues known as mesophyll cells to produce C_4 acids, which diffuse to and are decarboxylated in another type of specialized tissue, the bundle sheath cells. This process elevates the CO_2 concentration in the bundle sheath and inhibits Rubisco oxygenase activity, allowing Rubisco to operate close to its maximal rate (Fig. 1). In comparison with C_3 crops such as rice, C_4 crops (such as maize and sorghum) have higher yields and increased water- and nitrogen-use efficiency (*1*, *4*).

Building the C_4 Machinery

In an evolutionary context, the transition from C_3 to C_4 photosynthesis has occurred independently in more than 60 different plant taxa (*3*). Genomic and transcriptional sequence comparisons of cell-specific and leaf-developmental gradient transcription profiles between closely related C_3 and C_4 species are being used to identify C_4-specific regulatory genes (*4*). Combining this information in parallel with screens of mutagenized C_4 *Sorghum bicolor* and *Setaria viridis* along with activation-tagged rice populations hopefully will

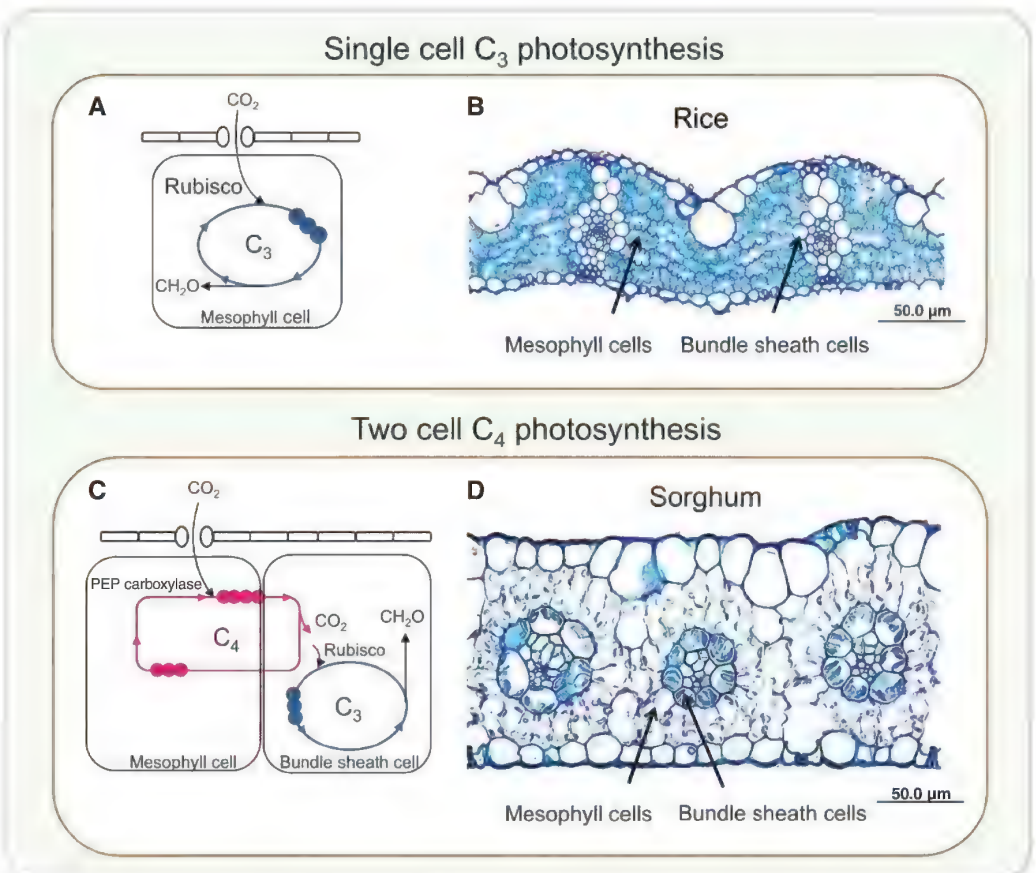

Fig. 1. **(A)** C_3 photosynthesis fixes atmospheric CO_2 into C_3 acids with Rubisco in single cells. **(C)** Two-cell C_4 photosynthesis requires spatial separation of fixation of atmospheric CO_2 into C_4 acids and the donation of CO_2 from these C_4 acids to Rubisco. Also shown are light microscopy images of transverse sections of leaves of **(B)** rice, a C_3 plant, and **(D)** sorghum, a C_4 plant. The rice section shows vascular bundles with few chloroplasts and large numbers of mesophyll cells between the vascular bundles typical for C_3 species. The sorghum leaf section shows chloroplasts in bundle sheath and only two or three mesophyll cells in between the vascular tissue typical of a C_4 species.

[1]Research School of Biology, Australian National University, Canberra, ACT 0200, Australia. [2]International Rice Research Institute, Los Banos, Philippines, and University of Sheffield, Sheffield S10 2TN, UK. [3]High Resolution Plant Phenomics Centre, Commonwealth Scientific and Industrial Research Organization (CSIRO) Plant Industry, Canberra, ACT 2601, Australia.

*To whom correspondence should be addressed. E-mail: susanne.caemmerer@anu.edu.au

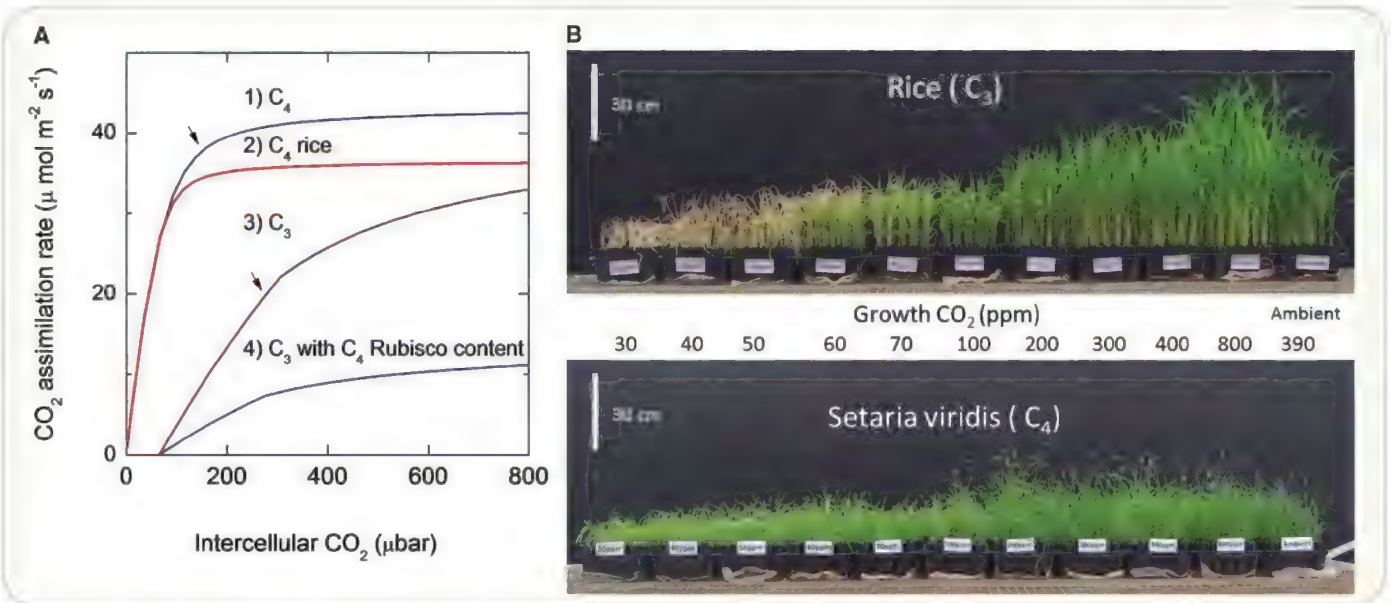

Fig. 2. (**A**) Modeled changes in CO_2 assimilation rate in response to changes in leaf intercellular CO_2 partial pressure for C_3 and C_4 photosynthesis and for a hypothetical C_4 rice. Curves 1, 2, and 4 have Rubisco levels typically found in a C_4 leaf (10 μmol m^{-2} catalytic Rubisco sites). Curve 3 shows a typical response for C_3 leaves with three times the Rubisco level of C_4 leaves. Curve 1 shows the response of a C_4 leaf with C_4 Rubisco kinetic properties. Curve 2 models how a C_4 leaf with C_3 Rubisco kinetic properties would respond (a hypothetical C_4 rice with C_3 Rubisco kinetics). The comparison of these two curves shows the increase in CO_2 assimilation rate achieved with C_4 compared with C_3 Rubisco kinetic properties within a functional C_4 mechanism. Arrows to curves 1 and 3 show intercellular CO_2 partial pressures typical at current ambient CO_2 partial pressures for C_4 and C_3 photosynthesis. To generate the curves, model equations were taken from (*11*) and comparative Rubisco kinetic constants from (*12*). (**B**) Growth of 21-day-old rice and *S. viridis* seedlings at different ambient CO_2 concentrations ranging from 30 to 800 parts per million.

reveal candidate genes in the C_3-to-C_4 switch that can be tested in transgenic rice and *S. viridis* (*5*). Because C_4 plants can carry out net CO_2 assimilation at very low CO_2 levels whereas C_3 plants cannot (Fig. 2), we can use growth screens to identify gain of function in activation-tagged rice mutants and loss of function in *S. viridis* mutants (Fig. 2). We are also using the fact that C_4 photosynthesis imparts a distinct carbon isotope signature on dry matter (*6*) in a loss-of-function screen for C_4 mutants.

A subset of genes required for the major biochemical components and metabolite transporters involved in the C_4 pathway have been cloned and coupled to suitable promoters to give cell-specific expression in rice (*7*). Attempts to install C_4 photosynthesis in plants lacking the appropriate anatomy show that a biochemical approach alone will not be enough (*8*). Bundle sheath cells in rice are smaller than in C_4 plants and have less chloroplasts, and there are a large number of mesophyll cells between vascular bundles (Fig. 1) (*4*). Promising mutants have been identified in rice that show reduced vein spacing. Combined with studies of sorghum, we are optimistic that we will be able to identify the genes controlling this aspect of anatomy (*4*, *7*).

Lessons Learned and Future Challenges

Although C_4 leaves have close veins and high rates of photosynthesis, C_4 photosynthesis is also naturally supported around widely spaced veins in maize husk tissue, albeit at lower rates (*6*). Thus, a prototype C_4 rice may be achievable with a subset of C_4 genes, but a "good" C_4 rice will require substantial fine tuning of biochemistry and anatomy. Particularly intriguing is the need for additional metabolite transport across membranes of organelles in C_4 photosynthesis (*4*). A functional C_4-concentrating mechanism in rice would allow for an approximately two-thirds reduction in Rubisco levels, relative to wild-type rice, but Rubisco would be sequestered in bundle sheath cells and ideally have a greater catalytic turnover rate (Fig. 2) (*2*). Antisense gene suppression of key photosynthetic enzymes has illuminated C_4 metabolism and engineering strategies, including the surprising find that phosphorylation of phosphoenolpyruvate (PEP) carboxylase by the regulatory enzyme PEP carboxylase phosphokinase is not needed for C_4 function (*9*). With the adoption of the C_4 model plant *S. viridis*—with its short life cycle, small stature, and genome size—along with advances in efficient transformation, we anticipate that much more will soon be learned (*5*). We expect to have a C_4 rice prototype within 3 years. However, we estimate that another 15 years of research are required for optimization of the phenotype and field testing for C_4 rice to become ready for cultivation in farmers' fields.

Norman Borlaug's green revolution was based on just a handful of genes (*10*). However, the need for even greater food plant production looms. The promise of C_4 rice has resulted in one of the largest consortia of plant biologists pursuing a common goal. We optimistically take on this challenge, anticipating that advances in our understanding of plant metabolism, and C_3 and C_4 photosynthesis in particular, will better serve humanity in years to come.

References and Notes

1. J. M. Hibberd, J. E. Sheehy, J. A. Langdale, *Curr. Opin. Plant Biol.* **11**, 228 (2008).
2. M. R. Badger *et al.*, *Can. J. Bot.* **76**, 1052 (1998).
3. R. F. Sage, P. A. Christin, E. J. Edwards, *J. Exp. Bot.* **62**, 3155 (2011).
4. J. A. Langdale, *Plant Cell* **23**, 3879 (2011).
5. T. P. Brutnell *et al.*, *Plant Cell* **22**, 2537 (2010).
6. J. J. L. Pengelly *et al.*, *Plant Physiol.* **156**, 503 (2011).
7. K. Kajala *et al.*, *J. Exp. Bot.* **62**, 3001 (2011).
8. M. Miyao, C. Masumoto, S. Miyazawa, H. Fukayama, *J. Exp. Bot.* **62**, 3021 (2011).
9. T. Furumoto, K. Izui, V. Quinn, R. T. Furbank, S. von Caemmerer, *Plant Physiol.* **144**, 1936 (2007).
10. N. Borlaug, *Science* **318**, 359 (2007).
11. S. von Caemmerer, *Biochemical Models of Leaf Photosynthesis*, vol. 2, *Techniques in Plant Sciences* (CSIRO Publishing, Collingwood, Australia, 2000).
12. A. B. Cousins, O. Ghannoum, S. von Caemmerer, M. R. Badger, *Plant Cell Environ.* **33**, 444 (2010).

Acknowledgments: This work was supported by the Bill and Melinda Gates Foundation. We are thankful for the scientific contributions of all the members of the C_4 Rice Consortium.

10.1126/science.1220177

REVIEW

Systems Biology for Enhanced Plant Nitrogen Nutrition

Rodrigo A. Gutiérrez

Nitrogen (N)–based fertilizers increase agricultural productivity but have detrimental effects on the environment and human health. Research is generating improved understanding of the signaling components plants use to sense N and regulate metabolism, physiology, and growth and development. However, we still need to integrate these regulatory factors into signal transduction pathways and connect them to downstream response pathways. Systems biology approaches facilitate identification of new components and N-regulatory networks linked to other plant processes. A holistic view of plant N nutrition should open avenues to translate this knowledge into effective strategies to improve N-use efficiency and enhance crop production systems for more sustainable agricultural practices.

Nitrogen (N) is the mineral nutrient required in the greatest amount by plants (*1*), and its availability, or lack thereof, limits plant growth and development (*2*), crop yield (*3*), and primary production at a planetary scale (*4*). Biologically available N forms, such as nitrate or ammonia, are in short supply in natural as well as agricultural systems. Consequently, N removed from the soil in crop products or by leaching must be replaced if agricultural productivity is to be sustained. Synthetic fertilizers, such as urea or ammonium nitrate, are the main sources of N applied to crops and represent up to 50% of the operational costs in agriculture (*3*). Out of ~120 Tg year^{-1} of N used for food production globally, only ~10% is consumed by people (*5*). Most of the unutilized N, between 50 and 75% of the N applied to the field, is not used by crops and hence is lost by leaching into the soil or is released to the atmosphere as nitrogen gases (*3*)—a fraction that has not substantially improved in 50 years (*6*). Excess N can cause eutrophication of terrestrial and aquatic systems, dramatically exemplified by dead zones such as the one found in the northern Gulf of Mexico (*7*). Of particular concern is that nitrogen can be transformed into different chemical forms in the environment, leading to diverse effects (*4*). In addition to negative environmental effects, excess nitrogen may also have direct negative consequences for humans (*8*, *9*). These concerns led the World Health Organization to set limits on the amount of nitrates in the drinking water. Recent reports however, describe potentially beneficial effects of nitrate in the diet (*10*), suggesting that we have yet to answer key questions regarding the contribution of nitrate and nitrite to human nutrition, physiology, and pathology.

N Perception, Signaling, and Responses

In addition to their role as nutrients, nitrate and other forms of N can act as signals to regulate plant gene expression, metabolism, physiology, and growth and development [reviewed in (*11*, *12*)]. Nitrate is sensed by NITRATE TRANSPORTER 1.1 (NRT1.1), which can switch from low to high affinity based on the phosphorylation of threonine-101 (T101) (*13*) (Fig. 1). Under low-nitrate conditions, CBL-INTERACTING PROTEIN KINASE 23 (CIPK23) can phosphorylate T101, making NRT1.1 a high-affinity nitrate carrier and leading to a weak induction of gene expression of *NRT2.1* (*13*). *NRT2.1* is a high-affinity nitrate transporter and one of several primary nitrate response genes that show a rapid induction of gene expression in response to nitrate treatments independent of protein synthesis. Conversely, under high-nitrate conditions, T101 is not phosphorylated, NRT1.1 functions as a low-affinity carrier, and *NRT2.1* gene expression is strongly induced. The NRT1.1 protein is involved in both nitrate perception and transport (*14*–*16*), functions that can be differentiated by the mutant allele *chl1-9*. *Chl1-9* carries a point mutation that changes the proline residue 492 to leucine. This mutation reduces NRT1.1 nitrate uptake in all affinity ranges but does not affect the primary nitrate response of *NRT2.1*. Thus, nitrate transport activity is not required for the sensing function of NRT1.1 (*13*).

In addition to NRT1.1, other receptors that sense nitrate as well as other forms of N may yet be discovered in plants. Nitrate induction of *NRT2.1* and other primary response genes is unaffected in *nrt1.1* mutants if nitrate treatments are carried out after N deprivation (*14*). Genetic evidence supports a role for NRT2.1 in a signaling pathway that represses lateral root initiation in response to nutritional cues by acting either as a nitrate sensor or signal transducer (*17*). The role of AMMONIUM TRANSPORTER 1.3 in regulating lateral root branching in response to ammonium is independent of ammonium transport, suggesting a signaling role for this transporter (*18*).

The first regulatory factor identified in N responses was the MADS box transcription factor *ARABIDOPSIS* NITRATE REGULATED 1 (ANR1). Transgenic plants with repressed expression levels of *ANR1* showed altered sensitivity to nitrate and did not show the characteristic root elongation response to a localized nitrate supply (*19*). Additional transcription factors known to regulate N responses include NIN-LIKE PROTEIN7 (NLP7), required for normal nitrate regulation of N-assimilatory genes in *Arabidopsis* and a putative repressor of the N starvation (*20*); members of the LATERAL ORGAN BOUNDARY DOMAIN (LBD37/38/39), found to repress anthocyanin biosynthesis and many other known N-responsive genes, including key genes required for nitrate uptake and assimilation (*21*); ELONGATED HYPOCOTYL 5 (HY5) and HY5-HOMOLOG (HYH), positive regulators of *NITRATE REDUCTASE* (*NIA*) *2* and negative regulators of NRT1.1 in *Arabidopsis* (*22*); and SQUAMOSA PROMOTER BINDING PROTEIN–LIKE 9, a negative regulator of *NIR* and *NIA2* (*23*) (Fig. 1).

Besides transcription, posttranscriptional mechanisms are implicated in plant N responses. The *Arabidopsis NITROGEN LIMITATION ADAPTATION* gene (*NLA*) coding for a RING-type ubiquitin ligase is a positive regulator of plant adaptation to N limitation (*24*). NLA controls phosphate homeostasis and interactions between N and phosphate metabolism in plants (*25*). The nitrate-responsive CIPK8 is required for normal nitrate regulation of primary nitrate-response genes in the low-affinity range (*26*). Repression of microRNA 169 (miR169) by N limitation may lead to drought tolerance by regulating the A5 subunit of NF-Y, a transcription factor crucial for expression of drought-resistance genes (*27*) (Fig. 1).

Despite progress in identifying some components in regulatory networks, a comprehensive view of the N signal transduction pathways and how they impinge upon metabolic and developmental processes is still lacking. What are the mechanistic relationships between the regulatory components and response networks identified thus far (Fig. 1)? We know that the N response in *Arabidopsis* has an important cell-specific component (*28*), yet we have a very limited understanding of spatiotemporal aspects (*2*). Where is the nitrate signal first sensed? How is the response of individual cells orchestrated to articulate organismal responses? How do these mechanisms change over developmental time? Answering these questions is important for generating the holistic view of plant N nutrition necessary to increase N-use efficiency in crops.

Systems Biology for Understanding Plant N Nutrition

Systems biology has accelerated the discovery of N-regulatory networks (Fig. 1) as well as integrated knowledge across traditionally disconnected fields of plant biology (Fig. 2). A systems biology approach to understanding N-regulatory networks is an iterative process that includes data collection and integration, system modeling, experimentation at a global level, and generation of new hypotheses for experimental validation (*29*–*31*). The increasing

FONDAP Center for Genome Regulation, Millennium Nucleus Center for Plant Functional Genomics, Departamento de Genética Molecular y Microbiología, Pontificia Universidad Católica de Chile, Avenida Libertador Bernardo O'Higgins 340, Santiago, Chile. E-mail: rgutierrez@bio.puc.cl

genome-wide information about components and their relationships in *Arabidopsis*, together with a growing database of experimental measurements under various N regimes, has provided a fertile terrain for addressing plant responses to N. Systems analysis of expression data in *Arabidopsis* roots identified molecular machines and cellular processes that are modulated by N and carbon and N interactions. This analysis highlighted the role of auxin and cytokinin signaling pathways and microRNAs as important players in N-regulatory networks (*32*). Systems analysis also showed that CIRCADIAN CLOCK ASSOCIATED 1 (CCA1), one of the master regulators of the circadian clock, coordinates the organic N response of N-assimilatory genes by direct binding to the promoters of *BASIC REGION/LEUCINE ZIPPER TRANSCRIPTION FACTOR 1* (*bZIP1*) (which in turn regulates *ASPARAGINE SYNTHETASE 1* (*ASN1*) expression), *GLUTAMINE SYNTHETASE 1.3*, and *GLUTAMATE DEHYDROGENASE 1* (*33*). CCA1 thus integrates N nutrition and circadian regulation of gene expression in *Arabidopsis* (*34*) (Fig. 2A). Systems analysis provided mechanisms to explain how root system architecture is modulated by N availability. Network analysis identified miR167 and one of its targets, *AUXIN RESPONSE FACTOR 8* (*ARF8*), in the control of lateral root development in response to nitrate (*28*) (Fig. 2B). Nitrate treatments repressed miR167 in pericycle cells, leading to an increase in *ARF8* transcript. *ARF8* induction in pericycle cells triggered an increase in the ratio between initiating and emerging lateral roots (*28*). Another study revealed an incoherent feed-forward mechanism that is induced by nitrate and repressed by N metabolites generated by nitrate assimilation (*35*) (Fig. 2C). The key components of this regulatory module are miR393 and one of its targets, the auxin receptor AFB3 (*35*). Induction of *AFB3* gene expression by nitrate leads to auxin responses in primary and lateral roots. Under sufficient N nutrition, miR393 is induced, repressing AFB3 expression and auxin sensitivity. This regulatory module is a simple mechanism that controls root system architecture in response to external and internal N availability in *Arabidopsis*. These examples illustrate the power of systems biology to address molecular mechanisms as well as to connect distinct biological processes. These findings represent first steps to develop biotechnological applications to improve N-use efficiency in crop production systems.

Future Prospects

World population is estimated to reach 9 billion inhabitants by 2050 and more beyond (*36*). Increased needs for food will impose a large stress on agriculture production worldwide. Nonfood use of crops—for example, for biofuel production—will also tax agricultural systems. Besides the direct implications for crop yield, the interactions between the nitrogen and carbon cycle are key players in Earth's climate and other planetary processes (*4*). The magnitude and seriousness of this challenge must not be underestimated. Increased understanding of N-use efficiency for increased

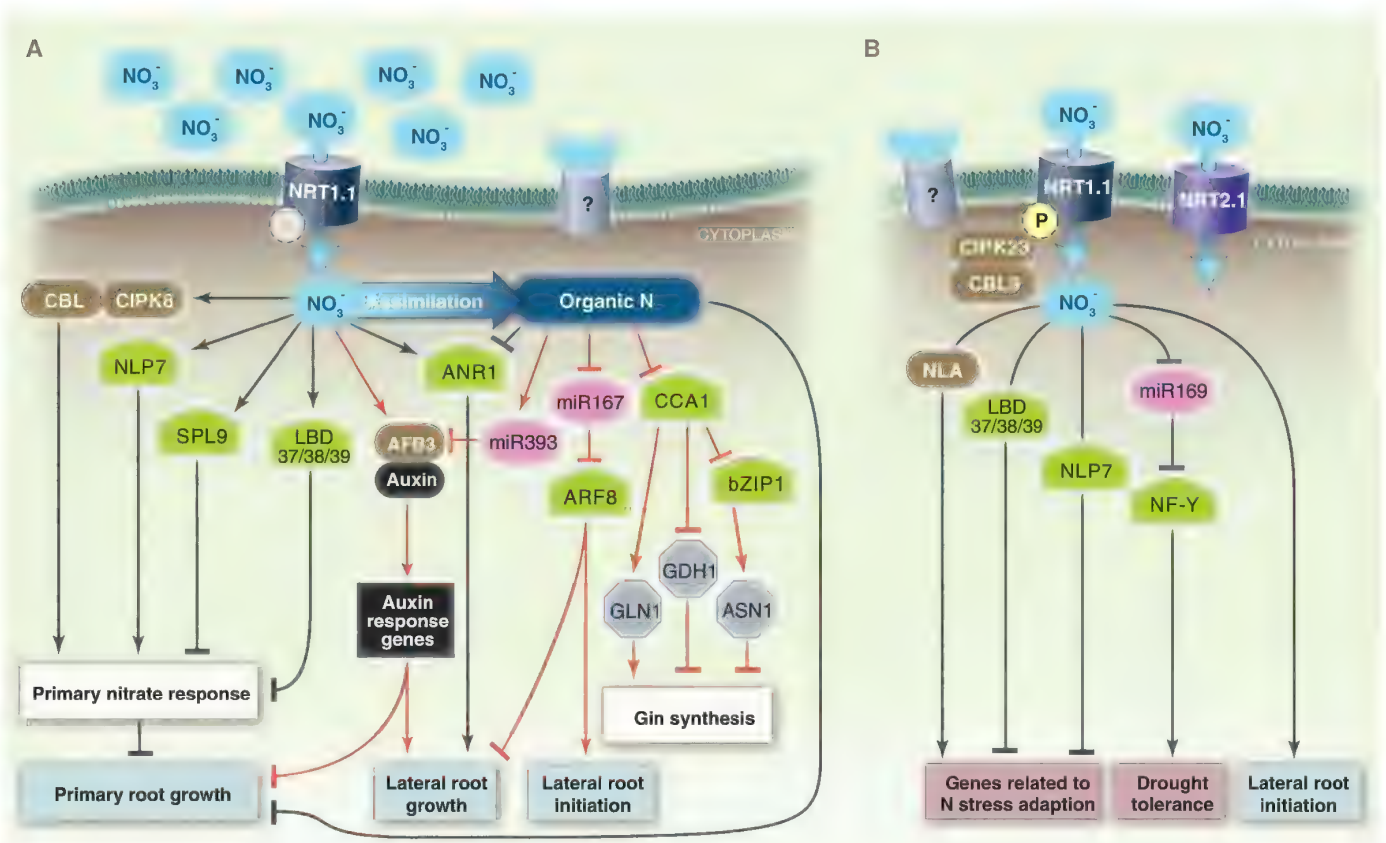

Fig. 1. A simplified summary of known regulatory components controlling *Arabidopsis* responses to N. At the perception layer, NRT1.1 stands out as the best-characterized sensor for nitrate. Additional receptors for nitrate as well as other N forms likely exist. At the regulatory network layer, several independent studies identified transcription factors and other putative components of N signaling pathways, mostly in *Arabidopsis thaliana*. Response networks correspond to metabolic, physiological, and growth and developmental pathways activated for adaptive responses to changes in N availability. Only responses that can be connected to upper regulatory components are shown. (**A**) Under high-nitrate conditions (>1 mM), NRT1.1 transporter functions as a low-affinity nitrate transporter. (**B**) Under low-nitrate conditions (<1 mM), NRT1.1 transporter is phosphorylated at T101 and functions as a high-affinity nitrate transporter. Under low-nitrate conditions, NRT2.1 may play a role in signaling. Green shapes represent transcription factors, gray octagons represent enzymes, pink octagons represent microRNAs, and brown shapes represent other regulatory molecules. Black lines represent relationships obtained by molecular genetic approaches, and red lines represent relationships discovered by systems biology approaches.

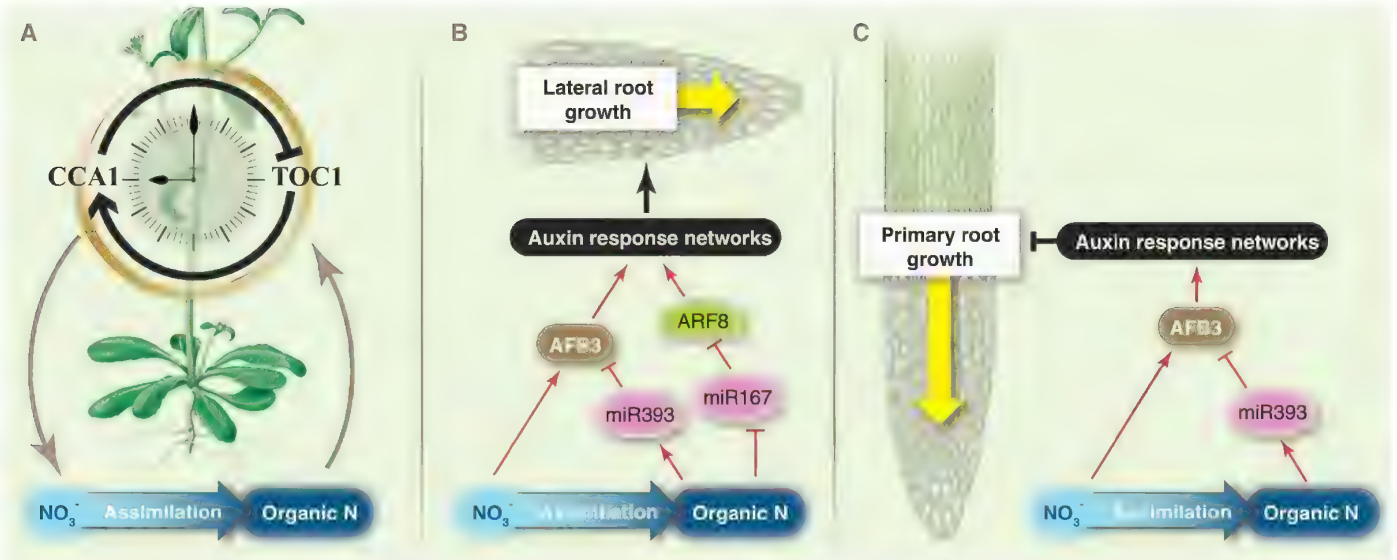

Fig. 2. Systems biology approaches to map N-regulatory networks. Systems biology approaches accelerate discovery of N-regulatory networks as well as connect N-regulatory networks to other plant processes. (**A**) A systems approach identifies a connection between genes in the N-assimilation pathway and the circadian clock. The circadian clock regulates N metabolism, and in turn N metabolites act as inputs to the clock. (**B**) A type I incoherent feed-forward loop motif including miR393 and AFB3 plays a role in modulating lateral root growth in response to N signals. Organic N affects lateral root growth through an independent pathway that requires miR167 and ARF8. (**C**) The miR393/AFB3 regulatory motif is also implicated in modulating primary root growth in *Arabidopsis*. This regulatory motif integrates both external inorganic N signals (nitrate) and internal N signals (e.g., Glu) to adjust primary root growth based on N demand.

productivity is urgently needed. N-use efficiency is a complex trait controlled by interwoven networks driving an array of physiological and developmental pathways. Environmental interactions and cell-, tissue-, and organ-specific adaptive responses for a given genotype add nuances. Traditional trial-and-error approaches to addressing N-use efficiency will continue to be slow and costly. When modifying intricate metabolic or regulatory networks, we must consider the system-wide implications of our alterations under a wide range of environmental conditions. Here the full power of systems biology should be harnessed.

Systems biology approaches are building a holistic understanding of N-regulatory networks and molecular mechanisms to control growth and development in plants. Ultimately, systems biology should provide us with a virtual plant model that can be used for in silico design and testing of network alterations. The new research field of synthetic biology can leverage this knowledge for biological engineering (*37*). Synthetic biology designs biological systems by combining simple genetic parts with robust biological functions to construct devices and circuits with new properties [e.g., (*38*)]. There is a long road ahead for synthetic biology to build complex traits in plants and other multicellular eukaryotes. A key bottleneck to advances in synthetic biology lies in the lack of shared resources. The plant research community should embrace the development of synthetic biology design principles and standards and should contribute physical plant DNAs to the Standard Registry of Biological Parts (*39*). The close interplay of systems biology and synthetic biology should help both advance our understanding of plant biology as well as facilitate design and construction of biotechnological solutions for enhanced N-use efficiency in crop production systems.

References and Notes

1. E. Epstein, A. J. Bloom, *Mineral Nutrition of Plants: Principles and Perspectives* (Sinauer, Sunderland, MA, 2005).
2. J. M. Alvarez, E. A. Vidal, R. A. Gutiérrez, *Curr. Opin. Plant Biol.* **15**, 185 (2012).
3. B. Hirel, T. Tétu, P. J. Lea, F. Dubois, *Sustainability* **3**, 1452 (2011).
4. N. Gruber, J. N. Galloway, *Nature* **451**, 293 (2008).
5. G. P. Robertson, P. M. Vitousek, *Annu. Rev. Environ. Resour.* **34**, 97 (2009).
6. K. G. Cassman, A. Dobermann, D. T. Walters, *Ambio* **31**, 132 (2002).
7. R. J. Diaz, R. Rosenberg, *Science* **321**, 926 (2008).
8. H. H. Comly, *J. Am. Med. Assoc.* **129**, 112 (1945).
9. J. K. Lin, *Clin. Biochem.* **23**, 67 (1990).
10. J. O. Lundberg *et al.*, *Nat. Chem. Biol.* **5**, 865 (2009).
11. G. Krouk *et al.*, *Trends Plant Sci.* **16**, 178 (2011).
12. E. A. Vidal, R. A. Gutiérrez, *Curr. Opin. Plant Biol.* **11**, 521 (2008).
13. C. H. Ho, S. H. Lin, H. C. Hu, Y. F. Tsay, *Cell* **138**, 1184 (2009).
14. R. Wang, X. Xing, Y. Wang, A. Tran, N. M. Crawford, *Plant Physiol.* **151**, 472 (2009).
15. A. Gojon, G. Krouk, F. Perrine-Walker, E. Laugier, *J. Exp. Bot.* **62**, 2299 (2011).
16. J. Dechorgnat *et al.*, *J. Exp. Bot.* **62**, 1349 (2011).
17. D. Y. Little *et al.*, *Proc. Natl. Acad. Sci. U.S.A.* **102**, 13693 (2005).
18. J. E. Lima, S. Kojima, H. Takahashi, N. von Wirén, *Plant Cell* **22**, 3621 (2010).
19. H. Zhang, B. G. Forde, *Science* **279**, 407 (1998).
20. L. Castaings *et al.*, *Plant J.* **57**, 426 (2009).
21. G. Rubin, T. Tohge, F. Matsuda, K. Saito, W. R. Scheible, *Plant Cell* **21**, 3567 (2009).
22. E. M. Jonassen, D. C. Sévin, C. Lillo, *J. Plant Physiol.* **166**, 2071 (2009).
23. G. Krouk, P. Mirowski, Y. LeCun, D. E. Shasha, G. M. Coruzzi, *Genome Biol.* **11**, R123 (2010).
24. M. Peng, C. Hannam, H. Gu, Y. M. Bi, S. J. Rothstein, *Plant J.* **50**, 320 (2007).
25. S. Kant, M. Peng, S. J. Rothstein, *PLoS Genet.* **7**, e1002021 (2011).
26. H. C. Hu, Y. Y. Wang, Y. F. Tsay, *Plant J.* **57**, 264 (2009).
27. B. D. Pant *et al.*, *Plant Physiol.* **150**, 1541 (2009).
28. M. L. Gifford, A. Dean, R. A. Gutierrez, G. M. Coruzzi, K. D. Birnbaum, *Proc. Natl. Acad. Sci. U.S.A.* **105**, 803 (2008).
29. T. Ideker, T. Galitski, L. Hood, *Annu. Rev. Genomics Hum. Genet.* **2**, 343 (2001).
30. R. A. Gutiérrez, D. E. Shasha, G. M. Coruzzi, *Plant Physiol.* **138**, 550 (2005).
31. H. Y. Chuang, M. Hofree, T. Ideker, *Annu. Rev. Cell Dev. Biol.* **26**, 721 (2010).
32. R. A. Gutiérrez *et al.*, *Genome Biol.* **8**, R7 (2007).
33. R. A. Gutiérrez *et al.*, *Proc. Natl. Acad. Sci. U.S.A.* **105**, 4939 (2008).
34. C. R. McClung, R. A. Gutiérrez, *Curr. Opin. Genet. Dev.* **20**, 588 (2010).
35. E. A. Vidal *et al.*, *Proc. Natl. Acad. Sci. U.S.A.* **107**, 4477 (2010).
36. United Nations, *World Population Prospects, the 2010 Revision*, http://esa.un.org/unpd/wpp/index.htm (2010).
37. S. Rollié, M. Mangold, K. Sundmacher, *Chem. Eng. Sci.* **69**, 1 (2012).
38. S. Basu, Y. Gerchman, C. H. Collins, F. H. Arnold, R. Weiss, *Nature* **434**, 1130 (2005).
39. Registry of Standard Biological Parts, http://partsregistry.org (2012).

Acknowledgments: Thanks to N. Crawford and Y.-F. Tsay for critical comments on the manuscript. Thanks also to J. M. Alvarez, E. Vidal, and O. Contreras for figures and constructive discussions. Research in our group is funded by International Early Career Scientist program from Howard Hughes Medical Institute, Fondo de Desarrollo de Areas Prioritarias (FONDAP) Center for Genome Regulation (15090007), Millennium Nucleus Center for Plant Functional Genomics (P10-062-F), Fondo Nacional de Desarrollo Científico y Tecnológico (1100698), Comisión Nacional de Investigación Científica y Tecnológica-ANR program (ANR-007), and Corporación de Fomento de la Producción Genome Program (CORFO07Genoma01).

10.1126/science.1217620

A Decade of Imaging Cellular Motility and Interaction Dynamics in the Immune System

Ronald N. Germain,[1]*† Ellen A. Robey,[2]*† Michael D. Cahalan[3]*†

To mount an immune response, lymphocytes must recirculate between the blood and lymph nodes, recognize antigens upon contact with specialized presenting cells, proliferate to expand a small number of clonally relevant lymphocytes, differentiate to antibody-producing plasma cells or effector T cells, exit from lymph nodes, migrate to tissues, and engage in host-protective activities. All of these processes involve motility and cellular interactions—events that were hidden from view until recently. Introduced to immunology by three papers in this journal in 2002, in vivo live-cell imaging studies are revealing the behavior of cells mediating adaptive and innate immunity in diverse tissue environments, providing quantitative measurement of cellular motility, interactions, and response dynamics. Here, we review themes emerging from such studies and speculate on the future of immunoimaging.

During embryonic development of complex metazoans, rapid cell division, large-scale movement of cells, and inductive interactions result in further differentiation and specialization. These latter events depend greatly on cellular location and take account of both contact-dependent and soluble signals. But this panoply of highly dynamic processes is largely absent from adult organisms, replaced by relatively stable tissue architectures and stereotypical spatial relocation of terminal cells in epithelial structures from basal progenitors. Neural networks undergo local modifications and pruning, but wide-scale cell position changes and replacement are rare.

The cells of the immune system stand out against this general landscape in retaining many of the properties of the embryonic state. Aside from the initial seeding of some resident myeloid and lymphoid cells into specific tissues and organs, there is widespread movement throughout life of many cell types from bone marrow to the thymus and secondary lymphoid organs, entry into a variety of tissue sites in response to damage or microbial invasion, extensive signaling through transient contacts lasting minutes to hours, transient exchange of differentiation-inducing or viability-sustaining information, and rapid cell division that rivals the rates seen during embryogenesis.

Although the existence of circulating and tissue-invading immune cells has been recognized for half a century (*1*), and the dynamic process of leukocyte extravasation from blood to tissue studied using video imaging for nearly 20 years (*2*), it is only in the past decade that multiplex, high-resolution, dynamic, in situ examination of this complex choreography of immune cell motion, interaction, and function has been possible. Starting with a series of papers in 2002, three of which appeared together in this journal (*3*–*5*), our understanding of how cell movement, positioning, and interaction contribute to effective immune responses has undergone explosive growth using one- and, more commonly, two-photon (2P) microscopy to visualize living cells in vivo and in tissue explant preparations (Box 1). The observations made during this period have changed concepts of the relationship between tissue organization and the development of adaptive immunity, provided new insights into how innate immune effectors carry out their search and destroy missions, yielded quantitative data that have altered previous models of adaptive immune response development, and helped provide insight into the effect of gene mutations on immunity that could not have been gained by other means. Other studies have revealed in colorful detail how immune cells interact with a diverse array of pathogens, the basis for immunoregulation in secondary lymphoid tissues, and the effects of immunosuppressive drugs on immune cell behavior in vivo. In short, in situ imaging has proved a powerful tool to investigate the cellular dynamics of the immune response in lymphoid organs and in peripheral tissues (Fig. 1). Here, we try to synthesize the key conceptual advances that have come from this research, not seeking a comprehensive review of the literature, but focusing on how the application of this technology has fundamentally changed our understanding of immune system organization and physiology. We end with some thoughts about the future.

Lymph Node Cellular Dynamics and the Initiation of T Cell Adaptive Immune Responses

Among the most striking findings to emerge from dynamic imaging analyses is the seemingly random pattern of robust cellular migration exhibited by many cell types under basal conditions and the efficiency with which cells direct their attention to particular targets by short- or long-range migrations during active immune responses. T cells are able to crawl more rapidly than any other cell type in the body. Similar amoeboid actin-based motility at a somewhat slower pace is

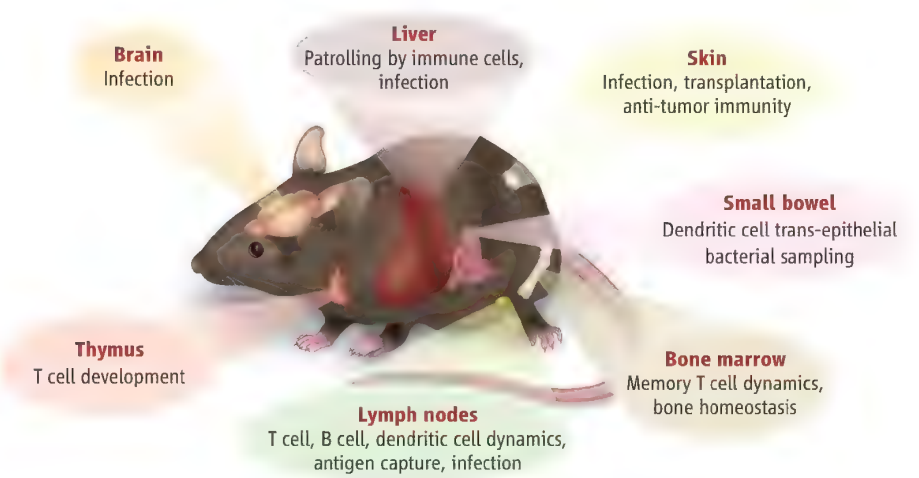

Fig. 1. Two-photon imaging of different anatomical sites in the mouse. Although early 2P studies of the immune system focused on T cell activation in the lymph node, in the past decade this approach has been extended to a variety of different tissues, using both intravital imaging approaches and tissue explants. Processes that have been examined include immune responses to infection, immune homeostasis, transplant immunology, antitumor immunology, and regulation of immune responses.

[1]Laboratory of Systems Biology, National Institute of Allergy and Infectious Diseases, National Institutes of Health, Bethesda, MD 20892, USA. [2]Department of Molecular and Cell Biology, University of California Berkeley, Berkeley, CA 94720, USA. [3]Department of Physiology and Biophysics, University of California Irvine, Irvine, CA 92697, USA.

*All authors contributed equally to this manuscript.
†To whom correspondence should be addressed. E-mail: rgermain@nih.gov (R.N.G.); erobey@berkeley.edu (E.A.R.); mcahalan@uci.edu (M.D.C.)

the default status of B lymphocytes (*4*, *6*), natural killer cells (*7*, *8*), neutrophils (*9*, *10*), and monocytes (*11*). Collectively, these cells can be regarded as the explorers, using cell surface receptors to sample the environment and responding with altered motility when signals are transmitted. On the other hand, antigen-presenting cells (APCs), such as dendritic cells (DCs) (*5*, *12*–*16*) and Langerhans cells (*17*, *18*), are generally sessile in tissue unless induced to migrate by microbial or inflammatory signals (*16*, *18*, *19*), actively waving their DC processes and displaying on their surface major histocompatibility complex (MHC)–encoded proteins a short-term historical record of pathogen invasion. When antigen receptors are engaged by antigen or chemokines, lymphocytes often stop (*5*, *12*, *13*, *20*, *21*) as signals begin to transform seemingly random motility into directed responses that reveal coordinated cellular behavior, including local swarming or directed migration from one region to another. Local motility can evolve into long-range migrations by cells leaving the tissue environment to migrate in blood or lymph to distant sites.

Lymph nodes are major sites of antigen capture, detection, and initial responses during an adaptive immune response (Fig. 2). After homing into lymph nodes from the blood, lymphocytes spend several hours to a day in a given lymph node (*22*). During this time, they sample the environment and most often leave the lymph node via efferent lymphatic vessels without finding antigen. Entry is regulated by the chemokine receptor CCR7, egress by the sphingosine-1-phosphate receptor 1 (S1P1); both G protein–coupled receptors ensure directed migration at the global level into and out of the lymph node (*22*). The dynamic nature of lymphocyte movement as revealed by the earliest imaging studies of these secondary lymphoid organs, first in explants (*4*, *12*) and then in intravital preparations (*13*, *23*), demonstrated that lymphocytes actively migrate to pass from their entry sites at high endothelial venules to their exit at efferent lymphatics. The remarkably rapid pace of T cell movement while in the dense paracortical region of the node, however, and the way in which the cells scanned for antigen, were nonetheless unexpected. When viewed in time lapse, it looks chaotic; in fact, naïve T and B cell tracks are well described as a random walk (*4*, *13*, *23*). When antigen is present, however, T and B cells respond by altering their ongoing random migration, initiating interactions that lead to antibody production, proliferation, differentiation to memory or effector cells, and exit from the lymph node.

Two-photon studies illuminated the remarkable process whereby cell types present in very small numbers (APCs or specific T and B cells) find each other in the large volume of a lymph node to drive effective adaptive immune responses. The robust motility in lymph nodes initially suggested an antigen search strategy carried out by lymphocytes acting autonomously (*23*). Later, it became clear that T lymphocytes migrate in a random walk–like manner in contact with a network of fibroblastic reticular cells (FRCs) that are tightly associated with DCs (*24*) and from which they acquire chemokinetic signals enabling more rapid migration (*25*). These imaging data refined earlier concepts based on static imaging that suggested a possible role of the FRC network in guiding intranodal lymphocyte movement (*26*). Inflammatory chemokine production by DCs or DC-T cell combinations can also influence the migration of T cells within the lymph node, leading to more directed movement on this network (*27*, *28*). On the APC side of the equation, individual resident and migratory DCs extend agile dendrites and contact hundreds or thousands of motile T cells per hour to enable efficient repertoire scanning (*14*). Together these observations suggest that structural and chemical cues are used to enhance the likelihood that rare cells will colocalize and come into contact in the shortest possible time after antigen entry, driving effective adaptive responses.

Intravital imaging has also uncovered a previously unappreciated sequence of kinetic behaviors in the T cell response to antigen-bearing DCs (Fig. 3A). This process evolves in three distinct phases for both $CD4^+$ and $CD8^+$ T cells (*13*, *15*). Initially, T cells contact antigen-bearing DCs intermittently, briefly pausing and then migrating again to sample several DCs. During this time, T cell signaling is initiated, resulting in a series of Ca^{2+} spikes (*29*). The Ca^{2+} signal reduces motility acutely and also acts synergistically with other signaling pathways, resulting in enhanced gene expression, cytokine secretion, and cell proliferation. T cell–DC contact durations later increase, leading to prolonged interactions as several T cells cluster around individual DCs. After 16 to 24 hours, T cells resume their motility, swarm in the local vicinity, and undergo several rounds of proliferation. Activated $CD4^+$ T cells then begin to interact with cognate B cells near the edge of the follicle.

Imaging the Induction of Humoral Immunity

If the scanning and motility data along with this newly revealed multistage progression of cell interaction dynamics first captured the field's attention, a second wave of enthusiasm came with studies revealing how antigen accessed the lymph node and became available for lymphocyte recognition (*30*). Antigen can arrive in the form of molecules or microbial particles that travel passively via afferent lymphatic vessels, or it can arrive as peptide-MHC ligands on the surface of tissue-derived DCs and Langerhans cells that deliver a representative sample of peripheral material. Large antigen molecules or virus particles in lymph are taken up by subcapsular macrophages in draining lymph nodes and then handed off to B cells and, in turn, to follicular DCs that provide a reservoir later sampled by B cells (*31*–*34*). Other pathways for delivery of soluble antigens include being conveyed directly to B cells in the follicle by conduits (*35*) or presented to B cells by DCs (*36*).

Beyond revealing this first wave of antigen acquisition by the B cell, 2P imaging of T and B

Box 1. Two-photon basics.

Although some important contributions have come from use of confocal imaging methods [as just two examples, (*5*, *82*)], most studies now use 2P microscopy as the technique of choice for relatively deep tissue imaging of living cells (*83*, *84*). Two-photon microscopy uses very bright pulses of near-infrared laser light, less than 1 ps in duration and focused to a spot by the objective lens of a microscope to illuminate fluorescently labeled cells inside the tissue environment. When the light is on during the laser pulse, the photon density at the spot is such that two photons are absorbed almost simultaneously by a fluorescent dye or protein inside the cell, and a lower-wavelength photon is then emitted. Despite the intensity of light, less damage is produced than with other imaging methods, because the light is off most of the time in between laser pulses, and fluorescence excitation is confined to the diffraction-limited spot. Moreover, the near-infrared light used for excitation penetrates better through the tissue environment than lower wavelengths. The laser is scanned rapidly in the *x*-*y* plane to produce an image; volume images are obtained by repositioning the objective up and down in the *z* axis; emitted photons are detected by photomultiplier tubes. This process is then repeated to obtain a time-lapse movie of cell behavior; volume sampling in less than 20 s is best to avoid blurring of rapidly migrating cells. Several detectors can be deployed to image differently labeled molecules or cell types simultaneously.

The first 2P imaging study of lymph nodes examined explanted lymph nodes that were superfused with warmed, oxygenated media (*4*). This study was followed shortly by studies in which lymph nodes were imaged in live, anesthetized mice (*13*, *23*). The practical limit to tissue depth for most studies is around 300 μm, and thus some studies have used sliced tissue preparations to provide access to deep regions of tissue, such as the splenic white pulp (*85*, *86*) and the thymic medulla (*54*, *56*). Other studies have succeeded in imaging in liver (*61*, *62*), lung (*87*, *88*), bone marrow (*89*, *90*), pancreas (*91*), and the gastrointestinal mucosa (*63*), as well as other sites. In general, the observations made with explanted and intravitally imaged tissues have been in close agreement. A crucial technical consideration for 2P tissue imaging is that care be given to maintain the health of the tissue during the experiment, regardless of what method is used to provide access for imaging.

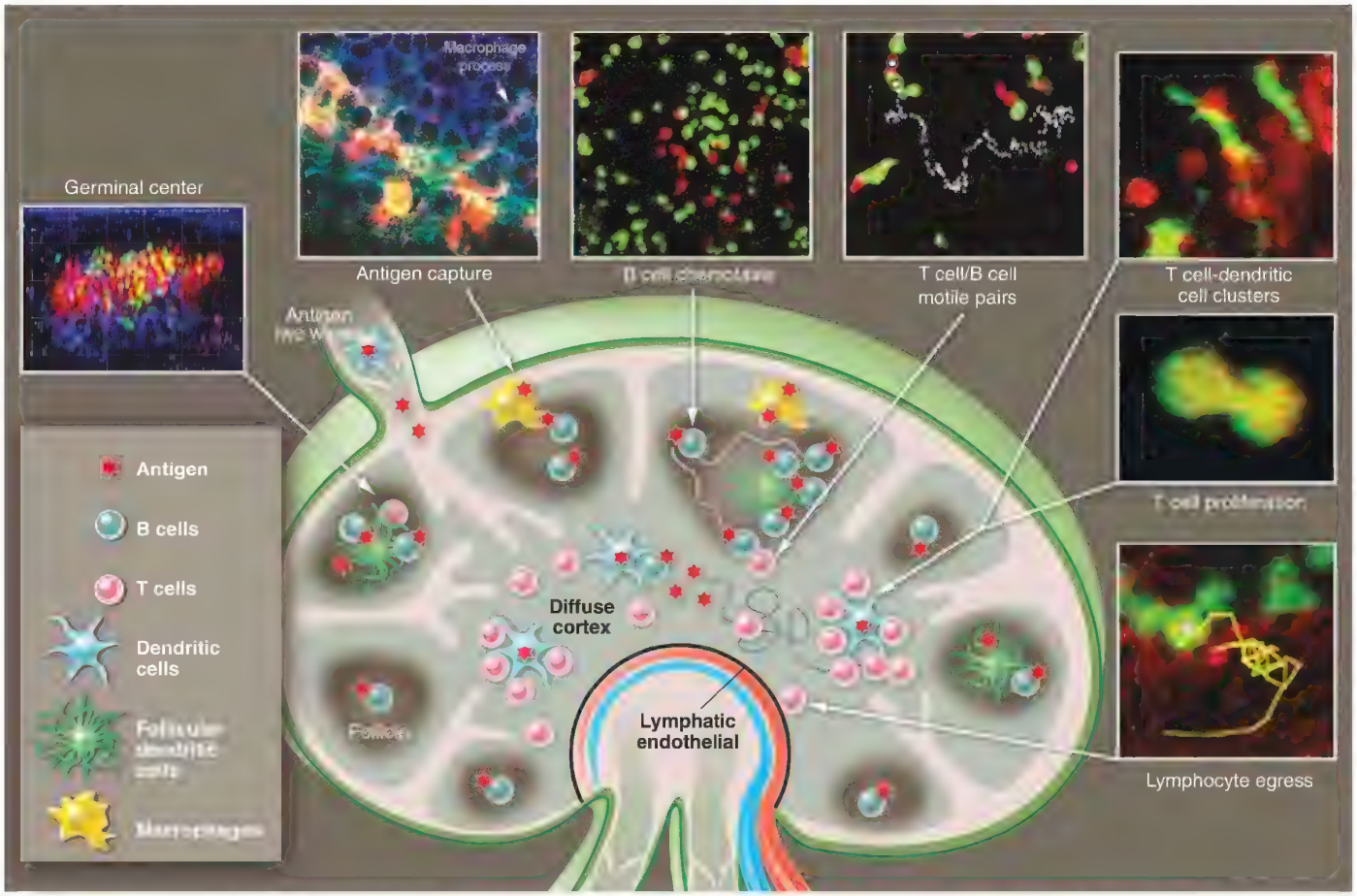

Fig. 2. Lymph node cellular choreography in response to antigen. T cells (T), B cells (B), DCs, follicular dendritic cells (FDCs), and macrophages (Mφ) during the response to antigen [adapted from (*6*)]. Diagram depicts 2P images of (clockwise from left): germinal center (*43*), antigen capture (*31*), B cell chemotaxis (*39*), T cell/B cell motile pairs (*39*), T cell–dendritic cell interactions (*15*), T cell proliferation (*15*), and lymphocyte egress (*72*). [Images adapted from the original sources: (*43*), figure 5C; (*31*), figure 2A; (*39*), figures 1B and 6A; (*15*), figures 1D and 6B; (*72*), figure 5A]

cell interaction provided additional insights. Activated B cells were known to take the initiative in seeking T cell help, moving by chemotaxis toward the follicle edge (*37*, *38*), but live imaging provided a much richer appreciation of the choreography of these critical first steps in humoral immunity. Antigen-activated B cells migrate randomly within the follicle until they enter a zone about 100 to 200 μm from the follicle edge. Then, newly expressed CCR7 receptors detect a gradient of CCL19 and CCL21 that guides them toward the T cell zone. Near the follicle edge, antigen presentation–dependent motile B-T conjugates are formed, the B cells leading the way (*39*). Both activated B and T cells then return to the deeper follicle to start the germinal center reaction.

The germinal center reaction, responsible for production of high-affinity, isotype-switched antibodies, had been well studied using static imaging and elegant molecular tools. It had also been the subject intensive efforts to quantitatively model immune function, specifically antibody affinity maturation. So it came as a surprise when the initial sets of results from live imaging of germinal centers did not fit easily into the established model of trafficking between germinal center subregions as implied by data from conventional histochemistry (*40*–*42*). Movement between these zones seemed more frequent and less regulated than expected, and a clear division of proliferation versus selective events in the two regions was less evident. However, recent studies using advances in tracking cells in vivo, especially employment of photo-activatable probes that permit cells to be tagged when present in one location and imaged as they move to another, have shown that the older model of selection based on T cell help in the light zone and proliferation in the dark zone was largely correct, while implicating the extent of interaction with T cells as a major determinant of interzonal migration and effective selection (*43*). Thus, intravital imaging combined with imaginative experimental design and new technology has substantially improved our understanding of a process at the heart of adaptive immunity.

Cell Migratory Dynamics Place a Threshold on Cell-Cell Communication

The first 2P images of rapid T cell migration in lymph nodes (*4*, *12*, *13*, *23*) necessitated a rethinking of intercellular communication and the impact of cell motility on this process. Although immunologists long appreciated that T cell responses require direct contact between a T cell and an antigen-bearing cell, these events had previously been examined using either end-stage assays of in vivo events that occur over a period of days or weeks or in vitro studies in which the interacting cells are maintained in a constrained culture environment for days. Striking images of the distinctive migratory patterns of T cells and their potential partners forcefully pointed out that independent cellular movement must be overcome to prevent partner cells from moving outside of the range needed for effective molecular communication. This in turn points to the existence of "go–no go" thresholds for antigen signaling intensity; such signaling must elicit an adequate adhesive change or override the propensity for continued cell movement to ensure useful intercellular communication.

With this concept in mind, we can now better appreciate seminal observations showing that during the phase of T-B adhesion in lymph nodes, the B cells drag the T cells behind them as they move (*39*) (Fig. 3B). The early in situ imaging studies, as confirmed by many subsequent reports, helped resolve an existing controversy about

whether T cells undergo a stop signal when the T cell receptor (TCR) is adequately engaged by antigen (*4*, *5*, *12*, *13*, *23*), a phenomenon initially described in vitro (*20*, *44*, *45*). In contrast, B cells that have acquired antigen through the B cell receptor (BCR) and become activated APCs do not get such a strong stop signal and continue to migrate. Therefore, to ensure a sufficient duration of cell-cell contact to permit up-regulation of key mediators by the T cells (CD40L, cytokines, and so on) and effective sensing of these signals by the antigen-activated B cells, the T cell needs to depolarize, then adhere to and passively follow the moving B cell.

The importance of overcoming dispersive cell movement by regulated adhesion was acutely revealed while exploring the basis for immune defects produced by mutation of the small adaptor protein SAP. Functional loss of SAP in T cells results in X-linked lymphoproliferative disease in humans and a syndrome in mice characterized by the lack of germinal center responses (*46*). Two-photon imaging studies revealed that the immunodeficiency resulted from an insufficient duration of cell-cell contact between SAP-deficient activated helper T cells and activated B cells (*47*). The reduced time available for these interactions when the T cells lacked SAP prevented delivery of the molecular help required for early B cell survival and clonal expansion. The critical role of adequate cell adhesion during developing T-dependent antibody responses was missed in vitro.

This theme of cell contact duration as a key regulatory checkpoint in immunity is further emphasized by data on how inhibitory receptors on effector T cells or how regulatory T cells mediate their suppressive effects. Operating in a cis manner, CTLA-4 (*48*) and PD-1 (*49*) have both been reported in imaging analyses to limit the duration of T cell interaction with antigen-bearing DCs. Other studies have implicated interference with stable T cell contact with antigen-presenting DCs or B cells as one way regulatory T cells interfere with CD4 T cell priming (*50*) or CD8 T cell effector activity (*51*). By reducing the duration of effective cell-cell contact, and thus how long cellular receptors remain engaged, these immunoregulatory components amplify any inhibitory effects they have directly on TCR or costimulatory molecule signaling.

In contrast to examples where mature T cells adhere tightly to antigen-bearing cells during productive responses, 2P imaging has revealed other settings in which T cells remain relatively motile and collect signals from serial brief encounters with multiple APCs. This mode of interaction may provide sufficient interactions to sustain TCR signaling under conditions where peptide-MHC ligands are broadly distributed on multiple APCs or when the directed release of effector molecules by T cells is not required. Behavior of this type has been reported for activation of CD8 T cells in lymph nodes under conditions of limiting antigen on DCs (*52*) and, in particular, developing T cells undergoing TCR repertoire selection in the thymus. Immature T cells in the thymus migrate relatively slowly via random walk through the cortex (*53*, *54*), and encounters with positive-selecting ligands lead to calcium-dependent pausing (*54*) and both dynamic and stable contacts with MHC-bearing stromal cells (*3*). These behaviors are consistent with the broadly distributed self-peptide MHC ligands that induce positive selection. On the other hand, the rapid and directional migration of positively selected thymocytes is incompatible with productive engagement of peptide-MHC ligands on immobile thymic epithelial cells (*53*, *55*), and thus cessation of strong MHC recognition must occur as positively selected thymocytes relocate from the cortex to the medulla. Once in the medulla, thymocytes undergo further screening for recognition of self-antigen. Two-photon imaging of thymocytes undergoing negative selection in the medulla revealed a motile, but highly confined migration pattern (*56*) (Fig. 3C), suggesting that some autoreactive thymocytes sample multiple APCs in a local area of the medulla for some time before eventually being eliminated by clonal deletion.

The duration of T cell contact with APCs has also been explored in peripheral tolerance induction. Some (*57*, *58*) but not other (*59*) papers have described a striking difference in the length of T-DC contact under immunogenic versus tolerogenic conditions, with the former being long-lived and the latter transient. Whether these different observations arise from the specific experimental systems employed remains to be determined, but such divergent results emphasize the need for further studies on how the length of cell-cell contact influences the quality and magnitude of T cell responses, not only with respect to events within secondary lymphoid tissues but also in terms of effector T cell activity in peripheral tissues, as we discuss in the next section.

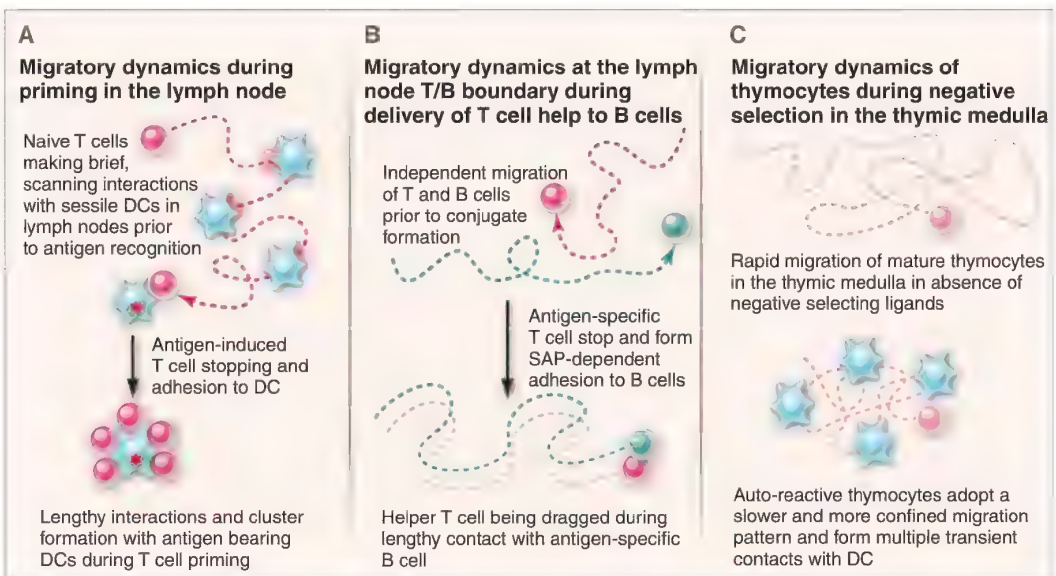

Fig. 3. Cell migratory dynamics and intracellular communication. Two-photon microscopy has revealed numerous examples in which T cells regulate their speed and cell adhesion to allow for efficient sampling of potential APCs and effective intracellular communication. (**A**) During T cell priming in lymph nodes, naive T cells (pink) migrate rapidly along FRCs (not depicted here), making brief and frequent contact with DCs (blue). Upon antigen detection, T cells arrest and adhere to DCs, leading to the formation of T cell swarms and clusters around individual DCs. In some cases, T cells undergo a phase of intermittent contacts before forming lengthy interactions with DCs (not depicted). (**B**) The independent migration of helper T cells and antigen-specific B cells (green) is overcome when T cells arrest and form stable SAP-dependent conjugates with B cells. B cells continue to migrate, dragging the T cell behind. (**C**) In the thymus, developing T cells (pink) undergo rapid migration in the medulla while scanning thymic APCs for self-antigens. Encounters with self-antigens can lead to slower and more confined migration, allowing for frequent, serial interactions with DCs (yellow) and other potential APCs in the vicinity.

Imaging Host-Pathogen Interactions and Understanding Effector Function in Tissues

Besides the basic understanding of immune cell behavior revealed by these imaging studies, 2P imaging has also become a key tool to investigate the interplay between pathogens and the host immune system (*60*). The ability to directly visualize fluorescent pathogens as they move through the body and interact with immune cells has provided a new dimension to studies of host-pathogen interactions in diverse tissues, including lymph nodes,

brain, liver, gut, and skin (*10*, *61*–*67*). Before 2P imaging, our understanding of pathogen–immune cell interactions relied largely on in vitro infection, which may miss the key role of specialized cell types that exist in vivo. Thus, 2P imaging combined with in vivo infection models has proved a powerful approach to reveal when, where, and how pathogens are engaged by the immune system.

One example is the key role of lymph node subcapsular macrophages in the initial encounters with pathogens. Besides conveying antigen to B cells, these macrophages also trap lymph-borne pathogens and impede their dissemination through the body. A particularly fascinating example involves the neurotropic vesicular stomatitis virus (*68*). In a normal lymph node, subcapsular macrophages prevent the virus from gaining access to other cells. When these macrophages are removed, however, the virus invades neurons within the lymph node and can spread rapidly to the central nervous system. In another example, by allowing themselves to be invaded by intracellular pathogens, including viruses and the protozoan parasite *Toxoplasma gondii* (*10*, *33*, *66*, *68*, *69*), subcapsular macrophages expose themselves to recognition and killing by $CD8^+$ T cells (*66*, *69*). These studies reveal that lymph node subcapsular macrophages provide an important battleground between host and pathogen during the initial phases of infection.

Two-photon imaging has also been used to visualize the standoff between pathogens and T cell effectors at sites of chronic infection (*61*, *62*, *64*, *67*). These studies reveal striking examples in which pathogens can remain undetected while surrounded by large numbers of actively migrating effector T cells. For example, effector $CD8^+$ T cells ignore *Toxoplasma*-containing cysts in the brains of chronically infected mice, despite the presence of abundant antigen, instead forming transient contacts with granuloma-like structures containing isolated parasites (*64*). Similarly, $CD4^+$ effector T cells at sites of *Leishmania major* infection focused their attention on certain parasites, while ignoring others in the immediate vicinity (*67*). Limited T cell effector responses at sites of chronic infection, and the ability of some pathogens to avoid detection altogether, help to explain the ability of pathogens to persist in the face of a T cell response and the ability of T cells to contain pathogens while avoiding collateral damage to host tissues.

The question of whether transient contacts between T cell effectors and APCs during chronic infection allow for delivery of effector functions remains controversial. Some studies suggested that short-lived interactions (called kinapses) mediated activation and function during antitumor or antiviral $CD8^+$ T cell responses (*70*, *71*). A different view emerged from analysis of chronic mycobacterial granulomas. In such lesions, a clear correlation between a low rate of antigen-induced stopping by effector T cells and a low frequency of interferon-γ–producing T cells was observed. Increasing the amount of antigen in the granuloma resulted in stopping by nearly all antigen-specific cells and in cytokine production by the same large fraction of cells (*62*). These results reinforce the notion that strong stop signals are required for elicitation of and/or delivery of T cell effector molecules, at least under many circumstances, and also indicate that only a small number of potential effectors may do so at one time when antigen is limited. This latter result has important implications for assessing whether antigen-induced stopping is critical for effector function when analyzing data on large populations of effector cells in a tissue setting. If only a small fraction of pathogen-specific cells stops at any moment, measurements such as average velocity or average confinement calculated for all the specific cells being imaged will show little difference from those seen for control (antigen-unspecific) cells, obscuring the behavior of the functionally critical subpopulation of effectors and suggesting that activation without stopping had occurred.

Many other key issues related to tissue entry and in situ function of innate and adaptive effectors have recently been highlighted by dynamic imaging studies. For example, how directional are cell paths within a tissue? Do neutrophils or effector T cells travel directly to foci of infection or tissue damage, or do they meander on the way to these end targets? Intravital imaging has shown that neutrophil migration from venules to sites of tissue damage is direct and linear, with little meandering and with essentially no neutrophils exiting an inflamed vessel on the side away from the damage (*9*, *10*), documenting a precise control of cell migration directionality at both the vessel and tissue level. In tissues, what is the effect of tissue density and architecture on effector movement, and how might this influence the search for pathogens and tumors? How long do T cells produce cytokines once in an antigen-rich tissue environment, and do they do so locally around static APCs or, in contrast, once activated by antigen within the tissue, do they move extensively, delivering effector cytokines to many distinct locations? These remain key questions for future studies.

Tracking Immunosuppression

Imaging has also been applied to investigate the action of drugs that interfere with immune processes. Two classes of immunosuppressants have been examined using this approach: egress blockers that resemble sphingosine and disrupt the normal trafficking of lymphocytes back into the circulation from the lymph node; and inhibitors of Kv1.3 potassium channels in T cells for specific suppression of effector T cells that are mediators of autoimmune disease and inflammatory responses. Several studies have imaged the egress step of lymphocytes traversing the lymphatic endothelial barrier in the medullary sinuses at particular sites, or portals, for egress to gain access to efferent lymphatic vessels (*72*–*75*). S1P1 is the target of FTY-720 (fingolimod), an agent that has shown efficacy in treatment of multiple sclerosis. After exposure to a metabolic product of this drug, lymphocytes fail to egress from lymph nodes, resulting in lymphopenia and a paucity of lymphocytes in the periphery. Intravital imaging showed that reversible agonists of S1P1 are able to prevent egress and, upon washout or addition of an S1P1 antagonist, lymphocytes were observed crossing into the medullary sinuses. Although some mechanistic aspects of egress are controversial (*22*), these studies documented the feasibility of 2P imaging to investigate drug action.

Imaging immunosuppression has also been accomplished in the periphery during chronic inflammatory immune responses. T effector memory cells recapitulate the events of antigen recognition in the lymph node, stopping in contact with tissue APCs and subsequently migrating on collagen as enlarged T cell blasts in dermal tissue during a delayed-type hypersensitivity response. Blockade of Kv1.3 channels selectively inhibits cell enlargement and motility of T effector memory cells in the tissue (*76*). Moreover, the Kv1.3 channel blockade spares the motility of naïve T cells in the lymph node and, correspondingly, does not inhibit the acute immune response to bacterial or viral infection. These experiments provide important validation for selective immunosuppression based on Kv1.3 channels as a target to ameliorate chronic autoimmune and inflammatory conditions without disrupting an acute immune response.

Future Directions

Imaging has opened a new window to observe cells of the immune system in real time and in vivo. However, current immunoimaging techniques are restricted in their ability to analyze the motility and interactions of cells over extended time and distance scales and to discriminate individual cells within a swarm of identically labeled cohorts. To address these limitations, novel approaches have been recently introduced using photoconvertible genetic probes to unambiguously mark specific cells and to image and track cells over long distances within intact tissue. This approach, called optical highlighting, eliminates ambiguity when cells cross tracks with one another and enables labeling of a subset of cells that have undergone specific behaviors, such as interactions with DCs. The method has recently been used to clarify germinal center dynamics (*43*). Other technological advances in optical imaging promise to markedly improve our ability to image deeper and faster. These new methods include sheet illumination rather than point illumination (*77*) and a shift to far red probes whose emitted photons are better able to penetrate tissue without scattering to improve signals at depth. Beyond allowing for the tracking of individual cells over greater depths and distances, these improvements will also permit following cells for longer periods, allowing better linkage between early signaling events and the subsequent differentiation and function of the imaged cells. Perhaps the most important frontier in intravital imaging of the immune system, however, is that of combining molecular imaging with the cell-level dynamic measurements that have dominated to date. The goal is not just to monitor the behavior of cells but

also to link cellular movement and positioning to changes in signaling and gene expression. Only by doing so can a robust and truly multidimensional picture of immune function in vivo be developed.

Although it is still early in this regard, progress is being made and there is an expectation of rapid advances in this arena. Existing fluorescent cytokine gene-reporter animals can be used to follow the behavior of cells that are marked as committed to a specific effector fate, but because of the longevity of the reporter fluorescent proteins, these present indicator lines are not useful for real-time analysis of contemporaneous gene expression and cytokine production. The use of rapidly degraded reporter proteins or secreted rather than cytoplasmic reporters will likely help overcome this present limitation. Ca^{2+} imaging with dyes has already been used in several published studies (*29*, *36*, *54*), and improved fluorescence resonance energy transfer–based reporters are likely to provide more robust systems for following this aspect of cellular signaling in the future. Fluorescent chimeric proteins with transcriptional factors whose nuclear translocation is important to their function have been described (*78*), as have adapters (*71*) or chimeric receptor proteins (*79*) that relocalize during TCR signaling. In addition, techniques for deconvolving the complex data involved in measuring such molecular relocation in moving cells using intravital methods have been published, so we can anticipate new insights from application of these methods in the near future. Other studies will benefit from improved physiological preparations for imaging of tissues not well studied to date, including the gastrointestinal tract, pancreas, spleen, and lung. Portable imaging setups with miniaturized light delivery systems in endoscopes or implantable devices will bring this approach into the realm of clinical diagnosis.

As the number of different colors used for such imaging increases, as the tissue volume examined and number of cells imaged enlarges, as the duration of imaging sessions lengthens, and as the use of subcellular probes becomes commonplace, there will be a critical need for new analytic methods for distilling useful information from the resulting complex data sets. Analysis of the collected images is now a time-limiting feature of many intravital studies, and this will only be an increasing bottleneck until more facile and robust ways of automated data processing are developed. Enhanced methods for tracking very large numbers of objects moving in three dimensions have been introduced in studies of embryogenesis (*80*) and certainly should be adapted for such work with immune cells, but many more computational tools for parsing the highly dynamic aspects of intravital data on immune cells will be needed to enable future studies to reach their full potential (*81*). In introducing more automated methods, it will be critical to avoid having investigators lose the intimate connection to their data that manual review now provides. The proper blend of computer assistance and direct viewing will be crucial so that unexpected behaviors that would not be automatically extracted from the data are not missed and so that artifacts that an algorithm would not notice are caught. In the end, the greatest value from imaging data comes from its integration with other modes of assessing the state and operation of the immune system. Imaging is just a tool, albeit a powerful one that has provided a new level of insight into the key dynamic aspects of immune system behavior. Systems biology methods for integrating diverse complex data sets will ultimately be a key element in extracting the greatest value from advanced imaging studies, helping to yield a more complete picture of immune function. Thus, although a decade of imaging has given rise to a new appreciation of the importance of cell motility and interaction dynamics in producing immune responses, current studies have only scratched the surface. We look forward to even greater progress in the next decade of research in this rapidly developing field.

References and Notes

1. J. L. Gowans, *Int. Rev. Exp. Pathol.* **5**, 1 (1966).
2. U. H. von Andrian, *Microcirculation* **3**, 287 (1996).
3. P. Bousso, N. R. Bhakta, R. S. Lewis, E. Robey, *Science* **296**, 1876 (2002).
4. M. J. Miller, S. H. Wei, I. Parker, M. D. Cahalan, *Science* **296**, 1869 (2002).
5. S. Stoll, J. Delon, T. M. Brotz, R. N. Germain, *Science* **296**, 1873 (2002).
6. M. D. Cahalan, I. Parker, S. H. Wei, M. J. Miller, *Nat. Rev. Immunol.* **2**, 872 (2002).
7. K. R. Garrod, S. H. Wei, I. Parker, M. D. Cahalan, *Proc. Natl. Acad. Sci. U.S.A.* **104**, 12081 (2007).
8. S. Celli, M. L. Albert, P. Bousso, *Nat. Med.* **17**, 744 (2011).
9. N. C. Peters *et al.*, *Science* **321**, 970 (2008).
10. T. Chtanova *et al.*, *Immunity* **29**, 487 (2008).
11. C. Auffray *et al.*, *Science* **317**, 666 (2007).
12. P. Bousso, E. Robey, *Nat. Immunol.* **4**, 579 (2003).
13. T. R. Mempel, S. E. Henrickson, U. H. Von Andrian, *Nature* **427**, 154 (2004).
14. M. J. Miller, A. S. Hejazi, S. H. Wei, M. D. Cahalan, I. Parker, *Proc. Natl. Acad. Sci. U.S.A.* **101**, 998 (2004).
15. M. J. Miller, O. Safrina, I. Parker, M. D. Cahalan, *J. Exp. Med.* **200**, 847 (2004).
16. R. L. Lindquist *et al.*, *Nat. Immunol.* **5**, 1243 (2004).
17. A. Kissenpfennig *et al.*, *Immunity* **22**, 643 (2005).
18. D. Sen, L. Forrest, T. B. Kepler, I. Parker, M. D. Cahalan, *Proc. Natl. Acad. Sci. U.S.A.* **107**, 8334 (2010).
19. O. Tal *et al.*, *J. Exp. Med.* **208**, 2141 (2011).
20. M. L. Dustin, S. K. Bromley, Z. Kan, D. A. Peterson, E. R. Unanue, *Proc. Natl. Acad. Sci. U.S.A.* **94**, 3909 (1997).
21. N. Kawakami *et al.*, *J. Exp. Med.* **201**, 1805 (2005).
22. J. G. Cyster, S. R. Schwab, *Annu. Rev. Immunol.* **30**, 69 (2012).
23. M. J. Miller, S. H. Wei, M. D. Cahalan, I. Parker, *Proc. Natl. Acad. Sci. U.S.A.* **100**, 2604 (2003).
24. M. Bajénoff *et al.*, *Immunity* **25**, 989 (2006).
25. T. Worbs, T. R. Mempel, J. Bölter, U. H. von Andrian, R. Förster, *J. Exp. Med.* **204**, 489 (2007).
26. J. E. Gretz, A. O. Anderson, S. Shaw, *Immunol. Rev.* **156**, 11 (1997).
27. F. Castellino *et al.*, *Nature* **440**, 890 (2006).
28. S. Hugues *et al.*, *Nat. Immunol.* **8**, 921 (2007).
29. S. H. Wei *et al.*, *J. Immunol.* **179**, 1586 (2007).
30. J. G. Cyster, *Nat. Immunol.* **11**, 989 (2010).
31. T. G. Phan, I. Grigorova, T. Okada, J. G. Cyster, *Nat. Immunol.* **8**, 992 (2007).
32. Y. R. Carrasco, F. D. Batista, *Immunity* **27**, 160 (2007).
33. T. Junt *et al.*, *Nature* **450**, 110 (2007).
34. T. G. Phan, J. A. Green, E. E. Gray, Y. Xu, J. G. Cyster, *Nat. Immunol.* **10**, 786 (2009).
35. R. Roozendaal *et al.*, *Immunity* **30**, 264 (2009).
36. H. Qi, J. G. Egen, A. Y. Huang, R. N. Germain, *Science* **312**, 1672 (2006).
37. P. Garside *et al.*, *Science* **281**, 96 (1998).
38. K. Reif *et al.*, *Nature* **416**, 94 (2002).
39. T. Okada *et al.*, *PLoS Biol.* **3**, e150 (2005).
40. C. D. Allen, T. Okada, H. L. Tang, J. G. Cyster, *Science* **315**, 528 (2007).
41. T. A. Schwickert *et al.*, *Nature* **446**, 83 (2007).
42. A. E. Hauser *et al.*, *Immunity* **26**, 655 (2007).
43. G. D. Victora *et al.*, *Cell* **143**, 592 (2010).
44. P. A. Negulescu, T. B. Krasieva, A. Khan, H. H. Kerschbaum, M. D. Cahalan, *Immunity* **4**, 421 (1996).
45. E. Donnadieu, G. Bismuth, A. Trautmann, *Curr. Biol.* **4**, 584 (1994).
46. J. L. Cannons, S. G. Tangye, P. L. Schwartzberg, *Annu. Rev. Immunol.* **29**, 665 (2011).
47. H. Qi, J. L. Cannons, F. Klauschen, P. L. Schwartzberg, R. N. Germain, *Nature* **455**, 764 (2008).
48. H. Schneider *et al.*, *Science* **313**, 1972 (2006).
49. B. T. Fife *et al.*, *Nat. Immunol.* **10**, 1185 (2009).
50. Q. Tang *et al.*, *Nat. Immunol.* **7**, 83 (2006).
51. T. R. Mempel *et al.*, *Immunity* **25**, 129 (2006).
52. S. E. Henrickson *et al.*, *Nat. Immunol.* **9**, 282 (2008).
53. C. M. Witt, S. Raychaudhuri, B. Schaefer, A. K. Chakraborty, E. A. Robey, *PLoS Biol.* **3**, e160 (2005).
54. N. R. Bhakta, D. Y. Oh, R. S. Lewis, *Nat. Immunol.* **6**, 143 (2005).
55. L. I. Ehrlich, D. Y. Oh, I. L. Weissman, R. S. Lewis, *Immunity* **31**, 986 (2009).
56. M. Le Borgne *et al.*, *Nat. Immunol.* **10**, 823 (2009).
57. S. Hugues *et al.*, *Nat. Immunol.* **5**, 1235 (2004).
58. S. D. Katzman *et al.*, *Proc. Natl. Acad. Sci. U.S.A.* **107**, 18085 (2010).
59. G. Shakhar *et al.*, *Nat. Immunol.* **6**, 707 (2005).
60. J. L. Coombes, E. A. Robey, *Nat. Rev. Immunol.* **10**, 353 (2010).
61. J. G. Egen *et al.*, *Immunity* **28**, 271 (2008).
62. J. G. Egen *et al.*, *Immunity* **34**, 807 (2011).
63. M. Chieppa, M. Rescigno, A. Y. Huang, R. N. Germain, *J. Exp. Med.* **203**, 2841 (2006).
64. M. Schaeffer *et al.*, *J. Immunol.* **182**, 6379 (2009).
65. B. John *et al.*, *PLoS Pathog.* **5**, e1000505 (2009).
66. H. D. Hickman *et al.*, *Nat. Immunol.* **9**, 155 (2008).
67. O. Filipe-Santos *et al.*, *Cell Host Microbe* **6**, 23 (2009).
68. M. Iannacone *et al.*, *Nature* **465**, 1079 (2010).
69. T. Chtanova *et al.*, *Immunity* **31**, 342 (2009).
70. J. V. Kim, S. S. Kang, M. L. Dustin, D. B. McGavern, *Nature* **457**, 191 (2009).
71. G. A. Azar, F. Lemaître, E. A. Robey, P. Bousso, *Proc. Natl. Acad. Sci. U.S.A.* **107**, 3675 (2010).
72. S. H. Wei *et al.*, *Nat. Immunol.* **6**, 1228 (2005).
73. M. G. Sanna *et al.*, *Nat. Chem. Biol.* **2**, 434 (2006).
74. I. L. Grigorova *et al.*, *Nat. Immunol.* **10**, 58 (2009).
75. S. M. Cahalan *et al.*, *Nat. Chem. Biol.* **7**, 254 (2011).
76. M. P. Matheu *et al.*, *Immunity* **29**, 602 (2008).
77. T. V. Truong, W. Supatto, D. S. Koos, J. M. Choi, S. E. Fraser, *Nat. Methods* **8**, 757 (2011).
78. H. J. Melichar *et al.*, *Immunol. Cell Biol.* **89**, 549 (2011).
79. R. S. Friedman, P. Beemiller, C. M. Sorensen, J. Jacobelli, M. F. Krummel, *J. Exp. Med.* **207**, 2733 (2010).
80. K. Khairy, P. J. Keller, *Genesis* **49**, 488 (2011).
81. F. Klauschen *et al.*, *Nat. Protoc.* **4**, 1305 (2009).
82. F. Geissmann *et al.*, *PLoS Biol.* **3**, e113 (2005).
83. R. N. Germain, M. J. Miller, M. L. Dustin, M. C. Nussenzweig, *Nat. Rev. Immunol.* **6**, 497 (2006).
84. M. D. Cahalan, I. Parker, *Annu. Rev. Immunol.* **26**, 585 (2008).
85. T. Aoshi *et al.*, *Immunity* **29**, 476 (2008).
86. M. Bajénoff, N. Glaichenhaus, R. N. Germain, *J. Immunol.* **181**, 3947 (2008).
87. D. Kreisel *et al.*, *Proc. Natl. Acad. Sci. U.S.A.* **107**, 18073 (2010).
88. M. R. Looney *et al.*, *Nat. Methods* **8**, 91 (2011).
89. L. L. Cavanagh *et al.*, *Nat. Immunol.* **6**, 1029 (2005).
90. M. Ishii *et al.*, *Nature* **458**, 524 (2009).
91. K. Coppieters, M. M. Martinic, W. B. Kiosses, N. Amirian, M. von Herrath, *PLoS ONE* **5**, e15732 (2010).

Acknowledgments: We would like to thank members of our laboratory groups for their contributions to the research described here and for comments on the manuscript. We apologize to the many authors who contributed importantly to the field of imaging the immune response but whose work could not be included in the references for lack of space. This research was supported by the Intramural Research Program of the National Institute of Allergy and Infectious Diseases, NIH (R.N.G.); AI-065537 and AI-064227 (E.A.R.); and NIH RO1 grant GM-41514 (M.D.C.).

10.1126/science.1221063

Hesperian Age for Western Medusae Fossae Formation, Mars

James R. Zimbelman* and Stephen P. Scheidt

The Medusae Fossae Formation (MFF) on Mars is an intensely eroded deposit near the northern edge of the cratered highlands, between ~130° and ~230°E longitude and ~15°S to ~15°N latitude (*1*–*3*). Recent geologic mapping of western and central MFF (*4*) identified outliers of MFF materials well beyond the previously mapped limits of the deposit (*5*), including outliers close to Gale crater, the landing site chosen for the Mars Science Laboratory (MSL) rover Curiosity, en route to an August 2012 landing.

Global mapping identified three members of MFF (upper, middle, and lower); Viking-based crater counts showed all members to be Amazonian in age (*1*, *2*), younger than the Hesperian and Noachian systems (*6*). Divisions between the three martian eras likely correspond to ~3.5 and ~3.8 billion years (Ga), although this is dependent on production functions used (*7*). We present crater size frequency distributions and inferred ages derived from craters counted on recent spacecraft imaging data for four mapped MFF subunits (*4*, *5*) (Fig. 1 and fig. S1). We subdivided the lower member of MFF into two units on the basis of superposition; the stratigraphically upper component has an early Amazonian age (Aml2), whereas the lower component has an age near the Amazonian-Hesperian boundary (AHml1). Craters on a nearby exposure of middle-member material (superposed on the lower member) indicate a late Hesperian age (Hmm). An exposure of lower-member materials in the central portion of MFF [Hml, MC-16 NW (*4*, *5*)] has a crater size frequency distribution statistically indistinguishable from those of the AHml1 and Hmm units. These results indicate that the crater retention ages for MFF units likely represent surface exposure ages rather than emplacement ages; the lower-member units experienced substantial erosion into the early Amazonian, even though late-Hesperian-aged middle-member material (showing less evidence of resurfacing) is superposed on some lower-member exposures. Therefore, emplacement of both the lower and middle members occurred before the late Hesperian, much earlier than indicated by prior investigations (*1*, *2*, *8*) but consistent with recent work that suggests a Hesperian age for portions of MFF (*9*).

A Hesperian age for western MFF has implications for materials at the MSL landing site. Aml2 materials consist of uniformly bedded materials quite similar to layers near the top of the Gale mound (fig. S2); both terrains are unlike the variable-thickness layers exposed in the lower portions of the mound (*10*). Our MFF results are consistent with recent cratering results for the entire Gale mound, which indicate a late Hesperian to early Amazonian exposure age (*11*). There may not be as substantial a time gap between the upper and lower portions of the Gale mound, despite the presence of an unconformity between the mound units (*10*). The hypothesized ignimbrite origin for MFF (*12*–*14*) may thus apply to the regularly layered upper units of the Gale mound. Curiosity may test this interpretation while exploring the Gale mound.

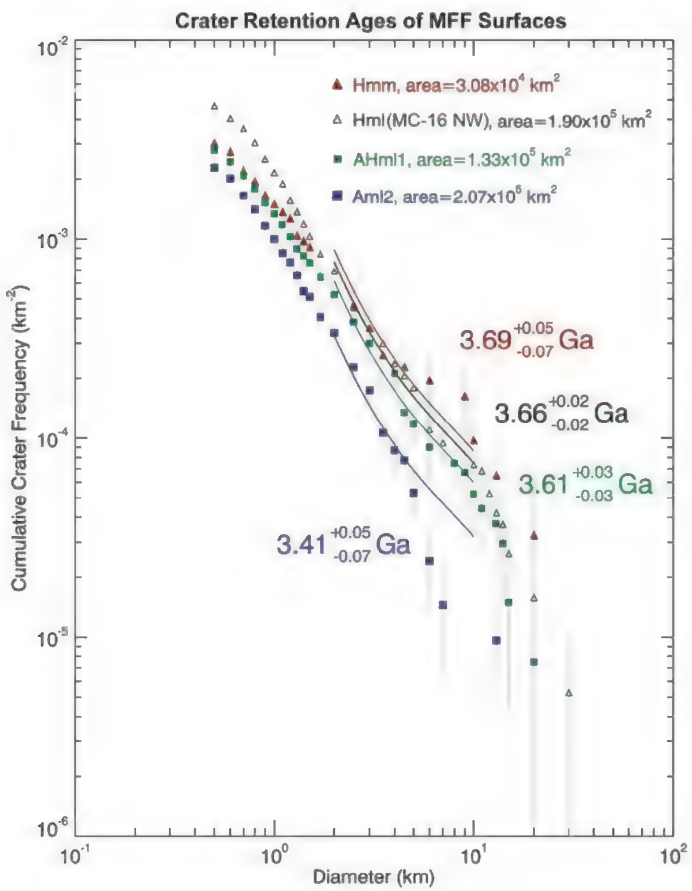

Fig. 1. Binned cumulative crater frequency data for three MFF units in quadrangle MC-23 NW and unit Hml from quadrangle MC-16 NW (black symbols). Crater retention ages (with 1σ error estimates) were derived from fitting craters in the 2- to 10-km-diameter range (*4*).

References and Notes

1. D. H. Scott, K. L. Tanaka, *U.S. Geol. Survey Map* I-1802-A, scale 1:15,000,000 (1986).
2. R. Greeley, J. E. Guest, *U.S. Geol. Survey Map* I-1802-B, scale 1:15,000,000 (1987).
3. J. R. Zimbelman, L. J. Griffin, *Icarus* **205**, 198 (2010).
4. Data and methods are available as supplementary materials on *Science* Online.
5. J. R. Zimbelman, S. P. Scheidt, *Lunar Planet. Sci.* **43**, Abs. 2052 (2012).
6. K. L. Tanaka, *J. Geophys. Res.* **91**, E139 (1986).
7. S. C. Werner, K. L. Tanaka, *Icarus* **215**, 603 (2011).
8. S. C. Werner, *Icarus* **201**, 44 (2009).
9. L. Kerber, J. W. Head, *Icarus* **206**, 669 (2010).
10. R. E. Milliken, J. P. Grotzinger, B. J. Thomson, *Geophys. Res. Lett.* **37**, L04201 (2010).
11. B. J. Thomson *et al.*, *Icarus* **214**, 413 (2011).
12. D. H. Scott, K. L. Tanaka, *J. Geophys. Res.* **87**, 1179 (1982).
13. B. A. Bradley, S. E. H. Sakimoto, H. Frey, J. R. Zimbelman, *J. Geophys. Res.* **107**, 5058 (2002).
14. K. E. Mandt, S. L. de Silva, J. R. Zimbelman, D. A. Crown, *J. Geophys. Res.* **113**, E12011 (2008).

Acknowledgments: This work was supported by NASA grant NNX07AP42G from the Planetary Geology and Geophysics program.

Supplementary Materials

www.sciencemag.org/cgi/content/full/science.1221094/DC1
Materials and Methods
Supplementary Text
Figs. S1 and S2
Table S1
References (*15*–*18*)

27 February 2012; accepted 25 April 2012
Published online 24 May 2012;
10.1126/science.1221094

Center for Earth and Planetary Studies, MRC 315, National Air and Space Museum, Smithsonian Institution, Washington, DC 20013–7012, USA.

*To whom correspondence should be addressed. E-mail: zimbelmanj@si.edu

Synthesis of Self-Pillared Zeolite Nanosheets by Repetitive Branching

Xueyi Zhang,[1] Dongxia Liu,[1] Dandan Xu,[1] Shunsuke Asahina,[2] Katie A. Cychosz,[3] Kumar Varoon Agrawal,[1] Yasser Al Wahedi,[1] Aditya Bhan,[1] Saleh Al Hashimi,[4] Osamu Terasaki,[5,6] Matthias Thommes,[3] Michael Tsapatsis[1]*

Hierarchical zeolites are a class of microporous catalysts and adsorbents that also contain mesopores, which allow for fast transport of bulky molecules and thereby enable improved performance in petrochemical and biomass processing. We used repetitive branching during one-step hydrothermal crystal growth to synthesize a new hierarchical zeolite made of orthogonally connected microporous nanosheets. The nanosheets are 2 nanometers thick and contain a network of 0.5-nanometer micropores. The house-of-cards arrangement of the nanosheets creates a permanent network of 2- to 7-nanometer mesopores, which, along with the high external surface area and reduced micropore diffusion length, account for higher reaction rates for bulky molecules relative to those of other mesoporous and conventional MFI zeolites.

Zeolites with structural features as small as the size of a unit cell (e.g., 1 to 5 nm), including those with lamellar structure (*1*–*4*), can be used as building blocks for thin films (*5*–*7*). Additionally, hierarchical adsorbents and catalysts constructed by introducing mesopores between the zeolitic domains allow access of bulkier molecules often encountered in oil and biomass processing (*8*, *9*). Methods for the preparation of mesoporous zeolites involve multifunctional structure-directing agents (SDAs) and/or postsynthesis processing, such as pillaring or desilication/dealumination (*8*, *10*–*12*). Crystal growth by repetitive branching of layers can constitute a simple, low-cost approach for bottom-up synthesis of hierarchical zeolites and pillared materials. Although branching (by twinning, rotational intergrowths, or polytypic overgrowths) has been used to design nanostructures (*13*, *14*), it has not been explored for the formation of pillared zeolites. Among several candidates of epitaxially and rotationally overgrown zeolites [e.g., MFI/MEL (*15*), EMT/FAU (*16*), ETS-4/ETS-10 (*17*), CAN/SOD (*18*), MFI (*19*), and CHA (*20*)], we focus on exploring the 90° rotational intergrowths (or twins) of the MFI framework [which contains sinusoidal 10-member ring (10-MR) channels along the *a* axis, interconnected with straight 10-MR channels along the *b* axis] motivated by the prominence of the corresponding aluminosilicate (called ZSM-5) as a catalyst in chemical processing. Such an approach uses a single, simple, and relatively inexpensive SDA. Here, we demonstrate the one-step synthesis of a hierarchical self-pillared zeolite composed of orthogonally connected single–unit cell lamellae (2 nm thick) resembling a house-of-cards construction (*21*).

We decided to explore tetrabutylphosphonium (TBP)–silica and tetrabutylammonium (TBA)–silica sols, which are known to yield MFI as well as mixtures of MFI with the related structure MEL (which contains straight 10-MR channels along the *a* axis, interconnected with straight 10-MR channels along the *b* axis) (*7*, *22*). Figure 1A shows particles obtained after 3 hours at 388 K starting from a clear sol with composition $1SiO_2$:0.3TBPOH:$10H_2O$:4EtOH (*23*) (TBPOH, tetrabutylphosphonium hydroxide; EtOH, ethyl alcohol). Figure 1B shows a high-resolution transmission electron microscopy (HRTEM) image along with the corresponding fast Fourier transform (FFT) confirming that the particles are MFI plates, thin along the *b* axis. Their thickness was determined by atomic force microscopy (AFM) (fig. S1) to be ~2 nm (i.e., a unit cell along the *b* axis), thinner than previously reported lamellae made by exfoliation (*24*). With further heat treatment, the lamellae became intergrown. After 40 hours at 388 K, the product contained crystalline particles with size varying between 100 and 200 nm (Fig. 2A). HRTEM images (Fig. 2B) showed that the particles consist of crystalline zeolite lamellae with a layer thickness of 2 nm. Remarkably, the zeolite lamellae are intergrown in a house-of-cards arrangement (i.e., with the lamellae arranged perpendicular to each other) to define pores between them. TEM images, taken after calcination in air at 823 K for 12 hours, do not reveal any change in the house-of-cards arrangement (Fig. 2C). The pores as well as the connectivity of the lamellae can also be seen by low-voltage scanning electron microscopy (SEM) from calcined samples (Fig. 2, D and E).

To further probe their internal structure, we embedded the calcined particles in polystyrene and studied thin sections by TEM. Intermittent lattice fringes, as shown in Fig. 2F, provide evidence for pores between adjacent lamellae penetrating throughout the particles. Further TEM imaging and FFT analysis (Fig. 3A) indicated that the thin dimension (~2 nm) of the lamellae is along the *b* axis of MFI and that the lamellae are longer along the *c* axis and shorter (~100 nm) along the *a* axis. Additional synthesis and characterization (figs. S2 and S3) show that the self-pillared zeolite can be prepared in a range of conditions that allow manipulation of composition and particle size (supplementary text).

Two plausible models for the local structure of the intergrown lamellae are shown in the

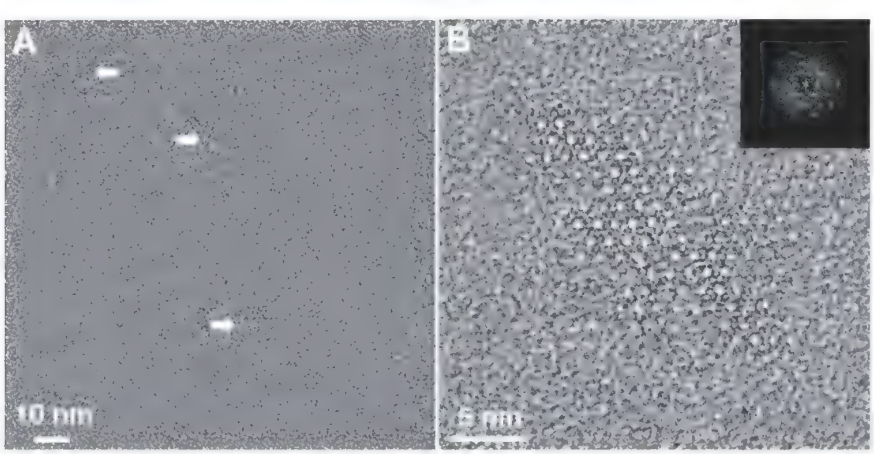

Fig. 1. (**A**) TEM image of zeolite nanoparticles obtained after 3 hours at 388 K. (**B**) High-resolution TEM image of a representative zeolite particle obtained after 7 hours at 388 K. Both samples were first aged at 353 K for 2 days. The inset in (B) is the fast Fourier transform (FFT) of the high-resolution TEM image.

[1]Department of Chemical Engineering and Materials Science, University of Minnesota, Minneapolis, MN 55455, USA. [2]SM Application Group, JEOL Ltd., Akisima, Tokyo 196-8558, Japan. [3]Quantachrome Instruments, 1900 Corporate Drive, Boynton Beach, FL 33426, USA. [4]Chemical Engineering Program, Petroleum Institute, Abu Dhabi, United Arab Emirates. [5]Graduate School of Energy, Environment, Water and Sustainability (EEWS), World Class University Program, Korea Advanced Institute of Science and Technology, 291 Daehak-ro (373-1 Guseong-dong), Yuseong-gu, Daejeon 305-701, Republic of Korea. [6]Department of Materials and Environmental Chemistry and Bezelii Center EXSELENT on Porous Materials, Stockholm University, SE-106 91 Stockholm, Sweden.

*To whom correspondence should be addressed. E-mail: tsapatsis@umn.edu

insets of Fig. 3B. According to these idealized fragment models, single–unit cell MFI lamellae (with thickness of one unit cell along the *b* axis of the MFI structure) are intergrown with their 90° twins or rotational intergrowths having a common *c* axis. In one of the idealized models, we hypothesize that the twins are connected through a needle of MEL (1 × 1 unit cell across and elongated along the *c* axis). The MEL connection runs through the entire interface of the MFI twins, ensuring full connectivity. There are 12 different ways to make the idealized connection; one of these is shown in the lower inset of Fig. 3B (see fig. S4 for the others). In the actual material, looser connections are possible (as depicted schematically in fig. S5, A to C), with partial overlay of the MFI lamellae. An idealized fragment with no connection between the MFI lamellae is also shown in the upper inset of Fig. 3B. TEM images from particles at an early stage of intergrowth (fig. S5, D and E) provide evidence for the presence of single–unit cell outgrowths emerging from the MFI plates. MEL/MFI intergrowths when using TBA and TBP ions have been reported before (*15*, *25*), and twining or rotational intergrowths are well known in MFI crystals. However, they were not associated with single–unit cell lamellae formation or with repetitive branching to create a hierarchical zeolite. The tetrabutyl SDA, which is stable at crystal growth conditions and is incorporated intact in the framework (fig. S6), appears to be an important contributor to the anisotropic growth giving rise to the single–unit cell lamellae. In the range of MFI and MEL reflections, the simulated powder x-ray diffraction (XRD) pattern of both fragment models, obtained using UDSKIP (*23*), are in good agreement with the experimental data (Fig. 3B). At lower angles, the simulation shows broad reflections (similar for both fragments) due to the small dimensions of the fragment model. As expected, these reflections are absent from the experimental diffraction pattern of the 100- to 200-nm crystals because even though they consist of numerous interconnected fragments, they preserve their crystallographic alignment (long-range order) due to the ordered branching growth mechanism. Because the new material could be an MFI/MEL intergrowth, we refer to it as self-pillared pentasil (SPP) zeolite, although it consists mostly of MFI with MEL being present, if at all, at the branching points.

We carried out the exfoliation procedure developed by Maheshwari *et al.* (*26*) on the as-synthesized material. As shown in fig. S7, it is possible to obtain individual lamellae. The high-resolution TEM image from one isolated lamella (fig. S7B) further confirms that the thickness of the lamellae is 2 nm. The exfoliated lamellar zeolites can be potentially used as building units for selective membranes according to the procedure recently reported in (*24*).

To explore the catalytic properties of SPP zeolites, we incorporated Al in the framework (fig. S8) at two different ratios of Si/Al: 253 and 75, both of which required the addition of NaOH (*23*). Synthesis in the presence of sodium and aluminum did not prevent branching and self-pillaring, as clearly seen by TEM imaging (fig. S8, A and B). Argon adsorption isotherms at 87.3 K and pore size analysis are given in figs. S10 to S12. The cumulative pore volume plots calculated from nonlocal density functional theory (NLDFT) (*27*) over the complete pore size range are shown in Fig. 3C and indicate the presence

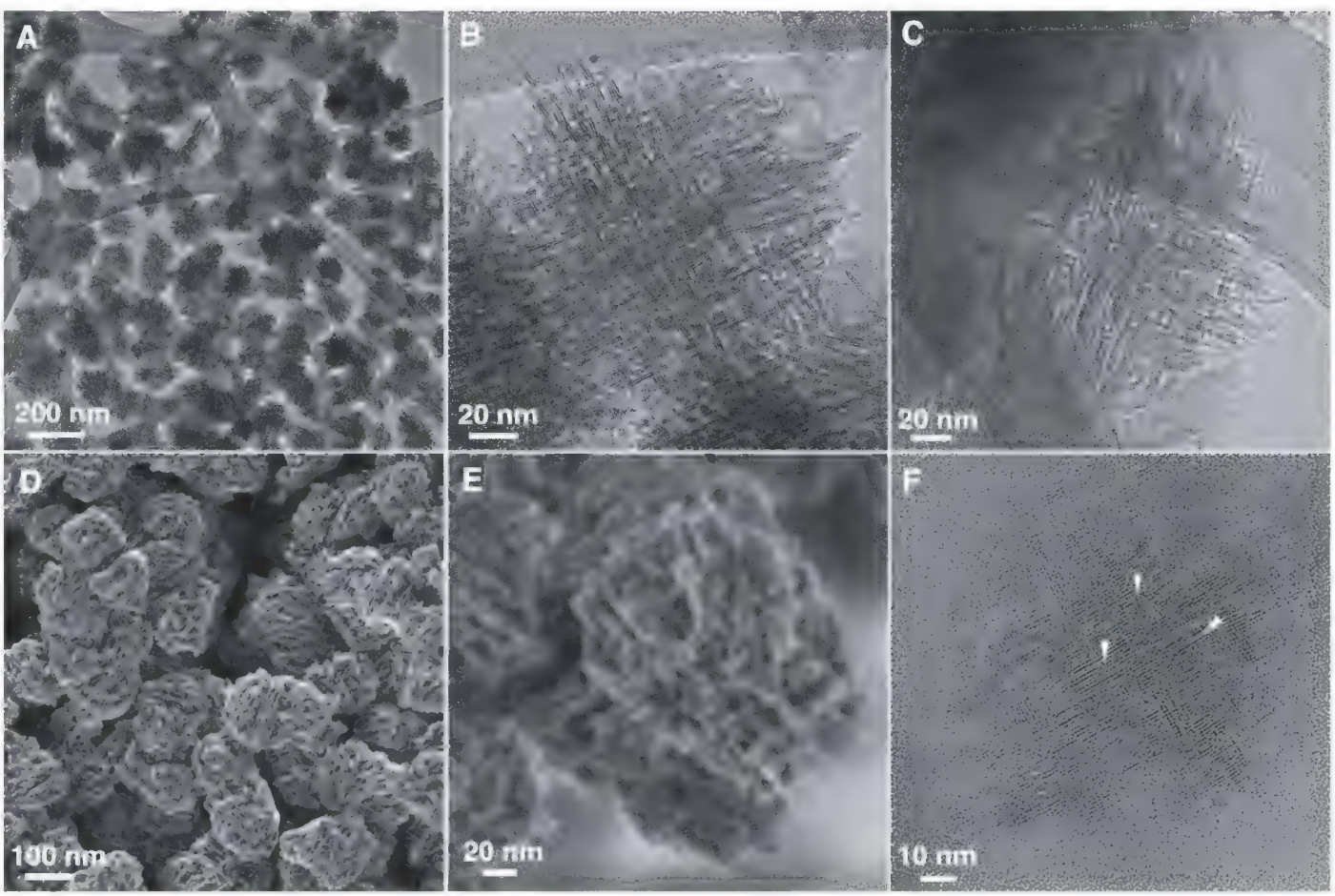

Fig. 2. Structure and morphology of the pure-silica self-pillared pentasil (SPP) zeolite particles after 40 hours of hydrothermal synthesis at 388 K. (**A** and **B**) Low-magnification (A) and high-magnification (B) TEM images of the particles before calcination, showing the morphology and the mesopores formed within the intersecting zeolitic lamellae. (**C**) TEM image of the particles after calcination, showing the retained mesoporosity. (**D** and **E**) Low-voltage, high-resolution SEM images of the calcined particles at two different magnifications, showing the mesopores and lamellar connectivity. (**F**) High-resolution TEM image of a thin section of the calcined zeolite embedded in polystyrene. Intermittent lattice fringes (arrows) suggest that mesopores exist throughout the particle.

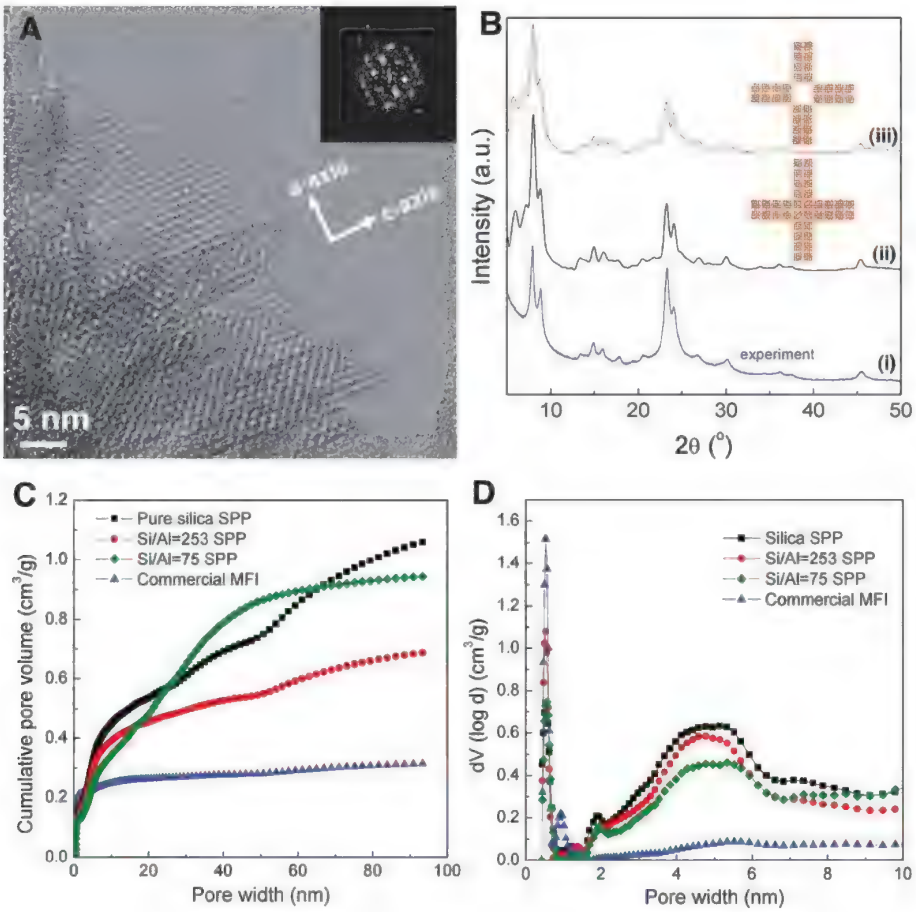

Fig. 3. (**A**) High-resolution TEM image of a SPP lamella viewed across its thin dimension; the FFT from the lamella is consistent with the [010]-zone axis of zeolite MFI. (**B**) Experimental (i) and simulated (ii and iii) powder XRD patterns of the pure-silica SPP zeolite. Insets show the intergrowth models from which the simulated XRD patterns were obtained; the model for trace ii is the idealized MFI/MEL model, that for trace iii is the idealized model with MEL removed, and the dimension of the model along the common *c* axis is 10 unit cells. (**C** and **D**) Argon (87.3 K) NLDFT cumulative pore volume plots over the entire pore width range (C) and pore size distributions up to 10 nm (D) for silica (squares), aluminosilicate SPP zeolite (circles, Si/Al = 253; diamonds, Si/Al = 75), and commercial MFI (triangles).

of micro- and mesoporosity in the SPP samples. The pore size distributions plotted up to 10 nm (Fig. 3D) indicate micropores centered around 0.522 nm, typical of MFI and MEL, and a broad distribution of mesopores (from ~2 to 7 nm) for both the silica and aluminosilicate SPP, in good agreement with the TEM and SEM images.

The catalytic properties of SPP were compared with those of pillared MFI (*3*), three-dimensionally ordered mesoporous-imprinted (3DOm-i) MFI, and three conventional MFI catalysts with different crystal size (17, 1.4, and 0.2 μm) (*23*). The Brønsted acid site concentrations of all zeolites, including that of the aluminosilicate SPP, were determined by chemical titration methods (*28*) and were found to agree well with those expected from the Si/Al ratio from elemental analysis (table S1). The fraction of acid sites present at the external surface was determined for each catalyst by means of a titrant molecule, 2,6-di-*tert*-butylpyridine (DTBP), that cannot enter the zeolite pores. The results were in good agreement with the values expected from the external surface areas of the corresponding catalysts (*9*) (table S1). Specifically, 30% and 45% of the acid sites in pillared MFI and SPP, respectively, are sites that are accessible by a molecule that cannot enter the micropores; for a micrometer-sized crystal, this fraction is ~2%. As a result of the increase in number of accessible acid sites, the pseudo–first-order rate constant for the liquid-phase alkylation of mesitylene (a molecule that is effectively excluded from the zeolite micropores) by benzyl alcohol was found to vary by more than two orders of magnitude (fig. S14 and table S2, column 2). However, when normalized per external acid site, the rate constant was found to be nearly invariant across all samples tested (Fig. 4A and table S2, column 3); this shows that the reactivity of external acid sites is similar among all samples tested, despite the different morphologies and synthesis conditions.

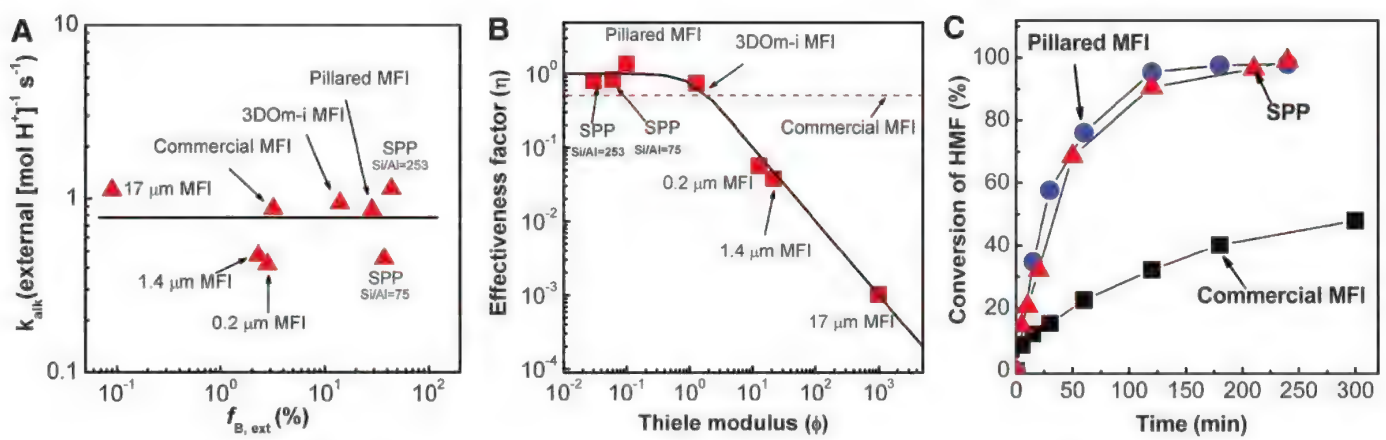

Fig. 4. Comparison of catalytic performance of SPP zeolite with pillared, 3DOm-i, and commercial and conventional (0.2, 1.4, and 17 μm) MFI. (**A**) Pseudo–first-order rate constant per external Brønsted acid site for mesitylene alkylation by benzyl alcohol. (**B**) Effectiveness factor versus Thiele modulus plot (solid line) and experimental data. The effectiveness factor of commercial MFI is indicated by the dashed line because the particle size of the commercial zeolite as determined by SEM is broad (0.1 to 1 μm) and therefore, its Thiele modulus cannot be determined. (**C**) Plots of HMF-to-OBMF conversion versus time for pillared MFI (circles), SPP zeolite (triangles), and commercial MFI (squares).

MFI lamellae are unique among the available aluminosilicate zeolite lamellae because they have pores that run across the lamella thickness (*3*). The nanometer-scale diffusion lengths of pillared MFI and SPP allow for fast transport even for molecules with small micropore diffusivity. In this respect, pillared MFI and SPP are valuable model materials for the quantitative assessment of diffusion limitations and intrinsic kinetics. The self-etherification of benzyl alcohol in the presence of DTBP (used in order to deactivate the external sites) was considered as an example. The plot of the effectiveness factor versus the Thiele modulus shows excellent agreement with the experimental data (*23*, *29*), from which it can be concluded that Brønsted acid sites in the micropores of SPP and pillared MFI have reactivity similar to those in conventional and nanocrystalline MFI, and that the observed differences in apparent reaction rates can be fully accounted for by diffusion limitations. A comparison of effectiveness factors with that of a commercially available ZSM-5 catalyst (dashed line in Fig. 4B) reveals that 3DOm-i, pillared MFI, and SPP catalysts exhibit higher apparent reaction rates. Improved behavior of pillared MFI and SPP was also established in other reactions. For example, etherification of 5-hydroxymethyl-2-furaldehyde (HMF) to 5,5′-oxy(bismethylene)-2-furaldehyde (OBMF) proceeds to completion, whereas commercial ZSM-5 suffers from deactivation (Fig. 4C). Because OBMF is a desirable biobased intermediate (*30*), this finding underscores the potential of single–unit cell layers in applications beyond petrochemical processing.

Branching of zeolite nanometer-sized lamellae, through repetitive twinning or other intergrowth processes, is a new low-cost approach toward hierarchical materials with interconnected micropores and mesopores. It is in principle applicable to all zeolite structures that can (i) be grown anisotropically as thin layers and (ii) can support branching at certain acute angles (supplementary text and fig. S16).

References and Notes

1. A. Corma, V. Fornes, S. B. Pergher, T. L. M. Maesen, J. G. Buglass, *Nature* **396**, 353 (1998).
2. Y. X. Wang, H. Gies, B. Marler, U. Muller, *Chem. Mater.* **17**, 43 (2005).
3. K. Na *et al.*, *J. Am. Chem. Soc.* **132**, 4169 (2010).
4. W. J. Roth, D. L. Dorset, *Micropor. Mesopor. Mater.* **142**, 32 (2011).
5. M. A. Snyder, M. Tsapatsis, *Angew. Chem. Int. Ed.* **46**, 7560 (2007).
6. M. Tsapatsis, *Science* **334**, 767 (2011).
7. Z. J. Li, C. M. Lew, S. Li, D. I. Medina, Y. S. Yan, *J. Phys. Chem. B* **109**, 8652 (2005).
8. J. Pérez-Ramírez, C. H. Christensen, K. Egeblad, C. H. Christensen, J. C. Groen, *Chem. Soc. Rev.* **37**, 2530 (2008).
9. D. Liu, A. Bhan, M. Tsapatsis, S. Al Hashimi, *ACS Catal.* **1**, 7 (2011).
10. J. Wang, W. Yue, W. Zhou, M.-O. Coppens, *Micropor. Mesopor. Mater.* **120**, 19 (2009).
11. D. P. Serrano *et al.*, *Catal. Today* **168**, 86 (2011).
12. K. Na *et al.*, *Science* **333**, 328 (2011).
13. L. Manna, D. J. Milliron, A. Meisel, E. C. Scher, A. P. Alivisatos, *Nat. Mater.* **2**, 382 (2003).
14. Y.- Jun, H.-W. Chung, J.- Jang, J. Cheon, *J. Mater. Chem.* **21**, 10283 (2011).
15. T. Ohsuna, O. Terasaki, Y. Nakagawa, S. I. Zones, K. Hiraga, *J. Phys. Chem. B* **101**, 9881 (1997).
16. M. M. J. Treacy, D. E. W. Vaughan, K. G. Strohmaier, J. M. Newsam, *Proc. R. Soc. A* **452**, 813 (1996).
17. H. K. Jeong, J. Krohn, K. Sujaoti, M. Tsapatsis, *J. Am. Chem. Soc.* **124**, 12966 (2002).
18. T. Okubo *et al.*, *Angew. Chem. Int. Ed.* **40**, 1069 (2001).
19. L. Karwacki *et al.*, *Nat. Mater.* **8**, 959 (2009).
20. G. R. Millward, S. Ramdas, J. M. Thomas, *Proc. R. Soc. A* **399**, 57 (1985).
21. K. Möller, T. Bein, *Science* **333**, 297 (2011).
22. L. Y. Hou, L. B. Sand, in *Proceedings of the Sixth International Zeolite Conference*, D. Olson, A. Bisio, Eds. (Butterworths, Guildford, UK, 1983), pp. 887–893.
23. See supplementary materials on *Science* Online.
24. K. Varoon *et al.*, *Science* **334**, 72 (2011).
25. A. Tuel, Y. B. Taarit, *Micropor. Mater.* **2**, 501 (1994).
26. S. Maheshwari *et al.*, *J. Am. Chem. Soc.* **130**, 1507 (2008).
27. P. I. Ravikovitch, A. V. Neimark, *Colloids Surf. A* **187–188**, 11 (2001).
28. P. Cheung, A. Bhan, G. J. Sunley, E. Iglesia, *Angew. Chem. Int. Ed.* **45**, 1617 (2006).
29. R. Aris, in *Elementary Chemical Reactor Analysis* (Dover, Boston, 1989), chap. 6.
30. O. Casanova, S. Iborra, A. Corma, *J. Catal.* **275**, 236 (2010).

Acknowledgments: We acknowledge support, for all aspects of SPP zeolite, from the Catalysis Center for Energy Innovation (award DESC00001004), an Energy Frontier Research Center funded by the U.S. Department of Energy, Office of Science, Office of Basic Energy Sciences. Partial support for synthesizing conventional, 3DOm-i, and pillared zeolites and their catalytic testing was provided by ADMIRE (Abu Dhabi–Minnesota Institute for Research Excellence), NSF Emerging Frontiers in Research and Innovation grant 0937706, and the Initiative for Renewable Energy and the Environment, a program of the University of Minnesota's Institute on the Environment. Portions of this work were conducted at the University of Minnesota Characterization Facility, which receives partial support from NSF through the NNIN program. Computing resources were provided by the Minnesota Supercomputing Institute. Supported by a University of Minnesota Graduate School doctoral dissertation fellowship (X.Z.) and by ADGAS and GASCO (Y.A.W.). We thank T. Ohsuna for helpful suggestions and S. Hwang for obtaining solid-state NMR spectra. M.T. has an equity interest in, and serves as the Chief Scientific Officer for, Argilex, a company that may commercially benefit from the results of this research. M.T., X.Z., and the University of Minnesota have financial interests arising from a right to receive royalty income under the terms of a license agreement with Argilex. These relationships have been reviewed and managed by the University of Minnesota in accordance with its conflict of interest policies. A U.S. patent application by M.T. and X.Z. was filed on 3 November 2011 (Application No. 13/288,595).

Supplementary Materials

www.sciencemag.org/cgi/content/full/336/6089/1684/DC1
Materials and Methods
Supplementary Text
Figs. S1 to S16
Tables S1 and S2
References (*31–40*)

27 December 2011; accepted 8 May 2012
10.1126/science.1221111

Seemingly Anomalous Angular Distributions in H + D_2 Reactive Scattering

Justin Jankunas,[1] Richard N. Zare,[1]* Foudhil Bouakline,[2] Stuart C. Althorpe,[3] Diego Herráez-Aguilar,[4] F. Javier Aoiz[4]

When a hydrogen (H) atom approaches a deuterium (D_2) molecule, the minimum-energy path is for the three nuclei to line up. Consequently, nearly collinear collisions cause HD reaction products to be backscattered with low rotational excitation, whereas more glancing collisions yield sideways-scattered HD products with higher rotational excitation. Here we report that measured cross sections for the H + D_2 → HD(v' = 4, j') + D reaction at a collision energy of 1.97 electron volts contradict this behavior. The anomalous angular distributions match closely fully quantum mechanical calculations, and for the most part quasiclassical trajectory calculations. As the energy available in product recoil is reduced, a rotational barrier to reaction cuts off contributions from glancing collisions, causing high-j' HD products to become backward scattered.

It is tempting and even at times quite insightful to describe the dynamics of chemical reactions in simple terms of classical billiard-ball collisions. In this picture, the impact parameter is defined as the distance of closest approach of the centers of the two billiard balls if they could travel without interaction in straight lines. Consider what happens when a billiard ball strikes another at rest. For a head-on collision, corresponding to zero impact parameter, the incoming billiard ball recoils backward in the center-of-mass frame. For a glancing collision between the two billiard balls, corresponding to a larger impact parameter, the incoming ball is scattered more sideways with respect to its initial direction. Next, consider the more complicated case of an atom A colliding with a diatomic molecule BC at rest to form by direct reaction the products AB and C. Furthermore, let us suppose that the

[1]Department of Chemistry, Stanford University, Stanford, CA 94305–5080, USA. [2]Institut für Chemie, Universität Potsdam, Karl-Liebknecht-Strasse 24-25, 14476 Potsdam-Golm, Germany. [3]Department of Chemistry, University of Cambridge, Lensfield Road, Cambridge CB2 1EW, UK. [4]Departamento de Química Física, Facultad de Química, Universidad Complutense, 28040 Madrid, Spain.

*To whom correspondence should be addressed. E-mail: zare@stanford.edu

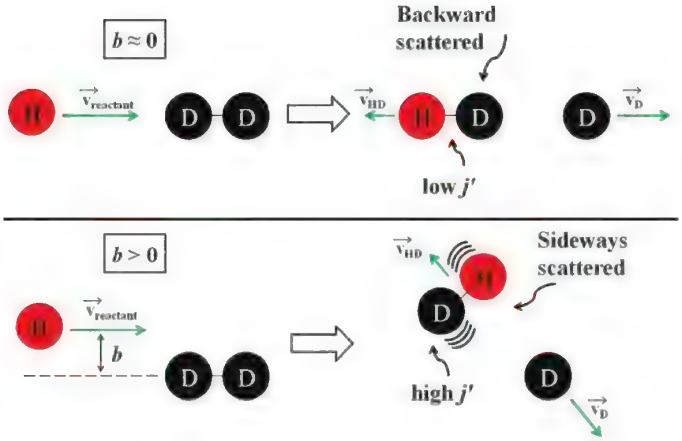

Fig. 1. Cartoon depicting a hypothetical H + D_2 → HD(v', j') + D reactive scattering event. $\vec{v}_{reactant}$ denotes the initial relative velocity of the reagents, and $\vec{v}_{HD}$ and $\vec{v}_D$ are the corresponding velocities of the HD and D products in the center-of-mass frame. The impact parameter b is defined as the distance of closest approach between the H atom and the center-of-mass of the D_2 molecule in the absence of interaction. Reactive collisions with small b lead to backward-scattered HD products in states of low rotational excitation (upper panel), whereas reactive collisions with large b lead to sideways-scattered HD products with high rotational excitation (lower panel).

preferred approach geometry for reaction is collinear, that is, with all three nuclei in a straight line. Under these conditions, it is natural to expect that for small impact parameters, the AB product of the direct reaction rebounds backward with little rotational excitation, whereas for larger impact parameters the AB product becomes increasingly sideways scattered with more rotational excitation (*1*, *2*). Indeed, this behavior has described all previous studies of direct [i.e., non–time-delayed (*3*, *4*)], collinear bimolecular reactions, including the benchmark reaction system H + D_2 → HD + D (*5*–*10*). Figure 1 illustrates schematically the impact parameter and other useful concepts for the H + D_2 → HD(v',j') + D reaction, where v' and j' are the vibrational and rotational quantum numbers, respectively, and the data in figs. S1 and S2 manifest the expected trend for the H + D_2 → HD(v' = 1, j') + D and H + D_2 → HD(v' = 3, j') + D reactions, respectively,

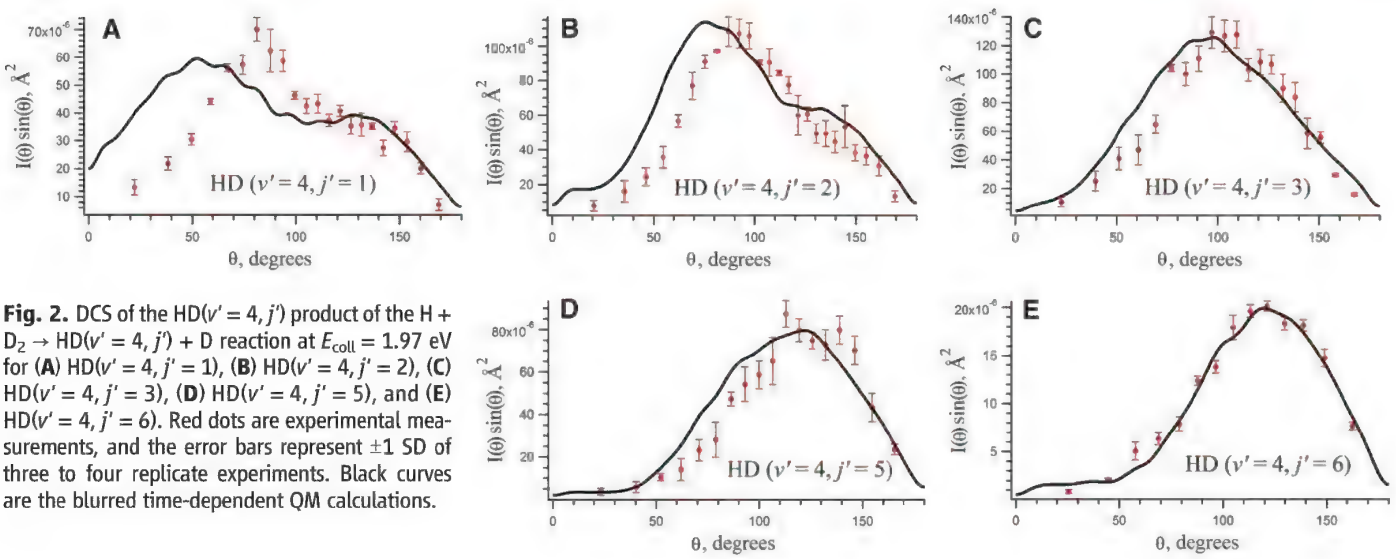

Fig. 2. DCS of the HD(v' = 4, j') product of the H + D_2 → HD(v' = 4, j') + D reaction at E_{coll} = 1.97 eV for (**A**) HD(v' = 4, j' = 1), (**B**) HD(v' = 4, j' = 2), (**C**) HD(v' = 4, j' = 3), (**D**) HD(v' = 4, j' = 5), and (**E**) HD(v' = 4, j' = 6). Red dots are experimental measurements, and the error bars represent ±1 SD of three to four replicate experiments. Black curves are the blurred time-dependent QM calculations.

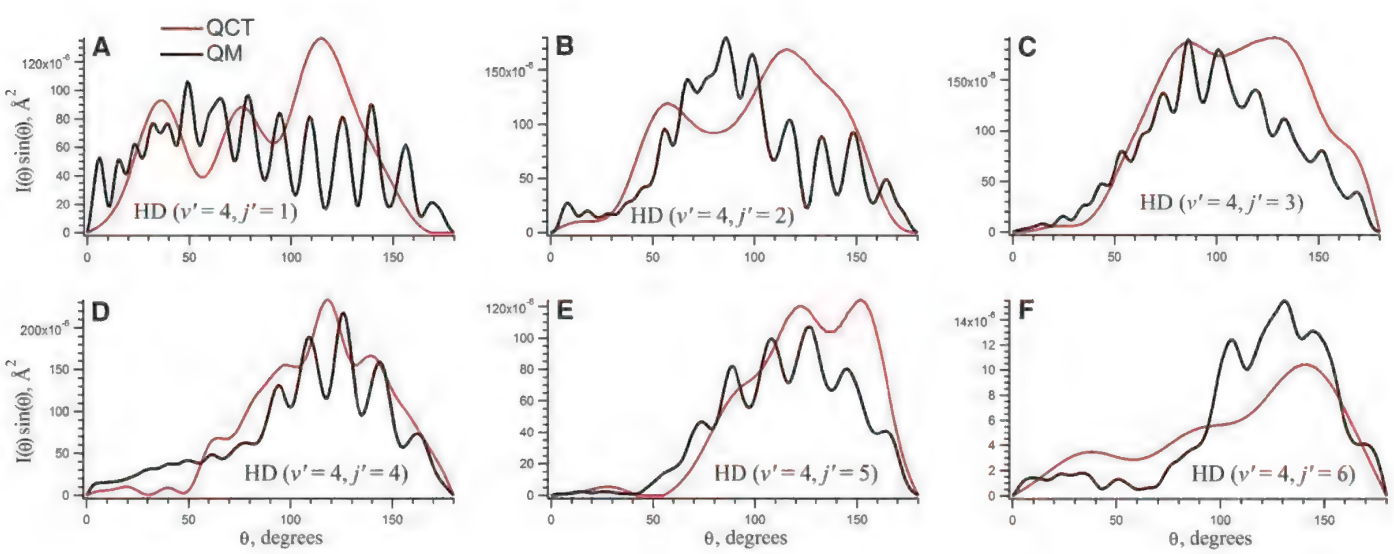

Fig. 3. Comparison between QCT (red curves) and unblurred time-independent QM (black curves) calculations for (**A**) HD(v' = 4, j' = 1), (**B**) HD(v' = 4, j' = 2), (**C**) HD(v' = 4, j' = 3), (**D**) HD(v' = 4, j' = 4), (**E**) HD(v' = 4, j' = 5), and (**F**) HD(v' = 4, j' = 6).

both at a collision energy of E_{coll} = 1.97 eV. This behavior has become one of the celebrated rules of reaction dynamics and encourages the belief that the classical motion of the nuclei on the ABC potential energy surface governs the reactive collision outcome when quantum tunneling effects are disregarded. Imagine, then, our initial surprise to find the opposite behavior for the reaction $H + D_2 \rightarrow HD(v' = 4, j') + D$ at E_{coll} = 1.97 eV in which with increasing product rotational excitation, the angular distribution of HD(v' = 4, j') increasingly shifts to the backward direction. Moreover, we show, experimentally and theoretically, that such anomalous angular distributions are general and to be expected for any direct collinear bimolecular reaction as the energy available for product recoil is reduced.

We employed a three-dimensional ion imaging apparatus (*11*) using the photoloc technique to record the differential cross section (DCS) of the HD(v' = 4, j') molecules in the same way we have studied the other H + D_2 reactions. In brief, a mixture of 1 to 3% HBr in D_2 was introduced through a 10-Hz pulsed valve into a vacuum chamber. The reactants underwent internal and translational cooling in a supersonic expansion, and almost all the D_2 was prepared in (v = 0, $j \leq 2$) internal states. Reaction was initiated by photolyzing HBr at 199 nm to produce fast H atoms. The resulting HD products were state-selectively ionized via [2+1] resonance-enhanced multiphoton ionization. As can be seen from Fig. 2, as the rotational excitation of the HD(v' = 4, j') increases, the DCS shifts in a backward direction. Fully quantum mechanical (QM) calculations were carried out using the wave-packet method of Althorpe (*12*), in which a quantum wave packet, containing a spread of desired energies, is propagated from the initial (H + D_2) to the final (HD + D) arrangements of the reaction, on the potential energy surface of Boothroyd–Keogh–Martin–Peterson (*13*). Time-independent QM calculations were also carried out at specific collision energies using the ABC code (*14*). The results are virtually identical to those obtained with the wave-packet calculations. We blurred the resulting DCSs (*10*) to account for the spread in the rotational levels of the D_2 reagent, the spread caused by imperfect translational cooling in the supersonic beam expansion, and the spread resulting from the finite instrument angular resolution. Figure 2 shows that each blurred DCS closely matches the corresponding experimental measurement, engendering confidence that the anomalous angular distributions reported here are accurate. The only disagreement occurs in the forward scattering direction for HD(v' = 4, j' = 1), for which we presently have no explanation. Data are not reported for HD(v' = 4, j' = 0) and HD(v' = 4, j' = 4) because of too much background interference for the wavelengths used to detect these reaction products.

To seek an explanation for this behavior, we performed quasiclassical trajectory (QCT) calculations on the same potential energy surface. To avoid the assignment of quantum numbers of states that are energetically inaccessible, we used the Gaussian binning procedure (*15*–*17*). Briefly, this entailed weighting each trajectory according to Gaussian functions centered on the correct QM vibrational action in such a way that the closer the (real) vibrational quantum number of one trajectory was to the nearest integer, the larger was the weight assigned to that trajectory. A batch of 15 million trajectories was run at 1.97-eV collision energy with a maximum impact parameter of 1.3 Å. Figure 3 presents a comparison of the unblurred fully quantum and the QCT results. Overall, the QCT calculations illustrate the same anomalous trend of increasing backward scattering with increasing rotational excitation of the HD(v' = 4, j') product, but some notable disagreements are apparent for HD(v' = 4, j' = 1 and 2). Such disagreements between quantum and QCT are to be expected because the recoil energy of the products ensures that the de Broglie wavelength of the separating particles is large in comparison with the dimensions of the collision process, and hence the semiclassical assumptions behind the QCT approach start to break down. The rapid oscillations (with a period of ~10°) in the quantum cross sections are the result of nearside-farside interference between products scattering into opposite hemispheres (*18*). The deviations between QCT and QM calculations seem most pronounced for HD(v' = 4, j' = 1, 2, and 6) so that the disagreement does not simply scale with increasing de Broglie wavelength.

We suggest that the anomalous angular distributions arise from the existence of a centrifugal barrier in the reaction path that impedes radial motion, leading to products with a high degree of internal excitation. Before collision, the relative velocity $\vec{v}$ of the approaching H and D_2 is perpendicular to the direction of the impact parameter b (see Fig. 1), and hence the magnitude of the total angular momentum of the colliding system is given by $L = \mu v b$, where μ is the reduced mass of the collision partners. Consequently, at a radial distance R between the reactants, the centrifugal energy is given by $L^2/2\mu R^2 = J(J+1)\hbar^2/2\mu R^2 = \frac{1}{2}\mu b^2 v^2/R^2 = E_{coll} b^2/R^2$, ignoring the small amount of angular momentum associated with D_2 rotation. Thus, as H and D_2 draw closer, R decreases and more energy of motion becomes bound up in centrifugal energy. Let $P(J)$ be the probability of reaction to produce the HD product in the internal state (v', j'). The cross section to produce HD(v', j') is found by summing $P(J)$ weighted by $(2J + 1)$ over all possible J values that contribute to this process. Note that J is proportional to the impact parameter b. As J increases, more of the HD(v', j') product becomes side scattered, but also more energy is bound up in the centrifugal energy

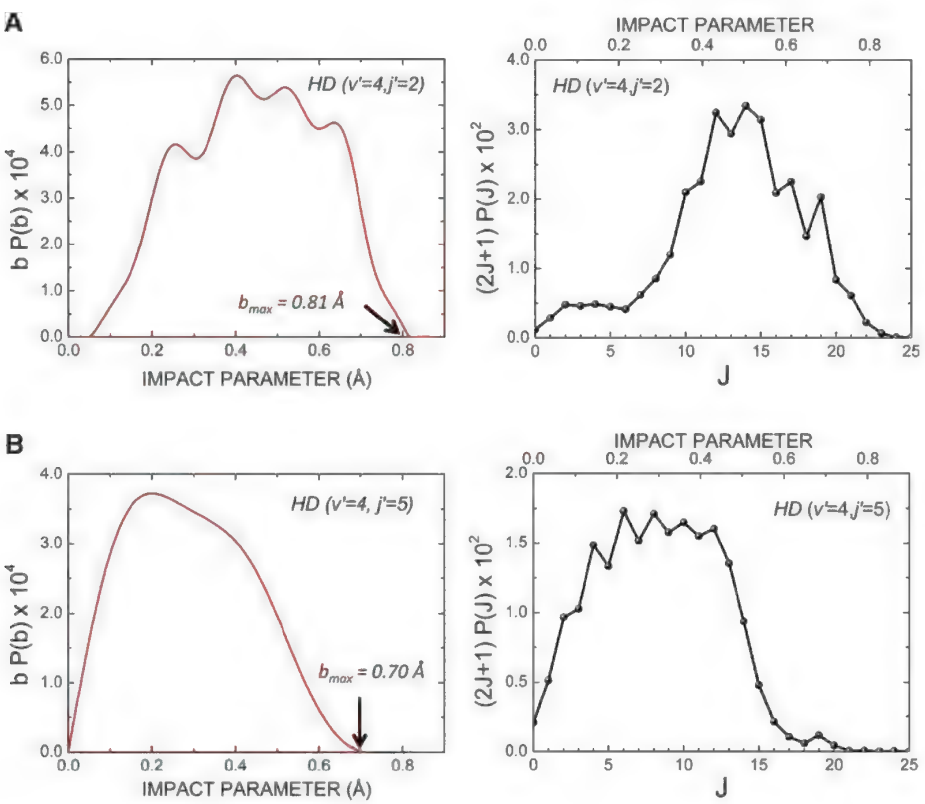

Fig. 4. Plots of the time-independent QM-derived $P(J)(2J + 1)$ versus J and the QCT-derived $bP(b)$ versus b for (**A**) HD(v' = 4, j' = 2) and (**B**) HD(v' = 4, j' = 5) for the reaction H + D_2 → HD(v' = 4, j') + D at a collision energy of 1.97 eV. As rotational excitation of the HD product increases, the contributions to the cross section from $P(J)(2J + 1)$ and $bP(b)$ for larger values of J and b diminish, causing backscattering of the HD(v' = 4, j') product.

and not available for radial motion to bring H and D_2 closer together for reaction to occur to produce the HD(v', j') product state. That is, for HD(v', j') products where most of the available energy is in internal excitation, H + D_2 collisions with high impact parameters (high J values) contribute less to product formation than those with low b values (low J values). Thus, as rotational excitation of the HD(v', j') product increases for a given fixed total collision energy, this product will at some point become more backscattered than an HD(v', j') product with somewhat less rotational excitation.

This explanation is supported by examining the form of $(2J+1)\,P(J)$ and $bP(b)$ for HD($v'=4$, $j'=2$) (Fig. 4A) and HD($v'=4$, $j'=5$) (Fig. 4B). Both QM and QCT plots show the same overall behavior. The exact details depend on the form of the potential energy surface, but we expect this phenomenon to be general. It is not surprising, then, to find that the H + D_2 → HD($v'=3$, $j'=8$ and 10) + D reactions at 1.97 eV show the same behavior as seen for HD($v'=4$, j'), as shown in fig. S3. We expect that this seemingly anomalous behavior will apply to other direct bimolecular reactions in which most of the energy of reaction becomes tied up in the internal motions of the reaction products.

References and Notes

1. R. D. Levine, *Molecular Reaction Dynamics* (Cambridge Univ. Press, Cambridge, UK, 2005).
2. P. Casavecchia, K. Liu, X. Yang, in *Tutorials in Molecular Reaction Dynamics*, M. Brouard, C. Vallance, Eds. (RSC, Cambridge, UK, 2010), p. 175.
3. S. C. Althorpe *et al.*, *Nature* **416**, 67 (2002).
4. S. A. Harich *et al.*, *Nature* **419**, 281 (2002).
5. E. Wrede *et al.*, *J. Chem. Phys.* **110**, 9971 (1999).
6. F. Fernández-Alonso *et al.*, *J. Chem. Phys.* **115**, 4534 (2001).
7. B. D. Bean, J. D. Ayers, F. Fernandez-Alonso, R. N. Zare, *J. Chem. Phys.* **116**, 6634 (2002).
8. F. J. Aoiz, L. Bañares, V. J. Herrero, *Int. Rev. Phys. Chem.* **24**, 119 (2005).
9. K. Koszinowski *et al.*, *J. Chem. Phys.* **127**, 124315 (2007).
10. N. C.-M. Bartlett *et al.*, *Phys. Chem. Chem. Phys.* **13**, 8175 (2011).
11. K. Koszinowski, N. T. Goldberg, A. E. Pomerantz, R. N. Zare, *J. Chem. Phys.* **125**, 133503 (2006).
12. S. C. Althorpe, *J. Chem. Phys.* **114**, 1601 (2001).
13. A. I. Boothroyd, W. J. Keogh, P. G. Martin, M. R. Peterson, *J. Chem. Phys.* **104**, 7139 (1996).
14. D. Skouteris, J. F. Castillo, D. E. Manolopoulos, *Comput. Phys. Commun.* **133**, 128 (2000).
15. L. Bonnet, J.-C. Rayez, *Chem. Phys. Lett.* **277**, 183 (1997).
16. L. Bañares, F. J. Aoiz, P. Honvault, B. Bussery-Honvault, J.-M. Launay, *J. Chem. Phys.* **118**, 565 (2003).
17. L. Bonnet, J.-C. Rayez, *Chem. Phys. Lett.* **397**, 106 (2004).
18. A. J. Dobbyn, P. McCabe, J. N. L. Connor, J. F. Castillo, *Phys. Chem. Chem. Phys.* **1**, 1115 (1999).

Acknowledgments: We gratefully acknowledge funding support from the U.S. National Science Foundation (grant NSF CHE-1025960 to J.J. and R.N.Z.), the Alexander von Humboldt Foundation (F.B.), the UK Engineering and Physical Sciences Research Council (S.C.A.), and the Spanish Ministry of Science and Innovation (MCINN) (grants CTQ2008-02578 and CSD2009-00038 to F.J.A. and D.H.). D.H. acknowledges the FPU fellowship AP2009-0038.

Supplementary Materials

www.sciencemag.org/cgi/content/full/336/6089/1687/DC1
Figs. S1 to S3

1 March 2012; accepted 19 April 2012
10.1126/science.1221329

Major Earthquakes Occur Regularly on an Isolated Plate Boundary Fault

Kelvin R. Berryman,[1]* Ursula A. Cochran,[1] Kate J. Clark,[1] Glenn P. Biasi,[2] Robert M. Langridge,[1] Pilar Villamor[1]

The scarcity of long geological records of major earthquakes, on different types of faults, makes testing hypotheses of regular versus random or clustered earthquake recurrence behavior difficult. We provide a fault-proximal major earthquake record spanning 8000 years on the strike-slip Alpine Fault in New Zealand. Cyclic stratigraphy at Hokuri Creek suggests that the fault ruptured to the surface 24 times, and event ages yield a 0.33 coefficient of variation in recurrence interval. We associate this near-regular earthquake recurrence with a geometrically simple strike-slip fault, with high slip rate, accommodating a high proportion of plate boundary motion that works in isolation from other faults. We propose that it is valid to apply time-dependent earthquake recurrence models for seismic hazard estimation to similar faults worldwide.

A long-standing acceptance of Reid's (*1*) elastic rebound theory of earthquakes combined with the knowledge that tectonic plates move steadily over geological time scales has led to an appealing—but rarely demonstrated—idea that major earthquakes on plate boundary faults occur relatively regularly (*2*–*5*). In contrast, several studies have suggested that faults rupture randomly or produce temporal clusters of earthquakes in response to various complexities, including fault interactions (*6*–*9*). The increasing popularity of models of random or clustered earthquake recurrence may reflect the paucity of earthquake histories from geometrically simple, rapidly slipping, isolated plate boundary faults. Paleoseismology provides evidence for the timing, size, and location of past major earthquakes on faults over longer time periods than the historical record, improving understanding of fault behavior and enabling estimates of future earthquake occurrence to be made (*5*, *7*, *9*, *10*).

We present a long earthquake record determined using paleoseismological techniques from the Alpine Fault in southwest New Zealand to assess the relationship between fault characteristics and patterns of earthquake recurrence. The Alpine Fault is ~850 km long and slips horizontally at average rates ranging from 14 mm/year in the north (*11*) to 31 mm/year in the south (*12*), with a subordinate amount of vertical slip (Fig. 1, A and B), making it one of the longest, straightest, and fastest-moving plate boundary transform faults on Earth. In the southwestern South Island, the Alpine Fault accommodates two-thirds of the relative motion between the Pacific and Australian tectonic plates (Fig. 1, A and B) (*13*, *14*). The remainder is accommodated by distributed deformation across the width of the plate boundary in the South Island (*13*–*15*). No major earthquake has occurred on the Alpine Fault since written records began (~170 years ago), but various lines of evidence indicate that the fault ruptures in large [moment magnitude (M_w) > 7] to possibly great (M_w > 8) earthquakes (*16*) and poses a substantial seismic hazard. Previous paleoseismic work has provided age constraints for the past four surface-rupturing earthquakes (*17*–*21*), but this yields only three interseismic intervals with which to assess the Alpine Fault's recurrence behavior. We extend the known record to a total of 24 major earthquakes over the past 8000 years at Hokuri Creek on the southern onshore section of the fault (Fig. 1C).

The formation and exposure of a long, fault-proximal, sedimentary earthquake record at Hokuri Creek is the result of specific geomorphological conditions. Hokuri Creek used to flow across the Alpine Fault through what is now an abandoned gorge (Fig. 1C). Holocene sediments accumulated against the fault over a 20-ha area adjacent to the creek to a total section thickness of 18 m (fig. S1). Deposition ceased when the creek changed course and flowed along the fault instead of across it at ~1000 C.E., before the penultimate Alpine Fault earthquake. Rapid incision around the junction of the north and south branches of Hokuri Creek has since exposed the sediments (Fig. 1C) (*22*). The sedimentary section comprises decimeter-thick beds of alternating shallow-water peat and silt units. Geomorphological investigations reveal that this cyclic stratigraphy is bounded to the northwest by the main scarp of the Alpine Fault.

Geologic and paleoenvironmental investigations indicate that the mechanism for formation of the cyclic peat-silt stratigraphy depends on surface rupture of the Alpine Fault. At the Hokuri

[1]GNS Science, Post Office Box 30-368, Lower Hutt 5040, New Zealand. [2]Seismological Laboratory, University of Nevada-Reno, Reno, NV 89557, USA.

*To whom correspondence should be addressed E-mail: k.berryman@gns.cri.nz

Creek locality, the uphill-facing scarp produced by the vertical component of slip on the Alpine Fault provides a natural dam to Hokuri Creek drainage. For example, in the most recent surface-rupturing earthquake, channels in the abandoned gorge were displaced by ~1 m vertically and 7.5 ± 0.5 m dextrally (fig. S2). Raising this dam periodically caused ponding against the fault scarp, with consequent deposition of catchment-derived silt. When drainage was reestablished across the scarp, autochthonous peat deposition resumed (Fig. 2). Raising the northwestern side of the fault in every surface-rupturing earthquake not only provides the mechanism for alternating between peat and silt deposition but also explains the intermittent creation of accommodation space required to sustain shallow-water sedimentation on the southeastern side of the fault for much of the Holocene. We interpret the appearance of silt in the stratigraphic section to mark the first sedimentation after an earthquake and every package of silt plus peat to represent the length of an earthquake cycle.

Aggradation of catchment-derived sediment on floodplains, and in the form of beach ridges, at the time of past Alpine Fault earthquakes has been documented at various sites north of Hokuri Creek (*18*, *20*, *23*). These studies illustrate that Alpine Fault earthquakes are the dominant control on large-scale sedimentation events in catchments that cross the fault. Climate events have not caused equivalent features to be preserved at the same sites. The west coast of the South Island has a very high and relatively constant rate of rainfall (*24*), which is consistent with regular flushing of catchments. In addition, the timing of peat-silt transitions does not correlate to any regional proxies of paleo-precipitation (*25*, *26*).

We developed a record of depositional events resulting from fault rupture using unit thickness, continuity, sedimentology, and paleoenvironment (*27*). Twenty-two silt-peat couplets, deposited between 6000 B.C.E. and 1000 C.E., are consistent with an earthquake origin. Although earthquake size cannot be measured directly at Hokuri Creek, we know from the inferred mechanism of formation that every earthquake was big enough to cause surface rupture with a vertical component of offset capable of altering site hydrology. Magnitude estimates for the two most recent events on the southern section of the fault ranged between M_w 7.6 and 8.3 (*16*). Eighty-two radiocarbon ages were used to produce our best estimate of the earthquake sequence (Fig. 3). The ages for event horizons were derived from bounding radiocarbon dates (usually multiple) on short-lived, fragile organic fractions such as single leaves and seeds. The two most recent earthquakes of the Alpine Fault chronology were adopted from paleoseismic trenches 100 km along strike to the northeast at Haast (*21*). One of these events is recognized as offsets in the abandoned gorge at Hokuri Creek, but it could not be dated in the stratigraphic section because deposition had ceased by this time. The third event identified at Haast (688 to 1066 C.E.) overlaps in time with the youngest event recognized in the Hokuri Creek stratigraphic section (730 to 921 C.E.). We assume, because of the overlap of these ages and similar large single-event displacements (7.5- to 9-m strike-slip) at both sites, that they represent a single earthquake, and we

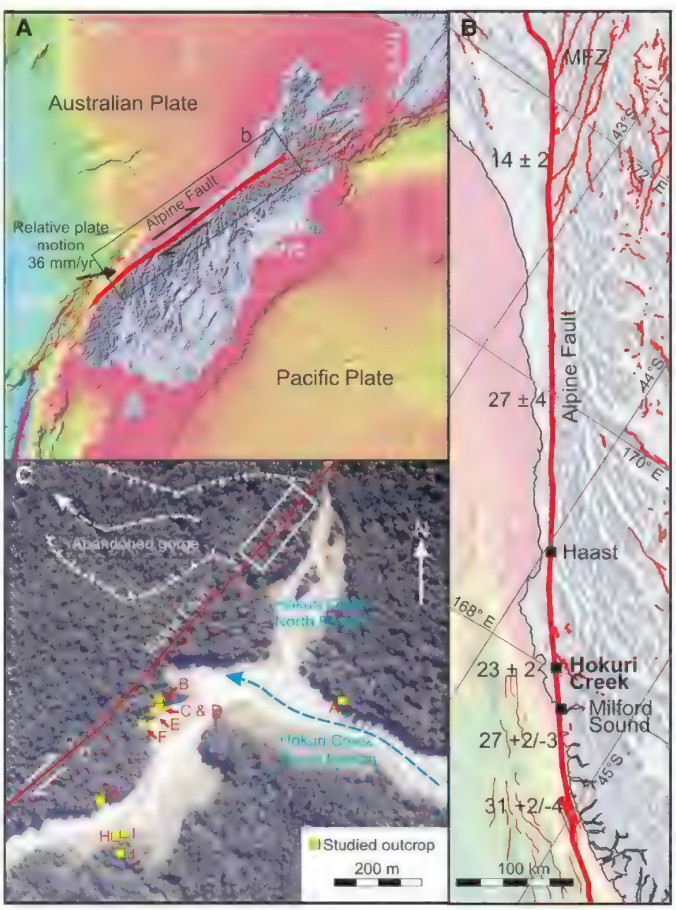

Fig. 1. Tectonic setting of the Alpine Fault and Hokuri Creek study site. (**A**) Australian-Pacific plate boundary through the South Island of New Zealand with plate motion rate after Sutherland *et al.* (*13*). (**B**) Detail of the Alpine Fault showing slip-rate estimates along the fault and other active faults in red (*11*–*13*, *32*). MFZ, Marlborough Fault Zone. Bathymetry is from the New Zealand Oceanographic Institute's Chart Miscellaneous Series No. 74. (**C**) Aerial photograph of Hokuri Creek study area. Letters A to J show locations of the studied outcrops (fig. S1). Present outflow direction of both north and south branches of Hokuri Creek is to the southwest. The former outflow was via a gorge across the fault (edges marked by white dashed lines). Box "1" shows the area of a topographic survey where channels are offset (fig. S2).

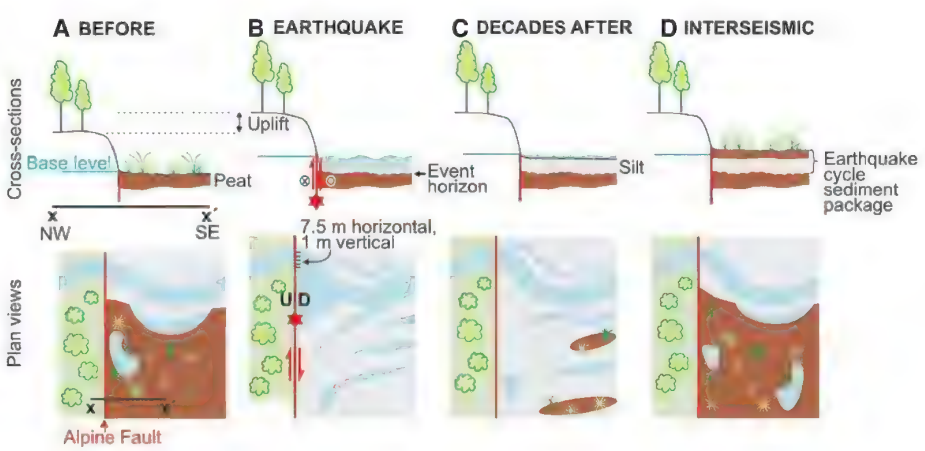

Fig. 2. Depositional model for fault-controlled sediment accumulation at Hokuri Creek. (**A**) Hokuri Creek flows across the fault scarp, and a wetland exists on the southeast side of the fault. In situ, organic sediment deposition occurs in wetlands and pond margins, forming peat. (**B**) Surface rupture of the Alpine Fault occurs (involving 7.5 ± 0.5 m dextral, and 1 m vertical offset). This displacement blocks the drainage of Hokuri Creek, causing a change in hydrological regime. Deposition on the southeast side of fault is dominated by transported, catchment-derived silt in shallow ponds. (**C**) Silt deposition continues, and the creek starts to reestablish drainage across the fault scarp. (**D**) Sedimentation on the southeast side of the fault returns to in situ peat formation.

combined the two dates to generate the age of event HK1 in Fig. 3. Thus, our composite record (Fig. 3) covers the past 24 surface-rupturing events on the southern onshore section of the Alpine Fault between 6000 B.C.E. and the present day.

We estimate a mean recurrence interval of 329 ± 68 years and a coefficient of variation (COV) of 0.33 for the 24-event data set (Fig. 3B). Kagan and Jackson (*6*) define completely random earthquake recurrences as having a COV of 1, whereas distributions with a COV < 1 are "quasi-periodic" and distributions with a COV > 1 are termed "clustering." Given the number of intervals examined, earthquake recurrence on the southern onshore section of the Alpine Fault is clearly quasi-periodic. Quasi-periodic earthquake recurrence conforms with elastic rebound theory and the idea that faults rupture in response to a specific amount of strain accumulation (*1*, *4*, *5*). Comparison with previous paleoseismic studies on the southern onshore section of the Alpine Fault highlights the strength of a long earthquake record in determining mean recurrence intervals. For example, the three earthquakes identified at Haast (*21*) indicate an average recurrence time of about 485 years, and although the same Haast events are incorporated into the earthquake record at Hokuri Creek, the mean recurrence interval using 24 earthquakes is 329 ± 68 years. Unlike the Haast study, this value is consistent with the long-term average slip rate on this part of the fault (Fig. 1B), probably because sufficient variation in recurrence is encompassed by the 8000-year time span.

The southern onshore section of the Alpine Fault exhibits more regular or periodic behavior than other major transform faults (Fig. 4). For example, a 3000-year, 29-event record from the San Andreas Fault at Wrightwood in California exhibited quasi-periodic behavior (*5*) but with a COV of about 0.7. Recent reanalysis of the

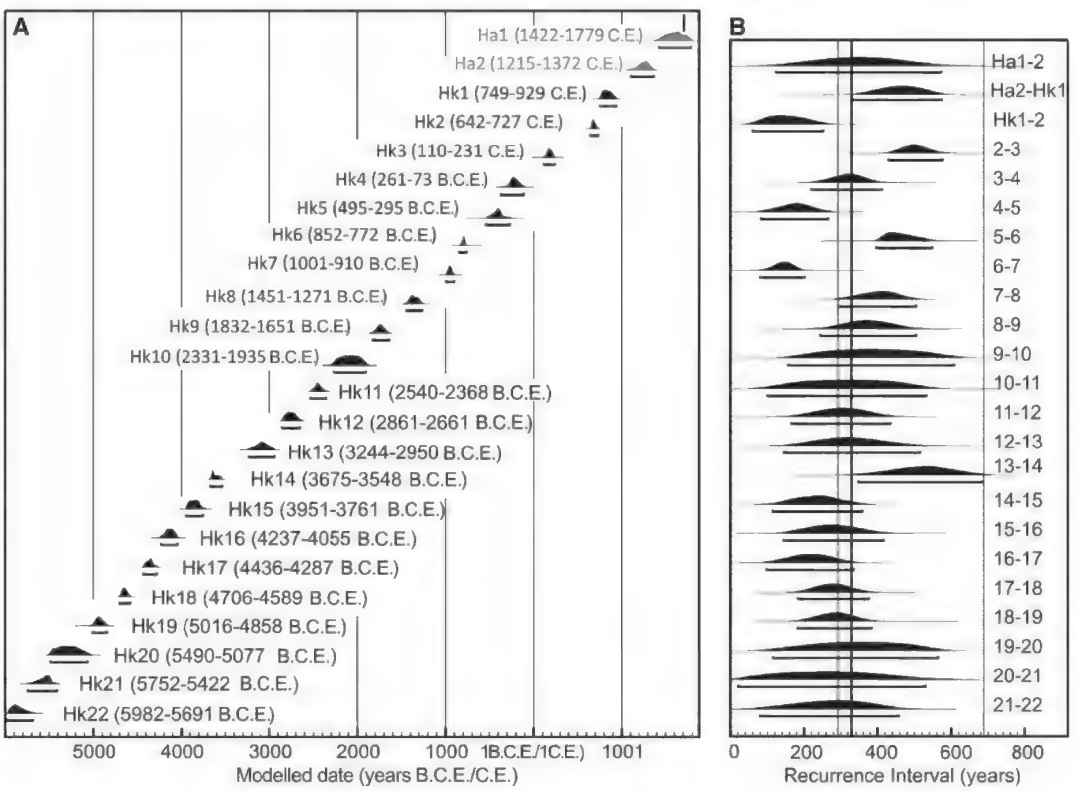

Fig. 3. Ages of surface-rupturing earthquakes on the Alpine Fault from Hokuri Creek and Haast. (**A**) Probability distributions for the earthquake ages modeled from bounding radiocarbon ages (table S1). Gray-shaded probability distributions are the events recorded at Haast. Calendar years in brackets after event names are the 95% ranges. The most recent event, Ha1, is shown with a small vertical bar at its inferred date of 1717 ± 5 C.E. (*18*). (**B**) Recurrence interval probability distributions for the events shown in (A). Horizontal bars under distributions indicate the 95% range. The black vertical line is the mean recurrence interval (329 years). The gray vertical line represents the elapsed time since the most recent earthquake (295 years).

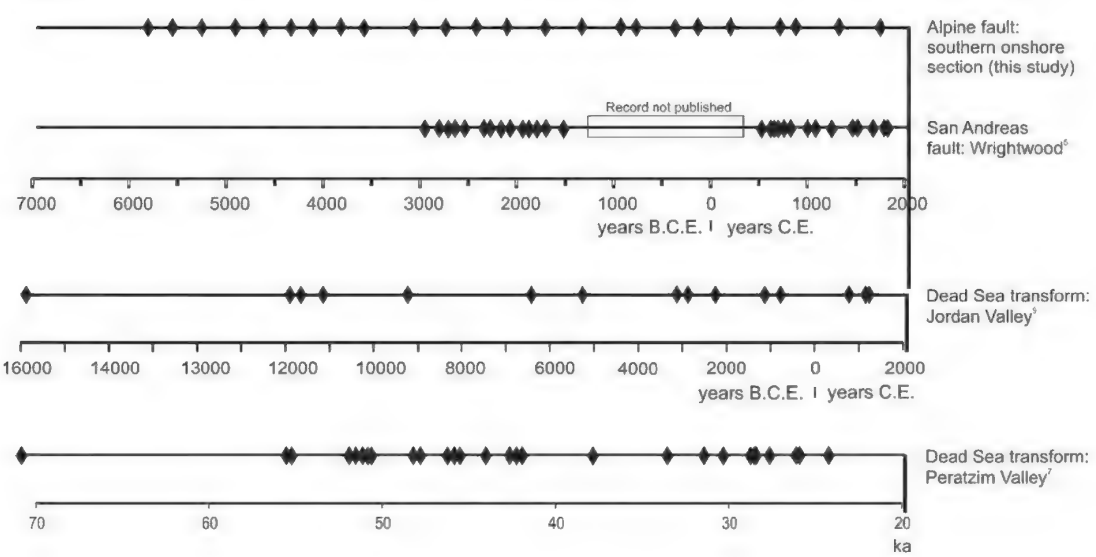

Fig. 4. Recurrence patterns of large earthquakes on major transform faults from long geological records. The timing of earthquakes on the Alpine Fault in New Zealand (top line, data from this study) is the closest to periodic with a coefficient of variation (COV) of 0.33. The timing of earthquakes on the San Andreas fault in the United States (second line down) (*5*) is quasi-periodic, with a COV of 0.7. The timing of earthquakes on the Dead Sea Transform in the Middle East (lower two lines) ranges from random to clustered with COVs of 1 to 1.75 (*7*, *9*).

10-event record at Pallett Creek near Wrightwood yielded a COV estimate of 0.60 (*28*). On the Jordan Valley Fault section of the Dead Sea Transform system, Ferry *et al.* (*9*) described clustered behavior from a 14,000-year, 12-event record in which recurrence intervals ranged from 280 to 1160 years. Marco *et al.* (*7*) estimated COVs for earthquake recurrence in the Dead Sea Graben ranging from 1 (random) to 1.75 (clustered).

In light of the periodicity exhibited by the Alpine Fault, we can identify characteristics that may be good indicators of quasi-periodic recurrence on other faults. In a global context, the Alpine Fault is a prime example of a transform plate boundary fault that has a simple structure (long, straight trace with few large step-overs), large total offset (~480 km), and a high slip rate (23 ± 2 mm/year at Hokuri Creek) (*13*, *29*). However, perhaps the most important feature in this context is the lack of other major structures nearby for much of the length of the fault. In the southwestern South Island, one third of relative plate motion (*13*, *14*) is taken up on structures other than the Alpine Fault, but these have little effect on regulating the timing of Alpine Fault earthquakes. Structures that accommodate residual motion in this part of the plate boundary have low slip rates and are distributed broadly across the margin (*14*, *15*). The slightly less periodic (higher COV) San Andreas fault is known to be influenced by major faults nearby (*30*), and the aperiodic Dead Sea Transform is a more complicated system and slower slipping (*9*) than either the San Andreas or the Alpine Fault. Other faults that have similar characteristics to the Alpine Fault are sections of the North Anatolian in Turkey and the Denali Fault in Alaska.

Existing examples of long earthquake records suggest a continuum of recurrence behavior with more periodic recurrence on fast-moving, simple and smooth at seismogenic depth, isolated structures at one end of the spectrum (such as this Alpine Fault example) and aperiodic recurrence on low slip-rate, complex, rough, and networked structures at the other end. Thus, in the absence of long paleoseismic records, fault characteristics such as total slip, slip rate, geometric complexity, and possible interaction with other nearby major faults can enable the choice of appropriate statistical models for use in earthquake forecasting and hazard analysis. Regular earthquake recurrence can be considered an end-member of fault behavior. Our study highlights that the regularly repeating earthquake cycle is a realistic foundation on which to base earthquake forecasting and seismic hazard efforts, especially where a fault is acting in isolation to accommodate a high proportion of plate motion.

References and Notes

1. H. F. Reid, *The Mechanics of the Earthquake* (Carnegie Institution of Washington, Washington, DC, 1910).
2. K. Shimazaki, T. Nakata, *Geophys. Res. Lett.* **7**, 279 (1980).
3. W. Thatcher, *J. Geophys. Res.* **89**, 5674 (1984).
4. T. Parsons, *Geophys. Res. Lett.* **35**, L21301 (2008).
5. K. M. Scharer, G. P. Biasi, R. J. Weldon, T. E. Fumal, *Geology* **38**, 555 (2010).
6. Y. Y. Kagan, D. D. Jackson, *Geophys. J. Int.* **104**, 117 (1991).
7. S. Marco, M. Stein, A. Agnon, H. Ron, *J. Geophys. Res.* **101**, 6179 (1996).
8. Y. Y. Kagan, D. D. Jackson, *Bull. Seismol. Soc. Am.* **89**, 1147 (1999).
9. M. Ferry, M. Meghraoui, N. A. Karaki, M. Al-Taj, L. Khalil, *Bull. Seismol. Soc. Am.* **101**, 39 (2011).
10. J. P. McCalpin, A. R. Nelson, in *Paleoseismology*, J. P. McCalpin, Ed. (Elsevier, London, 2009), vol. 95, pp. 1–27.
11. R. M. Langridge *et al.*, *Lithosphere* **2**, 139 (2010).
12. P. M. Barnes, *Geology* **37**, 3 (2009).
13. R. Sutherland, K. R. Berryman, R. J. Norris, *Geol. Soc. Am. Bull.* **118**, 464 (2006).
14. L. M. Wallace, J. Beavan, R. McCaffrey, K. Berryman, P. Denys, *Geophys. J. Int.* **168**, 332 (2007).
15. P. M. Barnes, R. Sutherland, J. Delteil, *Geol. Soc. Am. Bull.* **117**, 411 (2005).
16. R. Sutherland *et al.*, in *A Continental Plate Boundary: Tectonics at South Island, New Zealand*, D. Okaya, T. Stern, F. Davey, Eds. (American Geophysical Union, Washington, DC, 2007), pp. 235–251.
17. A. F. Cooper, R. J. Norris, *N.Z. J. Geol. Geophys.* **33**, 303 (1990).
18. A. Wells, M. D. Yetton, R. P. Duncan, G. H. Stewart, *Geology* **27**, 995 (1999).
19. L. E. Cullen, R. P. Duncan, A. Wells, G. H. Stewart, *J. R. Soc. N.Z.* **33**, 693 (2003).
20. A. Wells, J. Goff, *Holocene* **16**, 543 (2006).
21. K. R. Berryman *et al.*, *Bull. Seismol. Soc. Am.* **102**, 620 (2012).
22. R. Sutherland, J. Norris, *N.Z. J. Geol. Geophys.* **38**, 419 (1995).
23. J. Adams, *Geology* **8**, 72 (1980).
24. For example, Milford Sound (Fig. 1B) receives 6 to 7 m of rain annually, and ~186 days per year are wet (*31*).
25. A. Lorrey *et al.*, *Quat. Int.* **187**, 52 (2008).
26. K. P. Knudson, I. L. Hendy, H. L. Neil, *Quat. Sci. Rev.* **30**, 3124 (2011).
27. Materials and methods are available as supplementary materials on *Science* Online
28. K. M. Scharer, G. P. Biasi, R. J. Weldon II, *J. Geophys. Res.* **116**, B12111 (2011).
29. K. R. Berryman *et al.*, *Ann. Tectonicae* **6** (suppl.), 126 (1992).
30. J. F. Dolan, D. D. Bowman, C. G. Sammis, *Geology* **35**, 855 (2007).
31. National Institute of Water and Atmospheric Research climate summaries, available at www.niwa.co.nz/education-and-training/schools/resources/climate (accessed March 2012).
32. R. J. Norris, A. F. Cooper, *J. Struct. Geol.* **23**, 507 (2000).

Acknowledgments: This research was funded by the Marsden Fund of the Royal Society of New Zealand. The Department of Conservation provided permits for us to work in the field area. D. Barker, T. Bartholomew, M. Hemphill-Haley, N. Litchfield, S. Marco, N. Palmer, D. Pantosti, and R. Van Dissen contributed to the field work. T. Bartholomew, T. Dutton, L. Ingham, G. Turner, and J. West carried out laboratory work. C. Prior and her team produced all the radiocarbon analyses. N. Litchfield, A. Nicol, R. Sibson, M. Stirling, R. Sutherland, J. Townend, and L. Wallace made comments that improved the manuscript. Data reported in this paper are provided in the supporting online material. K.R.B. initiated the research, led the fieldwork, and contributed to all aspects of the project, especially interpretation. U.A.C. contributed to preliminary fieldwork, produced the diatom-based paleoenvironmental interpretations, contributed to figures, and led the writing of the manuscript. K.J.C. was involved in all fieldwork, led development of the stratigraphic model, organized laboratory analyses, and contributed to figures and writing. G.P.B. contributed to fieldwork, interpretation, figures, and writing and produced the event sequence using Oxcal. R.M.L. and P.V. contributed to a large proportion of the fieldwork and to interpretations presented in the manuscript.

Supplementary Materials

www.sciencemag.org/cgi/content/full/336/6089/1690/DC1
Materials and Methods
Figs. S1 and S2
Table S1
References (*33*–*36*)

10 January 2012; accepted 4 May 2012
10.1126/science.1218959

Bilaterian Burrows and Grazing Behavior at >585 Million Years Ago

Ernesto Pecoits,[1]* Kurt O. Konhauser,[1] Natalie R. Aubet,[1,2] Larry M. Heaman,[1] Gerardo Veroslavsky,[2] Richard A. Stern,[1] Murray K. Gingras[1]

Based on molecular clocks and biomarker studies, it is possible that bilaterian life emerged early in the Ediacaran, but at present, no fossils or trace fossils from this time have been reported. Here we report the discovery of the oldest bilaterian burrows in shallow-water glaciomarine sediments from the Tacuarí Formation, Uruguay. Uranium-lead dating of zircons in cross-cutting granite dykes constrains the age of these burrows to be at least 585 million years old. Their features indicate infaunal grazing activity by early eumetazoans. Active backfill within the burrow, an ability to wander upward and downward to exploit shallowly situated sedimentary laminae, and sinuous meandering suggest advanced behavioral adaptations. These findings unite the paleontological and molecular data pertaining to the evolution of bilaterians, and link bilaterian origins to the environmental changes that took place during the Neoproterozoic glaciations.

Animals with bilateral symmetry, segmentation, and musculature probably emerged in the Neoproterozoic and were a major part of the subsequent Cambrian "explosion," but it has proven difficult to date the appearance of the first bilaterians. Recent molecular clock analyses

give dates ranging from 1153 to 1443 million years ago (Ma) (*1*) to 580 to 635 Ma (*2*, *3*) for the emergence of stem-group bilaterians, yet no definite bilaterian fossils have been found within this broad time interval. Putative microscopic bilaterian fossils from the Doushantou Formation in China (*4*) are probably about 580 million years (My) old (*5*), but their attribution to bilaterians remains controversial (*6*, *7*). Similarly, putative trace fossils ranging in age between 565 My and 2.1 billion years have been described, but only those younger than about 555 My satisfy the strict criteria for bilaterian burrows (*8*–*11*). The oldest widely accepted evidence for bilaterians comes from fossil burrows and probable body fossils such as *Kimberella* in shallow-water deposits from Russia that are approximately 555 My old (*12*, *13*).

Here we report bilaterian burrows from shallow-water Ediacaran sediments in the Tacuarí Formation in east-central Uruguay. We found abundant trace fossils at six different localities, three of which are within 5 m of the intrusive contact (detailed geological data are presented in figs. S1 to S9). The Tacuarí Formation comprises basal diamictites, varved sandstones, and minor pelites that grade upward into fine-grained rhythmites containing abundant outsized clasts. The clasts, interpreted as dropstones within the diamictites, are faceted and striated and provide evidence for the glacial origin of the varve-containing strata. Trace fossils occur within the uppermost fine-grained rhythmites that mark the waning stages of glaciation (Fig. 1).

To provide accurate age constraints for the deposition of these sediments, we obtained laser ablation multicollector inductively coupled plasma mass spectrometry (LA-MC-ICPMS) (n = 10 spot analyses) and sensitive high-resolution ion microprobe (SHRIMP) (n = 20 spot analyses) U-Pb zircon ages from an intrusive granite that cross-cuts and deforms the Tacuarí Formation (*14*). These combined dates constrain the minimum depositional age for the fossil-bearing unit to 585 ± 3 Ma (see Fig. 1 and tables S1 and S2). A maximum depositional age for the Tacuarí Formation is 600 ± 9 Ma, based on the youngest detrital zircon age cluster recorded in the fossil-bearing unit (tables S2 and S3). This age reinforces the Neoproterozoic age previously assigned to the Tacuarí Formation, which was based on structural and stratigraphic relationships with more–precisely dated units (*15*). The cross-cutting rocks comprise leucocratic, undeformed granite that is discordant to the locally foliated sedimentary strata of the Tacuarí Formation (figs. S2 to S5). The granite shows a well-developed chill margin, whereas the sedimentary strata at the contact are sintered and show evidence of extensive silicification and hematitization (figs. S3 to S8). Additional evidence of the intrusive nature of the granite comes from the presence of country rock xenoliths (both rafts and stoped blocks) along the margin and in the roof zone of the intrusion (fig. S9).

The trace fossils are preserved in fine detail on laminae tops and soles in association with siltstone laminae. Two modes of preservation are observed (Fig. 2 and fig. S10). The most common comprises downward-protruding (concave hyporelief) bilobate grooves, locally containing a beaded backfill (inset in Fig. 2A and Fig. 2G). The beaded backfill consists of very small, ovate sediment piles, the long axes of which are oriented transverse to the burrow length. The second type of burrow preservation entails irregular burrows that generally are upward-protruding (convex epirelief) from the plane of preservation: These structures locally show collapse features on their tops (Fig. 2B). Both types of burrows are 2 to 3 mm in width, and some of the collected specimens pass laterally from one form to the other along the length of the burrow. The bilobate grooves commonly possess raised lateral ridges adjacent to the burrow margins. Rarely, small circular indentations are preserved near the edges of bilobate furrows (insets in Fig. 2, D and H). The dents are approximately 0.5 mm in diameter and are serially emplaced along the trail. Plan-view morphology ranges from straight (Fig. 2B) to curvilinear (Fig. 2, A and E) to low-amplitude sinusoidal (Fig. 2, B and C). Abrupt adjustments in curve radius accompanied by small lateral movements are observed (Fig. 2, E and F). Three of the specimens show the burrow abruptly leaving the plane of preservation and reappearing 4 to 10 mm away (Fig. 2E and fig. S10). We also observed several instances of one burrow crossing another, with no evidence of avoidance (Fig. 2A). In three examples, a later burrow intersects a preexisting burrow, turns, and follows the earlier structure, then resumes its initial trajectory (Fig. 2F).

The two modes of trace-fossil preservation suggest that these burrows were emplaced within the sediment (i.e., intrastratally). Well-preserved bilateral furrows represent the bottom of the burrow. The irregularly defined examples represent the top of the burrow. Given the shallow intrastratal occurrence of this trace fossil, it is likely that the animal grazed on organic material within the sedimentary laminae. Rare but clear depar-

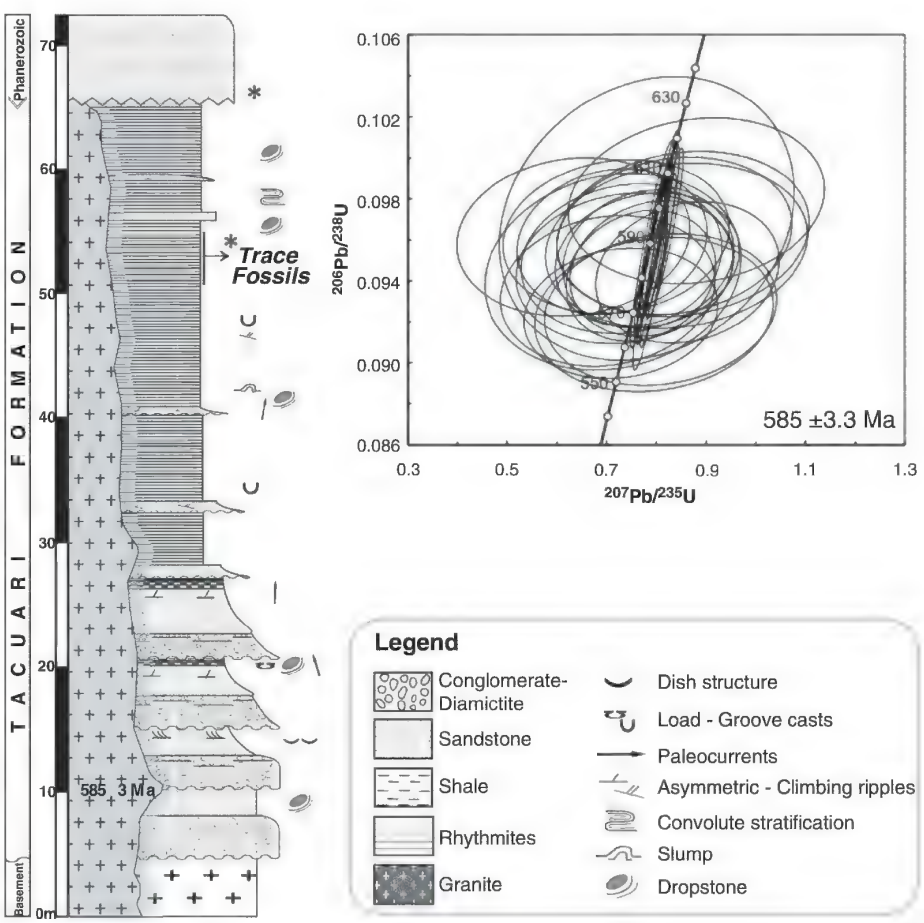

Fig. 1. Detailed stratigraphic section of the Tacuarí Formation with labeled trace-fossil horizon. Asterisks on the section indicate detrital zircon sampling sites (fig. S1). The U-Pb concordia diagram displays the LA-MC-ICPMS (narrow ellipses) and SHRIMP analyses of zircon grains from the granite intruding into the trace fossil–bearing strata.

[1]Department of Earth and Atmospheric Sciences, University of Alberta, Edmonton, Alberta T6G 2E3, Canada. [2]Instituto de Ciencias Geológicas, Universidad de la República, Iguá 4225, Montevideo 11400, Uruguay.

*To whom correspondence should be addressed. E-mail: epecoits@ualberta.ca

tures of some burrows from the plane of grazing may represent movement of the tracemaker to the sediment/water or sediment/biomat interface, or shifting to other shallow laminae in the search of food. The reappearance of the burrow nearby and in the same plane suggests the former, because these examples show the animal's subsequent return to the food source. Curvilinear to low-amplitude sinusoidal trails suggest that the tracemakers were engaged in rudimentary spatial optimization of patchy food resources or used a search pattern that improved the likelihood of intersecting optimal food resources. The lack of mutual burrow avoidance suggests that phobotaxis had not yet evolved. The specimens that show later burrows becoming coincident with preexisting burrows may imply primitive chemotaxis or may reflect the greater ease of burrowing through previously burrowed sediment.

The presence of raised lateral ridges and the preservation of a beaded backfill show that the animals moved by peristaltically pushing against the sediment. The spacing of the backfilled beads reveals forward movement of less than 0.5 mm (per peristaltic push); serial indentations along the burrow margin have a similar spacing. The indents further show that the tracemaker had prehensile "feet" of sorts and could extend those parts into the sediment to assist motility. Abrupt changes in the meander radius with abrupt lateral jogs further suggest that the animal, although possibly elongate, did not exceed 1 cm in length. The bilateral furrow reflects the bilateral symmetry of the tracemaker, and when coupled with the mode of locomotion, strongly points to an early bilaterian tracemaker.

A variety of inorganic sedimentary processes can superficially mimic the shape of simple burrows (*11*, *16*), but none of these seem applicable to the Uruguay trace fossils: All of the specimens exhibit remarkably consistent width and morphology. There is no evidence of alignment such as might be produced by depositional currents, nor are there abrupt changes in orientation, diameter, or relief along the length of the structures that might reflect tool markings or shrinkage cracks. The bilobate lower surface of the structures is typical of many modern and Phanerozoic bilaterian burrows, especially but not exclusively molluscan and annelid burrows, and would be difficult to produce consistently in numerous specimens by any known inorganic sedimentary process. Poorly preserved algal filaments or tubular animals can also mimic simple trace fossils (*16*, *17*), but there are no carbonaceous or calcareous films, and angular (i.e., broken) edges that might mark a body fossil are not observed (Fig. 2E).

The Uruguay structures exhibit abundant evidence for sediment displacement and processing in the formation of these structures. These include lateral ridges of displaced sediment flanking a bilobate furrow at the base, the meniscate fill of the structures, and the collapse features that followed the abandonment of partly open structures; the latter very strongly suggest that they represent the burrows of muscular organisms. Some prokaryotes and protists are capable of moving on sediment and can leave traces of their activity (*18*), but are too small and lack evidence for the strong musculature used in the construction of eumetazoan burrows. Although large protists have been shown to make traces similar to some surficial bilaterian traces (*19*), such animals are incapable of producing some of the features we observe in the Tacuarí tracks, including infaunal movements, meniscate backfill, and the small, regularly spaced indentations observed locally on either side of the medial furrow. Among the simple Eumetazoa, flatworms and anemones can produce lateral ridges of displaced sediment as they move across a surface using mucociliary creeping (*20*), but no modern Platyhelmininthes or Cnidaria are known to construct horizontal burrows that are either infaunal or backfilled. The combination of features seen in the Uruguay trace fossils makes it difficult to regard them as representing the activity of anything below the biological grade of the Eumetazoa, and in modern seas, these fossils are consistent only with those produced by bilaterian eumetazoans.

Although the internal structure of the Uruguay burrows is very similar to that of Phanerozoic and modern bilaterian burrows, their behavior

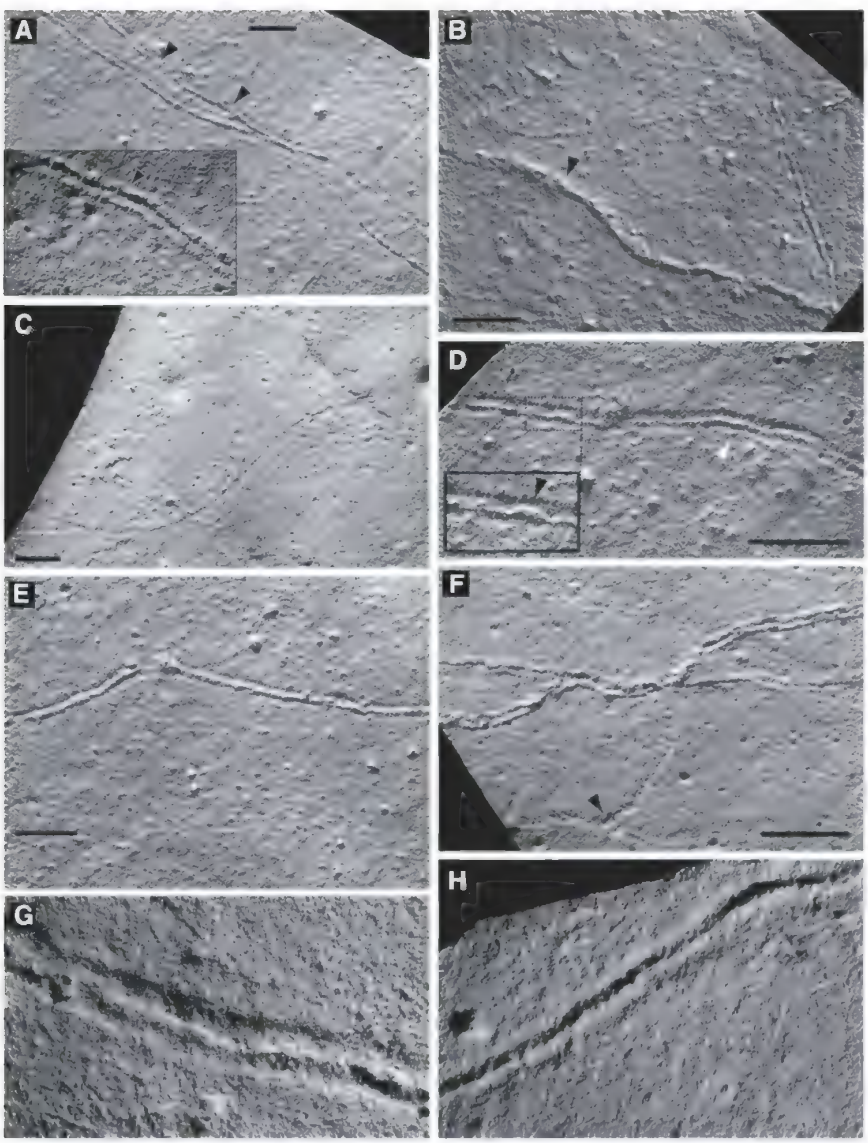

Fig. 2. Photographs of the Tacuarí trace fossils. (**A**) Typical bilobate furrow with beaded backfill/meniscae visible (black arrows). (**B**) Irregular trace fossil showing the collapsed top part of the burrow. (**C**) Sinuous trail illustrating the typical amplitude and wavelength. (**D**) Well-developed bilobate furrow with circular indentations (black arrow, inset) and raised burrow margins (white arrow). (**E**) Bilobate furrow showing departure from and return to the plane of preservation. (**F**) Later burrow intersecting and following a preexisting burrow. (**G**) Close-up of bedding plane (top view), clearly showing the bilobate furrow that is preserved in many of the burrows. (**H**) Close-up of the Ediacaran burrow-maker's trail, showing serial indentations along the furrow margin. Scale bars, 1 cm.

is considerably less complex, even in comparison with later Ediacaran burrows from northwest Canada (*21*) and Australia (*22*). Conspicuously absent are parallel meanders and three-dimensional avoidance that appeared later in the Ediacaran (*21*). Nevertheless, sinusoidal grazing probably marks the advent of more sophisticated grazing behaviors and is in itself evidence of early burrowing adaptation.

These findings extend the fossil record of bilaterian eumetazoans at least 30 million years backward to the early Ediacaran, a time consistent with the youngest ages for the appearance of bilaterians predicted by molecular clock analyses (*2*, *3*). The molecular clock dates for the Eumetazoa-sponge divergence have also been corroborated by the recently reported body fossil evidence of sponges from the Trezona Formation (Australia), immediately below the Marinoan-aged Elatina Formation (635.2 Ma), and lipid biomarkers suggestive of Demosponges in strata below the Hadash Formation (Marinoan) cap carbonate in Oman (*23*, *24*). Therefore, it appears as though a maximum interval of 50 My exists between the earliest definitive evidence of sponges and the bilaterians found in the Tacuarí Formation, which implies that early animal evolution took place on a geologically rapid time scale once environmental conditions proved favorable for higher forms of life to colonize the ocean realm. Presently, the occurrence of deep-sea bilaterian burrows at ~550 Ma (*25*) and the occurrence of deep-water Vendian fauna have led some researchers to suggest that bilaterians have a deep-sea origin (*26*–*29*). Based on the Tacuarí trace fossils, the possibility is reopened that bilaterians evolved in shallow-water settings (*30*), perhaps reflecting greater food availability in this environment and because their mobility and burrowing habit required higher oxygen levels than those of the sessile Ediacarans.

Finally, these early Ediacaran burrows demonstrate very early grazing activity by eumetazoans. The grazing behavior is facilitated by a low-amplitude sinusoidal search pattern and the ability to leave one sedimentary lamination for another. Evidence of active backfilling of the burrow is important, as well as the ability to pass sediment around or through the body and compact it in the animal's wake, which was a crucial advancement for infaunal life-styles. These behavioral characteristics, though primitive, are clearly derived from earlier animal ancestors.

References and Notes

1. S. B. Hedges, J. E. Blair, M. L. Venturi, J. L. Shoe, *BMC Evol. Biol.* **4**, 2 (2004).
2. K. J. Peterson, N. J. Butterfield, *Proc. Natl. Acad. Sci. U.S.A.* **102**, 9547 (2005).
3. K. J. Peterson, J. A. Cotton, J. G. Gehling, D. Pisani, *Philos. Trans. R. Soc. B* **363**, 1435 (2008).
4. J.-Y. Chen *et al.*, *Science* **305**, 218 (2004).
5. D. Condon *et al.*, *Science* **308**, 95 (2005).
6. T. Huldtgren *et al.*, *Science* **334**, 1696 (2011).
7. S. Xiao, A. H. Knoll, J. D. Schiffbauer, Ch. Zhou, X. Yuan, *Science* **335**, 1169; author reply 1169 (2012).
8. M. D. Brasier, D. McIlroy, *J. Geol. Soc. London* **155**, 5 (1998).
9. A. G. Liu, D. McIlroy, M. D. Brasier, *Geology* **38**, 123 (2010).
10. G. J. Retallack, *Geology* **38**, e223 (2010).
11. S. Jensen, M. L. Droser, J. G. Gehling, *Palaeogeogr. Palaeoclimatol. Palaeoecol.* **220**, 19 (2005).
12. M. A. Fedonkin, B. M. Waggoner, *Nature* **388**, 868 (1997).
13. M. W. Martin *et al.*, *Science* **288**, 841 (2000).
14. Materials and methods are available as supplementary materials on *Science* Online.
15. G. Veroslavsky, H. de Santa Ana, G. Daners, *Rev. Soc. Uru. Geol.* **13**, 23 (2006).
16. S. Jensen, M. L. Droser, J. G. Gehling, in *Neoproterozoic Geobiology and Paleobiology,* S. Xiao, A. J. Kaufman, Eds. (Springer, New York, 2006), pp. 115–157.
17. S. Jensen, T. Palacios, M. Martí Mus, in *The Rise and Fall of the Ediacaran Biota,* P. Vickers-Rich, P. Komarower, Eds. (Special Publication, Geological Society of London, 2007), pp. 223–235.
18. S. Bengtson, B. Rasmussen, B. Krapež, *Paleobiology* **33**, 351 (2007).
19. M. V. Matz, T. M. Frank, N. J. Marshall, E. A. Widder, S. Johnsen, *Curr. Biol.* **18**, 1849 (2008).
20. A. G. Collins, J. H. Lipps, J. W. Valentine, *Paleobiology* **26**, 47 (2000).
21. G. M. Narbonne, J. D. Aitken, *Palaeontology* **33**, 945 (1990).
22. M. L. Droser, J. G. Gehling, S. Jensen, in *Evolving Form and Function: Fossils and Development*, D. E. G. Briggs, Ed. (Peabody Museum of Natural History, New Haven, CT, 2005), pp. 125–138.
23. G. D. Love *et al.*, *Nature* **457**, 718 (2009).
24. A. C. Maloof *et al.*, *Nat. Geosci.* **3**, 653 (2010).
25. G. M. Narbonne, *Annu. Rev. Earth Planet. Sci.* **33**, 421 (2005).
26. D. E. Canfield, S. W. Poulton, G. M. Narbonne, *Science* **315**, 92 (2007).
27. K. A. McFadden *et al.*, *Proc. Natl. Acad. Sci. U.S.A.* **105**, 3197 (2008).
28. Y. Shen, T. Zhang, P. F. Hoffman, *Proc. Natl. Acad. Sci. U.S.A.* **105**, 7376 (2008).
29. L. M. Och, G. A. Shields-Zhou, *Earth Sci. Rev.* **110**, 26 (2012).
30. M. Gingras *et al.*, *Nat. Geosci.* **4**, 372 (2011).

Acknowledgments: This work was supported by Natural Sciences and Engineering Research Council (NSERC) of Canada Discovery Grants to K.O.K., M.K.G., and L.M.H.; by a Comisión Sectorial de Investigación Científica–UdelaR Grant ("El Ediacarano en Uruguay y su importancia en el contexto del origen de la vida animal") to K.O.K., G.V., M.K.G., E.P., and N.R.A.; and by an Agouron Institute Fellowship Program grant to E. Pecoits. Partial support for the U-Pb analyses was provided by an NSERC Major Resource Support Grant to L.M.H. Laboratory support for the thermal ionization mass spectrometry, LA-MC-ICPMS, and SHRIMP U-Pb analyses was provided by B. Herchuk, J. Schultz, G. Hatchard, A. DuFrane, and A. Simonetti. C. Magee and staff at Geoscience Australia facilitated SHRIMP analysis. We also thank G. Narbonne for many valuable insights. The data presented in this paper are available in the supplementary materials. The trace fossil collection can be found at the Department of Earth and Atmospheric Sciences, with accession nos. TF3 to TF16.

Supplementary Materials

www.sciencemag.org/cgi/content/full/336/6089/1693/DC1
Materials and Methods
Supplementary Text
Figs. S1 to S13
Tables S1 to S4
References (*31*–*46*)

7 November 2011; accepted 1 May 2012
10.1126/science.1216295

Early Pottery at 20,000 Years Ago in Xianrendong Cave, China

Xiaohong Wu,[1] Chi Zhang,[1] Paul Goldberg,[2,3] David Cohen,[2] Yan Pan,[1] Trina Arpin,[2] Ofer Bar-Yosef[4]*

The invention of pottery introduced fundamental shifts in human subsistence practices and sociosymbolic behaviors. Here, we describe the dating of the early pottery from Xianrendong Cave, Jiangxi Province, China, and the micromorphology of the stratigraphic contexts of the pottery sherds and radiocarbon samples. The radiocarbon ages of the archaeological contexts of the earliest sherds are 20,000 to 19,000 calendar years before the present, 2000 to 3000 years older than other pottery found in East Asia and elsewhere. The occupations in the cave demonstrate that pottery was produced by mobile foragers who hunted and gathered during the Late Glacial Maximum. These vessels may have served as cooking devices. The early date shows that pottery was first made and used 10 millennia or more before the emergence of agriculture.

Pottery making—the manufacture of fired, ceramic container forms—differs considerably from the baked clay figurines or small objects known from the Upper Paleolithic period (*1*) in its technological demands and in its significance both in subsistence activities, including food storage, processing, and cooking, and in social interactions (*2*). Pottery was until recently thought to have been developed during the so-called "Neolithic Revolution" and first made by settled, farming populations with domesticated plants and animals and ground stone tools, but recent discoveries have found earlier examples, from Late Pleistocene mobile or semimobile hunter-gatherer contexts in China, Japan, and the Russian Far East (*2*). One notable find, dating to ~18 to 17 thousand calendar years before the present (cal ky B.P.), is at Yuchanyan

[1]School of Archaeology and Museology, Peking University, Beijing 100871, China. [2]Department of Archaeology, Boston University, Boston, MA 02215, USA. [3]Eberhard Karls University Tübingen, The Role of Culture in Early Expansions of Humans, Rümelinstraße 23, D-72070 Tübingen, Germany. [4]Department of Anthropology, Harvard University, Cambridge, MA 02318, USA.

*To whom correspondence should be addressed. E-mail: obaryos@fas.harvard.edu

Cave (Hunan, China) (*3*–*5*). Here, we describe and date earlier pottery from Xianrendong Cave (Jiangxi, China).

Xianrendong Cave (28°44'10.05″N; 117°10'23.15″E) is located in Wannian County, northern Jiangxi Province, China, some 100 km south of the Yangtze River. The cave consists of a large, inner hall with a small entrance, ~2.5 m wide and 2 m high (Fig. 1). Xianrendong was excavated in 1961 and 1964 by Li (*6*, *7*), by Sino-American joint expeditions in 1993 and 1995 (*8*, *9*), and by Peking University and Jiangxi Provincial Institute of Cultural Relics and Archaeology in 1999 and 2000 (*10*). The excavations uncovered a long Late (or Upper) Paleolithic sequence, with a rich assemblage of stone, bone, and shell tools; animal bones; phytoliths; and pieces of locally made pottery vessels [(*6*–*11*) figs. S1 to S9].

The prehistoric deposits at Xianrendong are located in front of the cave hall entrance. For this study, in 2009 we reopened two trenches from the earlier excavations, here labeled as the "east" and "west" sections from their positions on either side of a modern path leading into the cave entrance (Fig. 1). The numbering of the layers here follows the original labeling: from top to bottom, layers 1 to 4B in the west section (Fig. 2 and fig. S10) and layers 1 to 6B in the east section (Fig. 3). There is no stratigraphic correlation between layers with the same numbering across the two trenches. Pottery sherds were found in previous excavations in layers 1A to 3C1B in the west and in layers 1A to 2B in the east, as well as in what the original excavators labeled as archaeological "features" but which actually include layers and lenses, and so profiles were redrawn in the field in 2009 (Figs. 2 and 3 and fig. S12).

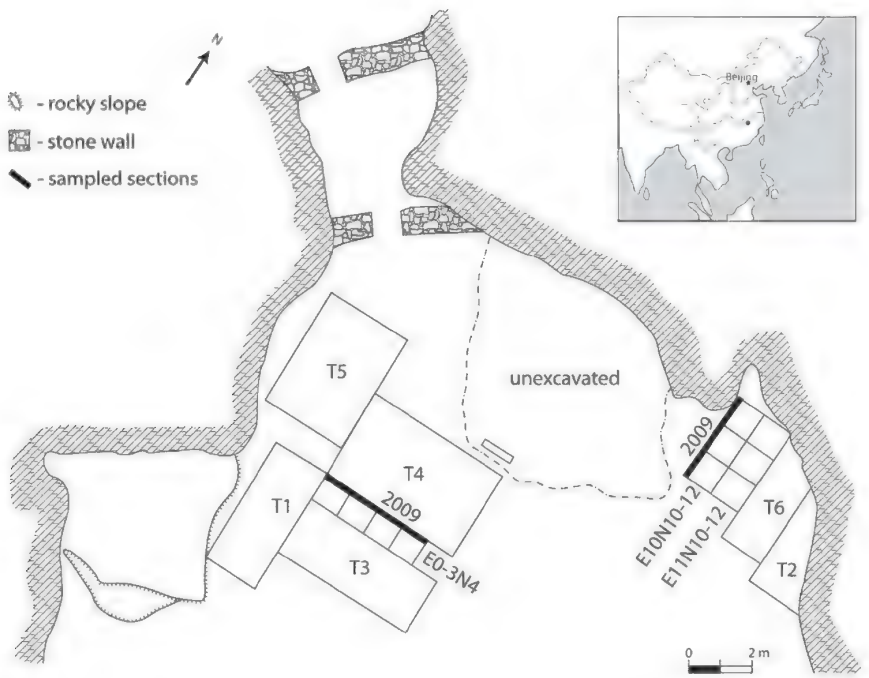

Fig. 1. Site map of Xianrendong showing the locations of the west and east sections reopened and sampled in 2009. Modified from (*10*) with permission. (**Inset**) The location of the cave in South China.

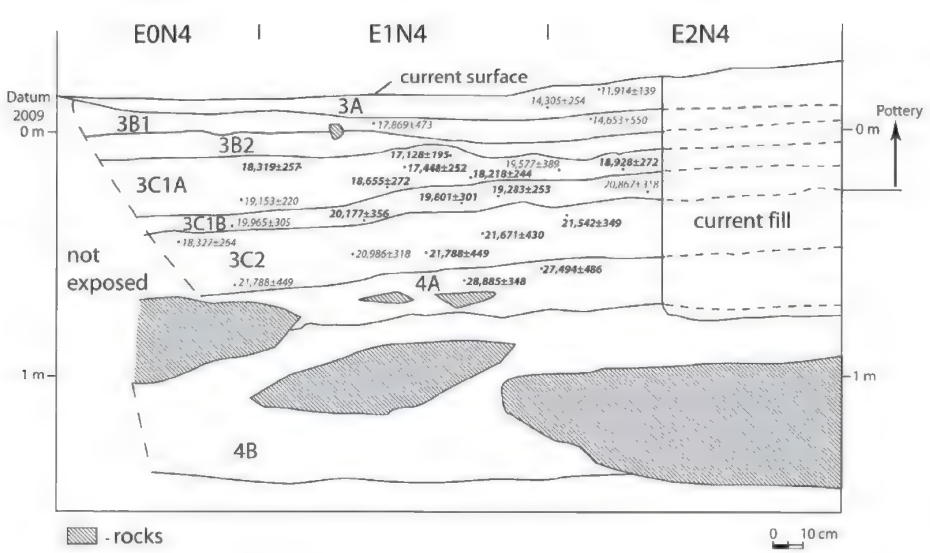

Fig. 2. The stratigraphy of the Xianrendong cave west section. Modified from (*10*) following field observations made in 2009. Dates indicated are calibrated cal yr B.P. dates calculated by CalPal_HULU 2007. For full information, see Table 1.

Although Xianrendong pottery was known to be Late Pleistocene in age, with only a limited number of radiocarbon determinations from the original excavations and no study of the complex formation processes of the cave's deposits, uncertainty persisted over the age of the earliest ceramics. We thus gathered systematically a new series of samples for radiocarbon determinations from the reopened and cleaned sections. We removed blocks of sediments for micromorphological analysis from the exposed sections concomitant with the collection of radiocarbon samples in order to establish the contextual integrity of both the pottery and the samples collected for dating (figs. S1 to S9) and to verify the integrity of the pottery-containing levels as recorded in earlier field observations (*12*–*14*).

Some 282 pottery sherds were retrieved during the 1993 excavations at Xianrendong, from contexts below the mixed layer 1A (figs. S1 to S8). We did not recover any sherds from the reopened sections but identified one piece in micromorphological sample 6 (figs. S1 to S9). All pottery is typically tempered with crushed quartzite or feldspar. Firing of the thick, more crudely made earliest pottery was probably carried out at relatively low temperatures in open fires. The earlier pottery is plain-surfaced or cord-marked, but some, from layer 3C1B, have parallel striations on the interior and exterior surfaces, probably from smoothing with grass fibers (fig. S1). Although no vessels could be reconstructed, they had rounded bottoms with walls 0.7 to 1.2 cm thick. Two vessel-forming techniques can be identified through visual observation: sheet laminating and coiling with paddling. Many sherds bear signs of burning on their exterior surface, possibly indicating their use in cooking. From a series of in situ bone fragments that we collected from the exposed profiles in the east and west trenches, we selected fragments larger than 1 cm for dating. We also selected similar fragments that were excavated previously. Because more than 90% of the bones recovered in Xianrendong were of deer—the largest mammal in the assemblage—most probably the thick fragments we used for dating were those of this group, although we could not identify specific species. Bone was chosen because it is short-lived, and we dated fragments of this size because it is unlikely that

the stratigraphic integrity of charcoal or bone samples of this size could have been disturbed after deposition (see below). Dating was done in the radiocarbon facility of Peking University (methodology is presented in the supplementary materials, section S3). In all, 45 samples have been dated. Thirteen of these were collected from the reopened sections in 2009, the dates of which are tabulated here and compared with samples collected in the 1999 and 2000 excavations and previously dated samples from the 1993 and 1995 excavations (*8*–*10*). Samples were measured by the laboratories of Peking University, University of California, Riverside, and the University of Arizona (Tables 1 and 2).

The radiocarbon dates suggest that the cave was in use with minor chronological gaps first from ~29,000 through Last Glacial Maximum (LGM) times until ~17,500 cal yr B.P. It was then abandoned and reoccupied from ~14,500 through 12,000 cal yr B.P. The earliest pottery appears in the Xianrendong sequence in layers 2B and 2B1 in the east trench and layer 3C1B in the west trench. The radiocarbon dating shows that both of these early contexts date to ~20,000 to 19,000 cal yr B.P. (Tables 1 and 2).

In order to assess the integrity and preservation of the layers and the associated samples, we studied thin sections of 24 micromorphological samples collected from the west and east trenches (*12*–*15*) (supplementary materials section S2). Although there are differences between the depositional sequences of each trench, the specific sample fabrics imply that the layers in both trenches had remained stable since deposition, with only minimal cracks on a scale of millimeters or centimeters. These are not large enough to affect the large bone fragments used for radiocarbon dating. In addition, the presence of intact ice lensing in layer 4B, which probably formed during the LGM, is further proof that the sediments have not been significantly reworked.

Alluvial sediments are present in the earliest layers of the sequence in both trenches, before the appearance of pottery (levels 4A and 4B in the west and 3A in the east trench). Above these sediments, the deposits in the west trench are overall similar, with minor changes in texture, composition, and fabric. They consist of moderately to poorly sorted sandy silty clay, with mm- to cm-sized inclusions of rock fragments derived from the cave's roof and walls. They represent a mixture of moderately sorted low-energy alluvial overbank deposits with anthropogenic contributions (charcoal, bones, sherds, and stone artifacts). The presence of bedding in layer 3C1B, where early pottery sherds, bones, and stone artifacts were found, indicates that these deposits are intact [samples 5 and 6 (*16*)].

The deposits in the east trench differ markedly from those of the west trench. They are generally calcareous, except for layer 3A, which is situated below the pottery bearing layers. Layer 3A [lower half of sample 19A (*16*)] is micaceous and strongly resembles the sediments from the west trench. A clear break is noted in the middle of sample 19A (layer 3A, Fig. 2B and fig. S13), where mica-rich sediment below changes to calcareous, ash-rich, and mica-poor sediment above.In these calcareous deposits in the east trench, the calcite is derived mostly from anthropogenic ash (accompanied by some charcoal) rather than from a geological source such as limestone: Both ash and charcoal indicate a lack of alluvial sediment, which is abundant in the western section. The lack of bedding and the virtual absence of mica in the east section in the layers from 2B2 and above suggest that most of the sediments were dumped near the cave wall by humans and were at least partially shielded from fluvial processes. It thus seems that the major occupation or activity areas at the site were located further outside the cave, beyond the excavated zone (Fig. 1), which is characterized by dumped deposits. This conclusion is supported by the lack of any intact combustion features (in spite of the large proportion of calcareous ashes), the absence of traces of bedding or any evidence of individual beds, and the mixing of a variety of materials, such as bone and charcoal: These components are chaotically arranged on a centimeter scale, whereas in occupation deposits they would normally be arranged more contiguously in a lateral direction (supplementary materials section S2).

Evidence of bioturbation by worms or similar-sized fauna, represented by centimeter-sized passage features (*15*), is common throughout the east trench and increases dramatically toward the top of the profile [e.g., samples 27, layer 2A1, and 28, layer 2A (*16*)]. Such bioturbation is responsible for the high porosity in many of the samples of the east trench [e.g., samples 27 and 28 (*16*)]. Bioturbation on this scale might have caused charcoal and bone with sizes of up to a centimeter to move, and thus millimeter-sized pieces of charcoal or bone would be inappropriate for dating. There is no evidence for

Table 1. Radiocarbon determinations from Xianrendong west section. Date column entries obtained by using Libby half-life. Calibration was done by using CalPal-HULU.2007 version, 1-Standard Deviation. Dates marked with an asterisk are cited by (*8*). Layer 3C1B contained the earliest pottery in this section. Laboratory numbers beginning with BA indicate those from Peking University radiocarbon laboratory; UCR, University of California, Riverside Radiocarbon Laboratory; AA, NSF-Arizona AMS Laboratory, Tucson. Ch indicates a charcoal sample.

Lab no.	Date	Calibrated age range yr B.P. 1δ	Material	Calibrated age B.P. 1δ
		Layer 2A		
BA09891	10,210 ± 50	11,774–12,053	Bone	11,914 ± 139
		Layer 3A		
BA09894	12,240 ± 55	14,050–14,559	Bone	14,305 ± 254
		Layer 3B1		
BA093181	14,610 ± 290	17,395–18,342	Ch	17,869 ± 473*
		Layer 3B2		
UCR3561	12,420 ± 80	14,302–15,003	Human bone	14,653 ± 350*
		Layer 3C1A		
BA09872	14,235 ± 60	17,448–17,700	Bone	17,448 ± 252
BA09868	14,925 ± 70	17,974–18,462	Bone	18,218 ± 244
BA09875	13,885 ± 55	16,933–17,333	Bone	17,128 ± 195
BA09874	15,165 ± 55	18,061–18,576	Bone	18,319 ± 257
BA00006	15,655 ± 194	18,655–19,200	Bone	18,928 ± 272
UCR3562	16,010 ± 70	18,932–19,373	Human bone	19,153 ± 220*
BA95143	16,340 ± 200	19,187–19966	Ch	19,577 ± 389*
		Layer 3C1B		
BA10264	16,165 ± 55	19,030–19,536	Bone	19,283 ± 253
BA10266	16,485 ± 55	19,500–20,102	Bone	19,801 ± 301
UCR3439	16,730 ± 120	19,659–20,270	Ch	19,965 ± 305*
BA00007	16,915 ± 186	19,821–20,533	Bone	20,177 ± 356
AA15005	17,420 ± 130	20,459–21,285	Ch	20,867 ± 318*
UCR3440	18,520 ± 140	21,784–22,455	Ch	22,120 ± 335*
		Layer 3C2		
UCR3300	15,180 ± 90	18,062–18,591	Human skull	18,327 ± 264*
UCR3522	17,580 ± 80	20,668–21,304	Ch	20,986 ± 318*
BA09878	17,915 ± 80	21,192–21,891	Bone	21,542 ± 349
BA00008	17,983 ± 177	21,326–22,042	Bone	21,671 ± 430
BA93182	18,110 ± 270	21,337–22,237	Ch	21,788 ± 449*
		Layer 4A		
BA00009	22,902 ± 322	27,008–27,980	Bone	27,294 ± 486
BA09880	24,080 ± 95	28,507–29,263	Bone	28,885 ± 378

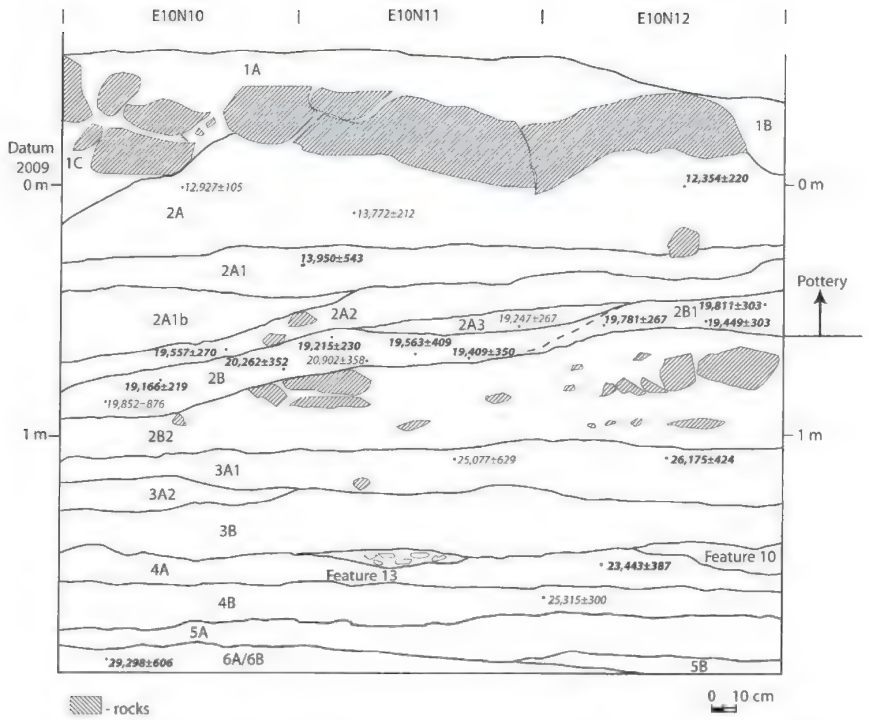

Fig. 3. The stratigraphy of the Xianrendong cave east section. Modified from (*10*) following field observations made in 2009. Dates indicated are calibrated cal yr B.P. dates calculated by CalPal_HULU 2007. For full information, see Table 2.

Table 2. Radiocarbon determinations from Xianrendong east section. Dates, calibrated age ranges, asterisks, and laboratory abbreviations as in Table 1. Layers with the earliest pottery are 2B1 and 2B.

Lab no.	Date	Calibrated age range cal yr B.P. 1δ	Material	Calibrated age cal yr B.P. 1δ
		Layer 2A		
BA00004	10,456 ± 118	12,134–12,574	Bone	12,354 ± 220
BA95138	11,840 ± 150	13,560–13,984	Ch	13,772 ± 212*
		Layer 2A1		
UCR3558	11,020 ± 60	12,871–13,032	Human bone	12,927 ± 105*
BA99038	11,840 ± 380	13,406–14,493	Bone	13,950 ± 543
		Layer 2A2		
BA09899	16,330 ± 65	19,286–19,827	Bone	19,557 ± 270
		Layer 2A3		
BA95139	16,110 ± 140	18,979–19,514	Ch	19,247 ± 267*
		Layer 2B1		
BA10263	16,030 ± 55	18,947–19,385	Bone	19,166 ± 219
BA09912	16,495 ± 60	19,508–20,114	Bone	19,811 ± 303
		Layer 2B		
BA09902	16,095 ± 65	18,983–19,443	Bone	19,215 ± 230
BA10268	16,270 ± 65	19,138–19,759	Bone	19,449 ± 310
BA00015	16,301 ± 157	19,148–19,849	Bone	19,499 ± 350
BA99037	16,330 ± 220	19,153–19,972	Bone	19,563 ± 409
BA09926	16,345 ± 70	19,313–19,848	Bone	19,581 ± 267
BA95141	16,580 ± 260	19,481–20,234	Ch	19,858 ± 376*
BA10271	17,105 ± 60	20,115–20,819	Bone	20,467 ± 352
BA95140	17,460 ± 210	20,543–21,260	Ch	20,902 ± 358*
		Layer 3A		
BA95142	20,940 ± 440	24,448–25,706	Ch	25,077 ± 629*
BA09921	21,820 ± 85	25,751–26,599	Bone	26,175 ± 424
		Layer 4		
BA00003	19,634 ± 186	23,046–23,820	Bone	23,433 ± 387
BA95144	21,090 ± 660	24,415–26,215	Ch	25,315 ± 900*
		Layer 6B		
BA99039	24,500 ± 370	28,691–29,904	Bone	29,298 ± 606

burrowing by larger animals such as rodents. Thus, we conclude that it is unlikely that either pottery sherds or the larger bone fragments that were used in dating were displaced in either section. Individual bone-rich layers can be observed in some of the thin sections [e.g., samples 19A, layer 3A; 22B, layer 2A3; 26, layer 2A2; and 29, A and B, both feature 4).

The tabulated radiocarbon dates (Tables 1 and 2) and Figs. 1 and 2 demonstrate a high degree of consistency in dating the contexts of the earliest appearance of pottery in the west and east trenches. In the west section, layer 3C1B, where the earliest sherds were uncovered, is ~10 cm thick and has five dates ranging from 20,867 ± 318 (AA15005) to 19,283 ± 283 (BA10267) cal yr B.P. The sixth date reported from this layer (UCR3440) of charcoal, calibrated as 22,120 ± 335, is an outlier. Given the observations concerning potential mobility of charcoal flecks (supplementary text S2) and uncertainty about their original location, it was not included in Fig. 2. The five dates of layer 3C1A are younger by a few centuries than those of layer 3C2 underneath and may indicate the particular time when making pottery began. A date of 18,327 ± 264 (UCR3300) on human bone from earlier excavations in layer 3C2 is likely intrusive; the same explanation holds for UCR-3561 (14,653 ± 550 cal yr B.P.) in layer 3B1 above. Layer 3CA1, directly above layer 3C1B, is definitely younger, with dates ranging from 19,577 ± 389 (BA95143) to 17,128 ± 195 cal yr B.P. (BA09875) (Fig. 2).

Dating in the east section is consistent with that in the west. In the east, layers 2B to 2B1, with the earliest pottery, contain 10 dates ranging from 20,902 ± 358 (BA95140; from the earlier excavations) to 19,166 ± 219 (BA10263) cal yr B.P. The overall thickness of layers 2B to 2B1 is about 15 cm (Fig. 3). Above this, layers 2A3 and 2A2 produced somewhat similar dates, after which there is a depositional break. We conclude that the two trenches, 8 m apart and separated by consolidated unexcavated deposits, provide the same chronological indicators for the early pottery in Xianrendong.

Pottery making introduces a fundamental shift in human dietary history, and Xianrendong demonstrates that hunter-gatherers in East Asia used pottery for some 10,000 years before they became sedentary or began cultivating plants (*17*–*19*). The age for pottery production at Xianrendong of ~20,000 years ago coincides with the peak period of the last ice age, when there was a decrease in the productivity of regional food resources (*20*–*22*). When used for cooking, pottery allows energy gains from starch-rich food as well as meat (*23*), and scorch and soot marks on sherd exterior surfaces indicate that Xianrendong pottery likely was used for cooking. Residue, starch, or other physiochemical analyses of recovered early pottery sherds from Xianrendong and other Late Pleistocene sites in China have not been reported, so the exact

function of this early pottery remains unknown. The Xianrendong assemblage contained a large number of fragmented bones, so the pottery could have been used in the extraction of marrow and grease (*24*, *25*). Other known uses of pottery in hunter-gatherer societies include food preparation and storage, as well as brewing alcoholic beverages, and could play a vital social role in feasting (*26*). Thus, the early invention of pottery may have played a key role in human demographic and social adaptations to climate change in East Asia, leading to sedentism, and eventually to the emergence of wild rice cultivation during the early Holocene (*17*, *27*).

References and Notes

1. P. B. Vandiver, O. Soffer, B. Klima, J. Svoboda, *Science* **246**, 1002 (1989).
2. P. Jordan, M. Zvelebil, Eds., *Ceramics Before Farming* (Left Coast Press, Walnut Creek, CA, 2009).
3. E. Boaretto *et al.*, *Proc. Natl. Acad. Sci. U.S.A.* **106**, 9595 (2009).
4. Y. V. Kuzmin, P. A. Kosintsev, D. I. Razhev, G. W. Hodgins, *J. Hum. Evol.* **57**, 91 (2009).
5. C. T. Keally *et al.*, *Radiocarbon* **48**, 345 (2004).
6. Jiangxi Provincial Cultural Relics Administration Committee, *Kao Gu Xue Bao* 1963.1, 1 (1963).
7. Jiangxi Provincial Museum, *Wen Wu* 1976.12, 23 (1976).
8. R. S. MacNeish, J. G. Libby, Eds., *Origins of Rice Agriculture: The Preliminary Report of the Sino-American Jiangxi (PRC) Project* (Publications in Anthropology no. 13, El Paso Centennial Museum, University of Texas at El Paso, El Paso, TX, 1995).
9. R. S. MacNeish *et al.*, *Revised Second Annual Report of the Sino-American Jiangxi (PRC) Origin of Rice Project (SAJOR)* (Andover Foundation for Archaeological Research, Andover, MA, 1998).
10. L. Wang, Ed., *Human Pottery Making and Rice Cultivation: World-Class Archaeological Discoveries and Studies on the Xianrendong and Diaotonghuan Sites of Wannian County* (in Chinese) (Jiangxi Meishu Chubanshe, Nanchang, Jiangxi, People's Republic of China, 2010).
11. Z. Zhao, *Antiquity* **72**, 885 (1998).
12. M.-A. Courty, P. Goldberg, R. I. Macphail, *Soils and Micromorphology in Archaeology* (Cambridge Univ. Press, Cambridge, 1989).
13. P. Goldberg, R. I. Macphail, *Geoarchaeology* **18**, 571 (2003).
14. P. Goldberg, S. C. Sherwood, *Evol. Anthropol.* **15**, 20 (2006).
15. H. Brammer, *Geoderma* **6**, 5 (1971).
16. Detailed information for samples can be found in the supplementary materials, section S2.
17. Z. Zhao, *Curr. Anthropol.* **52**, S295 (2011).
18. D. Cohen, *Curr. Anthropol.* **52**, S273 (2011).
19. O. Bar-Yosef, *Curr. Anthropol.* **52**, S175 (2011).
20. E. Huang, J. Tian, S. Steinke, *Quat. Res.* **75**, 196 (2011).
21. J. Ni, G. Yu, S. P. Harrison, I. C. Prentice, *Palaeogeogr. Palaeoclimatol. Palaeoecol.* **289**, 44 (2010).
22. L. Barton, P. J. Brantingham, D. Ji, *Dev. Quat. Sci.* **9**, 105 (2007).
23. R. N. Carmody, G. S. Weintraub, R. W. Wrangham, *Proc. Natl. Acad. Sci. U.S.A.* **108**, 19199 (2011).
24. M. E. Prendergast, J. Yuan, O. Bar-Yosef, *J. Archaeol. Sci.* **36**, 1027 (2009).
25. J. Yuan, in *The Origins of Pottery and Agriculture*, Y. Yasuda, Ed. (Roli Books, New Delhi, India, 2002), pp. 157–166.
26. B. Hayden, *World Archaeol.* **34**, 458 (2003).
27. Z. Zhao, *Archaeol. Anthropol. Sci.* **2**, 99 (2010).

Acknowledgments: We thank the State Administration of Cultural Heritage of China for permission to carry out this project and the Jiangxi Provincial Institute of Cultural Relics and Archaeology for their support, in particular C. Fan and G. Zhou. W. Yan (Peking University) and B. Wang (Cultural Relics Bureau, Wannian, Jiangxi) provided assistance and information concerning the earlier excavations. We also thank S. Liu (Jiangxi Provincial Institute) for assistance. Detailed descriptions of the stratigraphy and the pottery fragments are in (*17*). We thank K. Liu and X. Ding for the atomic mass spectrometry (AMS) radiocarbon measurements. The American School of Prehistoric Research (Peabody Museum, Harvard University) supported the fieldwork and, in part, the preparation of the samples for microscopic analysis. P.G. is grateful to the NSF (grant no. 0917739) for partial support of this project. W.X., Z.C., and O.B.-Y. contributed to conceiving the project and organizing the fieldwork. P.G. and T.A. analyzed the micromorphology of the thin sections. W.X. and P.Y. conducted the dating of the new radiocarbon samples. W.X., O.B.-Y., P.G., Z.C., and D.C. prepared the paper. The authors declare no competing financial interests. Correspondence and requests for materials should be addressed to O.B.-Y. and X.W. (wuxh@pku.edu.cn).

Supplementary Materials

www.sciencemag.org/cgi/content/full/336/6089/1696/DC1
Materials and Methods
Supplementary Text
Figs. S1 to S24
Tables S1 to S4
References (*28*–*32*)

3 January 2012; accepted 1 May 2012
10.1126/science.1218643

Photonic Crystal Light Collectors in Fish Retina Improve Vision in Turbid Water

Moritz Kreysing,[1,2]* Roland Pusch,[3]* Dorothee Haverkate,[4]* Meik Landsberger,[3]* Jacob Engelmann,[3,5]* Janina Ruiter,[6] Carlos Mora-Ferrer,[7] Elke Ulbricht,[6,8] Jens Grosche,[6] Kristian Franze,[1,6,8] Stefan Streif,[9] Sarah Schumacher,[3] Felix Makarov,[10] Johannes Kacza,[11] Jochen Guck,[1,12] Hartwig Wolburg,[13] James K. Bowmaker,[14] Gerhard von der Emde,[3] Stefan Schuster,[4] Hans-Joachim Wagner,[15] Andreas Reichenbach,[6]† Mike Francke[1,6,16]

Despite their diversity, vertebrate retinae are specialized to maximize either photon catch or visual acuity. Here, we describe a functional type that is optimized for neither purpose. In the retina of the elephantnose fish (*Gnathonemus petersii*), cone photoreceptors are grouped together within reflecting, photonic crystal–lined cups acting as macroreceptors, but rod photoreceptors are positioned behind these reflectors. This unusual arrangement matches rod and cone sensitivity for detecting color-mixed stimuli, whereas the photoreceptor grouping renders the fish insensitive to spatial noise; together, this enables more reliable flight reactions in the fish's dim and turbid habitat as compared with fish lacking this retinal specialization.

Most vertebrate retinae have two types of photoreceptor cells: rods, capable of sensing one or a few photons, and cones, less light-sensitive by two orders of magnitude but wired to contrast- and color-sensitive neuronal circuits. Cones are "blind" in the dark whereas rods are saturated when cones are active, so typically there is only a small ("mesopic") range of light intensities at which both rods and cones contribute to vision. All presently known retinae are specialized for either cone-dominated high-acuity vision at daylight or rod-dominated maximum sensitivity in dim environments (*1*, *2*). Fitting neither description, the so-called "grouped retina" was already described 100 years ago as a puzzling retinal anomaly in some fish (*3*). In such retinae, many cones are grouped together inside large crystalline cups (*4*), which is incompatible with high spatial resolution (*5*). But the short rods

[1]Cavendish Laboratory, Department of Physics, University of Cambridge, Cambridge CB3 0HE, UK. [2]Systems Biophysics, Department of Physics, Ludwig-Maximilians University, D-80799 Munich, Germany. [3]Institute of Zoology, University of Bonn, D-53115 Bonn, Germany. [4]University of Bayreuth, Department of Animal Physiology, D-95440 Bayreuth, Germany. [5]Department of Biology, University of Bielefeld, D-33501 Bielefeld, Germany. [6]Paul-Flechsig-Institute for Brain Research, University of Leipzig, D-04109 Leipzig, Germany. [7]Institute of Zoology, Neurobiology, University Mainz, D-55099 Mainz, Germany. [8]Department of Physiology, Development and Neuroscience, University of Cambridge, Cambridge CB2 3EG, UK. [9]Institute for Automation Engineering, Systems Theory and Automatic Control Lab, Otto von Guericke University Magdeburg, D-39106 Magdeburg, Germany. [10]Pavlov Institute of Physiology, 199034 St. Petersburg, Russia. [11]Institute of Anatomy, Histology and Embryology, Faculty of Veterinary Medicine, University of Leipzig, D-04109 Leipzig, Germany. [12]Technische Universität Dresden, Biotechnology Center, D-01062 Dresden, Germany. [13]Institute of Pathology and Neuropathology, University of Tübingen, D-72076 Tübingen, Germany. [14]Institute of Ophthalmology, University College London, London EC1V 9EL, UK. [15]Institute of Anatomy, University of Tübingen, D-72074 Tübingen, Germany. [16]Translational Centre for Regenerative Medicine, University of Leipzig, D-04103 Leipzig, Germany.

*These authors contributed equally to this work.
†To whom correspondence should be addressed. E-mail: reia@medizin.uni-leipzig.de

are located behind these light-shielding cups, so this retina is not adapted for very dim light vision either (*1*).

We investigated the function and purpose of the grouped retina in the elephantnose fish (*Gnathonemus petersii*), using a variety of complementary techniques. (i) Light and electron microscopy (EM) of the grouped retina (Fig. 1) were used as a quantitative basis for (ii) electrodynamical simulations of light propagation inside the crystalline cups. (iii) Absorption spectra measurements of isolated cone and rod outer segments, as well as electroretinography on intact eyes, were applied to reveal the spectral sensitivities of the photoreceptors. (iv) Electrophysiological field potential recordings from the optic tectum served to characterize the stimulus processing. Finally, (v) several behavioral experiments tested how well the fish can detect predator-mimicking visual stimuli in comparison with goldfish (*Carassius auratus*) and pumpkinseed (*Lepomis gibbosus*), both with well-studied visually guided behavior based on high-acuity color vision.

Gnathonemus has a typical grouped retina (Fig. 1). Large bundles of inner and outer segments of photoreceptor cells are embedded in a sandglass-shaped scabbard formed by six adjacent giant retinal pigment epithelial (RPE) cells (Fig. 1, B to F, and movie S1). The shape of the scabbard and its contents undergo some changes between the light- and dark-adapted states (*6*); all our data were obtained under the daytime conditions (40 lx) found in the fish's dim habitats (*7*–*10*). In this light-adapted state, the upper part of the scabbard forms a reflective cup that is terminated by a constriction. This cup (Fig. 1, B and G) is directed toward the light and contains the light-insensitive inner segments of rods and cones. It was noteworthy that only the light-sensitive outer segments of cones (COSs) are located at its base, whereas the rod outer segments (ROSs) are embedded in the less regularly shaped part of the scabbard below the cup (at bottom in Fig. 1, B and G). Confocal microscopy and EM suggest that the inner surface of the cup acts as a mirror (Fig. 1D), formed by a reflecting multilayer of four layers of thin, evenly spaced rows of guanine-crystal lamellae (Fig. 1J, and fig. S2). The scabbard below the cup lacks a mirror surface but contains light-scattering, submicron-sized guanine crystallites and light-absorbing melanin granules (Fig. 1, G and I to K, and fig. S3B).

To rationalize this peculiar arrangement, we simulated the intensity distributions of the incident light inside and below the reflecting cups (Fig. 1H and fig. S4) using a finite-difference time-domain (FDTD) implementation of Maxwell's equations [see (*11*) and supplementary materials for details] with our morphological data and published data for the refractive indices of retinal neurons [$n = 1.36$; (*12*)] and of guanine [$n = 1.83$; (*13*)] as input parameters. These simulations show that (i) light is efficiently reflected from the walls of the cup, (ii) local intensity is increased by factors >5 at the cup bottom where the COSs are located (particularly, for deep-red wavelengths) (compare Fig. 2A and fig. S4), and (iii) only a small fraction of light reaches the rods. The wavelength dependence of the reflection has to be seen in light of the absorption spectra of the rods and the one type of cone identified morphologically. The measured absorption spectra of mechanically dissociated ROSs (Fig. 2B) and COSs (Fig. 2C) verified that there were single photopigments with maximum absorption at 536 nm ("green," rods) and at 615 nm ("red," all cones), respectively. Electroretinograms (ERGs), used to record electrical activity in the retina in response to visual stimuli, showed two corresponding maxima close to the absorption peaks of individual rods and cones (Fig. 2D). Note that the cone-driven peak of the ERG was slightly shifted toward longer wavelengths (Fig. 2D

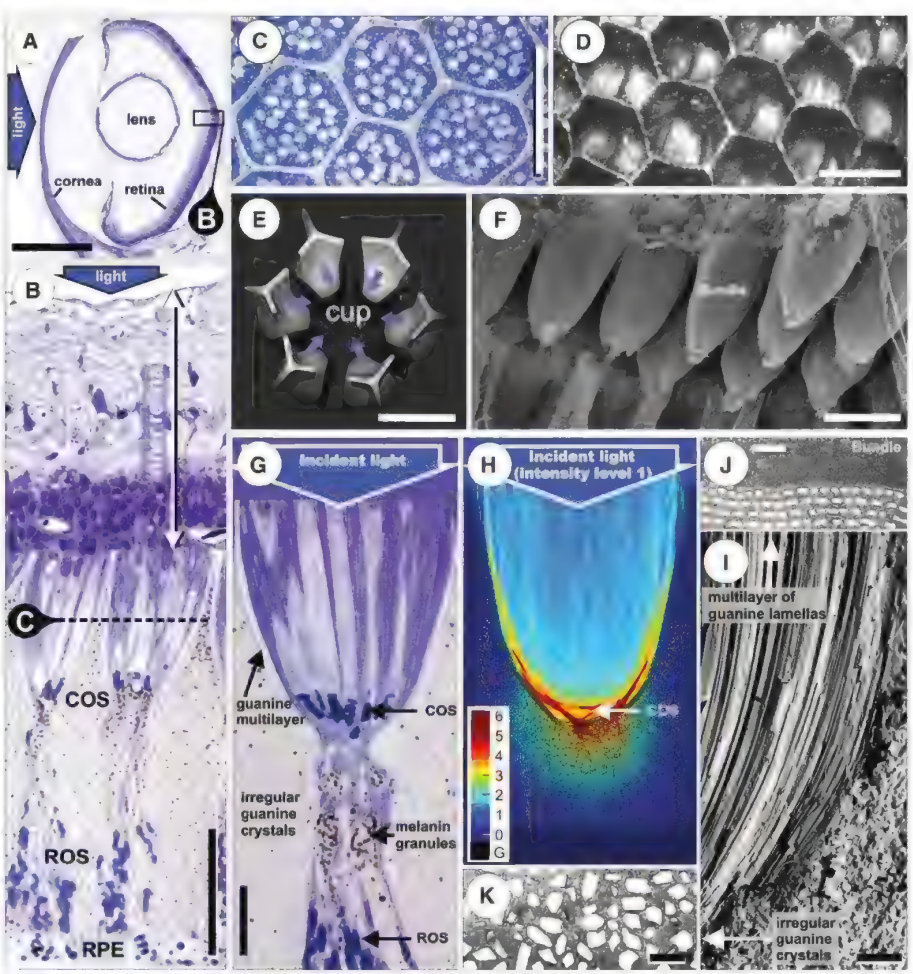

Fig. 1. The grouped retina of *Gnathonemus*. (**A**) Vertical section through an entire eye. (**B**) Radial semithin section at the region indicated in (A). The inner retina covers the crystalline cups, containing the COSs. ROSs are well below the cups and surrounded by RPE cells. (**C**) Transverse section through the cups at the level indicated in (B). The light blue circles are cone inner segments; rod inner segments are too thin to be visible. (**D**) Light reflection from the cups; top view onto intact retina using a confocal microscope in reflection mode. (**E**) Artistic rendering of six individual RPE cells, seen from top as in (D). The cells are here shifted away from each other, to demonstrate that the light-reflecting surfaces of six cells contribute to the formation of one cup (see also movie S1). (**F**) Scanning electron micrograph of several photoreceptor bundles—the filling of the cups. (**G**) Semithin section of a cup used as a model for the simulations with the COSs at its bottom and the ROSs far below, surrounded by RPE cells containing guanine crystals and melanin. (**H**) Simulation of the light intensity distribution in a cup for an incident plane wave of broad spectral range (525 to 725 nm). The COSs receive up to 500% of the incident light intensity, whereas the ROSs receive ≤20%. Color scale shows local gain; G stands for guanine (compare fig. S3). (**I**) Radial freeze-fracture electron micrograph of the guanine lamellae along the cup's inner surface. (**J**) and (**K**) Transmission electron micrographs of a transverse section through a cup wall, lined by rows of lamellae (J), and its bulk containing irregular crystals (K). Scale bars: 2 mm (A), 50 μm (B to F), 20 μm (G), 2 μm (I), 1 μm (J) and (K).

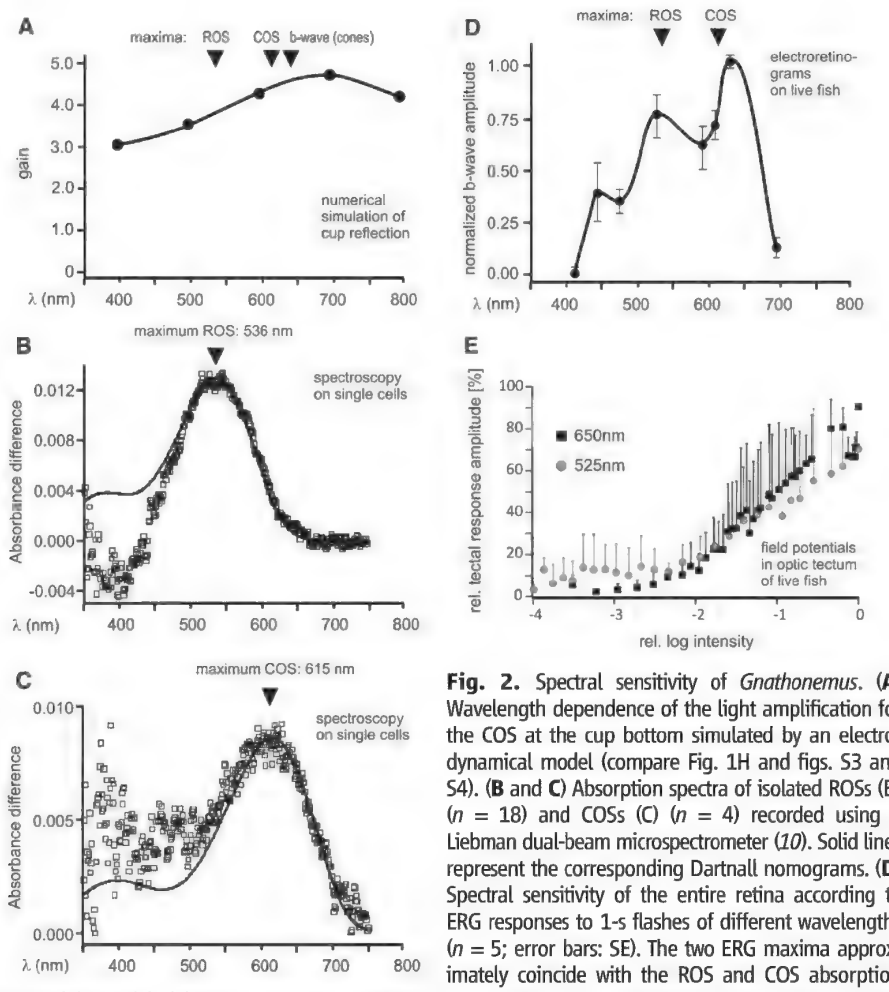

Fig. 2. Spectral sensitivity of *Gnathonemus*. **(A)** Wavelength dependence of the light amplification for the COS at the cup bottom simulated by an electrodynamical model (compare Fig. 1H and figs. S3 and S4). **(B** and **C)** Absorption spectra of isolated ROSs (B) (n = 18) and COSs (C) (n = 4) recorded using a Liebman dual-beam microspectrometer (*10*). Solid lines represent the corresponding Dartnall nomograms. **(D)** Spectral sensitivity of the entire retina according to ERG responses to 1-s flashes of different wavelengths (n = 5; error bars: SE). The two ERG maxima approximately coincide with the ROS and COS absorption maxima (B) and (C). **(E)** Field potentials recorded in the optic tectum in response to green and red light flashes of different intensities show that the tectal response of the fish is fully matched in sensitivity at both wavelengths.

versus 2C), in accordance with previously published data (*14*) that suggested a sensitivity of *Gnathonemus* to deep-red wavelengths, which is commensurate with the red-dominated turbid water it lives in (*8*, *14*, *15*) (fig. S1). This shift can be explained by the red-enhanced light reflection at the bottom of the photonic crystal cups (Fig. 2A and fig. S4).

The specific light distribution inside and below the crystalline cups holds the key for resolving the puzzle of the grouped retina, as it allows both cones and rods to be active simultaneously. The COSs—by themselves known to display a lower absolute light sensitivity than the ROSs (*16*, *17*)—receive an elevated level of illumination, whereas the illumination of the ROSs is drastically reduced. The latter is advantageous because it prevents bleaching of rod photopigment and allows their use even under light-adapted conditions. Indeed, the ERGs invariably displayed a mixed rod-and-cone contribution to retinal electrical activity (Fig. 2D), whereas, in other animals, identical illumination conditions eliminate the rod responses from ERG recordings (*18*). By measuring visually evoked potentials in the optic tectum of *Gnathonemus* (n = 4), we confirmed that cone and rod photoreceptors were simultaneously activated over a nearly identical range of intermediate light intensities (Fig. 2E).

The behavioral consequences of this shared working range of rods and cones lie in a superior response to visual stimuli in the dim mesopic range of illumination compared with fish without a grouped retina. In fact, dim stimuli elicited a startle response in *Gnathonemus*, triggered by a rapidly expanding circle, much more reliably than in *Carassius*, whereas the control experiment in bright light showed no difference (Fig. 3A). The

Fig. 3. *Gnathonemus* responds at low intensities and despite color camouflage. **(A)** Startle experiment with black circles expanding on a white background. The intensities of circles (I_C) and background (I_B) were varied. At low intensities, *Gnathonemus* (blue) performed better ($P < 0.05$) than *Carassius* (amber; n = 5 for both species). **(B)** Startle experiment with color-pooling task. The expanding circle was dynamically defined by the random exchange of red and green floating particles, with the particles inside the circle becoming stationary (compare movie S2). **(C)** *Gnathonemus* detected such color-camouflaged stimuli significantly better ($P < 0.05$) than *Carassius* (n = 5 for both species). The rate of false responses (right pair of columns) was not significantly different between species. Response percentages are relative to an expanding black circle that represents 1.0.

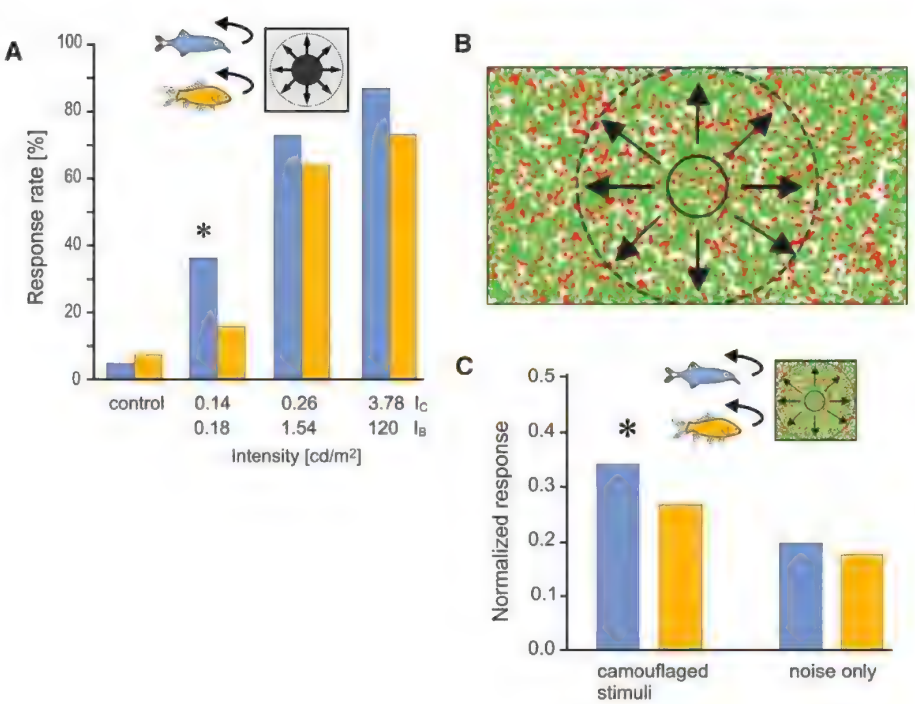

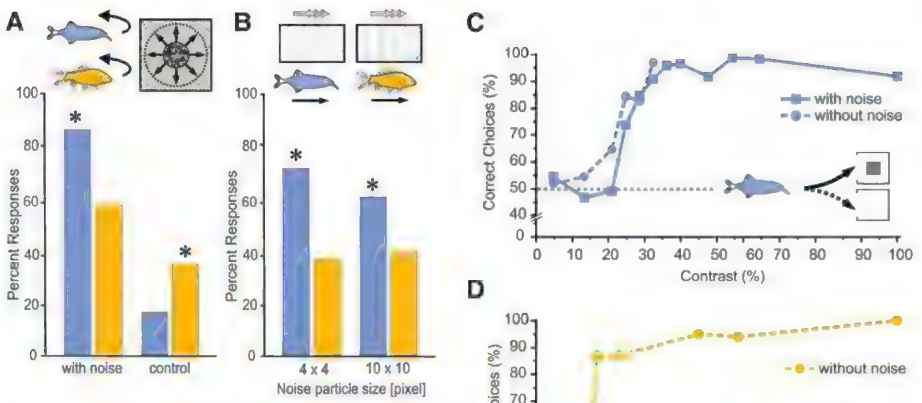

Fig. 4. *Gnathonemus* displays a high tolerance against spatial noise. (**A**) Startle experiment with an expanding circle disguised by dynamic gray noise particles (9000 particles). Flight responses declined in both species (percentage relative to no noise), but *Gnathonemus* (blue) was less affected than *Carassius* (amber; $P < 0.05$) and produced fewer false responses with noise only (control) ($P < 0.05$). (**B**) Percentage of optomotor responses to reversal of moving stripes relative to response rate without noise. When the stripes were obscured by dynamic white particles of varying size, *Gnathonemus* performed significantly better than *Carassius* ($P < 0.05$). (**C**) Contrast detection of *Gnathonemus* and (**D**) *Lepomis* with and without added dynamic noise particles. Fish were trained to approach a black square on a bright background; the contrast of the square was reduced stepwise. The performance of *Gnathonemus* decreased only slightly when noise particles were added (solid curve). Note that *Lepomis* refused to make any choices when images were overlaid by noise particles—even at 100% contrast.

color dependence of the startle response revealed a further remarkable advantage of *Gnathonemus*. Provided that *Gnathonemus* can add up signals from both cones (red) and rods (green) to generate responses to visual stimuli, such an addition (rather than a subtraction as required for color discrimination) should enable the detection of red-green color-camouflaged expanding stimuli, analogous to dichromatic human subjects and other dichromatic vertebrates (*19*, *20*). Indeed, *Gnathonemus* was better in detecting color-camouflaged objects, for example, when a rapidly expanding circle was only defined by randomly dynamic green and red dots (Fig. 3, B and C). Likewise, optomotor responses of *Gnathonemus*, assessed by its ability to follow the reversal of motion of a stripe pattern, could be elicited by green and red as well as white moving stripes (fig. S5A). This is in contrast to *Carassius*, whose optomotor response is selectively dependent on cone vision (*21*).

Additional behavioral advantages of *Gnathonemus* rest in the macroreceptor aspect of the grouped retina. On the one hand, behavioral tests confirmed that *Gnathonemus* detects only very large objects (4° and larger) (*5*, *6*, *22*), whereas objects of 3° visual field angle (corresponding to the sixfold diameter of the full moon in our eye) were not detected (fig. S5B). However, this apparent disadvantage was compensated for because *Gnathonemus* detected stimuli overlaid with noise in startle and optomotor tests better than *Carassius* and *Lepomis* did. When the expanding circle and the moving stripes were black on a white background, there was no statistical difference in the response between *Carassius* and *Gnathonemus*. But when a white or gray noise pattern was overlaid, *Gnathonemus* performed significantly better (Fig. 4, A and B). This improved noise tolerance was also obvious in the detection of large, stationary patterns, where *Gnathonemus* was only very little affected by the addition of small noise particles to the images, whereas *Lepomis* refused to accept noisy objects (Fig. 4, C and D). An obvious interpretation of these results is that the macroreceptors act as spatial low-pass filters before neuronal processing and render *Gnathonemus* incapable of resolving small-scale image information, whereas other fish with more acute vision get distracted by the image detail—an advantage *Gnathonemus* has when challenged with avoiding predators obscured by small debris and floating plant particles under poor lighting conditions.

Our results reveal that the photonic crystal cups in the grouped retina of *Gnathonemus* are effective, wavelength-sensitive light intensifiers that increase the sensitivity of cone photoreceptors in the red and match the dynamic ranges of rods and cones. This feature, together with the macroreceptor aspect of the grouped retina, enables these fish to perform better than species with conventional retinae, under experimental conditions mimicking the—visually challenging—habitat of *Gnathonemus*. We conclude that their grouped retina, as a unique type of retinal specialization, has emerged to provide the optical prerequisite to detect large, fast-moving predators as an adaptation to the survival demands of the fish's habitat. It might be expected that similar evolutionary advantages rationalize the grouped retina found in other species.

References and Notes

1. G. L. Walls, *The Vertebrate Eye and Its Adaptive Radiation* (Hafner Publ. Co, New York, 1963).
2. T. D. Lamb, S. P. Collin, E. N. Pugh Jr., *Nat. Rev. Neurosci.* **8**, 960 (2007).
3. A. Brauer, *Wiss. Ergebn. Tiefsee-Exped. "Valdivia" 1898-1899* **15**, 1 (1908).
4. N. A. Locket, *Proc. R. Soc. Lond. B Biol. Sci.* **178**, 161 (1971).
5. S. Schuster, S. Amtsfeld, *J. Exp. Biol.* **205**, 549 (2002).
6. M. Landsberger *et al.*, *J. Physiol. Paris* **102**, 291 (2008).
7. M. R. McEwan, *Acta Zool.* **19**, 427 (1938).
8. P. Moller, J. Serrier, P. Belbenoit, S. Push, *Behav. Ecol. Sociobiol.* **4**, 357 (1979).
9. P. Moller, *Electric Fishes: History and Behavior* (Chapman & Hall, London, 1995).
10. Materials and methods are available as supplementary materials on *Science* Online.
11. O. A. Oskooi *et al.*, *Comput. Phys. Commun.* **181**, 687 (2010).
12. K. Franze *et al.*, *Proc. Natl. Acad. Sci. U.S.A.* **104**, 8287 (2007).
13. M. C. J. Large, S. Wickham, J. Hayes, L. Poladian, *Physica B* **394**, 229 (2007).
14. S. Ciali, J. Gordon, P. Moller, *J. Fish Biol.* **50**, 1074 (1997).
15. R. D. Walmsley, M. Butty, H. Piepen, D. Grobler, *Hydrobiologia* **70**, 145 (1980).
16. F. S. Werblin, *Sci. Am.* **228**(1), 70 (1973).
17. R. A. Normann, F. S. Werblin, *J. Gen. Physiol.* **63**, 37 (1974).
18. M. W. Seeliger, A. Rilk, S. C. Neuhauss, *Doc. Ophthalmol.* **104**, 57 (2002).
19. M. J. Morgan, A. Adam, J. D. Mollon, *Proc. Biol. Sci.* **248**, 291 (1992).
20. S. Yokoyama, N. Takenaka, *Mol. Biol. Evol.* **22**, 968 (2005).
21. S. Schaerer, C. Neumeyer, *Vision Res.* **36**, 4025 (1996).
22. R. Rojas, P. Moller, *Brain Behav. Evol.* **59**, 211 (2002).

Acknowledgments: This work was financially supported by the Deutsche Forschungsgemeinschaft, the German Federal Ministry of Education and Research, and the Alexander-von-Humboldt Foundation. Help with freeze-fracturing by Ria Knittel is gratefully acknowledged. Numerical simulations were run on the Darwin Supercomputer, University of Cambridge. A.R., H.-J.W., S. Schuster, G.v.d.E., J. Guck, M.K., and M.F. developed the idea of the project, supervised the research, and wrote the manuscript; H.-J.W., J.E., F.M., E.U., R.P., J.R., H.W., J.K., and M.F. obtained morphological data; M.K. performed the electrodynamical simulations; J.B. measured the absorption spectra; K.F. measured light reflection of the eye; J. Grosche measured light reflection of the isolated retina and provided the 3D reconstructions of the RPE; M.L., D.H., and S. Schumacher obtained behavioral data; J.E. and R.P. performed tectum measurements; C.M.-F. and D.H. performed the electroretinogram; and S. Schuster designed and S. Streif developed the programs applied in the dynamic noise and color-pooling experiments.

Supplementary Materials

www.sciencemag.org/cgi/content/full/336/6089/1700/DC1
Materials and Methods
Figs. S1 to S5
References (*23*–*28*)
Movies S1 and S2

19 December 2011; accepted 14 May 2012
10.1126/science.1218072

A *Papaver somniferum* 10-Gene Cluster for Synthesis of the Anticancer Alkaloid Noscapine

Thilo Winzer,[1] Valeria Gazda,[1] Zhesi He,[1] Filip Kaminski,[1] Marcelo Kern,[1] Tony R. Larson,[1] Yi Li,[1] Fergus Meade,[1] Roxana Teodor,[1] Fabián E. Vaistij,[1] Carol Walker,[2] Tim A. Bowser,[2] Ian A. Graham[1]*

Noscapine is an antitumor alkaloid from opium poppy that binds tubulin, arrests metaphase, and induces apoptosis in dividing human cells. Elucidation of the biosynthetic pathway will enable improvement in the commercial production of noscapine and related bioactive molecules. Transcriptomic analysis revealed the exclusive expression of 10 genes encoding five distinct enzyme classes in a high noscapine–producing poppy variety, HN1. Analysis of an F_2 mapping population indicated that these genes are tightly linked in HN1, and bacterial artificial chromosome sequencing confirmed that they exist as a complex gene cluster for plant alkaloids. Virus-induced gene silencing resulted in accumulation of pathway intermediates, allowing gene function to be linked to noscapine synthesis and a novel biosynthetic pathway to be proposed.

Noscapine was first characterized from opium poppy, *Papaver somniferum*, by the distinguished French chemist Pierre Jean Robiquet in 1817 (*1*) but unlike codeine (which he also discovered) and several other opiates, noscapine is neither painkilling nor addictive. Noscapine has been used as a human cough suppressant for decades; its effect on the cough reflex and bronchial muscles was reported as early as 1954 (*2*), and the bioavailability and pharmacokinetics of its orally administered form were established in 1990 (*3*). The demonstration in 1998 that noscapine acts as a potent antitumor agent that binds to tubulin and affects its polymerization, thereby arresting cell division and inducing apoptosis (*4*), was followed by confirmation of its antitumor activity in various forms of cancer (*5*–*8*). Because of its history of safe use as an antitussive, rapid absorption after oral administration, and apoptosis-inducing effect on a number of cancer cell lines, noscapine may have an advantage over other tubulin-binding anticancer natural products such as the well-established taxanes (*9*).

Noscapine belongs to the phthalideisoquinoline subclass of the structurally diverse isoquinoline alkaloids, whereas codeine, morphine, thebaine, and oripavine belong to the morphinan subclass (*10*). Although the biosynthesis of morphinans has been elucidated at the molecular level (*11*–*16*), our knowledge of noscapine biosynthesis has not substantially advanced since the 1960s, when isotope-labeling experiments showed that it is derived from scoulerine (*17*). Understanding the biochemical genetics that underlie noscapine biosynthesis should enable improved production of this important pharmaceutical and related molecules in both poppy and other systems.

We created metabolite profiles of capsule extracts from three opium poppy varieties developed in Tasmania for alkaloid production, which we designate as high morphine 1 (HM1), high thebaine 1 (HT1), and high noscapine 1 (HN1) on the basis of the most abundant alkaloid in each case (Fig. 1A). Noscapine as well as 53 other

[1]Centre for Novel Agricultural Products, Department of Biology, University of York, York YO10 5DD, UK. [2]GlaxoSmithKline, 1061 Mountain Highway, PO Box 168, Boronia, VIC 3155, Australia.

*To whom correspondence should be addressed. E-mail: ian.graham@york.ac.uk

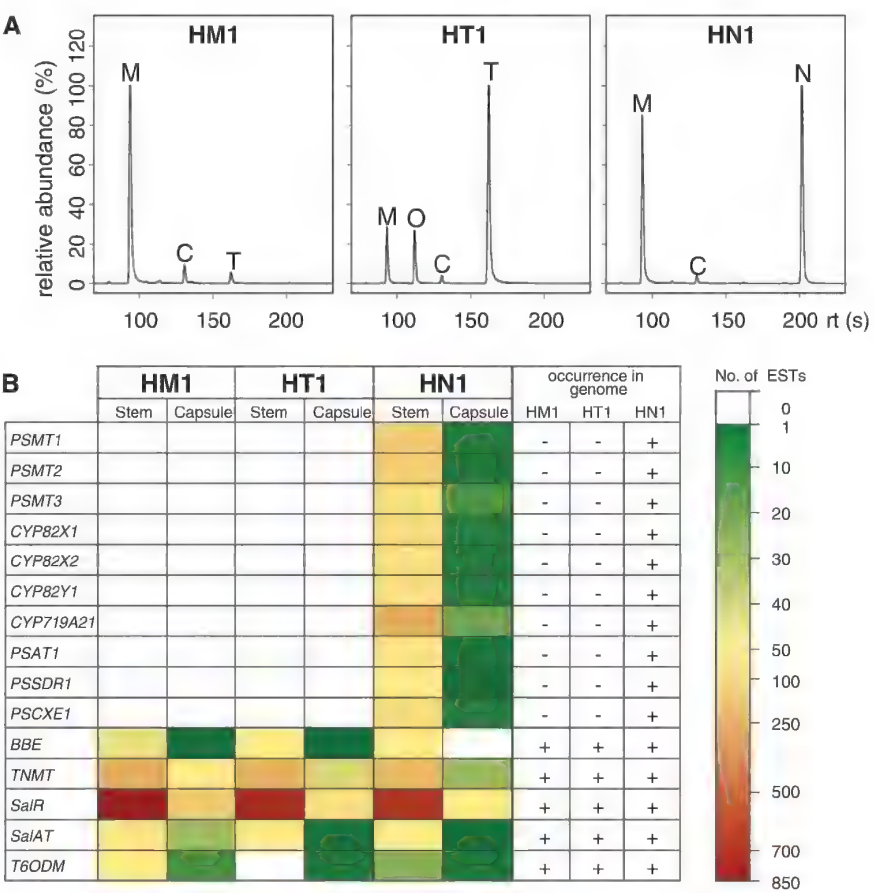

Fig. 1. Identification of genes exclusively present in the genome of a noscapine-producing poppy variety, HN1. (**A**) Relative abundance of the major alkaloids extracted from the capsules of three commercial varieties of poppy: HM1, HT1, and HN1. M, morphine; C, codeine; T, thebaine; O, oripavine; N, noscapine; rt, retention time in seconds. (**B**) EST libraries from stem and capsule were generated by pyrosequencing and unique contiguous sequences assembled as described (*18*). The first 10 genes are represented only in EST libraries from the HN1 variety; the last five genes are present in EST libraries from all three varieties. All genes are represented at consistently higher levels in stem than in capsule, as shown in color code. PCR on genomic DNA from all three varieties revealed that the 10 HN1-specific genes are absent from the genomes of the HM1 and HT1 varieties, whereas the five other functionally characterized genes are present in all three varieties (fig. S6).

low-abundance compounds, some of which are candidate intermediates in the noscapine biosynthetic pathway, are produced in HN1; none of these compounds appear in either HM1 or HT1 (table S1). We performed Roche 454 pyrosequencing on complementary DNA libraries derived from stem and capsule tissue from all three varieties. Analysis of expressed sequence tag (EST) abundance led to the discovery of a number of previously uncharacterized genes that are expressed in the HN1 variety but are completely absent from the HM1 and HT1 EST libraries (Fig. 1B). We putatively identified the corresponding genes as three O-methyltransferases (*PSMT1*, *PSMT2*, *PSMT3*; fig. S1), four cytochrome P450s (*CYP82X1*, *CYP82X2*, *CYP82Y1*, and *CYP719A21*; fig. S2), an acetyltransferase (*PSAT1*; fig. S3), a carboxylesterase (*PSCXE1*; fig. S4) and a short-chain dehydrogenase/reductase (*PSSDR1*; fig. S5). In contrast, a number of other functionally characterized genes associated with benzylisoquinoline alkaloid synthesis—including *Berberine Bridge Enzyme* (*BBE*), *Tetrahydroprotoberberine cis-N-MethylTransferase* (*TNMT*), *Salutaridine Reductase* (*SalR*), *Salutaridinol 7-O-AcetylTransferase* (*SalAT*), and *Thebaine 6-O-demethylase* (*T6ODM*)—were expressed in all three varieties (Fig. 1B). Polymerase chain reaction (PCR) analysis revealed that the genes exclusively expressed in HN1 are present as expected in the genome of HN1 but are absent from the genomes of HM1 and HT1 (Fig. 1B and fig. S6).

Using HN1 and HM1 as parents, we generated an F_2 mapping population of 271 individuals. Genotyping of the field-grown F_2 population revealed that the HN1-specific genes are tightly linked and associated with the presence of noscapine, which suggests that they occur as a gene cluster involved in noscapine biosynthesis (Fig. 2). Analysis of noscapine levels in field-grown F_2 capsules revealed that individuals containing this putative gene cluster fell into two classes. The first, containing 150 individuals, had relatively low levels of noscapine; the second, containing 63 individuals, exhibited the high-noscapine trait of the parental HN1 variety. The 58 F_2 individuals that lacked the putative gene cluster contained undetectable levels of noscapine (Fig. 2B). F_3 family analysis confirmed that F_2 individuals exhibiting the high-noscapine trait were homozygous for the gene cluster, whereas those exhibiting the

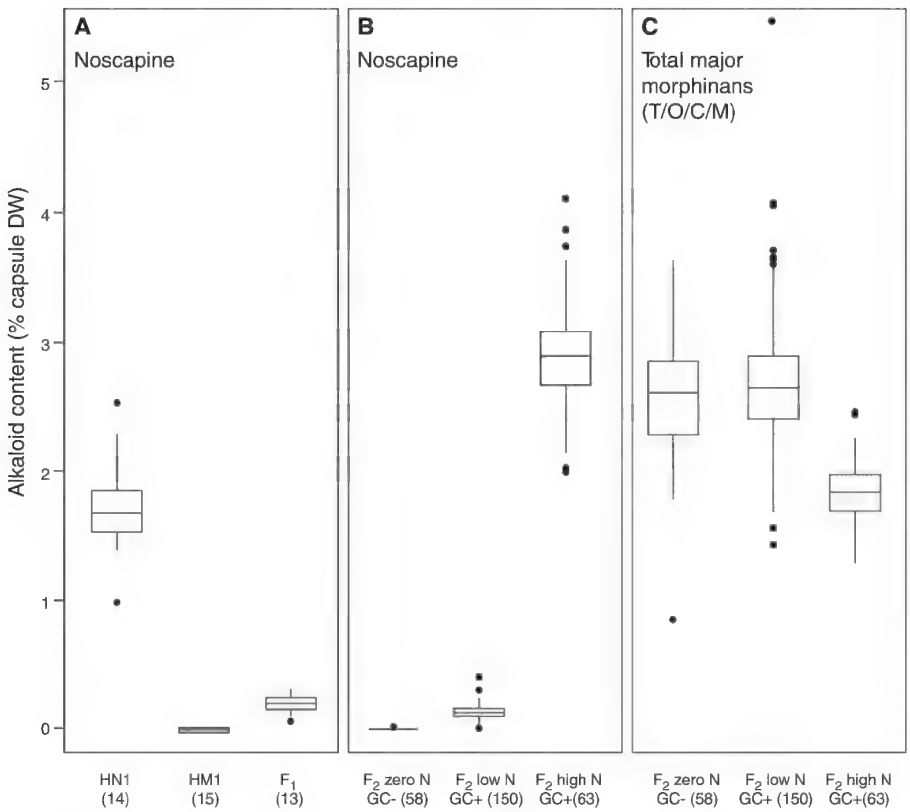

Fig. 2. Segregation analysis of noscapine content in an F_2 mapping population demonstrates requirement for the noscapine gene cluster. **(A)** Box plot depiction of noscapine levels as percentage dry weight (DW) in glasshouse-grown parental lines HN1 and HM1 and the F_1 generation. **(B)** The F_2 generation segregates into three classes of zero, low, and high noscapine (N); F_2 GC– and F_2 GC+ indicate the absence and presence, respectively, of the noscapine gene cluster. Numbers in parentheses indicate number of individuals in each class. **(C)** Total major morphinans as percentage capsule dry weight in the F_2 classes of zero, low, and high noscapine (T, thebaine; O, oripavine; C, codeine; M, morphine).

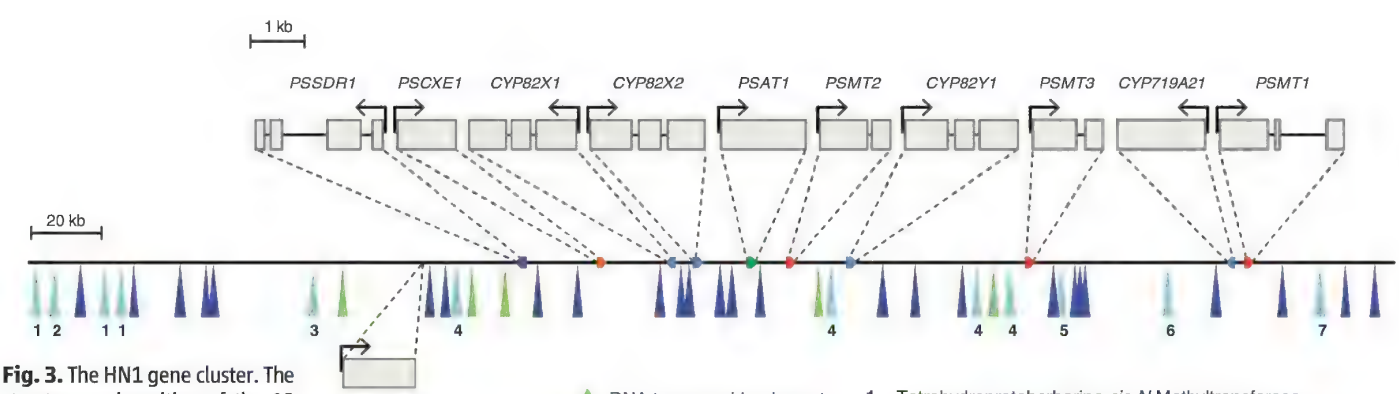

Fig. 3. The HN1 gene cluster. The structure and position of the 10 HN1-specific genes expressed in stems and capsule tissues are shown above the central black line, which represents 401 kb of genomic sequence. Exons are represented by solid gray boxes and introns by fine black lines. Arrows indicate the 5′ to 3′ orientation of each gene. Additional ORFs depicted below the central black line are as defined by the key. None of these ORFs are represented in the stem and capsule EST libraries. The location and annotation of all ORFs in the 401-kb sequence are detailed in table S5.

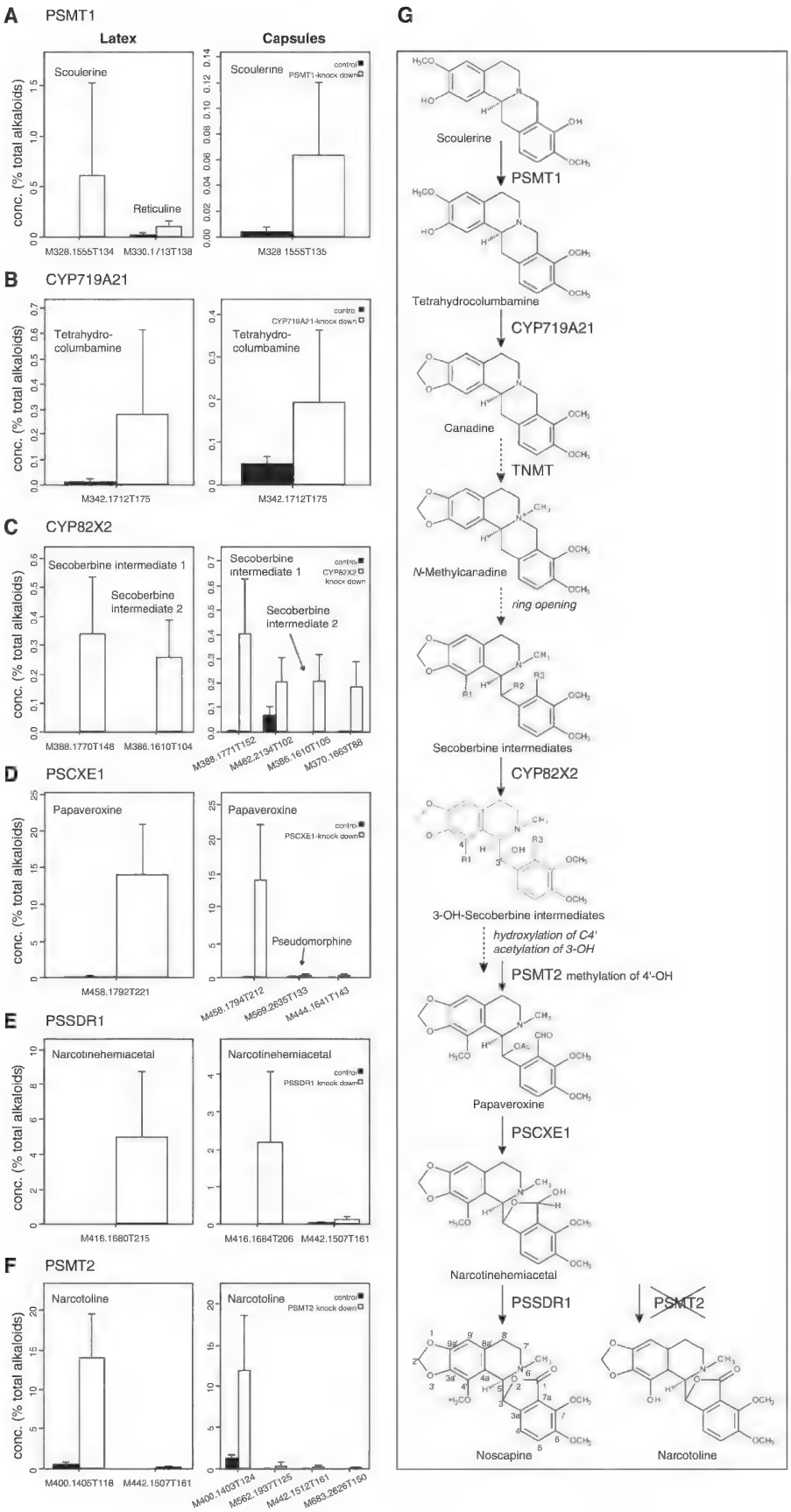

Fig. 4. Functional characterization using virus-induced gene silencing of six genes from the HN1 gene cluster. (**A** to **F**) Results from both leaf latex (left panels) and capsules (right panels) are consistent with each of these genes encoding enzymes involved in noscapine biosynthesis. All compounds that accumulate, apart from scoulerine, have been putatively identified on the basis of mass spectra (fig. S10). The mass-to-charge (*m/z*) value (M) followed by retention time in seconds (T) is shown for each compound on the horizontal axis. Metabolites showing a positive change by more than a factor of 2 (VIGS versus controls) and >0.05% total alkaloid profile are shown as percentage total metabolites. A complete list of all metabolites that were significantly changed in the VIGS experiments is shown in table S7. (**G**) Proposed pathway for noscapine biosynthesis based on VIGS data. Solid arrows depict steps supported by VIGS data; dashed arrows depict additional proposed steps. Italics depict those reactions that await gene assignment. The noscapine structure is numbered according to the IUPAC convention. Labeling of the 3-OH secoberbine intermediates is based on the numbering of the noscapine structure. For the secoberbine intermediates that accumulate in VIGS experiments, R1 = H or OH, R2 = H or OH, and R3 = CH_2OH, CHO, or COOH (fig. S10). The proposed pathway assumes R1 = H, R2 = H, and R3 = CHO in the secoberbine intermediates. The crossed-out PSMT2 depicts silencing of this gene product resulting in narcotoline accumulation, as described in the text.

low-noscapine trait were heterozygous (table S2). Noscapine levels in both the glasshouse-grown F_1 population and the heterozygous F_2 class were much lower than the intermediate levels expected for a semidominant trait, suggesting the involvement of some form of repression. A number of other HN1-specific metabolites were similarly decreased (table S3), suggesting global downregulation of this branch of alkaloid metabolism when the gene cluster is in the heterozygous state. However, quantitative reverse transcription PCR analysis did not detect any transcriptional repression in the heterozygous state on *PSMT1* and *PSMT2*, which we determine below to encode the first step and an intermediate step, respectively, in the noscapine pathway (fig. S7).

The morphinan branch of alkaloid metabolism, on the other hand, remained largely unaffected in F_1 (table S4) and heterozygous F_2 material, showing only a decrease in capsules producing high levels of noscapine, presumably due to substrate competition (Fig. 2C). The large step change to high noscapine in the homozygous F_2 class suggests that this trait is linked to the gene cluster locus rather than spread quantitatively among other loci.

To further characterize the putative noscapine gene cluster, we prepared a bacterial artificial chromosome (BAC) library from genomic DNA isolated from HN1 and identified six overlapping BACs containing genes from the cluster. Next-generation and Sanger sequencing were used to generate a high-quality assembly of 401 kb, confirming the arrangement of the 10 genes in a cluster spanning 221 kb (Fig. 3 and table S5) (*18*). The homology and intron-exon structure of the *CYP82* and *PSMT* genes suggest tandem gene duplication after genome reorganization of the progenitor genes. A similar case can be made for *PSCXE1* because a second homolog, *PSCXE2*, is present in the region flanking the gene cluster (Fig. 3 and fig. S4), but this gene is not represented in any of our EST libraries. However, on only one occasion are members of the same gene family adjacent in the cluster, when *CYP82X1* and *CYP82X2* are inverted with respect to each other. *CYP82Y1* is separated from *CYP82X2* by a gap of 45 kb containing *PSAT1* and *PSMT2*. *PSMT3* and *PSMT2* are separated by a gap of 73 kb containing *CYP82Y1*. Interspersed among the 10 genes are both retrotransposon and DNA transposable element (TE) sequences (Fig. 3 and table S5), which may have some function in gene rearrangement for cluster formation, as is thought to be the case for the thalianol and marneral clusters from *Arabidopsis thaliana* (*19*). A search of the PLACE database of plant cis-acting DNA elements (*20*) revealed a number of short motifs (four or five bases) present in the 1-kb predicted promoter regions upstream of the open reading frames (ORFs) of the 10 genes, among which the WRKY elements are noteworthy (*21*, *22*) (table S6).

To functionally characterize the genes in the HN1 cluster, we performed virus-induced gene silencing (VIGS) on poppy seedlings by established methods (*18*). VIGS in poppy seedlings persists through to mature plant stages (*23*), and we therefore routinely assayed both leaf latex and capsule extract (Fig. 4). We managed to silence six of the eight genes we tested by VIGS, as determined by mRNA abundance in infected leaf tissue (fig. S8). Silencing *PSMT1*, which shows high homology with scoulerine-9-*O*-methyltransferase from *Coptis japonica* (*24*) (fig. S1A), resulted in accumulation of scoulerine in both latex and capsules, as well as low levels of reticuline in latex (Fig. 4A). We expressed the *PSMT1* gene product in *Saccharomyces cerevisiae* and, consistent with the VIGS data, this converted scoulerine to tetrahydrocolumbamine at high efficiency (fig. S9). We therefore conclude that *PSMT1* is responsible for the first committed step in the pathway to noscapine synthesis.

The product of PSMT1, tetrahydrocolumbamine, accumulated in latex and capsules that were silenced for *CYP719A21*, indicating that this gene is responsible for the second step in the pathway (Fig. 4B and fig. S10). CYP719A21 shows high homology to cytochrome P450 oxidases that act as methylenedioxy bridge-forming enzymes, and we therefore propose that *CYP719A21* encodes a canadine synthase (*25*, *26*) (fig. S2B). We propose that canadine is methylated to form *N*-methylcanadine, which in turn is converted to secoberbine intermediates (Fig. 4G). Consistent with this, canadine and *N*-methylcanadine are HN1-specific metabolites (table S1). The product of *TNMT* has previously been shown to specifically N-methylate protoberberine alkaloids, including canadine (*27*). *TNMT* is present and expressed in HN1, HM1, and HT1 (Fig. 1B) and does not appear to be associated with the HN1 gene cluster (Fig. 3). Three other ORFs with *TNMT* homology are present in the flanking region of the HN1 gene cluster, but these are not expressed in stems or capsules, further implicating *TNMT* as having a role in the pathway.

Silencing of a second cytochrome P450 gene, *CYP82X2*, resulted in accumulation of several secoberbine intermediates, some of which may represent side products to the main synthetic pathway (Fig. 4C). The fragmentation pattern of intermediate 1 (fig. S10) is consistent with the compound being narcotolinol (R1 = OH, R2 = H, and R3 = CH_2OH), implying CYP82X2 hydroxylates at the R2 position. The production of these secoberbine intermediates from *N*-methylcanadine requires breakage of the berberine bridge and ring opening, as depicted in Fig. 4G. Silencing of the carboxylesterase gene *PSCXE1* resulted in accumulation of up to 20% total alkaloid content of the acetylated compound papaveroxine (Fig. 4D and fig. S10). Synthesis of papaveroxine from secoberbine intermediates requires hydroxylation and methylation at the position equivalent to the C4′ position of noscapine as well as acetylation of the hydroxyl group at the C3 position (Fig. 4G). The accumulation of papaveroxine in material silenced for *PSCXE1* implies that the corresponding enzyme removes an acetyl group from this compound to produce narcotinehemiacetal. That narcotinehemiacetal is an intermediate in the pathway to noscapine synthesis is substantiated by the fact that it accumulates upon silencing of the short-chain dehydrogenase/reductase gene *PSSDR1* (Fig. 4E and fig. S10). Conversion of narcotinehemiacetal to noscapine requires dehydrogenation, and we therefore conclude that PSSDR1 is involved in this final synthetic step (Fig. 4G).

The VIGS data for *PSCXE1* and *PSSDR1* therefore support a biosynthetic route to noscapine that involves O-methylation of secoberbine intermediates at the position equivalent to the C4′ hydroxyl group of noscapine (Fig. 4G). However, silencing *PSMT2* did not show any impact on secoberbine intermediates but instead led to accumulation of narcotoline at up to 20% total alkaloids (Fig. 4F). These results suggest that narcotoline is an end product of a desmethyl pathway that accumulates when PSMT2-mediated methylation at the 4′OH group of secoberbine intermediates is compromised. As for the noscapine pathway, the production of narcotoline via a desmethyl pathway is expected to require acetyltransferase, carboxylesterase, and dehydrogenase activities.

Our findings provide evidence for the involvement of 6 of the 10 genes from the HN1 gene cluster in noscapine biosynthesis. The remaining oxidation and acetyltransferase steps in the proposed pathway remain unaccounted for; they could be encoded by the *CYP82X1*, *CYP82Y1*, and *PSAT1* genes, which remain to be characterized.

This discovery extends the involvement of gene clusters to the alkaloid class of secondary metabolites in higher plants. Noscapine has been reported in a number of *Papaver* species, and it will be interesting to establish whether it has evolved as a single event prior to speciation of *P. somniferum* or independently multiple times, as recently reported for the glucosinolate gene cluster in *Lotus japonicus* (*28*). As with the other plant gene clusters reported to date (*19*, *28*–*31*), donor sequences could be recruited from genes encoding related plant enzymes in a process involving gene duplication and neofunctionalization. The arrangement of the HN1 cluster suggests that genome reorganization is an ongoing process, occurring in some cases before duplication, as evidenced by the small gene families (*PSCXE*, *PSCYP82*, and *PSMT*), or after duplication, as evidenced by the single-copy genes (*PSSDR1*, *PSAT1*, and *CYP719A21*). The selective advantage to drive cluster evolution in this way could come from co-inheritance of favorable combinations of alleles and coordinate regulation of gene expression at the level of chromatin (*32*). This work provides a platform for the improved production of noscapine and related bioactive molecules through the molecular breeding of commercial poppy varieties or engineering of new production systems.

References and Notes

1. P. J. Robiquet, *Annales de Chimie et de Physique* **5**, 275 (1817).
2. H. Konzett, E. Rothlin, *Experientia* **10**, 472 (1954).
3. M. O. Karlsson, B. Dahlström, S.-Å. Eckernäs, M. Johansson, A. T. Alm, *Eur. J. Clin. Pharmacol.* **39**, 275 (1990).
4. K. Ye *et al.*, *Proc. Natl. Acad. Sci. U.S.A.* **95**, 1601 (1998).
5. Y. Ke *et al.*, *Cancer Immunol. Immunother.* **49**, 217 (2000).
6. J. Zhou *et al.*, *J. Biol. Chem.* **277**, 39777 (2002).
7. M. Mahmoudian, P. Rahimi-Moghaddam, *Recent Pat. Anti-Cancer Drug Discov.* **4**, 92 (2009).
8. J. W. Landen *et al.*, *Cancer Res.* **62**, 4109 (2002).
9. D. G. I. Kingston, *J. Nat. Prod.* **72**, 507 (2009).
10. J. Ziegler, P. J. Facchini, *Annu. Rev. Plant Biol.* **59**, 735 (2008).
11. R. Lenz, M. H. Zenk, *J. Biol. Chem.* **270**, 31091 (1995).
12. B. Unterlinner, R. Lenz, T. M. Kutchan, *Plant J.* **18**, 465 (1999).
13. T. Grothe, R. Lenz, T. M. Kutchan, *J. Biol. Chem.* **276**, 30717 (2001).
14. J. Ziegler *et al.*, *Plant J.* **48**, 177 (2006).
15. A. Gesell *et al.*, *J. Biol. Chem.* **284**, 24432 (2009).
16. J. M. Hagel, P. J. Facchini, *Nat. Chem. Biol.* **6**, 273 (2010).
17. A. R. Battersby, M. Hirst, D. J. McCaldin, R. Southgate, J. Staunton, *J. Chem. Soc. Perkin 1* **17**, 2163 (1968).
18. See supplementary materials on *Science* Online.
19. B. Field *et al.*, *Proc. Natl. Acad. Sci. U.S.A.* **108**, 16116 (2011).
20. K. Higo, Y. Ugawa, M. Iwamoto, T. Korenaga, *Nucleic Acids Res.* **27**, 297 (1999).
21. N. R. Apuya *et al.*, *Plant Biotechnol. J.* **6**, 160 (2008).
22. N. Kato *et al.*, *Plant Cell Physiol.* **48**, 8 (2007).
23. L. C. Hileman, S. Drea, G. Martino, A. Litt, V. F. Irish, *Plant J.* **44**, 334 (2005).
24. N. Takeshita *et al.*, *Plant Cell Physiol.* **36**, 29 (1995).
25. M. L. Díaz Chávez, M. Rolf, A. Gesell, T. M. Kutchan, *Arch. Biochem. Biophys.* **507**, 186 (2011).
26. N. Ikezawa, K. Iwasa, F. Sato, *Plant Cell Rep.* **28**, 123 (2009).
27. D. K. Liscombe, P. J. Facchini, *J. Biol. Chem.* **282**, 14741 (2007).
28. A. M. Takos *et al.*, *Plant J.* **68**, 273 (2011).
29. B. Field, A. E. Osbourn, *Science* **320**, 543 (2008).
30. M. Frey *et al.*, *Science* **277**, 696 (1997).
31. S. Swaminathan, D. Morrone, Q. Wang, D. B. Fulton, R. J. Peters, *Plant Cell* **21**, 3315 (2009).
32. H.-Y. Chu, E. Wegel, A. Osbourn, *Plant J.* **66**, 66 (2011).

Acknowledgments: We thank the laboratory and field staff at GlaxoSmithKline Australia for valuable technical assistance and J. Mitchell for administrative support. Supported by GlaxoSmithKline Australia and by the Garfield Weston Foundation for the Centre for Novel Agricultural Products. The identities of three of the P450s and the methyltransferase genes associated with noscapine production have been disclosed in PCT patent applications WO2011/161431 and WO2012/010872, respectively. The sequences of four BAC clones and genomic sequences of the 10 genes are available through the National Centre for Biotechnology Information under GenBank accession nos. JQ659009 to JQ659012 and JQ658999 to JQ659008. HN1, HM1, and HT1 are available from GSK Australia for experimental purposes, subject to a material transfer agreement.

Supplementary Materials

www.sciencemag.org/cgi/content/full/science.1220757/DC1
Materials and Methods
Figs. S1 to S10
Tables S1 to S8
References (*33*–*48*)

20 February 2012; accepted 18 May 2012
Published online 31 May 2012;
10.1126/science.1220757

Structural Basis for Prereceptor Modulation of Plant Hormones by GH3 Proteins

Corey S. Westfall,[1]* Chloe Zubieta,[2]* Jonathan Herrmann,[1] Ulrike Kapp,[2] Max H. Nanao,[3,4] Joseph M. Jez[1]†

Acyl acid amido synthetases of the GH3 family act as critical prereceptor modulators of plant hormone action; however, the molecular basis for their hormone selectivity is unclear. Here, we report the crystal structures of benzoate-specific *Arabidopsis thaliana* AtGH3.12/PBS3 and jasmonic acid–specific AtGH3.11/JAR1. These structures, combined with biochemical analysis, define features for the conjugation of amino acids to diverse acyl acid substrates and highlight the importance of conformational changes in the carboxyl-terminal domain for catalysis. We also identify residues forming the acyl acid binding site across the GH3 family and residues critical for amino acid recognition. Our results demonstrate how a highly adaptable three-dimensional scaffold is used for the evolution of promiscuous activity across an enzyme family for modulation of plant signaling molecules.

Plants produce a variety of bioactive signaling compounds, including jasmonates, auxins, and benzoates, in response to intrinsic and environmental cues (*1*–*4*). Modification of hormones and other small signaling molecules by conjugation reactions is a general mechanism for regulation of their activity and stability in all organisms. In plants, amino acid conjugation of chemically diverse compounds, including jasmonic acid (JA), the auxin indole acetic acid (IAA), and salicylic acid (SA), alters the cellular concentrations of their bioactive forms to control plant growth, developmental processes, and defense responses (*5*–*8*). For example, formation of amino acid conjugates of JA, IAA, or SA differentially affects the potency of each molecule (fig. S1A). Conjugation of isoleucine to JA yields jasmonyl-isoleucine (JA-Ile), the active jasmonate hormone that binds to the F-box protein COI1 to trigger JA-mediated degradation of jasmonate ZIM domain proteins and subsequent hormone responses (fig. S1B) (*9*–*11*). Formation of IAA-Asp and IAA-Glu targets auxin for degradation and leads to attenuation of auxin signaling. In contrast, conjugation of IAA with either alanine or leucine results in hydrolysable auxin storage forms (*3*, *12*). Similarly, modification of SA can alter its biological activity to modulate defense responses (*4*, *13*). In each system, the GH3 family of acyl acid amido synthetases contributes to the active levels of critical plant hormones necessary for regulating distinct physiological responses.

[1]Department of Biology, Washington University, St. Louis, MO 63130, USA. [2]European Synchrotron Radiation Facility, 38000 Grenoble, France. [3]European Molecular Biology Laboratory, Grenoble, France. [4]Unit of Virus Host-Cell Interactions, Université Joseph Fourier–European Molecular Biology Laboratory–CNRS, Grenoble, France.

*These authors contributed equally to this work.
†To whom correspondence should be addressed. E-mail: jjez@biology2.wustl.edu

The GH3 enzyme family conjugates amino acids to diverse acyl acid substrates through a two-step mechanism involving adenylation and transferase activities (*6*–*8*, *14*–*17*) (fig. S1C). GH3 proteins are widespread in plants, and multiple mutant phenotypes connect these enzymes to JA, auxin, and SA responses in *Arabidopsis*, rice, and other species (*6*–*8*, *14*, *15*, *18*–*20*). Two of the best-studied *Arabidopsis* GH3 proteins are AtGH3.11 (JAR1) (*14*, *20*) and AtGH3.12 (PBS3) (*18*, *19*). The *Arabidopsis jar1* mutant is defective in AtGH3.11, which prevents formation of JA-Ile and blocks JA-mediated responses (*2*, *11*). Similarly, the *Arabidopsis* SA-response mutant *pbs3* disrupts AtGH3.12, resulting in enhanced susceptibility to *Pseudomonas syringae* infection due to SA signaling defects (*18*). Surprisingly, SA is an extremely poor substrate of AtGH3.12

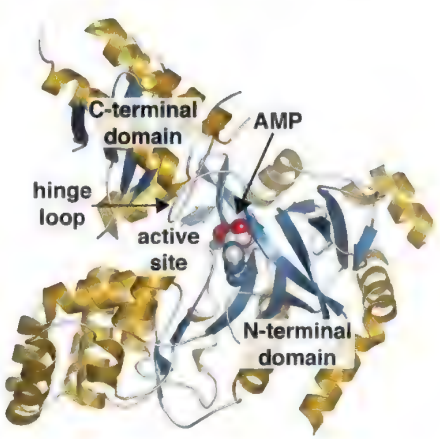

Fig. 1. Overall structure of AtGH3.12. Ribbon diagram showing the N- and C-terminal domains with α helices and β strands colored gold and blue, respectively. AMP in the active site is shown as a space-filling model. The hinge loop that switches conformation during the reaction sequence is also indicated.

compared with other benzoates such as 4-hydroxybenzoate (4HBA) and acts as an inhibitor in vitro (*19*). To understand the metabolic versatility of the GH3 proteins for modulating plant signaling molecules, we determined the x-ray crystal structures of AtGH3.12 and AtGH3.11.

Recombinant AtGH3.11 and AtGH3.12 functioned as monomeric proteins and were active with reported substrates (*16*, *19*–*21*) (table S1). We used single-wavelength anomalous dispersion phasing from selenomethionine-substituted proteins to determine the AtGH3.12•adenosine monophosphate (AMP)•SA ternary complex structure (Fig. 1, figs. S2 and S3A, and table S2). Subsequently, we determined structures of the AtGH3.12•AMP and AtGH3.12•AMP–carboxypiperazin-4-yl-propyl-1-phosphonic acid (CPP) binary complexes by molecular replacement (table S2). For structural comparison of benzoate- and JA-specific GH3 proteins, we also solved the structure of AtGH3.11•JA-Ile. Structures of AtGH3.12 with different ligands provide insight on nucleotide binding, conformational changes during catalysis, and reaction chemistry, whereas comparison of the AtGH3.11 and AtGH3.12 structures highlights the active site plasticity leading to differential biochemical roles of GH3 proteins in plants.

AtGH3.11 and AtGH3.12 share a common tertiary structure (Fig. 1 and fig. S2) consisting of a large N-terminal domain and a smaller C-terminal domain typical of the adenylating firefly luciferase (ANL) enzyme superfamily (*22*). These structures support the hypothesis of Staswick *et al.* (*14*) that the GH3 proteins are distantly related to firefly luciferase. The large N-terminal domain contains a β barrel and two β sheets flanked by α helices, and the C-terminal domain consists of a single four-stranded β sheet bracketed by two α helices on each side. The active site is located at the interface of the two domains. A flexible hinge loop (Val^{420}-Glu^{432} in AtGH3.12; Leu^{427}-Arg^{439} in AtGH3.11) between β15 and α15 connects the two domains and pivots the C-terminal domain during catalysis.

The nucleotide-bound AtGH3.12 structures reveal a conserved adenosine triphosphate (ATP)/AMP binding site defined by three sequence motifs (*22*) (Fig. 2A and fig. S3B). The first motif (S_{95}SGTSGGANK$_{104}$; S, Ser; G, Gly; T, Thr; A, Ala; N, Asn; K, Lys) is a canonical phosphate-binding (P) loop with the Ser^{95} and Ser^{96} hydroxyls contacting the α-phosphate. A second motif (S_{322}TTYGSSE$_{329}$; Y, Tyr; E, Glu) forms a β-turn-β structure, with Ser^{328} hydrogen bonding the α-phosphate group and Tyr^{325} stacking with the adenine ring. Previous studies of ANL proteins indicate that the glutamate residue (Glu^{329}) in this motif is critical for Mg^{2+} binding and orientation of ATP for catalysis (*22*). The third motif (G_{391}LYLYRGD$_{398}$; L, Leu; R, Arg; D, Asp) contains a conserved aspartate (Asp^{398}) that binds the nucleotide ribose. Although no nucleotide was bound in the AtGH3.11 structure, the site is similar to that of AtGH3.12 and is conserved across the 19 *Arabidopsis* GH3 proteins (fig. S3B).

The AtGH3.12•AMP and AtGH3.12•AMP-CPP structures show that the C-terminal domain pivots about the hinge loop (Fig. 2, B and C, and fig. S3C). With AMP-CPP bound, the hinge loop is directed away from the ligand, and the α18/α19 loop is positioned toward the N-terminal domain to cap the nucleotide β- and γ-phosphates (Fig. 2B). With AMP bound, the hinge and α18/α19 loops swap positions (Fig. 2B). Pivoting of the C-terminal domain toggles the active site between open (ATP-bound) and closed (AMP-bound) forms (Fig. 2C) and is probably linked to the adenylation and transferase half-reactions (fig. S1C). The open conformation allows binding of ATP, Mg^{2+}, and the acyl acid for the adenylation reaction and provides a solvent-accessible channel for pyrophosphate release. Comparison with the AMP bound form suggests that upon adenylation and loss of pyrophosphate, interaction of Lys^{550} in the α18/α19 loop with the β- and γ-phosphates of ATP is disrupted, triggering rotation of the C-terminal domain, repositioning of the P-loop serines near the α-phosphate, and enclosure of the activated intermediate for the transferase step. This rotation also positions Lys^{428} near the amino acid for the second half-reaction catalyzed by AtGH3.12.

The AtGH3.12 structures suggest mechanistic roles for active-site residues (fig. S4). Ser^{328} and Lys^{550} are positioned to interact with the ATP phosphates, Asp^{398} with the ATP ribose moiety, and Glu^{329} with Mg^{2+} for the adenylation reaction (fig. S4A). Ser^{95} and Ser^{96} in the P loop were disordered in the AMP-CPP structure, but these residues interact with the α-phosphate in the AMP structure and are positioned at the interface between the nucleotide and acyl acid sites. Kinetic analysis of mutants (table S1) shows that the Glu^{329}→Gln^{329} (E329Q) and D398N mutants are inactive for both the overall and adenylation reactions, which probably reflects a loss of nucleotide and/or Mg^{2+} binding (*22*). Although the S96A, S328A, and K550A mutants were inactive for the overall reaction, each catalyzed the adenylation step with varied efficiency (table S1). The 211-fold lower adenylation activity with the S96A mutant versus the wild type indicates that Ser^{96} may either stabilize the transition state or orient the acyl acid substrate for adenylation (fig. S4A). In contrast, the S328A mutant retained adenylation activity similar to that of the wild type, suggesting a key role for Ser^{328} in the transferase step, possibly by positioning the acyl acid portion of the adenylated intermediate for the second half-reaction (fig. S4B). The 26-fold reduction in adenylation activity with the K550A mutant is also consistent with a role for this C-terminal residue in the first half-reaction.

Clearly defining the acyl acid interaction site (Fig. 3), SA and JA-Ile bind adjacent to the β-turn-β motif of the nucleotide site in a pocket delineated by residues from α5, α6, β8, and β9 in the N-terminal domains of AtGH3.12 and AtGH3.11, respectively. In the AtGH3.12•AMP•SA structure, unambiguous electron density for SA (fig. S3A) shows that this ligand preferentially binds as an inhibitor with the carboxylate positioned away from the α-phosphate of AMP, which is consistent with this molecule's inhibitory effect versus 4HBA (*19*). Hydrogen bonds with Arg^{123} and Tyr^{120} orient the SA carboxylate away from AMP in a nonproductive binding mode (Fig. 3A). Presumably, the location of the

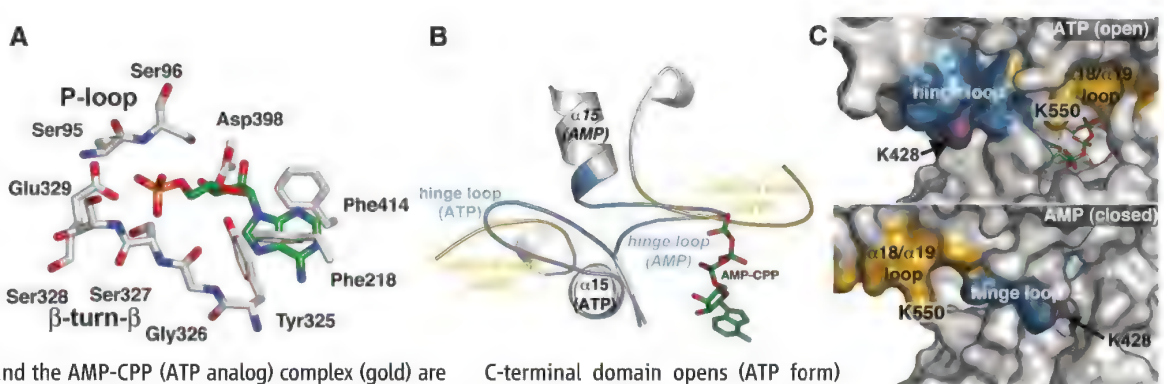

Fig. 2. Nucleotide binding site and C-terminal domain movement in AtGH3.12. (**A**) Active site residues in AtGH3.12•AMP. Residues from the P-loop, β-turn-β, and ribose interaction motifs are shown. (**B**) C-terminal domain pivot. Positions of the hinge loop (residues 420 to 432) and the α18/α19 loop (residues 543 to 554) in the AMP complex (blue) and the AMP-CPP (ATP analog) complex (gold) are shown. AMP-CPP is shown for reference. (**C**) Conformational change of active site. Surface views of the open and closed forms are shown. In each view, the bound nucleotide is shown as a stick model. Residues in the hinge C-terminal domain opens (ATP form) and closes (AMP form) access to the and α18/α19 loops are colored blue and gold, respectively. Positions of Lys^{428} and Lys^{550} in each conformation are indicated for reference.

ligand hydroxyl group at the ortho (SA) versus para (4HBA) position alters contacts to position the carboxylate of 4HBA near the ATP α-phosphate in the adenylation reaction. Mutagenesis of residues in the acyl acid site of AtGH3.12 indicates that Thr[161], Leu[217], and Phe[218] largely contribute to efficient catalysis with 4HBA (table S1).

In AtGH3.11 (Fig. 3, B and C), JA-Ile occupies a large apolar binding site with the cyclopentane ring in the same location as SA in AtGH3.12. A racemic mixture of JA was used for reaction before crystallization, but only (–)JA-Ile is observed in the structure. It is likely that AtGH3.11 uses only (–)JA, which after conjugation rapidly converts in solution to the bioactive hormone (+)JA-Ile (*10*, *11*). Thr[166], Val[222], Phe[223], and Ile[304] surround the cyclopentane ring of JA-Ile with a water-mediated hydrogen bond formed between the ligand 3-keto group and His[328]. Trp[336] and residues from α5 (Leu[117], Thr[121], Phe[125]) and α6 (Thr[166], Val[169]) provide a hydrophobic pocket for the pentenyl tail. The isoleucine moiety is oriented with its carboxylate toward the active site P loop (Fig. 3C).

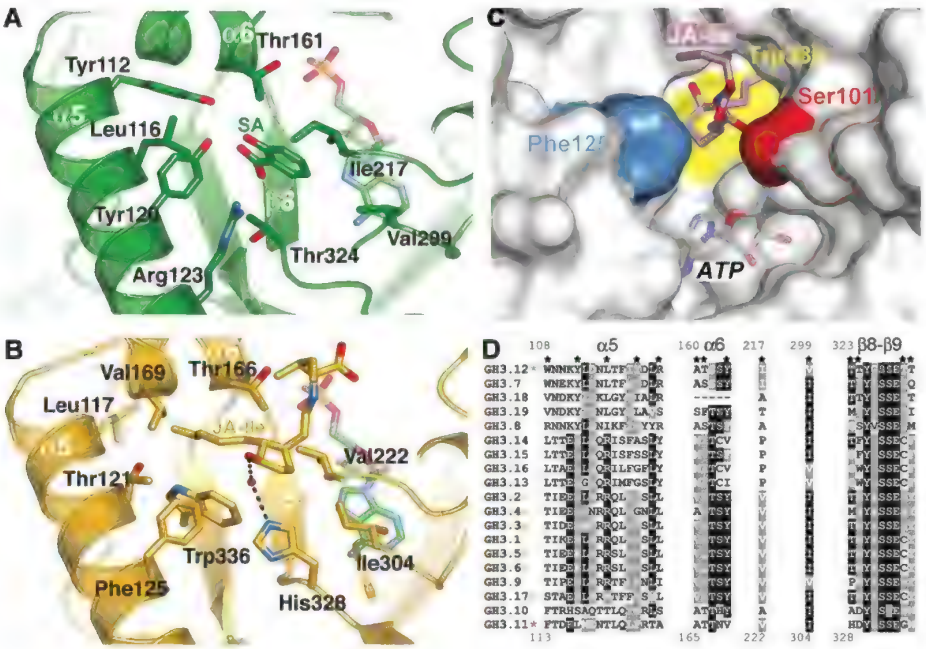

Fig. 3. Structural diversity of the acyl acid binding site in GH3 proteins. (**A**) Residues in the SA binding site of the AtGH3.12•AMP•SA complex are shown. (**B**) Residues of the JA-Ile binding site of AtGH3.11 are shown. The position of AMP from AtGH3.12 is shown for reference. (**C**) Surface view of the JA-Ile binding site in AtGH3.11, looking down the amino acid binding site toward the acyl acid substrate cavity. For clarity, the C-terminal domain has been removed. Surfaces associated with acyl acid substrate binding, Trp[336], Phe[125], and Ser[101] (part of the P loop), are shown in yellow, blue, and red, respectively. The position of ATP in the nucleotide binding site is modeled on the AtGH3.12 structures. (**D**) Sequence comparison of residues in the acyl binding site of GH3 proteins from *Arabidopsis*. Numbering at the top and bottom correspond to AtGH3.12 and AtGH3.11, respectively. Stars across the top of the alignment indicate residues with side chains in the pocket; shading indicates conservation. Asterisks near the GH3 protein names indicate known acyl acid specificity as follows: light blue, benzoate; yellow, IAA; red, JA.

Remodeling of the JA and benzoate binding pockets of AtGH3.11 and AtGH3.12, respectively, underlies the metabolic versatility of the GH3 proteins. Although the substrates for a limited number of plant GH3 proteins are known (*6*, *8*, *14*, *16*, *17*, *19*), structural insights and sequence comparisons suggest features leading to acyl acid preference (Fig. 3D). For example, residues in the acyl acid site of IAA-using *Arabidopsis* GH3 proteins show consistent changes in residues of α5, including substitution of Leu[117] and Thr[121] in AtGH3.11 to Asp/Glu and Arg/Lys, respectively. From these structures, comparison of the acyl acid sites from GH3 proteins in *Arabidopsis*, rice, soybean, maize, and mosses suggests that the family can be divided into eight subgroups based on conserved motifs in α5, α6, β8, and β9 (fig. S5). Three of these subgroups correspond to GH3 family members that use JA, benzoates, and IAA, respectively, as substrates and aid in the identification of homologs across plant species. One subgroup has a dwarf-in-light phenotype associated with AtGH3.10/DFL2 (*23*), but no information on its substrate specificity is available. Four of these subgroups have not been biochemically or genetically characterized, making predictive comparisons of function problematic; however, it is possible that acyl binding site changes may tailor the subgroups for the conjugation of metabolic precursors or variants of plant signaling molecules.

Amino acid specificity in the GH3 proteins is also not well understood; however, the AtGH3.11 and AtGH3.12 structures suggest a basis for

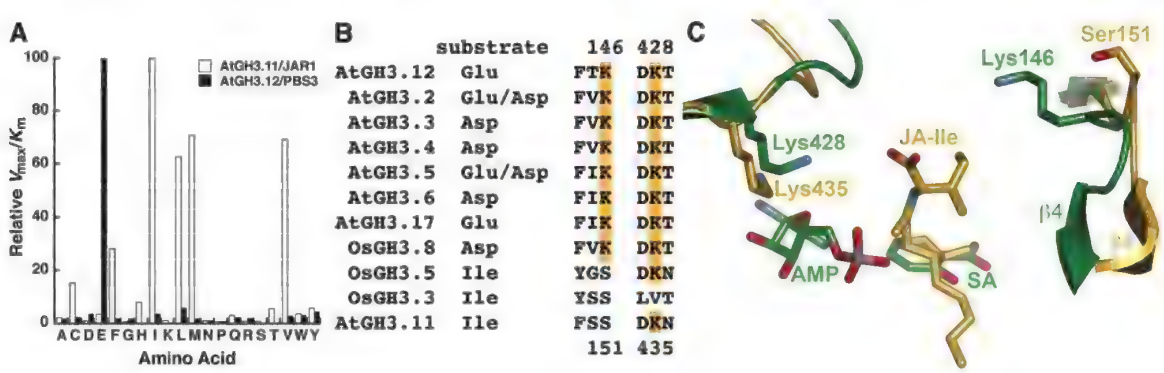

Fig. 4. Amino acid specificity and binding site. (**A**) Amino acid specificity of AtGH3.11 and AtGH3.12. Relative catalytic efficiency (V_{max}/K_m) for each amino acid was determined using JA and ATP for AtGH3.11/JAR1 and using 4HBA and ATP for AtGH3.12/PBS3. C, Cys; F, Phe; H, His; I, Ile; P, Pro; V, Val; W, Trp. (**B**) Targeted sequence comparison of *Arabidopsis* (At) and rice (Os) GH3 proteins with known amino acid preferences. Numbering at the top and bottom corresponds to AtGH3.12 and AtGH3.11, respectively. (**C**) Structural comparison of the AtGH3.12•AMP•SA (green) and AtGH3.11•JA-Ile (gold) complexes, showing the positions of the highly conserved lysine residues (Lys[428]/Lys[435]) proposed to interact with amino acid substrates and the second lysine (Lys[146]) proposed to interact with the R group of acidic amino acids.

discrimination of apolar (i.e., Ile) and acidic (i.e., Asp/Glu) substrates in the transferase reaction (Fig. 4 and fig. S4B). AtGH3.12 is specific for Glu, and AtGH3.11 prefers Ile but also accepts Met, Val, and Leu with reduced efficiency (Fig. 4A). In addition, the amino acid preferences of other GH3 proteins are known (*6*, *8*, *19*, *22*) (Fig. 4B). Within the active site, a lysine residue (Lys^{428} in AtGH3.12 and Lys^{435} in AtGH3.11) is positioned near AMP in AtGH3.12 and the carboxylate of JA-Ile in AtGH3.11 (Fig. 4C). In GH3 proteins with known amino acid preference, this residue is highly conserved (Fig. 4B) and may interact with the amino acid carboxylate during the second half-reaction. Comparison of the AtGH3.12 and AtGH3.11 structures (Fig. 4C) shows that Lys^{146} in AtGH3.12 is oriented toward the side-chain group of the reaction product. Ser^{151} in AtGH3.11 occupies the same position as Lys^{146} in AtGH3.12 (Fig. 4C). Interestingly, Lys^{146} is conserved in GH3 proteins that accept acidic amino acids, whereas Ser^{151} is conserved in enzymes specific to isoleucine conjugation (Fig. 4B). The K146M and K428M (M, Met) mutants of AtGH3.12 decrease the catalytic efficiency with glutamate by 35- and 2300-fold, respectively (table S1), but do not alter activity in the first half-reaction. Moreover, the K146M mutant does not affect the activity of AtGH3.12 with isoleucine, leucine, methionine, or valine, further demonstrating the likely role of Lys^{146} for efficient recognition of acidic amino acids in the transferase reaction.

The GH3 proteins are a noteworthy example of gene family expansion in plants, leading to diversification of substrate specificity and the evolution of positive and negative metabolic control systems for JA, auxin, and benzoate signaling molecules. Based on the ANL scaffold of adenylating enzymes, the GH3 family added amino acid transferase activity through an elegant reconfiguration of the active site via C-terminal domain rotation, providing a mechanism for activation and inactivation of a variety of bioactive molecules in plants. The structures presented here identify key features of substrate recognition and offer a molecular view of how plants co-opted the ANL scaffold to provide a chemically versatile platform for the exquisite control of hormone levels for plant growth, development, and defense.

References and Notes

1. A. Santner, L. I. Calderon-Villalobos, M. Estelle, *Nat. Chem. Biol.* **5**, 301 (2009).
2. J. Browse, *Annu. Rev. Plant Biol.* **60**, 183 (2009).
3. A. W. Woodward, *Ann. Bot. (London)* **95**, 707 (2005).
4. G. Loake, M. Grant, *Curr. Opin. Plant Biol.* **10**, 466 (2007).
5. G. Hagen, A. Kleinschmidt, T. Guilfoyle, *Planta* **162**, 147 (1984).
6. P. E. Staswick *et al.*, *Plant Cell* **17**, 616 (2005).
7. J. Terol, C. Domingo, M. Talon, *Gene* **371**, 279 (2006).
8. C. S. Westfall, J. Herrmann, Q. Chen, S. Wang, J. M. Jez, *Plant Signal. Behav.* **5**, 1607 (2010).
9. L. Katsir, A. L. Schilmiller, P. E. Staswick, S. Y. He, G. A. Howe, *Proc. Natl. Acad. Sci. U.S.A.* **105**, 7100 (2008).
10. S. Fonseca *et al.*, *Nat. Chem. Biol.* **5**, 344 (2009).
11. L. B. Sheard *et al.*, *Nature* **468**, 400 (2010).
12. K. Ljung *et al.*, *Plant Mol. Biol.* **50**, 309 (2002).
13. T. Gaffney *et al.*, *Science* **261**, 754 (1993).
14. P. E. Staswick, I. Tiryaki, M. L. Rowe, *Plant Cell* **14**, 1405 (2002).
15. R. A. Okrent, M. C. Wildermuth, *Plant Mol. Biol.* **76**, 489 (2011).
16. Q. Chen, B. Zhang, L. M. Hicks, S. Wang, J. M. Jez, *Anal. Biochem.* **390**, 149 (2009).
17. Q. Chen, C. S. Westfall, L. M. Hicks, S. Wang, J. M. Jez, *J. Biol. Chem.* **285**, 29780 (2010).
18. K. Nobuta *et al.*, *Plant Physiol.* **144**, 1144 (2007).
19. R. A. Okrent, M. D. Brooks, M. C. Wildermuth, *J. Biol. Chem.* **284**, 9742 (2009).
20. W. P. Suza, P. E. Staswick, *Planta* **227**, 1221 (2008).
21. Materials and methods are available as supplementary materials on *Science* Online.
22. A. M. Gulick, *ACS Chem. Biol.* **4**, 811 (2009).
23. T. Takase, M. Nakazawa, A. Ishikawa, K. Manabe, M. Matsui, *Plant Cell Physiol.* **44**, 1071 (2003).

Acknowledgments: This work was supported by NSF grant MCB-1157771 to J.M.J. C.S.W. was supported by a U.S. Department of Agriculture–National Institute of Food and Agriculture predoctoral fellowship (MOW-2010-05240), and J.H. was supported by an American Society of Plant Biologists–Summer Undergraduate Research Fellowship award and the Howard Hughes Medical Institute–Washington University Summer Scholars Program in Biology and Biomedical Research. Portions of this research were carried out at the European Synchrotron Radiation Facility and the Argonne National Laboratory Structural Biology Center of the Advanced Photon Source, a national user facility operated by the Univ. of Chicago for the U.S. Department of Energy Office of Biological and Environmental Research (DE-AC02-06CH11357). Atomic coordinates and structure factors have been deposited in the PDB (accession codes are noted in table S2).

Supplementary Materials

www.sciencemag.org/cgi/content/full/science.1221863/DC1
Materials and Methods
Figs. S1 to S5
Tables S1 and S2
References (*24*–*30*)

13 March 2012; accepted 11 May 2012
Published online 24 May 2012;
10.1126/science.1221863

Uniform ripening Encodes a *Golden 2-like* Transcription Factor Regulating Tomato Fruit Chloroplast Development

Ann L. T. Powell,[1]*† Cuong V. Nguyen,[2]† Theresa Hill,[1] KaLai Lam Cheng,[1] Rosa Figueroa-Balderas,[1] Hakan Aktas,[1]‡ Hamid Ashrafi,[1] Clara Pons,[3] Rafael Fernández-Muñoz,[4] Ariel Vicente,[1,5] Javier Lopez-Baltazar,[1]§ Cornelius S. Barry,[6] Yongsheng Liu,[7]‖ Roger Chetelat,[1] Antonio Granell,[3] Allen Van Deynze,[1] James J. Giovannoni,[2,7]* Alan B. Bennett[1]

Modern tomato (*Solanum lycopersicum*) varieties are bred for *uniform ripening* (*u*) light green fruit phenotypes to facilitate harvests of evenly ripened fruit. *U* encodes a *Golden 2-like* (*GLK*) transcription factor, *SlGLK2*, which determines chlorophyll accumulation and distribution in developing fruit. In tomato, two *GLKs*—*SlGLK1* and *SlGLK2*—are expressed in leaves, but only *SlGLK2* is expressed in fruit. Expressing *GLKs* increased the chlorophyll content of fruit, whereas *SlGLK2* suppression recapitulated the *u* mutant phenotype. *GLK* overexpression enhanced fruit photosynthesis gene expression and chloroplast development, leading to elevated carbohydrates and carotenoids in ripe fruit. *SlGLK2* influences photosynthesis in developing fruit, contributing to mature fruit characteristics and suggesting that selection of *u* inadvertently compromised ripe fruit quality in exchange for desirable production traits.

For ~70 years, breeders have selected tomato varieties with uniformly light green fruit before ripening, a characteristic that facilitates maturity determinations and promotes even ripening at the stem end (*1*, *2*). However, light green fruit ripen with reduced sugars, compromising traits that are valuable for processed products and the flavor of fresh fruit (fig. S1) (*3*–*5*). The *uniform ripening* (*u*) locus determines the intensity and pattern of chlorophyll distribution in unripe fruit (*3*, *5*–*7*). The dominant *U* allele results in fruit with dark green shoulders at the

[1]Plant Sciences Department, University of California, Davis, CA 95616, USA. [2]Departments of Plant Breeding and Genetics and Plant Biology, Cornell University, Ithaca, NY 14853, USA. [3]Instituto de Biología Molecular y Celular de Plantas, Consejo Superior de Investigaciones Científicas–Universidad Politécnica de Valencia, Valencia E-46022, Spain. [4]Instituto de Hortofruticultura Subtropical y Mediterranea La Mayora, Consejo Superior de Investigaciones Científicas–Universidad de Málaga, Málaga E-29750, Spain. [5]Centro de Investigación y Desarrollo en Criotecnología de Alimentos (Consejo Nacional de Investigaciones Científicas y Técnicas)–Universidad Nacional de La Plata (UNLP) and Facultad de Ciencias Agrarias y Forestales, Universidad Nacional de La Plata, CP 1900, Argentina. [6]Department of Horticulture, Michigan State University, East Lansing, MI 48824, USA. [7]Boyce Thompson Institute for Plant Research and USDA-ARS Robert W. Holley Center, Cornell University, Ithaca, NY 14853, USA.

*To whom correspondence should be sent. E-mail: alpowell@ucdavis.edu (A.L.T.P.); jjg33@cornell.edu (J.J.G.)
†These authors contributed equally to this work.
‡Present address: Department of Horticulture, Faculty of Agriculture, University of Suleyman Demirel, Isparta 32260, Turkey.
§Present address: Instituto Tecnologico del Valle de Oaxaca, Oaxaca 68120, Mexico.
‖Present address: School of Biotechnology and Food Engineering, Hefei University of Technology, Hefei 230009, P. R. China.

stem end adjacent to the pedicel; *u/u* fruit are uniformly light green.

Chloroplast formation, chlorophyll synthesis, and photosystem assembly require exposure to light and genetically defined developmental cues (*8*). Developing tomato fruit are capable of photosynthesis and contribute up to 20% of the fruit's photosynthate, with the remainder translocated from leaves (*9*). Light-harvesting electron transfer and CO_2 fixation proteins are conserved in fruit (*9–12*) and regulated by light and developmental signals, as in leaves. However, differences suggest additional levels of fruit-specific regulation (*13–17*).

Two GARP family Myb transcription factors [*Golden 2-like 1* (*GLK1*) and *GLK2*] determine the capacity for light-stimulated photosynthesis by controlling chloroplast formation (*18–20*). In C_3 photosynthesizing tissues, *GLK1* and *GLK2* act redundantly, but each may have undefined specialized roles in C_4 tissues (*19*). Although the *Atglk2* and *Atglk1-Atglk2 Arabidopsis* mutants have pale siliques (*18*), the contributions of *GLKs* to fleshy fruit chloroplast development are unknown. Expression of *AtGLK1* or *AtGLK2* is sufficient for leaf chloroplast development through control of similar photosystem, light-harvesting complex, and chlorophyll biosynthetic genes (*18*, *20–22*), although aspects of their function and/or regulation may have evolved distinctions (*23*, *24*). We report the identification of tomato *GLKs* and show that the *u* phenotype results from a mutation in *SlGLK2*.

Using two interspecific populations segregating for the *u* locus (*1–3*, *25–27*) (Fig. 1A), *U* mapped to a 60,507–base pair (bp) region on the short arm of chromosome 10 containing eight predicted genes, including *SlGLK2*, located at position Sl2.40chr10:2291209-2295578 (Fig. 2A). Sequencing full-length *SlGLK2* transcripts predicted that in *U* genotypes, *SlGLK2* encodes a 310–amino acid protein (fig. S2A), but in *u*, *Slglk2* encodes a truncated 80–amino acid protein because of a single base insertion that causes a frameshift and a premature stop codon (fig. S2B). The additional adenine (A) between SL2.40ch10:2292260-2292267 is the only difference in the *SlGLK2* sequence that is common to all light green *u/u* varieties and absent in all dark-green shouldered *U/U* varieties (Fig. 2B).

SlGLK2 and an additional GLK homolog (*SlGLK1*) were identified in tomato and related *Solanaceae* species (fig. S2A). The amino acid sequences of the *Solanaceae* GLKs are similar to other dicot GLKs and are approximately 45% identical to their *Arabidopsis* counterparts (fig. S2, A, C, and D).

SlGLK1 and *SlGLK2* expression predicts their roles in leaves and fruit. Transcripts from both *SlGLK1* and *SlGLK2* accumulate in cotyledons, sepals, and leaves, but only *SlGLK2* transcripts accumulate in green fruit (Fig. 3A). *SlGLK2* is eightfold more abundant in the pedicel (shoulder) than in the blossom (stylar) portions, suggesting that *SlGLK2* contributes to the pattern and intensity of chlorophyll accumulation (table S2). Maturation in the absence of light reduces, but does not eliminate, *SlGLK2* expression, which remains 40- to 300-fold greater than that of *SlGLK1* (table S3). Therefore, *SlGLK2* expression is partially regulated by light. In *u/u* fruit, *Slglk2* expression was 26 to 40% of *SlGLK2* levels (Fig. 3A and table S2). Fruit that develop in the dark with either *SlGLK2* allele are pale (fig. S4), confirming that light is essential for fruit chloroplast development and chlorophyll synthesis, but the pattern and extent of chloroplast development is determined by *SlGLK2* (table S3).

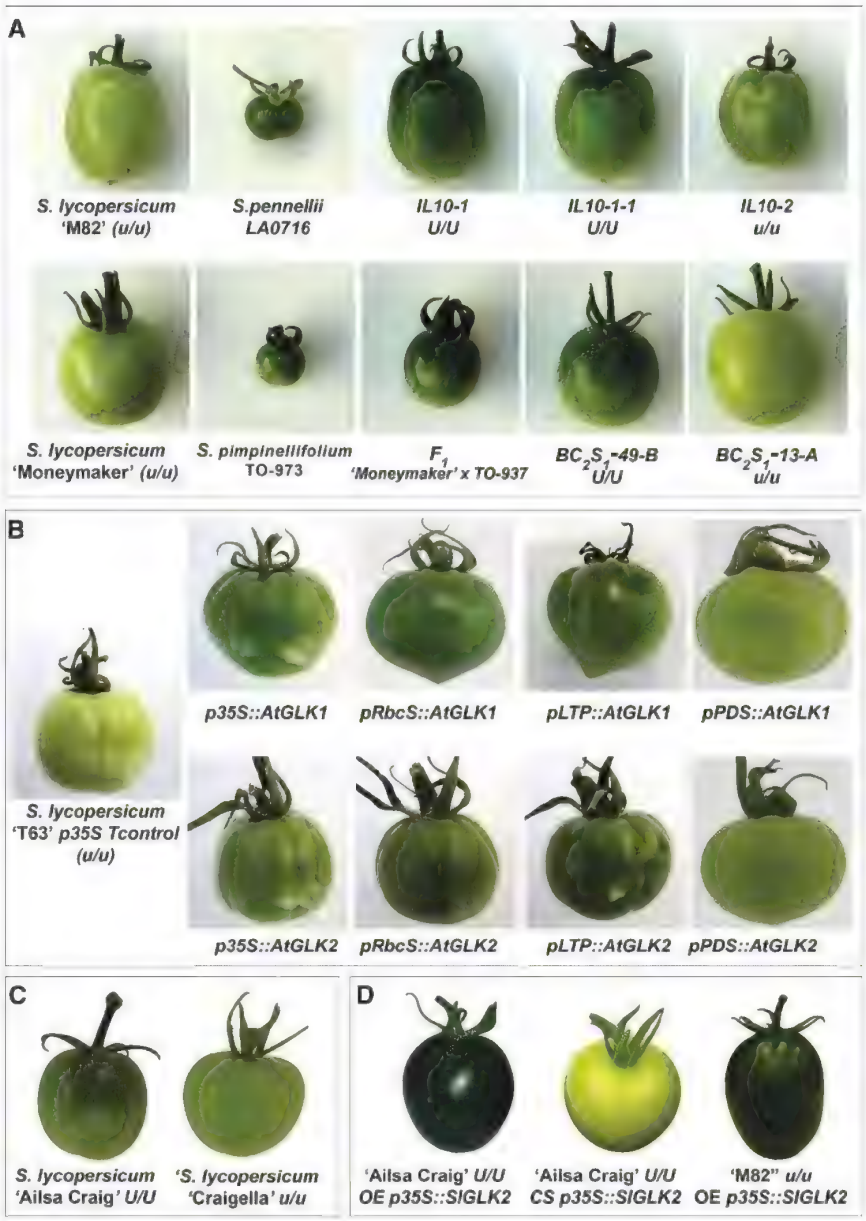

Fig. 1. Fruit phenotypes. (**A**) Immature green fruit (IM, 15 dpa) from the *S. lycopersicum* "M82" x *S. pennellii* introgression population and *S. lycopersicum* "Moneymaker" x *S. pimpinellifolium* backcross lines. (**B**) IM fruit from *S. lycopersicum* "T63" containing the *CaMV35S* promoter (Tcontrol) or *AtGLK1* or *AtGLK2* with the *Ca35S* (*p35S*), *RbcS* (*pRbcS*), *LTP* (*pLTP*), or *PDS* (*pPDS*) promoter. (**C**) Mature green (32 dpa) fruit from "Ailsa Craig" *U/U* and "Craigella" *u/u*. (**D**) Mature green fruit from Ailsa Craig *U/U* containing *p35S::SlGLK2* with overexpression (OE) or cosuppression (CS) of *SlGLK2* and from M82 *u/u* overexpressing *p35S::SlGLK2*.

We tested whether the *u* phenotype is altered by *GLK* expression. Expression of *AtGLK1* or *AtGLK2* in a *u/u* tomato variety (*28*) with promoters expressed before ripening resulted in homogeneously dark green unripe fruit (Fig. 1B and fig. S3, A to C), with three- to sixfold elevated chlorophyll contents (Fig. 3B). With a promoter expressed later in fruit development, *AtGLK1* or *AtGLK2* mRNA was not detected, and chlorophyll was not elevated (Figs. 1B and 3,

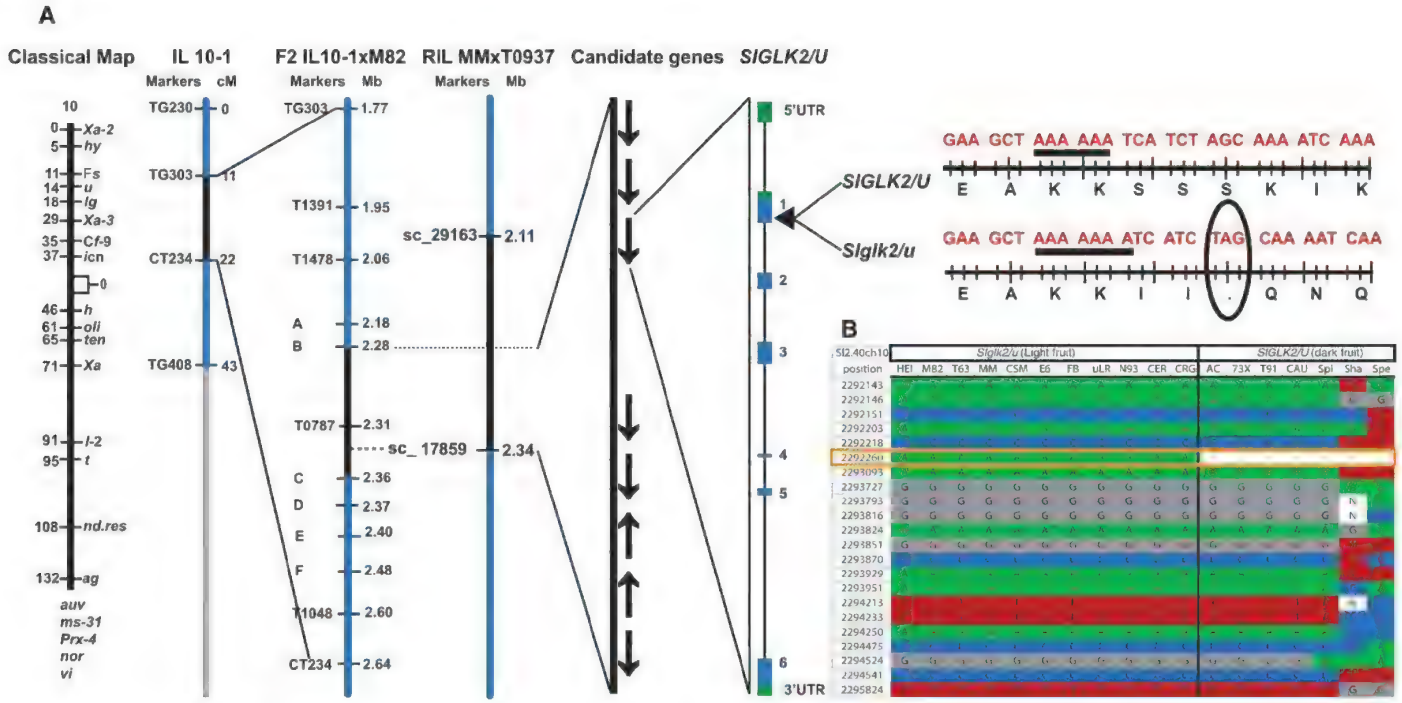

Fig. 2. Map position and sequence of *SlGLK2* alleles. (**A**) Left to right, the classical morphological map (*26*), IL map (*27*), maps derived from the IL 10-1 F_2 and the MM x "T0937" populations, candidate genes in the 60,507-bp region defined by markers, and gene model of *SlGLK2* with the additional A underlined and the resulting stop codon in *Slglk2/u* allele circled. (**B**) *SlGLK2/U* and *Slglk2/u* coding sequences. Nucleic acid calls between SL2.40ch10:2292143-2295824 (SGN tomato release 2.4) from cDNA and genomic sequencing of the *u/u S. lycopersicum* varieties "Heinz 1706" (HEI), M82, T63, Moneymaker (MM), "Castlemart" (CSM), "E6203" (E6), "Fireball" (FB), "Long Red" (uLR), "N93," *S. lycopersicum* var. *cerasiforme* PI114490 (Cer), and Craigella (CRG) and the *U/U S. pimpinellifolium* (Spi), *S. pennellii* (Spe), and *S. lycopersicoides* (*Sha*) wild tomato relatives and *S. lycopersicum* varieties Ailsa Craig (AC), "73X," "T91," and a "Cuatomate" (CAU) landrace. Translated reverse transcription polymerase chain reaction (RT-PCR) products and Basic Local Alignment Search Tool (BLAST) searches predicted the start codon at 2292050; no differences were detected until position 2292143. The sequence differences at 2292260-2292267 of all *u/u* varieties compared with all *U/U* varieties is boxed in orange.

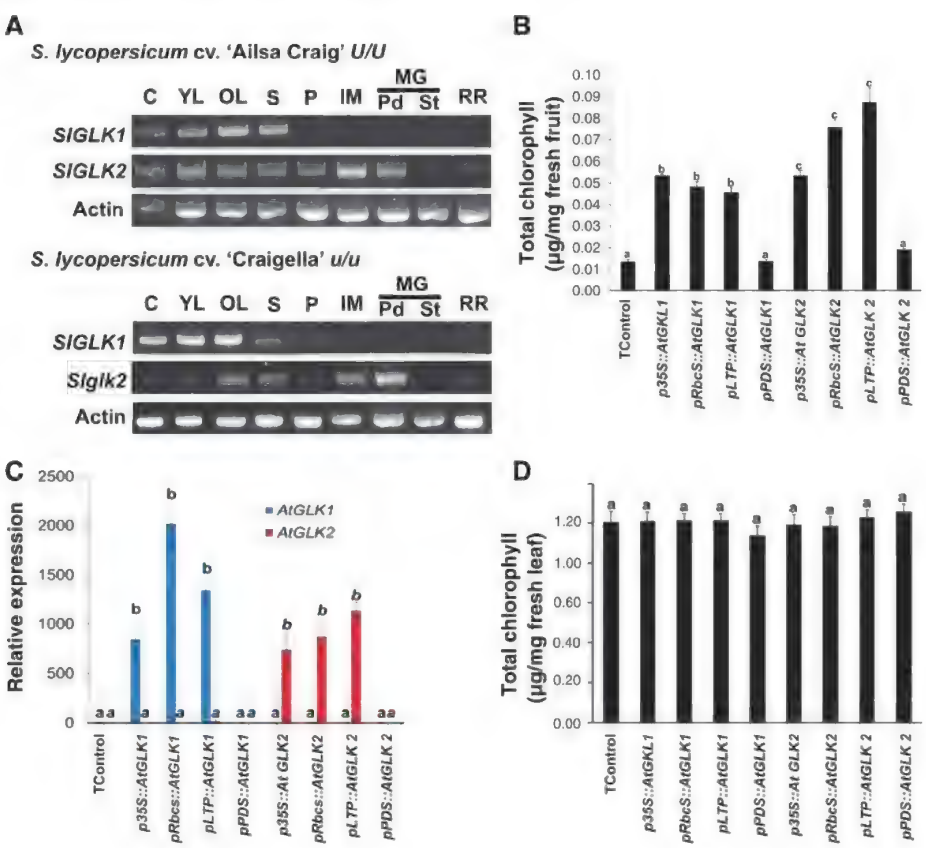

Fig. 3. GLK expression and chlorophyll accumulation. (**A**) *SlGLK1* and *SlGLK2* RT-PCR products from Ailsa Craig *U/U* and Craigella *u/u* cotyledons (C), young leaves (YL), developed leaves (OL), flower petals (P), stamens (S), immature fruit (IM, 10-15 dpa), and the pedicel shoulders (Pd) or the stylar ends (St) of mature green (MG, 32 dpa) fruit and ripe fruit (RR, 46 dpa). Results are typical of replicated RNA samples. (**B**) Chlorophyll in the outer pericarp and epidermis of IM fruit from *AtGLK1*- or *AtGLK2*-expressing lines. Statistical significance by means of general linear model (GLM) and Bonferroni multiple comparison test (MCT) at $P < 0.05$ are indicated. (**C**) Quantitative RT-PCR of *AtGLK1* and *AtGLK2* expression in IM fruit. Statistical significance by means of GLM and Tukey's honestly significant difference (HSD) test at $P < 0.05$ are indicated by roman (*AtGLK1*) and italic (*AtGLK2*) letters, respectively. (**D**) Chlorophyll in leaves from *AtGLK*-expressing lines. Statistical significance determined by means of GLM and Bonferroni MCT at $P < 0.05$ are indicated.

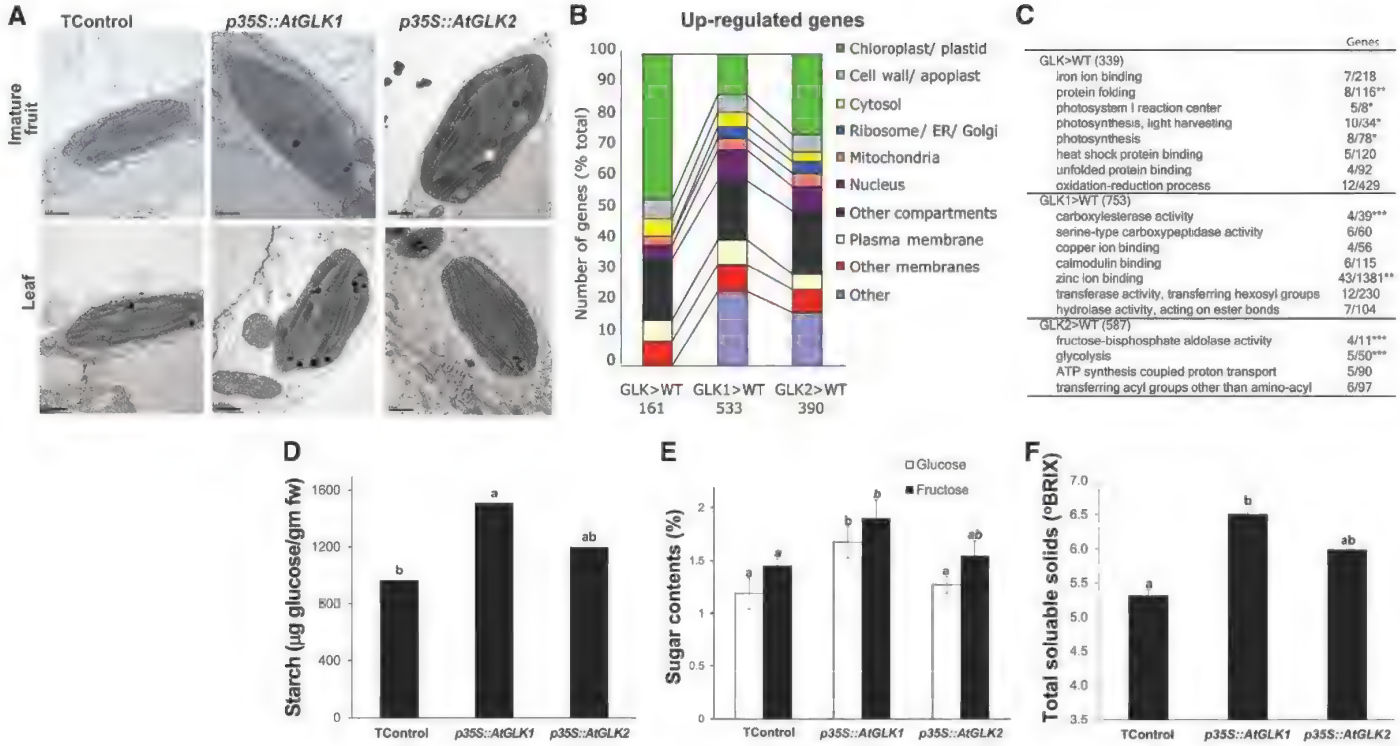

Fig. 4. *AtGLK*-expressing fruit characteristics. (**A**) TEM of IM (15 dpa) green fruit (top row) and leaf (bottom row) chloroplasts, 0.5 µm scale. (**B**) Cellular components Gene Ontology (GO) terms for significantly ($P < 0.05$, fold change >2) overexpressed genes in IM fruit identified in microarray hybridizations. The total number of genes with known GO terms is shown below bars. (**C**) GO categories of overrepresented genes ($P < 0.05$, $n > 3$ genes) whose transcript abundance were different ($P < 0.05$, fold change >2). *$P < 0.0001$; **$0.0001 < P < 0.001$; ***$0.001 < P < 0.01$. (**D**) Starch in IM fruit pericarp and epidermis. (**E**) Glucose (dark bar) and fructose (light bar) in red ripe (RR, 42 dpa) fruit. (**F**) Total soluble solids in RR fruit. Statistical significance determined by means of GLM and Tukey's HSD at $P < 0.05$ are indicated.

B and C). The chlorophyll contents of the leaves were not different from controls (Fig. 3D). The chlorophyll *a*/*b* ratio was unchanged by the expression of *AtGLK1* or *AtGLK2*. Fruit set, size, overall color, and time to ripen were indistinguishable from the control fruit (fig. S3). We also examined the effects of ectopic expression of *SlGLK2* in *U*/*U* and *u*/*u* genotypes. Expression of a full-length *SlGLK2* cDNA in either genotype resulted in homogeneously dark green unripe fruit (Fig. 1D). Cosuppression of *SlGLK2* in four *U*/*U* transgenic lines (*28*) converted the dark green shoulder *U* trait to light green, confirming that *SlGLK2* is *U* (Fig. 1D and fig. S5). The dark green fruit phenotype is confined to the shoulder region, where *SlGLK2* is more highly expressed in *U*/*U* varieties (Fig. 1, C and D), and all lines expressing *GLK*s with promoters expressed throughout the fruit produced homogeneously dark green fruit, affirming that the manifestation and intensity of the phenotype depends on the spatial pattern and level of *GLK* expression.

Transmission electron microscopy (TEM) revealed that *AtGLK1* or *AtGLK2* expression increased the number (twofold) and size of green fruit chloroplasts and promoted accumulation and development of grana thylakoids (Fig. 4A). Chloroplasts of green fruit expressing *AtGLK*s had 6.6 ± 0.45 thylakoids/granum; green control fruit had 3.1 ± 0.84 thylakoids/granum. No obvious alterations of leaf chloroplasts were observed (Fig. 4A).

Analysis of transcript abundance in immature green fruit (*28*) demonstrated that constitutive expression of *AtGLK1* or *AtGLK2* in *u*/*u* increased accumulation of transcripts from 672 genes (fig. S6), especially those with photosynthetic functions (Fig. 4C). Of the 127 genes with known cellular compartments, 47% of those up-regulated by *AtGLK1* and *AtGLK2* are predicted to function in chloroplasts (Fig. 4B). Expression of genes associated with chlorophyll biosynthesis, light-harvesting complexes, photosystem, and starch metabolism increased owing to expression of *AtGLK1* or *AtGLK2* (Fig. 4C and tables S4 to S6). In *atglk1-atglk2* lines constitutively overexpressing rice or *Arabidopsis GLK*s, similar classes of genes are up-regulated (*20*, *22*). Expression of the photomorphogenic regulators *DE-ETIOLATED1* (*DET1*), *UV-DAMAGED DNA-BINDING PROTEIN 1* (*DDB1*), and ELONGATED HYPOCOTYL5 (*HY5*) was not altered by *AtGLK* expression (table S4). Constitutive photomorphogenesis in the tomato *hp1* (*DDB1*) mutant does not reduce the low levels of *SlGLK1* expression (*29*) and only slightly elevates *SlGLK2* expression, suggesting distinct routes to plastid regulation via photomorphogenesis and *GLK* expression. Chloroplast development is exaggerated with costs to yield when the negative regulators of photomorphogenesis, *DET1* and *DDB1*, are down-regulated, with or without *GLK* expression (*30*, *31*). Expression of *AtGLK1* or *AtGLK2* did not affect fruit yield.

In further characterizing the effects of GLKs on fruit biology and quality, increased starch levels in green fruit were observed in response to *AtGLK* expression (*28*). Furthermore, *AtGLK* expression increased fructose and glucose 40% in red fruit (Fig. 4, D and E). Ripe fruit expressing *AtGLK1* or *AtGLK*2 had a 21% increase in soluble solids (Fig. 4F). A quantitative trait locus for increased soluble solids was reported near the *U* locus (*5*). The increase in soluble solids in *U*/*U* compared with that of *u*/*u* was 10% (fig. S1), presumably because *SlGLK2* expression was enhanced in the green fruit shoulders. Lycopene (*28*) increased 10 to 60% with ectopic expression of *AtGLK*s (fig. S8), supporting the conclusion that *GLK* expression regulating chloroplast development in unripe fruit affects sugars and the predominant carotenoid in ripe fruit.

Whereas *u*—that is, *Slglk2*—results in reduced soluble solids in ripe fruit (Fig. 4F and fig. S1), the soluble solids in red *u*/*u* fruit that develop in the dark decreased by an additional 30% (fig. S7). Thus, both GLK activity and light

regulate photosynthetic capacity in green fruit through their regulation of chlorophyll accumulation and chloroplast development and ultimately contribute to sugars that accumulate in ripe fruit.

As in many other plants, two *GLK* genes are present and expressed in tomato, but in fruit, *SlGLK2* mRNA predominates and accumulates in a spatial pattern consistent with chlorophyll biosynthesis and chloroplast development. All *u/u* cultivars examined contain a *Slglk2* allele encoding a truncated loss-of-function GLK protein. Our results suggest that breeding selections for the *u* fruit trait that is helpful for harvesting methods may have had an unintended negative impact on fruit quality because suboptimal chloroplasts develop, and consequently, ripe fruit sugar and lycopene levels decrease. Manipulation of *GLK* levels or spatial expression patterns represents an opportunity to recover and enhance production and quality traits in tomato and other crop species.

References and Notes

1. L. Butler, *J. Hered.* **43**, 25 (1952).
2. A. F. Yeager, *Proc. Am. Soc. Hort. Sci.* **33**, 512 (1935).
3. S. M. Kinzer, S. J. Schwager, M. A. Mutschler, *Theor. Appl. Genet.* **79**, 489 (1990).
4. C. M. Rick, *Hilgardia* **42**, 493 (1974).
5. S. D. Tanksley, J. Hewitt, *Theor. Appl. Genet.* **75**, 811 (1988).
6. G. A. Kemp, I. L. Nonnecke, *Can. J. Plant Sci.* **40**, 306 (1960).
7. C. M. Rick, L. Butler, *Adv. Genet. Incorp. Mol. Gen. Med.* **8**, 267 (1956).
8. M. T. Waters, J. A. Langdale, *EMBO J.* **28**, 2861 (2009).
9. S. Hetherington, R. Smillie, W. Davies, *J. Exp. Bot.* **49**, 1173 (1998).
10. M. M. Blanke, F. Lenz, *Plant Cell Environ.* **12**, 31 (1989).
11. S. Carrara, A. Pardossi, G. F. Soldatini, F. Tognoni, L. Guidi, *Photosynthetica* **39**, 75 (2001).
12. A. J. Matas *et al.*, *Plant Cell* **23**, 3893 (2011).
13. T. Manzara, P. Carrasco, W. Gruissem, *Plant Mol. Biol.* **21**, 69 (1993).
14. M. Sugita, W. Gruissem, *Proc. Natl. Acad. Sci. U.S.A.* **84**, 7104 (1987).
15. L. A. Wanner, W. Gruissem, *Plant Cell* **3**, 1289 (1991).
16. B. Piechulla, W. Gruissem, *EMBO J.* **6**, 3593 (1987).
17. B. Piechulla, R. E. Glick, H. Bahl, A. Melis, W. Gruissem, *Plant Physiol.* **84**, 911 (1987).
18. D. W. Fitter, D. J. Martin, M. J. Copley, R. W. Scotland, J. A. Langdale, *Plant J.* **31**, 713 (2002).
19. J. A. Langdale, *Plant Cell* **23**, 3879 (2011).
20. M. T. Waters *et al.*, *Plant Cell* **21**, 1109 (2009).
21. M. T. Waters, E. C. Moylan, J. A. Langdale, *Plant J.* **56**, 432 (2008).
22. H. Nakamura *et al.*, *Plant Cell Physiol.* **50**, 1933 (2009).
23. A. Bravo-Garcia, Y. Yasumura, J. A. Langdale, *New Phytol.* **183**, 133 (2009).
24. Y. Yasumura, E. C. Moylan, J. A. Langdale, *Plant Cell* **17**, 1894 (2005).
25. A. H. Paterson *et al.*, *Nature* **335**, 721 (1988).
26. S. D. Tanksley, M. A. Mutschler, C. M. Rick, in *Genetic Maps*, S. J. O'Brien, Ed. (Cold Spring Harbor Laboratory, Cold Spring Harbor, New York, 1987), pp. 655–669.
27. Y. Eshed, D. Zamir, *Genetics* **141**, 1147 (1995).
28. Materials and methods are available as supplementary materials on *Science* Online.
29. J. Rohrmann *et al.*, *Plant J.* **68**, 999 (2011).
30. E. M. A. Enfissi *et al.*, *Plant Cell* **22**, 1190 (2010).
31. Y. Liu *et al.*, *Proc. Natl. Acad. Sci. U.S.A.* **101**, 9897 (2004).

Acknowledgments: Minimum Information About a Microarray Experiment (MIAME)–compliant microarray data are available at http://ted.bti.cornell.edu. and at http://www.ebi.ac.uk/arrayexpress/(accession E-MEXP-3652). F. Carrari and A. Fernie provided *S. pennellii SlGLK2*, and J. Maloof provided *S. habrochaites SlGLK2* sequences. The U.S. Department of Agriculture (USDA)/National Institute of Food and Agriculture Solanaceae Coordinated Agricultural Project provided potato data. We are grateful to the Tomato Genome Consortium and the SOL Genomics Network for prepublication access to the tomato genome sequence. The *S. pennellii* introgression lines were provided by the C. M. Rick Tomato Genetics Resource Center; the *S. pimpinellifolium* populations were provided by the Instituto de Hortofruticultura Subtropical y Mediterranea "La Mayora," Consejo Superior de Investigaciones Cientificas; and both populations are available by request from the sources. The *AtGLK*-expressing lines were provided by Mendel Biotechnology and Seminis/Monsanto Vegetable Seeds. *SlGLK2*, the corresponding lines, and the F2 10-1 IL x M82 population lines and seeds are available from J.J.G. without restriction. Seminis/Monsanto will make available, upon request, and under a material transfer agreement indicating they are to be used for noncommercial purposes, the following lines: LexA:AtGLK1:p35S:LexA-Gal4; LexA:AtGLK1:pLTP:LexA-Gal4; LexA:AtGLK1:pRbcS:LexA-Gal4; LexA:AtGLK1:pPDS:LexA-Gal4; LexA:AtGLK2:p35S:LexA-Gal4; LexA:AtGLK2:pLTP:LexA-Gal4; LexA:AtGLK2:pRbcS:LexA-Gal4; LexA:AtGLK2:pPDS:LexA-Gal4; plus the T63 control line. Other biological materials are available by request from A.L.T.P. or J.J.G. A.L.T.P., T.H., K.L.-C., R.F.-B., and A.B.B. have filed a provisional U.S. patent application UC #2011-841, "Introduction of wild species *GLK* genes for improved ripe tomato fruit quality," through the University of California. A.L.T.P. and A.B.B. have filed the U.S. patent application #2010/0154078, "Transcription factors that enhance traits in plant organs," through Mendel Biotechnology. Assistance from B. Blanco-Ulate, S. Phothiset, S. Reyes, A. Abraham, L. Gilani, and G. Arellano is gratefully acknowledged. J. Langdale provided helpful advice regarding *GLK* phylogeny and nomenclature. G. Adamson and P. Kysar, Electron Microscopy (EM) Laboratory, University of California Davis Medical Center did the EM work. University of California Discovery and partners funded the pepper analysis and the initial investigations of the *Arabidopsis GLKs*. The Vietnam Education Foundation supported C.N. Fundación Genoma España ESPSOL Project provided partial funding to A.G. USDA–Agricultural Research Service, USDA–National Research Initiative (2007-02773), and NSF (Plant Genome Program IOS-0923312) provided support to J.J.G.

Supplementary Materials

www.sciencemag.org/cgi/content/full/336/6089/1711/DC1
Materials and Methods
Figs. S1 to S8
Tables S1 to S8
References (*32*–*58*)

21 March 2012; accepted 5 June 2012
10.1126/science.1222218

The Paleozoic Origin of Enzymatic Lignin Decomposition Reconstructed from 31 Fungal Genomes

Dimitrios Floudas,[1] Manfred Binder,[1] Robert Riley,[2] Kerrie Barry,[2] Robert A. Blanchette,[3] Bernard Henrissat,[4] Angel T. Martínez,[5] Robert Otillar,[2] Joseph W. Spatafora,[6] Jagjit S. Yadav,[7] Andrea Aerts,[2] Isabelle Benoit,[8,9] Alex Boyd,[6] Alexis Carlson,[1] Alex Copeland,[2] Pedro M. Coutinho,[4] Ronald P. de Vries,[8,9] Patricia Ferreira,[10] Keisha Findley,[11] Brian Foster,[2] Jill Gaskell,[12] Dylan Glotzer,[1] Paweł Górecki,[13] Joseph Heitman,[11] Cedar Hesse,[6] Chiaki Hori,[14] Kiyohiko Igarashi,[14] Joel A. Jurgens,[3] Nathan Kallen,[1] Phil Kersten,[12] Annegret Kohler,[15] Ursula Kües,[16] T. K. Arun Kumar,[17] Alan Kuo,[2] Kurt LaButti,[2] Luis F. Larrondo,[18] Erika Lindquist,[2] Albee Ling,[1] Vincent Lombard,[4] Susan Lucas,[2] Taina Lundell,[19] Rachael Martin,[1] David J. McLaughlin,[17] Ingo Morgenstern,[20] Emanuelle Morin,[15] Claude Murat,[15] Laszlo G. Nagy,[1] Matt Nolan,[2] Robin A. Ohm,[2] Aleksandrina Patyshakuliyeva,[9] Antonis Rokas,[21] Francisco J. Ruiz-Dueñas,[5] Grzegorz Sabat,[22] Asaf Salamov,[2] Masahiro Samejima,[14] Jeremy Schmutz,[23] Jason C. Slot,[21] Franz St. John,[12] Jan Stenlid,[24] Hui Sun,[2] Sheng Sun,[11] Khajamohiddin Syed,[7] Adrian Tsang,[20] Ad Wiebenga,[9] Darcy Young,[1] Antonio Pisabarro,[25] Daniel C. Eastwood,[26] Francis Martin,[15] Dan Cullen,[12] Igor V. Grigoriev,[2]* David S. Hibbett[1]*

Wood is a major pool of organic carbon that is highly resistant to decay, owing largely to the presence of lignin. The only organisms capable of substantial lignin decay are white rot fungi in the Agaricomycetes, which also contains non–lignin-degrading brown rot and ectomycorrhizal species. Comparative analyses of 31 fungal genomes (12 generated for this study) suggest that lignin-degrading peroxidases expanded in the lineage leading to the ancestor of the Agaricomycetes, which is reconstructed as a white rot species, and then contracted in parallel lineages leading to brown rot and mycorrhizal species. Molecular clock analyses suggest that the origin of lignin degradation might have coincided with the sharp decrease in the rate of organic carbon burial around the end of the Carboniferous period.

Lignin is a heterogeneous polymer that provides strength and rigidity to wood, protects cellulose and hemicellulose from microbial attack, and is the major precursor of coal (*1*). Genomic studies of wood decay organisms have focused on model fungal systems for white rot (in which all plant cell wall components are degraded), such as *Phanerochaete*

chrysosporium (*2*), and brown rot (in which lignin is modified but not appreciably degraded), such as *Postia placenta* (*3*) and *Serpula lacrymans* (*4*). However, these species represent just two of the 18 recognized orders of Agaricomycetes, of which five contain brown rot taxa. To reconstruct the evolution of lignin decay mechanisms, we analyzed 31 diverse fungal genomes, including 12 newly sequenced species of Agaricomycotina (Table 1). The new genomes comprise six white rot species, five brown rot species, and one mycoparasite, representing nine orders (Fig. 1 and figs. S1 to S5) (*5*).

To estimate phylogenetic relationships among these taxa, we constructed data sets using 71 or 26 single-copy genes, with varying alignment criteria and treatments for fast-evolving sites, yielding matrices of 10,002 to 34,257 amino acids, which we analyzed with maximum likelihood (ML) and Bayesian methods (*5*–*7*). All but six nodes receive maximal support values in all analyses, and the rest are strongly supported (bootstrap ≥99% or posterior probability ≥0.99) in at least three analyses. The tree topology is consistent with prior analyses and resolves four independent brown rot lineages (Fig. 1A and fig. S6).

We searched all 31 genomes for 27 gene families encoding oxidoreductases and carbohydrate-active enzymes (CAZymes) that have been implicated in wood decay (Table 1). CAZymes, particularly those acting on crystalline cellulose, are abundant in white rot genomes, which have 61 to 148 (average 87) copies of genes encoding CAZymes, representing 14 to 17 gene families, whereas brown rot genomes have 32 to 68 copies (average 46) from 9 to 12 families. The ectomycorrhizal (ECM) *Laccaria bicolor* resembles brown rot species in this regard, possessing 28 CAZyme genes in eight families (Table 1). Notably, glycoside hydrolase (GH) families GH6 and GH7, which include cellobiohydrolases that are involved in the attack of crystalline cellulose (*8*), are present in all white rot lineages, but they are absent in brown rot lineages (except Boletales) and *L. bicolor*. Similar patterns of enrichment in white rot genomes are shown by genes encoding GH61 enzymes, which have a copper-dependent oxidative mechanism for disrupting crystalline cellulose (*9*), and cellulose binding modules (CBM1), which effectively increase the concentration of the enzymes on the surface of crystalline cellulose (*10*) (Table 1).

To gain access to cellulose, wood-decaying fungi must overcome or circumvent lignin; thus, we focus on fungal class II peroxidases (PODs), which degrade lignin in *P. chrysosporium* and other species (*11*) (figs. S7 to S19). We classified PODs into four major groups, including three ligninolytic forms—lignin peroxidase (LiP), manganese peroxidase (MnP), and versatile peroxidase (VP)—and a fourth POD type, defined here as "generic peroxidase" (GP), which is expected to include nonligninolytic low–redox potential peroxidases with catalytic properties similar to those of the peroxidase of *Coprinopsis cinerea* or the product of the *nop*A gene in *P. chrysosporium* (*5*, *12*). LiPs possess a tryptophan residue on the surface of the enzyme corresponding to Trp^{171} in *P. chrysosporium* LiP-H8 that enables direct oxidation of lignin compounds via long-range electron transfer; MnPs possess two or three residues corresponding to Glu^{35}, Glu^{39}, and Asp^{175} of *P. chrysosporium* MnP1 that function in binding Mn (*13*). VPs possess both the Trp^{171} homolog and Mn-binding residues, whereas all are lacking in GPs.

Consistent with a central role for PODs in lignin degradation, white rot species have 5 to 26 copies (average 14) of genes encoding ligninolytic PODs, but all brown rot species lack these enzymes, as do the ECM *L. bicolor*, the soil saprotroph *C. cinerea*, and *Schizophyllum commune*, which has been regarded as a white rot fungus but has a limited capacity to degrade lignin (*14*). Moreover, analyses of gene diversification with binary state speciation analysis (*15*) confirmed that the rate of duplication of POD genes is elevated in white rot lineages versus non–white rot lineages (*5*).

To reconstruct the functional evolution of PODs, we performed Bayesian and ML analyses (*6*, *16*) using the GPs of Ascomycota as outgroups, and we estimated the ancestral states of the key residues of ligninolytic PODs using BayesTraits (*17*). Our results indicate that the ancestor of all PODs likely lacked the Mn-binding and Trp^{171} residues of MnP, LiP, and VP, suggesting that it was nonligninolytic (Fig. 1B). The most recent ancestor of all ligninolytic Agaricomycete PODs is reconstructed as an MnP, suggesting that there was a single origin of LiP (gain of Trp^{171} and loss of Mn-binding residues), with parallel expansions in the *P. chrysosporium* and *Trametes versicolor* (Polyporales, each with 10 LiP copies; Fig. 1B and figs. S7 and S17). We also identified two origins of VP in the Polyporales, where *T. versicolor* and *Dichomitus squalens* each have three VP copies (Fig. 1B and fig. S7). VPs are also produced in the "oyster mushroom" *Pleurotus ostreatus* (Agaricales) (*18*), indicating further convergent evolution of this class of enzymes.

To localize the diversification of PODs in the organismal phylogeny, we performed gene tree/species tree reconciliation analyses using CAFE (*19*), Notung (*20*), and DrML (*21*). All methods suggest that a single POD gene copy was present in the common ancestor of Basidiomycota, with parallel losses in lineages leading to the Pucciniomycotina, Ustilaginomycotina, Tremellomycetes, and *Dacryopinax* sp. (Fig. 1A). Diversification of PODs occurred in the lineage leading to the most recent common ancestor of the Agaricomycetes (node "A" in Fig. 1A), which is reconstructed as having two to seven POD gene copies in the various analyses. In addition, reconciliation analyses suggest that the ancestor of the Agaricomycetes possessed one or two genes encoding dye-decolorizing peroxidases (DyP), which are heme peroxidases that have been shown to degrade lignin model compounds (*22*), as well five to eight genes encoding oxidases (including glyoxal oxidase) involved in peroxide generation (*5*, *23*). Collectively, these results suggest that the ancestor of Agaricomycetes was a white rot species that possessed a ligninolytic system with PODs, DyPs, and multiple pathways for H_2O_2 production.

The "backbone" nodes in the Agaricomycete phylogeny (labeled "B" in Fig. 1A) are reconstructed as having 3 to 16 POD gene copies, which suggests that the white rot mechanism was retained throughout the early evolution of Agaricomycetes. Subsequently, all reconciliation analyses suggest that there were parallel expansions of POD genes in terminal lineages, leading to white rot species in five orders (Auriculariales, Hymenochaetales, Corticiales, Russulales, and Polyporales). In contrast, parallel contractions of PODs are resolved within lineages leading to the brown rot *Dacryopinax* sp., *Gloeophyllum trabeum*, the Boletales, and the brown rot Polyporales,

[1]Biology Department, Clark University, Worcester, MA 01610, USA. [2]U.S. Department of Energy Joint Genome Institute, Walnut Creek, CA 94598, USA. [3]Department of Plant Pathology, University of Minnesota, St. Paul, MN 55108, USA. [4]Architecture et Fonction des Macromolécules Biologiques, Aix-Marseille Université, CNRS UMR 6098, 13288 Marseille Cedex 9, France. [5]Centro de Investigaciones Biológicas, CSIC, Ramiro de Maeztu 9, E-28040 Madrid, Spain. [6]Department of Botany and Plant Pathology, Oregon State University, Corvallis, OR 97331, USA. [7]Environmental Genetics and Molecular Toxicology Division, Department of Environmental Health, University of Cincinnati College of Medicine, Cincinnati, OH 45267, USA. [8]Microbiology and Kluyver Centre for Genomics of Industrial Fermentation, Utrecht University, Padualaan 8, 3584 CH Utrecht, Netherlands. [9]CBS-KNAW Fungal Biodiversity Centre, Uppsalalaan 8, 3584 CT Utrecht, Netherlands. [10]Department of Biochemistry and Molecular and Cellular Biology and Institute of Biocomputation and Physics of Complex Systems, Zaragoza University, 50009, Zaragoza, Spain. [11]Department of Molecular Genetics and Microbiology, Duke University Medical Center, Durham, NC 27710, USA. [12]USDA Forest Products Laboratory, Madison, WI 53726, USA. [13]Institute of Informatics, Warsaw University, Warsaw, 02-097, Poland. [14]Department of Biomaterial Sciences, Graduate School of Agricultural and Life Sciences, University of Tokyo, 1-1-1, Yayoi, Bunkyo-ku, Tokyo 113-8657, Japan. [15]INRA, UMR 1136, INRA-Nancy Université, Interactions Arbres/Microorganismes, 54280 Champenoux, France. [16]Molecular Wood Biotechnology and Technical Mycology, Büsgen-Institute, Georg-August-University Göttingen, Büsgenweg 2, D-37077 Göttingen, Germany. [17]Department of Plant Biology, University of Minnesota, St. Paul, MN 55108, USA. [18]Departamento de Genética Molecular y Microbiología, Facultad de Ciencias Biológicas, Pontifica Universidad Católica de Chile, Casilla 114-D, Santiago 833-1010, Chile. [19]Department of Applied Chemistry and Microbiology, Viikki Biocenter, P.O. Box 56, Biocenter 1, University of Helsinki, FIN-00014 Helsinki, Finland. [20]Centre for Structural and Functional Genomics, Concordia University, 7141 Sherbrooke Street West, Montreal, Quebec H4B 1R6, Canada. [21]Department of Biological Sciences, Vanderbilt University, Nashville, TN 37235, USA. [22]University of Wisconsin Biotechnology Center, Madison, WI 53726, USA. [23]HudsonAlpha Institute for Biotechnology, Huntsville, AL 35806, USA. [24]Department of Forest Mycology and Pathology, Swedish University of Agricultural Sciences, Box 7026, Ulls v 26A, 750 07 Uppsala, Sweden. [25]Genetics and Microbiology Research Group, Public University of Navarre, 31006 Pamplona, Spain. [26]College of Science, University of Swansea, Singleton Park, Swansea SA2 8PP, UK.

*To whom correspondence should be addressed. E-mail: ivgrigoriev@lbl.gov (I.V.G.); dhibbett@clarku.edu (D.S.H.)

Table 1. Gene contents in 11 oxidoreductase and 17 CAZyme families in the genomes of 20 Agaricomycotina and 11 other fungi. **Species:** New genomes: Ad, *Auricularia delicata*; Cp, *Coniophora puteana*; Da, *Dacryopinax* sp., Ds, *Dichomitus squalens*; Fm, *Fomitiporia mediterranea*; Fp, *Fomitopsis pinicola*; Gt, *Gloeophyllum trabeum*; Pu, *Punctularia strigosozonata*; Sh, *Stereum hirsutum*; Tm, *Tremella mesenterica*, Tv, *Trametes versicolor*; Wc, *Wolfiporia cocos*. Others: An, *Aspergillus niger*; Bd, *Batrachochytrium dendrobatidis*; Cc, *Coprinopsis cinerea*; Cn, *Cryptococcus neoformans*; Cr, *Cryphonectria parasitica*; Ha, *Heterobasidion annosum* (has been reclassified as *H. irregulare*); Lb, *Laccaria bicolor*; Mg, *Malassezia globosa*; Ml, *Melampsora laricis-populina*; Pb, *Phycomyces blakesleeanus*; Pc, *Phanerochaete chrysosporium*; Pp, *Postia placenta*; Ps, *Pichia stipitis*; Sc, *Schizophyllum commune*; Sl, *Serpula lacrymans*; Sn, *Stagonospora nodorum*; Sr, *Sporobolomyces roseus*; Tr, *Trichoderma reesei*; Um, *Ustilago maydis*. **Ecologies:** WR, white rot; BR, brown rot; ECM, mycorrhiza; S, non-wood decay saprotroph; MP, mycoparasite; AP, animal pathogen/parasite; PP, plant pathogen; Y, yeast. **Genes:** GH, glycoside hydrolases; CE, carbohydrate esterases; POD, class II peroxidases; MCO, multicopper oxidases; CRO, copper-radical oxidases; CDH, cellobiose dehydrogenase; Cytb562, cytochrome b562; OXO, oxalate oxidase/decarboxylases; GLP, Fe(III)-reducing glycopeptides; QRD, quinone reductases; DyP, dye-decolorizing peroxidases; HTP, heme-thiolate peroxidases; P450, cytochromes P450. *P* values indicate strength of rejection of model of random diversification in CAFE analyses.

Taxonomy		Basidiomycota																								Ascomycota						
		Agaricomycotina																													Ch	Mu
		Agaricomycetes																	Dac	Trem		Ust		Pucc		Pez				Sc		
		Ha	Sh	Pu	Fm	Ad	Tv	Ds	Pc	Pp	Wc	Fp	Gt	Sl	Cp	Lb	Sc	Cc	Da	Tm	Cn	Mg	Um	Ml	Sr	An	Cr	Tr	Sn	Ps	Bd	Pb
Ecology		WR								BR						ECM	WR	S	BR	MP	AP	AP	PP	PP	Y	AP	PP	S	PP	Y	AP	S
		CAZymes																														
Genes	*P*																															
GH3*	0.000	11	15	12	7	12	11	7	9	5	7	12	9	9	12	2	11	7	8	3	7	1	3	3	3	16	15	11	16	7	1	2
GH5†	0.305	7	6	6	6	8	5	5	5	5	4	5	5	8	8	3	3	6	5	0	0	0	1	7	2	4	7	3	5	0	1	1
GH6	0.916	1	1	1	2	2	1	1	1	0	0	0	0	1	2	0	1	5	0	0	0	0	0	0	0	2	2	1	4	0	0	0
GH7	0.000	1	3	5	2	6	4	4	8	0	0	0	0	0	2	0	2	6	0	0	0	0	0	9	0	2	5	2	5	0	0	0
GH10	0.004	2	6	5	4	4	6	5	6	4	4	2	3	1	3	0	5	6	3	0	0	0	2	6	0	2	4	1	7	1	0	0
GH11	0.687	0	1	1	0	3	0	0	1	0	0	0	0	0	0	0	1	6	0	0	0	0	1	0	0	3	4	3	7	0	0	0
GH12	0.483	4	5	2	3	1	5	3	2	2	2	2	2	1	4	3	1	1	1	0	0	0	0	5	0	3	5	2	4	0	0	0
GH28‡	0.000	8	17	13	16	10	11	7	4	7	9	13	10	7	13	7	3	3	6	0	1	0	1	3	0	22	21	4	4	0	0	9
GH61	0.000	10	16	14	13	19	18	15	15	2	2	4	4	5	10	5	22	35	0	0	1	0	0	0	0	7	12	3	29	0	0	0
GH74	0.923	1	2	2	4	1	1	1	4	0	0	0	1	1	0	0	1	1	0	0	0	0	0	0	0	1	2	1	0	0	0	0
GH43	0.000	4	10	7	6	26	3	7	4	1	1	7	5	1	6	0	12	4	5	0	0	1	2	4	0	7	14	2	10	0	0	0
CE1	0.129	1	1	2	0	3	3	0	4	0	0	0	1	0	0	0	4	3	0	0	0	0	1	0	0	1	2	0	6	0	0	0
CE16	0.000	5	10	8	6	29	7	10	2	5	6	11	6	3	6	3	10	5	4	1	0	0	0	0	2	3	7	2	2	0	0	2
CE5	0.002	0	1	1	0	3	0	0	0	0	0	0	0	0	1	1	2	6	0	0	0	0	4	14	0	5	15	4	11	0	0	0
CE8	0.347	3	4	6	3	3	2	3	2	1	1	2	2	2	2	4	2	0	3	0	0	0	1	5	0	3	4	0	2	0	0	4
CE12	0.796	2	3	0	2	1	0	2	0	0	0	0	0	0	0	0	1	1	0	0	0	0	0	0	0	1	2	0	1	0	0	0
CE15	0.488	1	1	2	1	6	2	2	2	1	1	1	1	0	0	0	2	8	1	0	0	0	0	0	0	0	2	1	1	0	0	0
		Oxidoreductases																														
POD	0.000	8	6	11	17	19	26	12	16	1	1	1	0	0	0	1	0	1	0	0	0	0	0	0	0	0	1	0	5	0	0	0
MCO	0.000	17	20	13	11	10	10	13	5	5	5	7	4	6	8	11	6	17	5	4	5	9	6	20	1	14	16	8	9	2	3	5
CRO§	0.000	5	8	9	4	9	9	9	7	3	4	4	2	3	6	11	2	6	3	2	3	1	3	4	3	0	0	1	2	0	3	1
CDH‖	0.575	1	1	1	1	1	1	1	1	0	0	0	1	2	2	0	1	1	0	0	0	0	0	0	0	2	3	0	3	0	0	0
Cytb562	0.177	1	1	0	0	0	1	1	1	0	0	0	0	2	3	0	2	0	0	0	0	0	0	0	0	0	1	0	2	0	0	0
OXO	0.026	3	3	2	3	3	5	5	7	5	4	5	4	3	2	1	5	1	2	0	0	0	0	1	0	2	2	3	3	0	0	0
GLP	0.000	1	11	6	8	1	2	6	3	5	10	10	6	3	11	1	7	0	3	0	0	0	0	2	0	0	0	0	0	0	0	0
QRD	0.496	2	1	3	3	4	1	1	4	1	1	1	3	2	2	2	4	3	1	1	2	0	1	1	1	1	1	1	1	4	1	4
DyP	0.000	1	2	5	3	11	2	1	0	2	0	0	0	0	0	2	0	4	0	1	1	0	0	2	0	0	0	0	0	0	0	0
HTP	0.000	5	10	8	4	16	3	4	3	5	5	4	6	3	2	5	3	8	6	0	0	0	3	17	0	5	2	4	13	0	0	0
P450	0.000	144	215	144	130	249	190	187	149	250	206	190	130	164	238	101	115	139	126	9	13	7	17	28	7	156	125	71	125	10	9	52

*GH3 does not include β-N-acetylhexosaminidase genes. †GH5 includes only models with similarity to endo-1,4-β-D-glucanases and mannan endo-β-1,4-mannosidases. ‡One model (Fompi1 162677) is a potential pseudogene. §One model in *A. delicata* is a potential pseudogene. ‖One CDH gene in *C. puteana* lacks a cyt domain and may not be functional.

suggesting that these lineages lost PODs as they shifted to a nonligninolytic mode of wood decay (Fig. 1A).

To place the origin of lignin degradation in the context of geologic time, we performed Bayesian relaxed molecular clock analyses using BEAST (*16*) and PhyloBayes (*7*), with fossil-based calibrations at three nodes, including the ancestors of the Boletales, Agaricales, and Ascomycota (*5*). The mean age of the Agaricomycetes is ~290 Ma (millions of years ago) in both BEAST and PhyloBayes analyses [95% highest posterior density interval (hpd) = 222 to 372 Ma], with the mean age of the Agaricomycotina placed at ~430 to 470 Ma (95% hpd = 329 to 557 Ma), consistent with basidiomycete fossils that were not used as calibration points, including hyphae with clamp connections from the Mississippian (*24*) from ~330 Ma. BEAST analyses of the POD genes, calibrated with the split between Ascomycota and Basidiomycota according to the organismal phylogeny, suggest that the first ligninolytic MnP arose at ~295 Ma (95% hpd = 195 to 399 Ma; Fig. 1), which is slightly earlier than (and therefore consistent with) the oldest definitive white rot fossils from the Permian (~260 Ma) and Triassic (~230 Ma) (*25*).

Organic carbon accumulated at an exceptionally high rate during the Carboniferous and Permian, resulting in the formation of vast coal deposits, derived primarily from lignin (*26*). A frequently cited explanation for this phenomenon is that decay was inhibited in the anoxic sediments of widespread coastal swamp forests. Our results are consistent with a complementary hypothesis (*1*), which posits that the sharp decline in the rate of organic carbon burial at the

Fig. 1. (**A**) Organismal phylogeny (chronogram) produced with BEAST from a 26-gene data set. Light blue bars are 95% highest posterior density intervals for node ages; mean ages of selected nodes (millions of years) are in parentheses. Blue and red branches indicate significant expansion and contraction, respectively, of PODs inferred using CAFE. Numbers in red following taxon names are POD gene counts. Numbers in red at nodes, separated by commas, are numbers of POD gene copies estimated with CAFE, Notung (with two different edge weight threshold settings), and DrML, respectively. The node labeled A is the ancestor of Agaricomycetes; nodes labeled B are "backbone" nodes in Agaricomycetes (see text). Asterisks indicate nodes that do not receive maximal support in all analyses (see fig. S6 for support values). See Table 1 for full species names. (**B**) POD gene phylogeny estimated in BEAST with ancestral state reconstructions for manganese-binding site (colored pies) and Trp^{171} residues (black and white pies) estimated with BayesTraits. Bars to right of gene IDs indicate presence of functional residues (*13*). Mean ages for selected nodes in parentheses are followed by 95% highest posterior density ranges.

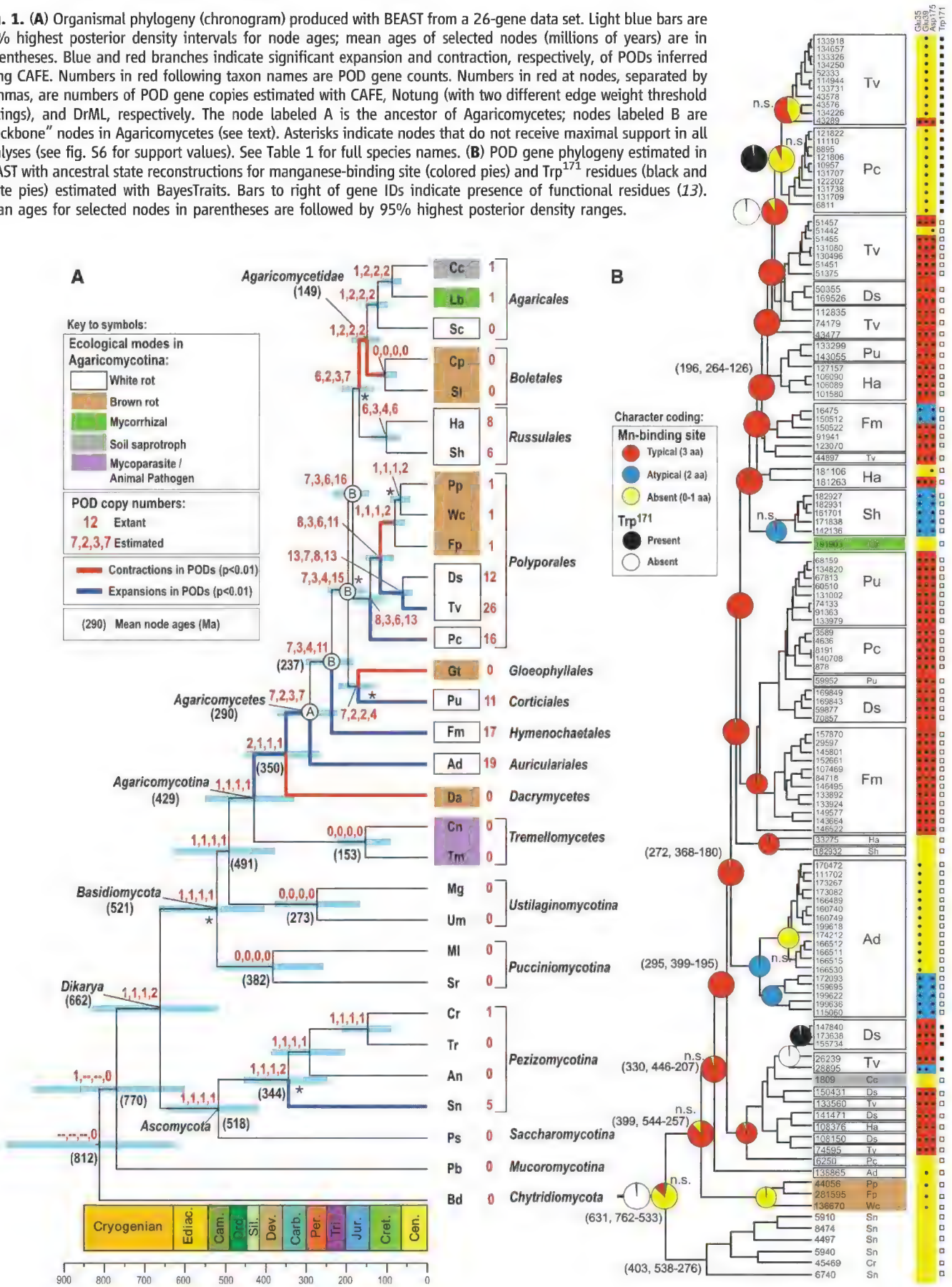

end of the Permo-Carboniferous was caused, at least in part, by the evolution of lignin decay capabilities in white rot Agaricomycetes.

References and Notes

1. J. M. Robinson, *Geology* **18**, 607 (1990).
2. D. Martinez *et al.*, *Nat. Biotechnol.* **22**, 695 (2004).
3. D. Martinez *et al.*, *Proc. Natl. Acad. Sci. U.S.A.* **106**, 1954 (2009).
4. D. C. Eastwood *et al.*, *Science* **333**, 762 (2011).
5. See supplementary materials on *Science* Online.
6. A. Stamatakis, *Bioinformatics* **22**, 2688 (2006).
7. N. Lartillot, T. Lepage, S. Blanquart, *Bioinformatics* **25**, 2286 (2009).
8. P. Baldrian, V. Valásková, *FEMS Microbiol. Rev.* **32**, 501 (2008).
9. R. J. Quinlan *et al.*, *Proc. Natl. Acad. Sci. U.S.A.* **108**, 15079 (2011).
10. D. Guillén, S. Sánchez, R. Rodríguez-Sanoja, *Appl. Microbiol. Biotechnol.* **85**, 1241 (2010).
11. A. T. Martínez, F. J. Ruiz-Dueñas, M. J. Martínez, J. C. Del Río, A. Gutiérrez, *Curr. Opin. Biotechnol.* **20**, 348 (2009).
12. L. Larrondo, A. González, T. Perez Acle, D. Cullen, R. Vicuña, *Biophys. Chem.* **116**, 167 (2005).
13. F. J. Ruiz-Dueñas *et al.*, *J. Exp. Bot.* **60**, 441 (2009).
14. O. Schmidt, W. Liese, *Holzforschung* **34**, 67 (1980).
15. R. G. FitzJohn, W. P. Maddison, S. P. Otto, *Syst. Biol.* **58**, 595 (2009).
16. A. J. Drummond, A. Rambaut, *BMC Evol. Biol.* **7**, 214 (2007).
17. D. Barker, A. Meade, M. Pagel, *Bioinformatics* **23**, 14 (2007).
18. F. J. Ruiz-Dueñas, E. Fernández, M. J. Martínez, A. T. Martínez, *C. R. Biol.* **334**, 795 (2011).
19. T. De Bie, N. Cristianini, J. P. Demuth, M. W. Hahn, *Bioinformatics* **22**, 1269 (2006).
20. D. Durand, B. V. Halldórsson, B. Vernot, *J. Comput. Biol.* **13**, 320 (2006).
21. P. Górecki, G. J. Burleigh, O. Eulenstein, *BMC Bioinformatics* **12** (suppl. 1), S15 (2011).
22. M. Hofrichter, R. Ullrich, M. J. Pecyna, C. Liers, T. Lundell, *Appl. Microbiol. Biotechnol.* **87**, 871 (2010).
23. A. Vanden Wymelenberg *et al.*, *Appl. Environ. Microbiol.* **72**, 4871 (2006).
24. M. Krings, N. Dotzler, G. Galtier, T. N. Taylor, *Mycoscience* **52**, 18 (2011).
25. S. P. Stubblefield, T. N. Taylor, *Bot. Gaz.* **147**, 116 (1986).
26. R. A. Berner, *The Phanerozoic Carbon Cycle: CO_2 and O_2* (Oxford Univ. Press, Oxford, 2004).

Acknowledgments: The work conducted by the U.S. Department of Energy Joint Genome Institute was supported by the Office of Science of the U.S. Department of Energy under contract DE-AC02-05CH11231. Also supported by the Assembling the Fungal Tree of Life (AFTOL) project under NSF awards DEB-0732968 (D.S.H.), DEB-0732993 (J.W.S.), and DEB-0732550 (D.J.M.). We thank R. H. Petersen for the strain of *A. delicata*. The organisms *A. delicata* and *Dacryopinax* sp. were obtained in Costa Rica and can only be used for research purposes. Assemblies and annotations of the 12 genomes reported here are available from the JGI fungal portal MycoCosm (http://jgi.doe.gov/fungi) and from DDBJ/EMBL/GenBank under the following accessions: AFVO00000000, AEIT00000000, AEUS00000000, AEID00000000, AEJJ00000000, AEHC00000000, AFVP00000000, AEGM00000000, AEGX00000000, AEJI00000000, AFVY00000000, and AEHD00000000. Aligned sequence data for organismal and gene family phylogenies and molecular clock analyses, and secretome results are available at DRYAD (http://dx.doi.org/10.5061/dryad.5k3t47p0).

Supplementary Materials

www.sciencemag.org/cgi/content/full/336/6089/1715/DC1
Materials and Methods
Supplementary Text
Tables S1 to S16
Figs. S1 to S22
References

12 March 2012; accepted 7 May 2012
10.1126/science.1221748

Leucine-tRNA Initiates at CUG Start Codons for Protein Synthesis and Presentation by MHC Class I

Shelley R. Starck,[1] Vivian Jiang,[1] Mariana Pavon-Eternod,[2] Sharanya Prasad,[1] Brian McCarthy,[3] Tao Pan,[2] Nilabh Shastri[1]*

Effective immune surveillance by cytotoxic T cells requires newly synthesized polypeptides for presentation by major histocompatibility complex (MHC) class I molecules. These polypeptides are produced not only from conventional AUG-initiated, but also from cryptic non–AUG-initiated, reading frames by distinct translational mechanisms. Biochemical analysis of ribosomal initiation complexes at CUG versus AUG initiation codons revealed that cells use an elongator leucine-bound transfer RNA (Leu-tRNA) to initiate translation at cryptic CUG start codons. CUG/Leu-tRNA initiation was independent of the canonical initiator tRNA (AUG/Met-tRNA$_i^{Met}$) pathway but required expression of eukaryotic initiation factor 2A. Thus, a tRNA-based translation initiation mechanism allows non–AUG-initiated protein synthesis and supplies peptides for presentation by MHC class I molecules.

In almost all nucleated cells, newly translated polypeptides supply antigenic precursors for loading major histocompatability complex (MHC) class I molecules (*1*). Peptide-loaded MHC class I (pMHC I) molecules reveal the presence of viral or mutated proteins to circulating cytotoxic T cells (CTLs), which bind pMHC I through their T cell receptors to eliminate infected or transformed cells. Antigenic precursors are translated from conventional AUG-initiated open reading frames (ORFs) by the canonical initiator transfer RNA (tRNA), Met-tRNA$_i^{Met}$ (*2*, *3*). Cryptic, non–AUG-initiated ORFs (*4*–*7*) also generate pMHC I during viral infections (*8*–*12*) and oncogenesis (*13*–*15*) by unknown mechanisms. Cryptic CUG start codons can also be decoded with leucine at the initiation stage of translation in mammalian cells (*5*–*7*, *16*). However, this decoding is incompatible with the current model of translation, which indicates that ribosomes are preloaded with initiator Met-tRNA$_i^{Met}$ before recognition of AUG or even non-AUG start codons (*17*).

Our previous study suggested that translation of antigenic precursors from a CUG start codon using leucine represents a distinct initiation pathway (*16*). To determine the molecular mechanism of CUG/leucine initiation, we first screened a series of compounds described as inhibitors of eukaryotic protein synthesis (*18*) using primer extension inhibition analysis (toeprinting) (*19*) of AUG-YL8 and CUG-YL8 mRNA ribosome initiation complexes (fig. S1). We found that NSC119893, which inhibits Met-tRNA$_i^{Met}$ association with eukaryotic initiation factor 2 (eIF2) (*20*), selectively inhibits AUG-YL8 initiation (table S1) in a dose-dependent fashion, whereas CUG-YL8 toeprints were resistant to NSC119893 treatment (Fig. 1A). Structurally unrelated protein synthesis inhibitors, such as suramine and aurin tricarboxylic acid, also inhibited AUG initiation yet enhanced initiation at the CUG start codon (table S1). In contrast, the small molecule acriflavine inhibited CUG initiation more than AUG initiation in a dose-dependent fashion (Fig. 1A). Thus, a structurally diverse set of compounds can distinguish ribosomal recognition of AUG and CUG start codons.

We next assessed the effect of these protein synthesis inhibitors on translation of antigenic precursors in living cells by biochemically analyzing peptides from extracts of cells transfected with the AUG-YL8 or CUG-YL8 plasmids (*5*). As expected, a single peak of antigenic activity—corresponding to the methionine-initiated peptide (MYL8)—was detected from AUG-YL8–transfected cells (Fig. 1B). Yet, CUG-YL8–transfected cells yielded the leucine-initiated peptide (LYL8) as well as the MYL8 peptide, arising from Met-tRNA$_i^{Met}$ "wobble" initiation (Fig. 1C). Although NSC119893 inhibited the expression of MYL8 from AUG and CUG start codons, it did not inhibit decoding of the CUG initiation codon with leucine (LYL8) (Fig. 1, B to D). In contrast, and consistent with the toeprint analysis (Fig. 1A), translation of LYL8 was inhibited by acriflavine, a nucleic acid intercalator, whereas MYL8 initiation from either AUG or CUG codons was unaffected (Fig. 1, B to D). This inhibitor effect was not limited to translation of antigenic precursors, because NSC119893 inhibited AUG-GFP, but not CUG-GFP, expression (fig. S2, A and B). Conversely, CUG-GFP, but not AUG-GFP, expression was inhibited by acriflavine treatment in cultured cells

[1]Division of Immunology and Pathogenesis, Department of Molecular and Cell Biology, University of California, Berkeley, CA 94720, USA. [2]Department of Biochemistry and Molecular Biology, University of Chicago, Chicago, IL 60637, USA. [3]DNA Sequencing Facility, University of California, Berkeley, CA 94720, USA.

*To whom correspondence should be addressed. E-mail: nshastri@berkeley.edu

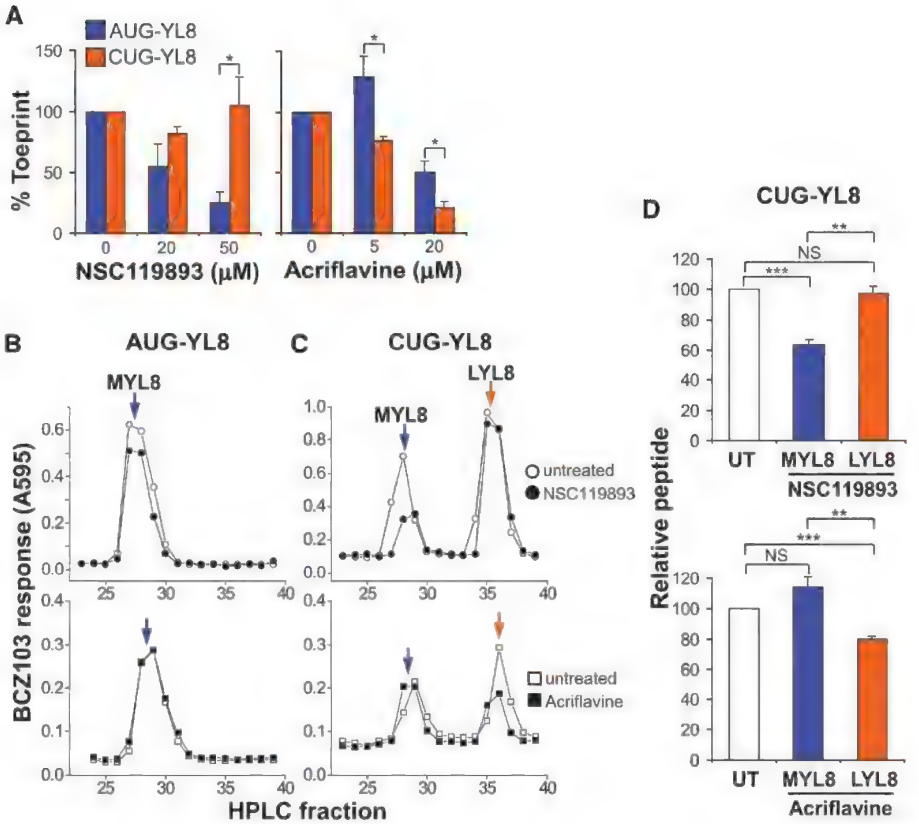

Fig. 1. Cryptic CUG/leucine initiation is differentially affected by protein synthesis inhibitors. (**A**) Toeprint analysis of AUG-YL8 and CUG-YL8 mRNAs (fig. S1), which encode a peptide, either MYL8 or LYL8, respectively, by using RRL in the presence of indicated concentrations of NSC119893 or acriflavine. Data are presented as a percentage of untreated samples (means ± SEM; $n = 2$ or 3). T cell hybridoma response (BCZ103) to (**B**) AUG-YL8 versus (**C**) CUG-YL8–translated peptides from COS-7 cells transfected with plasmid DNAs and treated with NSC119893 (50 μM) or acriflavine (10 μM) for 3 hours (data are representative of three independent experiments). Peptides were acid-extracted and analyzed by reversed-phase high-performance liquid chromatography to resolve the methionine (MYL8)– versus leucine (LYL8)–initiated peptides. Activation of BCZ103 T cell hybridoma was used to measure the amount and identity of peptides produced by initiation at AUG or CUG start codons. (**D**) Peptide abundance from CUG-YL8 in the presence of NSC119893 and acriflavine from (C) (area under the curve) are relative to untreated samples (UT) (means ± SEM; $n = 3$). Statistical significance was evaluated with the unpaired t test (*$P < 0.05$; **$P < 0.01$; ***$P < 0.001$).

(fig. S2C). Because NSC119893 inhibits global protein synthesis (fig. S3) and induces stress by limiting Met-tRNA$_i^{Met}$ availability (*20*, *21*), our analysis suggests that CUG/leucine initiation proceeds independently of the Met-tRNA$_i^{Met}$ initiation pathway and persists during host translation shutoff and stress.

To study cryptic translation in professional antigen-presenting cells (APCs), we used primary APCs from transgenic mice expressing a bicistronic ORF with an AUG/methionine-initiated peptide (WI9) followed by a cryptic CUG/leucine-initiated peptide (LYL8) (fig. S4), both detected by T cell hybridomas (*6*). NSC119893 treatment reduced WI9 presentation to the level observed with the elongation inhibitor cycloheximide (CHX) (Fig. 2A) and induced complete host translation shutoff (fig. S5) in bone marrow–derived dendritic cells (BM-DCs). Unlike inhibition by CHX treatment, however, presentation of the cryptic LYL8 peptide persisted with NSC119893 treatment in BM-DCs (Fig. 2A) and splenocytes (fig. S6A). Thus, NSC119893 inhibited AUG-initiated presentation of the WI9 peptide, such that more than twice the number of NSC119893-treated APCs were required for a half-maximal T cell response (Fig. 2B, blue bar) compared with an equivalent number of APCs presenting the CUG/leucine-initiated LYL8 peptide (Fig. 2B, orange bar). These results show that professional APCs can use distinct initiation mechanisms to translate antigenic precursors during host translation shutoff, such as during stress or viral infection.

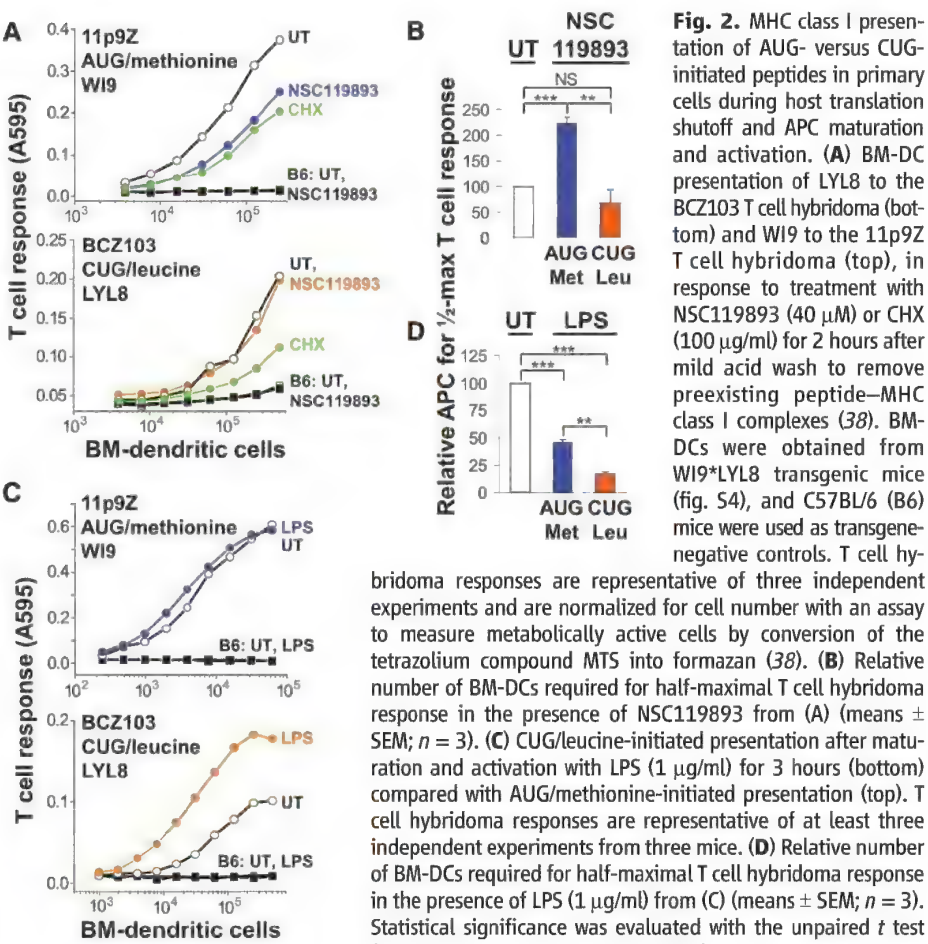

Fig. 2. MHC class I presentation of AUG- versus CUG-initiated peptides in primary cells during host translation shutoff and APC maturation and activation. (**A**) BM-DC presentation of LYL8 to the BCZ103 T cell hybridoma (bottom) and WI9 to the 11p9Z T cell hybridoma (top), in response to treatment with NSC119893 (40 μM) or CHX (100 μg/ml) for 2 hours after mild acid wash to remove preexisting peptide–MHC class I complexes (*38*). BM-DCs were obtained from WI9*LYL8 transgenic mice (fig. S4), and C57BL/6 (B6) mice were used as transgene-negative controls. T cell hybridoma responses are representative of three independent experiments and are normalized for cell number with an assay to measure metabolically active cells by conversion of the tetrazolium compound MTS into formazan (*38*). (**B**) Relative number of BM-DCs required for half-maximal T cell hybridoma response in the presence of NSC119893 from (A) (means ± SEM; $n = 3$). (**C**) CUG/leucine-initiated presentation after maturation and activation with LPS (1 μg/ml) for 3 hours (bottom) compared with AUG/methionine-initiated presentation (top). T cell hybridoma responses are representative of at least three independent experiments from three mice. (**D**) Relative number of BM-DCs required for half-maximal T cell hybridoma response in the presence of LPS (1 μg/ml) from (C) (means ± SEM; $n = 3$). Statistical significance was evaluated with the unpaired t test (*$P < 0.05$; **$P < 0.01$; ***$P < 0.001$).

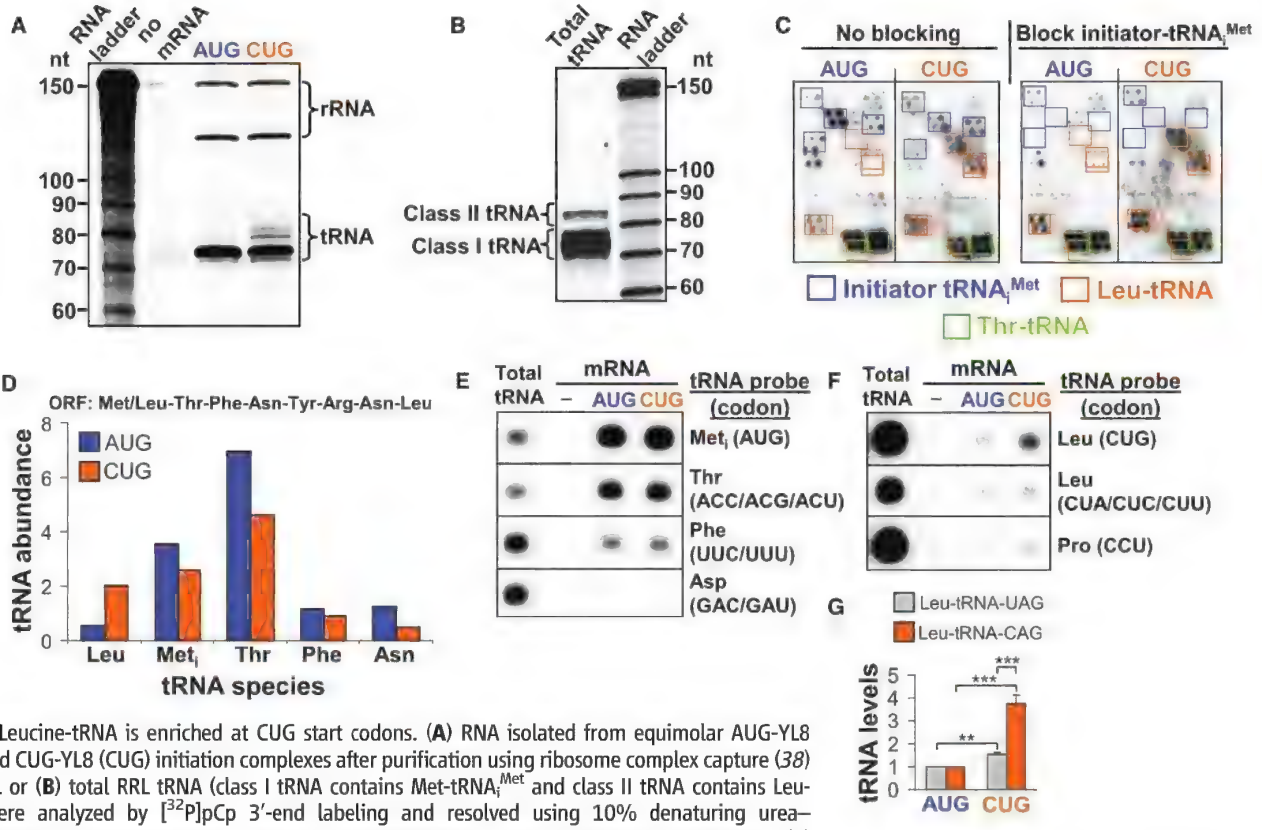

Fig. 3. Leucine-tRNA is enriched at CUG start codons. (**A**) RNA isolated from equimolar AUG-YL8 (AUG) and CUG-YL8 (CUG) initiation complexes after purification using ribosome complex capture (*38*) from RRL or (**B**) total RRL tRNA (class I tRNA contains Met-tRNA$_i^{Met}$ and class II tRNA contains Leu-tRNA) were analyzed by [^{32}P]pCp 3′-end labeling and resolved using 10% denaturing urea–polyacrylamide gel electrophoresis. Data are representative of three independent experiments. (**C**) tRNA microarray analysis of AUG and CUG initiation complexes in the absence (left) or presence (right) of an unlabeled initiator Met-tRNA$_i^{Met}$ probe. tRNA was analyzed using at least three independent microarrays. (**D**) Relative tRNA abundance at AUG and CUG start codons (from C) (presented relative to total tRNA signal quantified) is shown for initiator tRNAs (leucine and methionine) and tRNA present from ribosome elongation (Thr, Phe, and Asn) along the ORF (shown). (**E** and **F**) Northern blot analysis of AUG versus CUG initiation complex tRNAs. Minimal mRNAs (*38*) were used containing only one AUG or CUG start codon. (E) Thr- and Phe-tRNAs are derived from A-site occupancy and elongation, respectively. The same Northern blot was stripped and reprobed with the indicated full-length tRNA probes, and each blot shown is from an equivalent PhosphoImager exposure. Data are representative of four independent experiments. (**G**) Quantification of Leu-tRNA with anticodon 5′-CAG-3′ (Leu-tRNA-CAG) in CUG initiation complexes from (F) (means ± SEM; $n = 4$). Statistical significance was evaluated with the unpaired t test (*$P < 0.05$; **$P < 0.01$; ***$P < 0.001$).

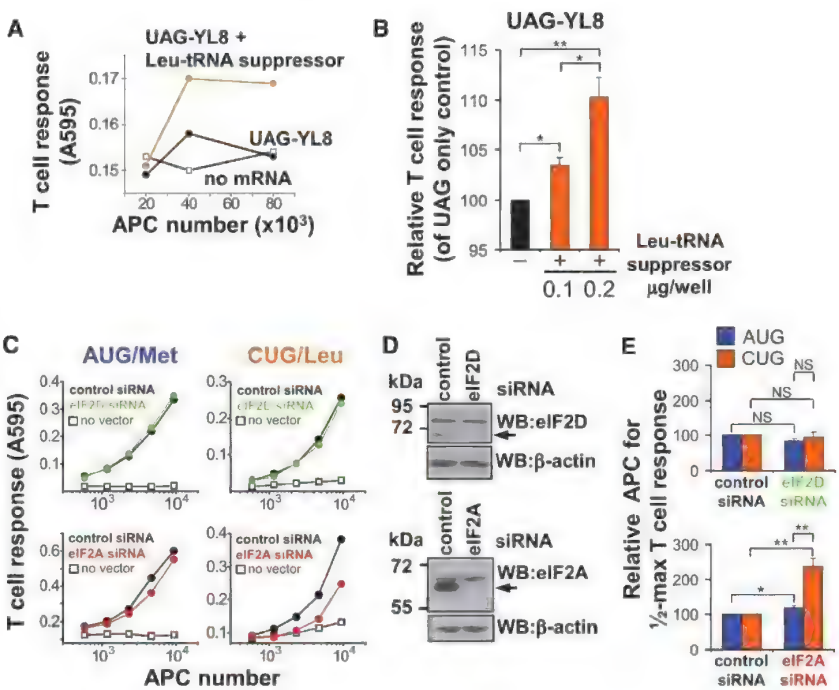

Fig. 4. Leu-tRNA participates in a distinct translation initiation pathway. (**A**) HeLa H2-K^b cells (APCs) were transfected with UAG-YL8 mRNA alone or with Leu-tRNA-CAG containing a 5′-CUA-3′ anticodon (Leu-tRNA suppressor) to recognize the UAG stop codon. T cell hybridoma (BCZ103) activation measures the generation of the leucine-initiated LYL8 peptide in the presence of Leu-tRNA suppressor (data are representative of three independent experiments) (**B**) in a dose-dependent manner (means ± SEM; $n = 3$). (**C**) L-cell fibroblasts expressing H2-K^b (APCs) were subjected to control, eIF2D, or eIF2A siRNA-mediated knockdown before transfection with plasmid DNAs encoding the bicistronic WI9*LYL8 sequence (fig. S4) and H2-D^b. AUG/methionine-initiated presentation of WI9 was measured with the 11p9Z T cell hybridoma and CUG/leucine-initiated presentation of LYL8 was measured with the BCZ103 T cell hybridoma. (**D**) Western blot analysis of control, eIF2D, and eIF2A siRNA knockdown in cells from (C). Data in (C) and (D) are representative of three independent experiments. (**E**) Relative number of APCs required for half-maximal T cell hybridoma response in the presence of either eIF2D (top) or eIF2A (bottom) siRNA knockdown from (C) (means ± SEM; $n = 3$). Statistical significance was evaluated with the unpaired t test (*$P < 0.05$; **$P < 0.01$).

Dendritic cells are key for initiating immune responses (*22*) and, upon activation, undergo numerous modifications (*23*, *24*). We therefore analyzed antigen presentation of LYL8 and WI9 peptides in immature versus lipopolysaccharide (LPS)–activated APCs. Although LPS exposure enhanced AUG/methionine-initiated WI9 presentation (Fig. 2C), CUG/leucine-initiated antigen presentation of LYL8 peptide was substantially enhanced (Fig. 2C), despite comparable expression of pMHC I on LPS-activated cells (fig. S7, A and B). With ex vivo (Fig. 2D) and in vivo LPS exposure (fig. S7, D and E), less than one-quarter of the number of BM-DCs (Fig. 2D, orange bar) and splenocytes (fig. S7, C to E) presenting LYL8 were required for a half-maximal T cell response. This effect is also seen with a lower Met-tRNA$_i^{Met}$ inhibitor concentration (NSC119893) (fig. S6B), which indicates that different cell stimuli profoundly increase cryptic CUG/leucine-initiated translation. Thus, the cryptic pMHC I repertoire can be enhanced in vivo by even a short LPS exposure in professional APCs.

To understand the molecular basis of CUG/leucine initiation, we developed a technique to analyze initiator tRNAs from ribosome initiation complexes stalled at the start codons of either the AUG-YL8 or CUG-YL8 mRNAs (fig. S8). Using this technique, we isolated intact ribosomal initiation complexes bound to AUG or CUG start codons as indicated by the enrichment of ribosomal RNA (rRNA) relative to the control with no mRNA (Fig. 3A). In addition, material migrating at the size expected for type I tRNAs (74 to 77 nucleotides), such as initiator Met-tRNA$_i^{Met}$, was observed from both AUG and CUG initiation complexes (Fig. 3A). However, a single nucleotide substitution of A to C (AUG to CUG) in the mRNA yielded at least one additional distinct band (Fig. 3A) migrating with larger type II tRNAs, which typically contain Leu-tRNA isoacceptors bearing longer variable loops (Fig. 3B).

Next, tRNA microarray analysis (*25*) showed that both AUG and CUG initiation complexes contained Met-tRNA$_i^{Met}$ hybridization signals that could be blocked with an unlabeled Met-tRNA$_i^{Met}$ probe (Fig. 3C, blue boxes). However, Leu-tRNA was enriched in CUG initiation complexes (Fig. 3C, orange boxes, and Fig. 3D). In addition, Thr-tRNA signal was observed from both AUG and CUG initiation complexes, because the second codon of the ORF codes for threonine (ACC) (Fig. 3, C and D). Furthermore, lower amounts of both Phe-tRNA and Asn-tRNA were also detected, which indicated that some ribosomes could participate in up to two rounds of elongation (Fig. 3D).

The nature of tRNA present in AUG and CUG initiation complexes was further confirmed by Northern blot analysis with full-length tRNA probes. As expected, initiator Met-tRNA$_i^{Met}$ was detected at both start codons (Fig. 3E), whereas Asp-tRNA (no aspartic acid codons in the ORF) was not detected. The presence of Thr-tRNA and Phe-tRNA indicated that both AUG and CUG initiation complexes were competent for A-site selection and elongation (Fig. 3E). As the tRNA microarray results indicated, the larger migrating bands from the CUG initiation complex (Fig. 3A) were of Leu-tRNA origin, as a strong signal for Leu-tRNA with the anticodon 5′-CAG-3′ (Leu-tRNA-CAG), but not Leu-tRNA-UAG or Pro-tRNA, was enriched in the sample (Fig. 3, F and G).

To test whether Leu-tRNA initiation at CUG start codons can be extended to non–AUG-initiated cellular mRNAs, we analyzed the CUG-initiated isoform of Myc, a factor implicated in oncogenesis (*26*) and previously found associated with initiation complexes using ribosome profiling (*27*). Initiation complexes were detected at the Myc CUG start codon by using toeprinting (fig. S9A) and were also found to contain Leu-tRNA-CAG (fig. S9B). Together, these results indicate that leucine initiation (*5*, *6*) is not the result of initiator tRNA$_i^{Met}$ misacylation (*28*, *29*) but is a mechanistically distinct pathway for Leu-tRNA decoding of CUG start codons

To our surprise, analysis of ribosome assembly (toeprinting) in the presence of Leu-tRNA-CAG and Leu-tRNA-UAG, but not Leu-tRNA-UAA, inhibited AUG but not CUG toeprints in rabbit reticulocyte lysate (RRL) (fig. S10, A and B). Moreover, added tRNA per se did not inhibit initiation, because an equivalent amount of total tRNA, which contains initiator Met-tRNA$_i^{Met}$, actually enhanced both AUG and CUG toeprints (fig. S10, A and B). Further, when we used tRNA-depleted RRL (fig. S10C) (*30*), Leu-tRNA-CAG specifically stimulated CUG but not AUG initiation, whereas total tRNA enhanced initiation at both the AUG and CUG start codons (fig. S10D). This suggests that a portion of ribosomal subunits is not preloaded with initiator tRNA and is receptive to both Met-tRNA$_i^{Met}$ and Leu-tRNA-CAG loading for initiation at CUG start codons.

We next tested whether Leu-tRNA initiates translation of antigenic precursors in living cells, using a stop-codon suppression technique that utilizes a tRNA suppressor to decode a unique stop codon present within the ORF (*31*, *32*). HeLa H2-K^b–expressing cells were transfected with UAG-YL8 mRNA (UAG replaced CUG) with or without Leu-tRNA suppressor. Activation of the T cell hybridoma by the H2-K^b–presented LYL8 peptide was observed only when Leu-tRNA suppressor was also present (Fig. 4A) and was enhanced in a dose-dependent manner (Fig. 4B). Thus, Leu-tRNA can function as an initiator tRNA in cells to generate an antigenic precursor for presentation by MHC class I molecules.

How Leu-tRNA is delivered to the P-site of the ribosome independent of the Met-tRNA$_i^{Met}$•eIF2 pathway is unclear. Previously, the initiation factors eIF2D (formerly called ligatin and functionally complemented by MCT-1 and DENR) (*33*, *34*) and eIF2A (*35*, *36*) have been shown in vitro to stimulate initiation with elongator tRNAs (e.g., Phe-tRNA) in addition to canonical initiator Met-tRNA$_i^{Met}$. Therefore, we tested the effect of small interfering RNA (siRNA)–mediated knockdown of eIF2D or eIF2A on the presentation of AUG-initiated WI9 versus CUG-initiated LYL8. Neither AUG/methionine- nor CUG/leucine-initiated presentation was altered with eIF2D knockdown (Fig. 4, C to E). In contrast, eIF2A knockdown significantly inhibited CUG/leucine-initiated, not AUG/methionine-initiated, presentation (Fig. 4, C and D) and required more than twice the number of eIF2A-siRNA–treated APCs to achieve a half-maximal T cell response (Fig. 4E). The finding that CUG/leucine-initiated presentation required at least eIF2A, yet was insensitive to reduced Met-tRNA$_i^{Met}$•eIF2 levels (Fig. 1C, Fig. 2A, and fig. S2A), indicated that initiation at CUG start codons with leucine utilizes an eIF2A-dependent pathway, which may be necessary during infection (*37*) or translation of endogenous CUG-initiated proteins.

Degeneracy is a hallmark of biological systems. Just as multiple codons are decoded with the same amino acid, CUG start codons may be decoded by more than one initiator tRNA. We propose that the highly regulated step of translation initiation is governed by at least two mechanistically distinct pathways at the level of the initiator tRNA. The alternative initiation pathway that uses Leu-tRNA to decode CUG start codons can explain why usage of CUG-initiated 5′-untranslated regions occurs frequently in cells (*27*) and can also provide polypeptide precursors for presentation by MHC class I (*4*).

References and Notes

1. N. Shastri, S. Schwab, T. Serwold, *Annu. Rev. Immunol.* **20**, 463 (2002).
2. M. Kozak, *J. Mol. Biol.* **196**, 947 (1987).
3. T. V. Pestova, S. I. Borukhov, C. U. Hellen, *Nature* **394**, 854 (1998).
4. S. R. Starck, N. Shastri, *Cell. Mol. Life Sci.* **68**, 1471 (2011).
5. S. Malarkannan, T. Horng, P. P. Shih, S. Schwab, N. Shastri, *Immunity* **10**, 681 (1999).
6. S. R. Schwab, K. C. Li, C. Kang, N. Shastri, *Science* **301**, 1367 (2003).
7. S. R. Schwab, J. A. Shugart, T. Horng, S. Malarkannan, N. Shastri, *PLoS Biol.* **2**, e366 (2004).
8. S. M. Mayrand, D. A. Schwarz, W. R. Green, *J. Immunol.* **160**, 39 (1998).
9. N. J. Maness *et al.*, *J. Exp. Med.* **204**, 2505 (2007).
10. A. Bansal *et al.*, *J. Exp. Med.* **207**, 51 (2010).
11. N. J. Maness *et al.*, *J. Virol.* **84**, 11569 (2010).
12. C. T. Berger *et al.*, *J. Exp. Med.* **207**, 61 (2010).
13. H. Dolstra *et al.*, *J. Exp. Med.* **189**, 301 (1999).
14. C. Ronsin *et al.*, *J. Immunol.* **163**, 483 (1999).
15. A. O. Weinzierl *et al.*, *Cancer Res.* **68**, 2447 (2008).
16. S. R. Starck *et al.*, *PLoS ONE* **3**, e3460 (2008).
17. T. V. Pestova, C. U. T. Hellen, *Cell. Mol. Life Sci.* **57**, 651 (2000).
18. O. Novac, A. S. Guenier, J. Pelletier, *Nucleic Acids Res.* **32**, 902 (2004).
19. M. Kozak, *Nucleic Acids Res.* **26**, 4853 (1998).
20. F. Robert *et al.*, *Mol. Biol. Cell* **17**, 4632 (2006).
21. S. Mokas *et al.*, *Mol. Biol. Cell* **20**, 2673 (2009).
22. J. Banchereau, R. M. Steinman, *Nature* **392**, 245 (1998).
23. I. Mellman, R. M. Steinman, *Cell* **106**, 255 (2001).
24. H. Lelouard *et al.*, *J. Cell Biol.* **179**, 1427 (2007).
25. K. A. Dittmar, J. M. Goodenbour, T. Pan, *PLoS Genet.* **2**, e221 (2006).
26. S. R. Hann, M. W. King, D. L. Bentley, C. W. Anderson, R. N. Eisenman, *Cell* **52**, 185 (1988).
27. N. T. Ingolia, L. F. Lareau, J. S. Weissman, *Cell* **147**, 789 (2011).

28. A. L. Németh *et al.*, *FEBS J.* **274**, 1610 (2007).
29. N. Netzer *et al.*, *Nature* **462**, 522 (2009).
30. R. J. Jackson, S. Napthine, I. Brierley, *RNA* **7**, 765 (2001).
31. M. Sisido, in *Chemical Biology: From Small Molecules to Systems Biology and Drug Design*, S. L. Schreiber, T. M. Kapoor, G. Wess, Eds. (Wiley-VCH Verlag, Weinheim, Germany, 2007), vol. 1, pp. 271–284.
32. R. Geslain, T. Pan, *J. Mol. Biol.* **396**, 821 (2010).
33. S. E. Dmitriev *et al.*, *J. Biol. Chem.* **285**, 26779 (2010).
34. M. A. Skabkin *et al.*, *Genes Dev.* **24**, 1787 (2010).
35. W. C. Merrick, W. F. Anderson, *J. Biol. Chem.* **250**, 1197 (1975).
36. S. L. Adams, B. Safer, W. F. Anderson, W. C. Merrick, *J. Biol. Chem.* **250**, 9083 (1975).
37. J. H. Kim, S. M. Park, J. H. Park, S. J. Keum, S. K. Jang, *EMBO J.* **30**, 2454 (2011).
38. Materials and methods are available as supplementary materials on *Science* Online.

Acknowledgments: We thank K. Collins, A. H. Bakker, K. Chen, N. Nagarajan, and T. Greene for helpful discussions and advice; Y. Ow for initial experiments with NSC119893; and N. Nagarajan and K. Lind for assistance with intravenous injections. The data presented in this paper are tabulated in the main paper and in the supplementary materials. S.R.S. was supported in part by an NIH training grant, a postdoctoral fellowship from the Cancer Research Institute, and a National Research Service Award (NRSA) fellowship from the NIH. M.P.-E was supported by an NIH training grant and by the Ruth Kirschstein NRSA predoctoral fellowship. This research was supported by grants from the NIH to N.S. and T.P. and the International AIDS Vaccine Initiative to N.S. The authors declare no competing financial interests.

Supplementary Materials

www.sciencemag.org/cgi/content/full/336/6089/1719/DC1
Materials and Methods
Figs. S1 to S10
Table S1
References (*39*–*42*)

8 February 2012; accepted 25 April 2012
10.1126/science.1220270

CTD Tyrosine Phosphorylation Impairs Termination Factor Recruitment to RNA Polymerase II

Andreas Mayer,[1]* Martin Heidemann,[2]* Michael Lidschreiber,[1] Amelie Schreieck,[1] Mai Sun,[1] Corinna Hintermair,[2] Elisabeth Kremmer,[3] Dirk Eick,[2]† Patrick Cramer[1]†

In different phases of the transcription cycle, RNA polymerase (Pol) II recruits various factors via its C-terminal domain (CTD), which consists of conserved heptapeptide repeats with the sequence Tyr[1]-Ser[2]-Pro[3]-Thr[4]-Ser[5]-Pro[6]-Ser[7]. We show that the CTD of transcribing yeast Pol II is phosphorylated at Tyr[1], in addition to Ser[2], Thr[4], Ser[5], and Ser[7]. Tyr[1] phosphorylation stimulates binding of elongation factor Spt6 and impairs recruitment of termination factors Nrd1, Pcf11, and Rtt103. Tyr[1] phosphorylation levels rise downstream of the transcription start site and decrease before the polyadenylation site, largely excluding termination factors from gene bodies. These results show that CTD modifications trigger and block factor recruitment and lead to an extended CTD code that explains transcription cycle coordination on the basis of differential phosphorylation of Tyr[1], Ser[2], and Ser[5].

The C-terminal domain (CTD) is a flexible, tail-like extension of RNA polymerase (Pol) II and consists of 26 (yeast) or 52 (human) highly conserved heptapeptide repeats of the consensus sequence Tyr[1]-Ser[2]-Pro[3]-Thr[4]-Ser[5]-Pro[6]-Ser[7]. During the transcription cycle, changes in CTD phosphorylation patterns coordinate the recruitment of transcription and mRNA processing factors to Pol II (*1*–*3*). During early transcription, Ser[5] phosphorylation recruits the mRNA capping enzyme (*4*, *5*). Ser[2] phosphorylation occurs during transcription elongation and functions in recruitment of RNA 3′-processing and termination factors (*6*). Phosphorylations at Ser[7] (*7*–*9*) and Thr[4] (*10*) have roles in processing of specific RNAs. Tyr[1] phosphorylation was described for human Pol II almost two decades ago (*11*), but whether this has a functional role and whether it exists in other species are unknown.

We generated a monoclonal antibody against a Tyr[1]-phosphorylated CTD peptide (3D12, Methods). Because the functional CTD unit is a pair of repeats (*12*), we determined antibody specificity by using di-heptapeptides bearing combinations of phosphorylations (Fig. 1A and fig. S1). This revealed a high affinity for the Tyr[1]-phosphorylated CTD that was not impaired by adjacent Ser[2] phosphorylation and no affinity to other CTD peptides (Fig. 1A and fig. S1). The antibody immunoprecipitated Pol II from extracts of the yeast *Saccharomyces cerevisiae* (Fig. 1B), and the precipitated polymerases were also phosphorylated at Ser[2], Ser[5], and Ser[7] (fig. S2). The antibody also recognized Pol II that was purified from human cells with antibody 1C7 (fig. S1) and phosphorylated in vitro by the Tyr[1] kinase c-Abl (*13*) (Fig. 1C). Thus, antibody 3D12 specifically recognizes the Tyr[1]-phosphorylated CTD, and Tyr[1] phosphorylation occurs in yeast.

To investigate whether genome-associated Pol II is phosphorylated at Tyr[1], we used high-resolution chromatin immunoprecipitation (ChIP) profiling in proliferating yeast (*14*). Data from two biological replicates ($R = 0.94$) were averaged and revealed strong signals over protein-coding and small nucleolar RNA genes (fig. S3). To test whether Tyr[1] phosphorylation occurs on all transcribed protein-coding genes, we measured covariation in ChIP data for other CTD phosphorylations by singular value decomposition (*14*). The first singular vector explained 83.8% of the variance (fig. S4), indicating a similar occurrence of phosphorylations at Tyr[1],

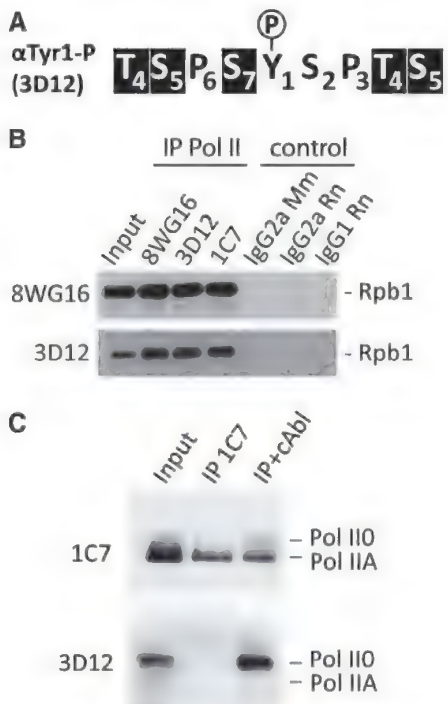

Fig. 1. Pol II CTD is phosphorylated at Tyr[1]. (**A**) Part of the CTD sequence around phosphorylated Tyr[1] (Y_1). Residues Ser[2], Pro[3], Thr[4], Ser[5], Pro[6], and Ser[7] are denoted S_2, P_3, T_4, S_5, P_6, and S_7, respectively. CTD residues that interfere with 3D12 antibody binding upon phosphorylation are highlighted in black. (**B**) Western blot analysis of whole-cell extract from proliferating yeast (Input). Pol II was immunoprecipitated with antibodies 8WG16, 3D12, and 1C7 (IP Pol II) and probed with 8WG16 or 3D12. Isotype controls are shown. Ig, immunoglobulin. (**C**) Antibody 3D12 detects CTD Tyr[1] phosphorylation in HeLa cells (Input). Pol II was immunoprecipitated with antibody 1C7 (IP 1C7, fig. S1) and incubated with cAbl kinase, leading to a 3D12 signal (IP+cAbl). The hyper- (IIO) and hypophosphorylated forms (IIA) of Pol II are indicated.

[1]Gene Center and Department of Biochemistry, Center for Integrated Protein Science Munich (CIPSM), Ludwig-Maximilians-Universität München, Feodor-Lynen-Strasse 25, 81377 Munich, Germany. [2]Department of Molecular Epigenetics, Helmholtz Zentrum München and CIPSM, Marchioninistrasse 25, 81377 Munich, Germany. [3]Institute of Molecular Immunology, Helmholtz Zentrum München, Marchioninistrasse 25, 81377 Munich, Germany.

*These authors contributed equally to this work.
†To whom correspondence should be addressed. E-mail: eick@helmholtz-muenchen.de (D.E.); cramer@genzentrum.LMU.de (P.C.).

Ser^2, and Ser^5. A correlation between levels of Tyr^1 phosphorylation and mRNA expression (*15*) (fig. S5A) further indicated that Tyr^1 phosphorylation is functionally relevant.

Gene-averaging of ChIP profiles (*14*) revealed Tyr^1 phosphorylation in the coding region (Fig. 2, A and B). Whereas Tyr^1 phosphorylation signals were low at promoters, they increased downstream of the transcription start site (TSS). The gene-averaged profile resembled that for Ser^2 phosphorylation, except that Ser^2 phosphorylation signals persist downstream of the polyadenylation (pA) site for ~200 nucleotides (nt), whereas Tyr^1 phosphorylation signals decrease already around 180 nt upstream of the pA site (Fig. 2, A, B, and D). The point of Tyr^1 phosphorylation signal increase was dependent on the TSS, whereas the point of decrease was dependent on the pA site but not on gene length or expression level (Fig. 2D and figs. S5B and S6). These results indicate that Tyr^1 phosphorylation marks are set and removed within the transcription cycle.

To investigate whether Tyr^1 phosphorylation influences factor recruitment to Pol II, we determined genomic occupancy profiles for termination factors Nrd1, Rtt103, and Pcf11, which contain a CTD-interacting domain (CID). The gene-averaged Nrd1 occupancy peaked at the beginning of the transcribed region, 193 ± 44 nt downstream of the TSS (Fig. 2C). This region also showed maximum signals in Ser^5 phosphorylation, and genomic Nrd1 and Ser^5 phosphorylation profiles correlate (R = 0.6), consistent with Nrd1 binding to the Ser^5-phosphorylated CTD (*16*). The general presence of Nrd1 at protein-coding genes extends previous results (*17*, *18*) and befits a role of Nrd1 in early transcription termination (*2*, *19*–*21*). Rtt103 showed peak occupancy at the end of genes, 112 ± 27 nt downstream of the pA site, where peak levels of Pcf11 were also observed (*14*) (Fig. 2C and fig. S7). Because this region shows the maximum difference between Ser^2 and Tyr^1 phosphorylation signals, Tyr^1 phosphorylation may impair recruitment of Rtt103 and Pcf11 upstream of the pA site. Consistent with this, genome-wide occupancies of Rtt103 and Pcf11 do not correlate well with Ser^2 phosphorylation signals (R = 0.4, for both), although both proteins bind the Ser^2-phosphorylated CTD (*22*, *23*).

To test whether Tyr^1 phosphorylation impairs CTD binding of termination factors, we determined the affinity of purified recombinant CIDs of yeast Nrd1, Pcf11, and Rtt103 for various CTD diheptad phosphopeptides (table S1) by using fluorescence anisotropy (Fig. 3, A to C, and fig. S8). None of the CIDs bound to an unphosphorylated CTD peptide. Consistent with previous results (*16*, *23*), Pcf11-CID and Rtt103-CID bound to the Ser^2-phosphorylated CTD peptide [dissociation constants (K_D) = 54 ± 6 μM (±SD) and 12 ± 2 μM, respectively; Methods], whereas the Nrd1-CID preferentially bound to a Ser^5-phosphorylated CTD peptide (K_D = 85 ± 25 μM). In contrast, none of the CIDs bound Tyr^1-phosphorylated CTD peptides, regardless of whether additional phosphorylations were present or not. Thus, Tyr^1 phosphorylation blocks CID binding to the CTD in vitro, consistent with the hypothesis that it impairs termination factor recruitment in vivo.

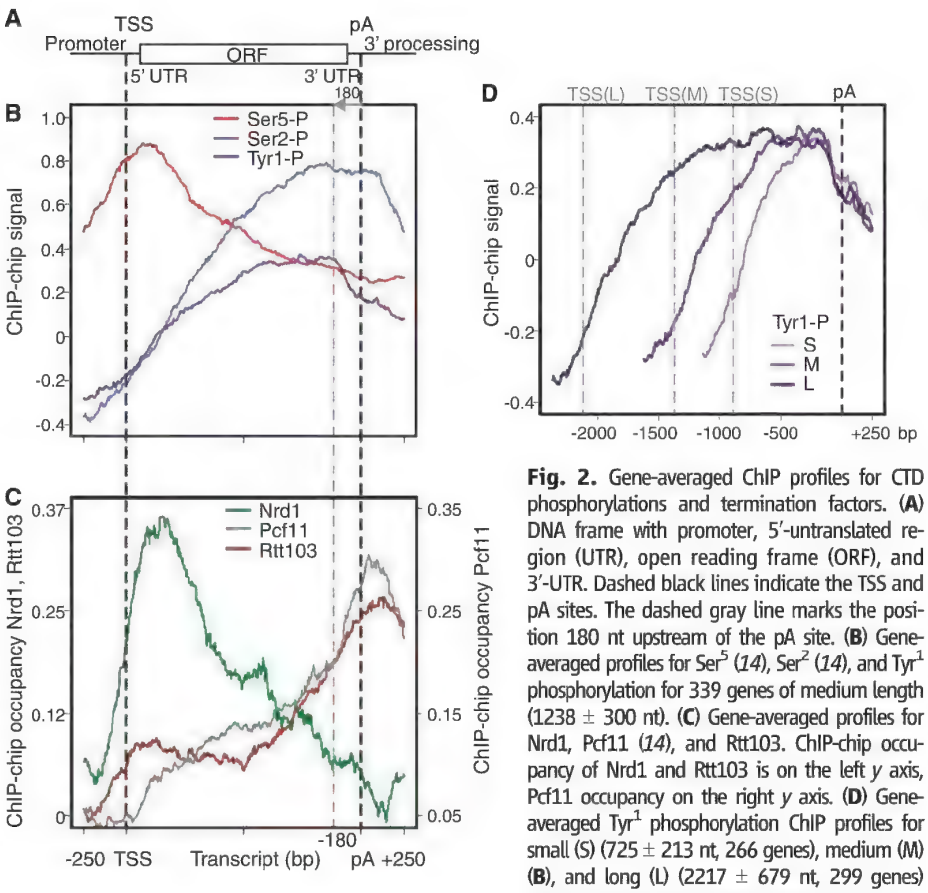

Fig. 2. Gene-averaged ChIP profiles for CTD phosphorylations and termination factors. **(A)** DNA frame with promoter, 5′-untranslated region (UTR), open reading frame (ORF), and 3′-UTR. Dashed black lines indicate the TSS and pA sites. The dashed gray line marks the position 180 nt upstream of the pA site. **(B)** Gene-averaged profiles for Ser^5 (*14*), Ser^2 (*14*), and Tyr^1 phosphorylation for 339 genes of medium length (1238 ± 300 nt). **(C)** Gene-averaged profiles for Nrd1, Pcf11 (*14*), and Rtt103. ChIP-chip occupancy of Nrd1 and Rtt103 is on the left *y* axis, Pcf11 occupancy on the right *y* axis. **(D)** Gene-averaged Tyr^1 phosphorylation ChIP profiles for small (S) (725 ± 213 nt, 266 genes), medium (M) (B), and long (L) (2217 ± 679 nt, 299 genes) gene-length classes, aligned at the pA site.

Structural modeling reveals how Tyr^1 phosphorylation blocks the CID-CTD interaction. Crystal structures of Ser^2-phosphorylated CTD peptides bound to Pcf11-CID (*22*) and Rtt103-CID (*23*) are available, and the structure of the Nrd1-CID (*16*) is known. In the Pcf11-CTD structure, the Tyr^1 hydroxyl group forms a hydrogen bond with the Asp^{68} side chain in the CID (*22*) (fig. S9A). This indicates that Tyr^1 phosphorylation blocks CTD binding because of electrostatic repulsion of two negatively charged groups, the Asp^{68} side chain and the Tyr^1 phosphate. The CTD-binding aspartate residue is conserved in the Nrd1 CID (*16*). In the Rtt103-CTD structure, the corresponding residue, Asn^{65}, forms a hydrogen bond with the Tyr^1 hydroxyl group (*23*) that is incompatible with Tyr^1 phosphorylation. Generally, a Tyr^1 phosphate group modeled onto CTD peptides in CID complex structures results in steric clashes (fig. S9B).

Structural considerations also indicated that Thr^4 phosphorylation (*10*) interferes with CID binding by destabilizing the bound CTD conformation (*22*). This predicted that Thr^4 phosphorylation levels at the pA site are low, to enable recruitment of Pcf11 and Rtt103. Indeed, ChIP profiling revealed that Thr^4 phosphorylation is limited to the transcribed region (fig. S10). Modeling further indicated that Ser^7 phosphorylation is unlikely to interfere with CTD-CID binding, consistent with Nrd1 recruitment in the 5′ region of genes where Ser^7 phosphorylation levels are high (*14*). Thus, genome-wide signals of CTD phosphorylation at Thr^4 and Ser^7 are consistent with the function of Tyr^1 phosphorylation in impairing termination factor recruitment.

To investigate whether Tyr^1 phosphorylation also impairs CTD interactions of factors with other CTD-binding domains, we investigated the tandem Src homology 2 (SH2) domain of elongation factor Spt6. This domain binds the Ser^2-phosphorylated CTD (*24*–*27*) and is required for high Spt6 occupancy on transcribed genes (*14*), suggesting that Tyr^1 phosphorylation does not interfere with its CTD binding. Indeed, the recombinant domain (residues 1250 to 1444) bound very well to CTD peptides phosphorylated at Tyr^1, Tyr^1 and Ser^2, or Tyr^1 and Ser^5 but not to unphosphorylated CTD (Fig. 3D). These results were consistent with recent data (*26*, *27*) and showed that interactions with Tyr^1-phosphorylated CTD peptides were even stronger than for peptides with phosphorylations at Ser^2 or Ser^5 alone. This shows that Tyr^1 phosphorylation stimulates CTD binding of a bona fide elongation factor.

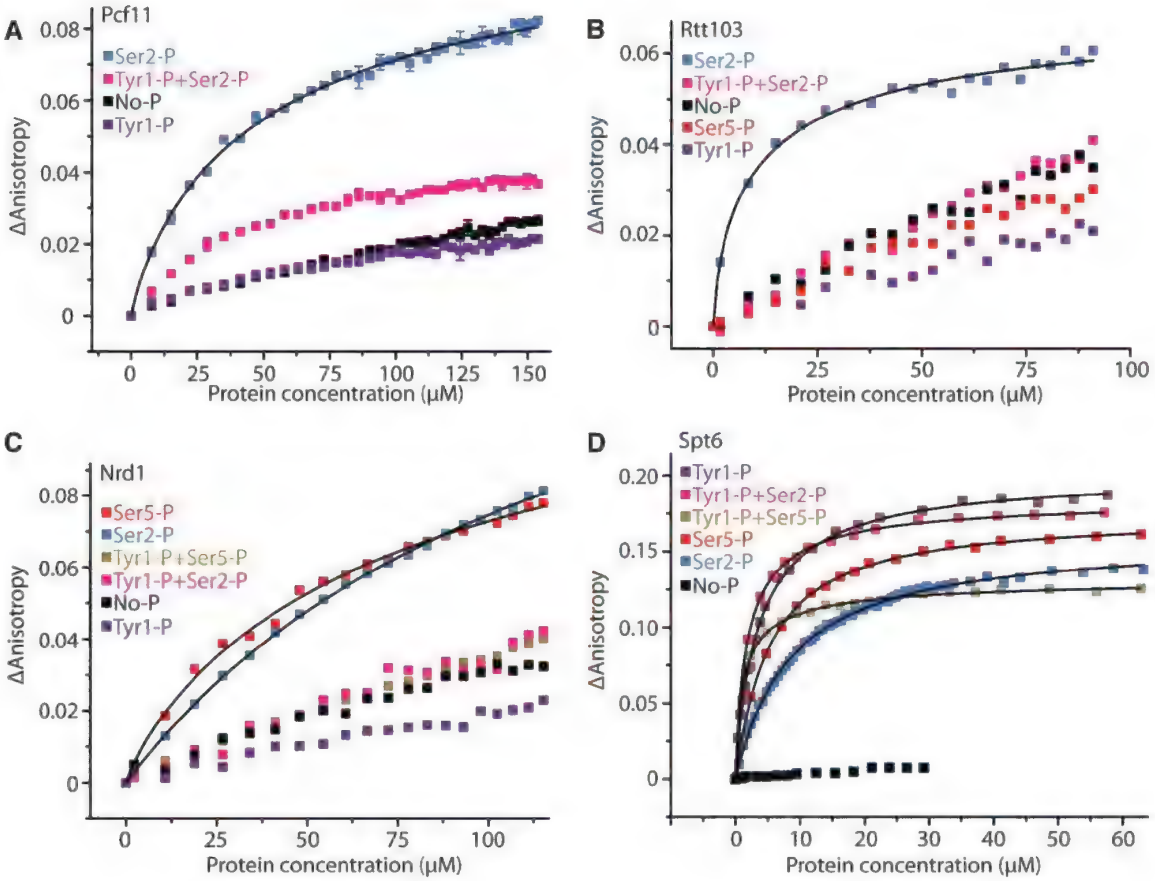

Fig. 3. CTD Tyr^1 phosphorylation blocks termination factor binding. Fluorescence anisotropy titration of CTD peptides with recombinant Pcf11-CID (**A**), Rtt103-CID (**B**), Nrd1-CID (**C**), and Spt6 tandem SH2 domain (**D**). When possible, binding affinity was determined as the protein concentration at half-maximum binding by nonlinear Hill fit (Origin). The remaining affinity of Pcf11-CID for the Tyr^1/Ser^2-phosphorylated CTD peptide was not observed at higher salt concentration (fig. S7). Tyr^1-phosphorylated CTD peptides were not bound by CIDs [(A) to (C)], but by Spt6 tandem SH2 domain (for Tyr1-P, K_D = 3.6 ± 0.15 μM; Tyr1-P+Ser2-P, K_D = 1.9 ± 0.04 μM; Tyr1-P+Ser5-P, K_D = 1.3 ± 0.06 μM; Ser2-P, K_D = 8.4 ± 0.19 μM; Ser5-P, K_D = 5.2 ± 0.09 μM).

We tested whether Tyr^1 phosphorylation depends on one of the yeast CTD kinases, Kin28, Srb10, Bur1, or Ctk1, which correspond to human Cdk7, Cdk8, Cdk9, and Cdk12, respectively. Inhibition of these kinases in vivo did not significantly affect Tyr^1 phosphorylation signals (table S2 and fig. S11). This indicates that Tyr^1 phosphorylation of the yeast CTD depends on a kinase other than the known CTD kinases. Consistent with this, Tyr^1 phosphorylation in human cells is achieved by c-Abl (*13*), a kinase that lacks a yeast homolog.

Our results extend the previously proposed CTD code (*3*, *28*, *29*), which was based on Ser^2 and Ser^5 phosphorylation, leading to an extended CTD code for the coordination of the transcription cycle with factor recruitment (fig. S12). During initiation and early elongation, the CTD is phosphorylated on Ser^5, which facilitates recruitment of the capping enzyme and Nrd1. Peak occupancy levels are reached for Nrd1 and Pol II 150 to 200 nt downstream of the TSS (*14*), likely marking a decision point where Pol II transiently pauses and either terminates or continues elongation (*2*). When Tyr^1 and Ser^2 phosphorylation levels rise, Pol II binds elongation factors stably and continues elongation. Tyr^1 phosphorylation releases Nrd1 and impairs recruitment of Rtt103 and Pcf11, suppressing termination during elongation. Before the pA site, Tyr^1 phosphorylation levels drop, whereas Ser^2 phosphorylation levels remain high. This enables recruitment of Rtt103 and Pcf11 that is enhanced by cooperative interactions between factors (*23*) and with nascent RNA (*18*), resulting in 3′-RNA processing and transcription termination. Our results indicate that Tyr^1 CTD phosphorylation is a target to activate transcription by suppressing Pol II termination and explain why mutation of Tyr^1 to phenylalanine, which lacks the oxygen atom required for phosphorylation, is lethal (*30*).

References and Notes

1. R. D. Chapman, M. Heidemann, C. Hintermair, D. Eick, *Trends Genet.* **24**, 289 (2008).
2. S. Buratowski, *Mol. Cell* **36**, 541 (2009).
3. J. L. Corden, *Science* **318**, 1735 (2007).
4. P. Komarnitsky, E.-J. Cho, S. Buratowski, *Genes Dev.* **14**, 2452 (2000).
5. S. C. Schroeder, B. Schwer, S. Shuman, D. Bentley, *Genes Dev.* **14**, 2435 (2000).
6. S. H. Ahn, M. Kim, S. Buratowski, *Mol. Cell* **13**, 67 (2004).
7. R. D. Chapman *et al.*, *Science* **318**, 1780 (2007).
8. M. Kim, H. Suh, E.-J. Cho, S. Buratowski, *J. Biol. Chem.* **284**, 26421 (2009).
9. S. Egloff *et al.*, *Science* **318**, 1777 (2007).
10. J.-P. Hsin, A. Sheth, J. L. Manley, *Science* **334**, 683 (2011).
11. R. Baskaran, M. E. Dahmus, J. Y. Wang, *Proc. Natl. Acad. Sci. U.S.A.* **90**, 11167 (1993).
12. J. W. Stiller, M. S. Cook, *Eukaryot. Cell* **3**, 735 (2004).
13. R. Baskaran, S. R. Escobar, J. Y. J. Wang, *Cell Growth Differ.* **10**, 387 (1999).
14. A. Mayer *et al.*, *Nat. Struct. Mol. Biol.* **17**, 1272 (2010).
15. S. Dengl, A. Mayer, M. Sun, P. Cramer, *J. Mol. Biol.* **389**, 211 (2009).
16. L. Vasiljeva, M. Kim, H. Mutschler, S. Buratowski, A. Meinhart, *Nat. Struct. Mol. Biol.* **15**, 795 (2008).
17. H. Kim *et al.*, *Nat. Struct. Mol. Biol.* **17**, 1279 (2010).
18. T. J. Creamer *et al.*, *PLoS Genet.* **7**, e1002329 (2011).
19. K.-Y. Kim, D. E. Levin, *Cell* **144**, 745 (2011).
20. E. J. Steinmetz, N. K. Conrad, D. A. Brow, J. L. Corden, *Nature* **413**, 327 (2001).
21. A. G. Rondón, H. E. Mischo, J. Kawauchi, N. J. Proudfoot, *Mol. Cell* **36**, 88 (2009).
22. A. Meinhart, P. Cramer, *Nature* **430**, 223 (2004).
23. B. M. Lunde *et al.*, *Nat. Struct. Mol. Biol.* **17**, 1195 (2010).
24. M. Sun, L. Larivière, S. Dengl, A. Mayer, P. Cramer, *J. Biol. Chem.* **285**, 41597 (2010).
25. M.-L. Diebold *et al.*, *J. Biol. Chem.* **285**, 38389 (2010).
26. D. Close *et al.*, *J. Mol. Biol.* **408**, 697 (2011).
27. J. Liu *et al.*, *J. Biol. Chem.* **286**, 29218 (2011).
28. S. Buratowski, *Nat. Struct. Mol. Biol.* **10**, 679 (2003).
29. S. Egloff, S. Murphy, *Trends Genet.* **24**, 280 (2008).
30. M. L. West, J. L. Corden, *Genetics* **140**, 1223 (1995).

Acknowledgments: We thank S. Etzold and K. Leike for help and S. Hahn for providing yeast strains. P.C. was supported by the Deutsche Forschungsgemeinschaft (DFG), SFB646, SFB960, TR5, NIM, the BioImaging Network, a European Research Council (ERC) Advanced Grant, and the Jung-Stiftung. D.E. was supported by DFG, TR5, and SFB684. Microrray data have been deposited in ArrayExpress under accession code E-MTAB-1060. A.M. carried out ChIP-chip and fluorescence anisotropy experiments. M.H. and C.H. validated antibodies. M.L. analyzed ChIP-chip data. M.S. carried out modeling. A.S. carried out additional ChIP assays. E.K. generated the 3D12 antibody. D.E. and P.C. designed and supervised research. A.M. and P.C. prepared the manuscript, with help from all authors.

Supplementary Materials

www.sciencemag.org/cgi/content/full/336/6089/1723/DC1
Materials and Methods
Figs. S1 to S12
Tables S1 and S2
References (*31*–*35*)

25 January 2012; accepted 7 May 2012
10.1126/science.1219651

Elastic Coupling Between RNA Degradation and Unwinding by an Exoribonuclease

Gwangrog Lee,[1,2] Matthew A. Bratkowski,[3] Fang Ding,[3] Ailong Ke,[3] Taekjip Ha[1,4]*

Rrp44 (Dis3) is a key catalytic subunit of the yeast exosome complex and can processively digest structured RNA one nucleotide at a time in the 3′ to 5′ direction. Its motor function is powered by the energy released from the hydrolytic nuclease reaction instead of adenosine triphosphate hydrolysis as in conventional helicases. Single-molecule fluorescence analysis revealed that instead of unwinding RNA in single base pair steps, Rrp44 accumulates the energy released by multiple single nucleotide step hydrolysis reactions until about four base pairs are unwound in a burst. Kinetic analyses showed that RNA unwinding, not cleavage or strand release, determines the overall RNA degradation rate and that the unwinding step size is determined by the nonlinear elasticity of the Rrp44/RNA complex, but not by duplex stability.

The cellular levels of RNA species are tightly regulated by balancing transcription and degradation, controlling the temporal and spatial distribution of RNA (*1*). The exosome complex is a major player in the 3′ to 5′ RNA degradation and processing pathways (*1*, *2*). In yeast, Rrp44, also named Dis3, is the only catalytically active component of the 10-subunit core exosome complex. Rrp44 is a multifunctional enzyme containing endo- and exoribonuclease activities that reside in two distinct regions (*3*, *4*). The endonuclease activity of Rrp44 is carried out by the N-terminal PIN domain (*3*, *4*). The RNA-binding CSD1, CSD2, and S1 domains, together with the RNB domain at its C-terminal region, organize into a typical RNase (ribonuclease) II-type exoribonuclease (Fig. 1A) (*5*, *6*). The exoribonuclease removes nucleotides (nt) one at a time in a processive manner from the 3′ end of RNA (*7*) and can unwind structured RNA for degradation. Structural and functional studies suggest an occlusion-based mechanism where a narrow entryway to the active site allows the passage of single-stranded RNA (ssRNA) but sterically restricts double-stranded RNA (dsRNA) (*5*, *6*). Unwinding of the duplex is presumably achieved by a translocation of the exonuclease active site pulling the 3′ tail at the junction of the RNA duplex (ds-ss junction) (*6*). Rrp44 can be considered as a 3′ to 5′ RNA helicase except that its translocation seems powered by the chemical energy released from hydrolysis of the RNA chain; thus, it burns its own track.

How does Rrp44 couple its processive nuclease activity with duplex unwinding? Does it unwind a single base pair (bp) of RNA each time it cleaves a single nucleotide? Similar mechanistic questions have been debated for adenosine triphosphate (ATP)–dependent helicases (*8*–*12*). To address these questions, we developed an RNA unwinding assay based on single-molecule fluorescence resonance energy transfer (FRET) (*13*). The RNA substrate is a duplex RNA (60% GC content, 43 base pairs); the substrate strand further contains a 3′-$(A)_{15}$ overhang for Rrp44 loading to initiate degradation (Fig. 1B). The donor fluorophore (Cy3) is placed at the 5′ end of the complementary strand to mark the beginning of the duplex, and the acceptor fluorophore (Cy5) is placed 25 bp into the duplex on the substrate strand. The annealed RNA was immobilized on a polymer-coated quartz surface by a biotin-streptavidin interaction and imaged using a two-color total internal reflection fluorescence microscope. The RNA construct was incubated with Rrp44 protein (~30 nM) in the absence of Mg^{2+} for ~2 min at room temperature to load the enzyme, and the reaction was initiated by flowing in 100 μM of Mg^{2+}. The flow also removed free proteins in solution, so only the prebound Rrp44 contributes to the reaction. Degradation of the substrate strand triggers RNA duplex unwinding, and the displaced donor-containing complementary strand experiences larger conformational freedom, which causes an increase in FRET due to a decrease in the time-averaged distance between the two fluorophores (*14*–*16*).

Indeed, upon addition of Mg^{2+}, we observed a FRET increase (Fig. 1C and fig. S1). Interestingly, FRET increased with a discrete stepwise pattern that most commonly exhibited four apparent steps (Fig. 1C and fig. S1) (*17*), in contrast to the smooth FRET changes observed during single-stranded RNA degradation by an archaeal exosome (*18*). To determine whether the endo- or exoribonuclease activity of Rrp44 is responsible for the stepwise FRET increases, we tested four mutants: $Rrp44_{D171N}$ (endonuclease mutant), $Rrp44\Delta N_{PIN}$ (N-terminal PIN domain deletion mutant), $Rrp44_{D551N}$ (exonuclease mutant), and $Rrp44_{D171N,\ D551N}$ (double mutant in both active sites). The FRET increase was not observed from $Rrp44_{D171N,\ D551N}$ or $Rrp44_{D551N}$, whereas a similar stepwise FRET increase was observed from $Rrp44_{D171N}$ and $Rrp44\Delta N_{PIN}$ (fig. S2). We therefore attribute the stepwise FRET increases to the exoribonuclease activity of Rrp44. A gel assay confirmed that the enzyme indeed unwinds and degrades the 25-nt region flanked by the fluorophores (fig. S3).

To quantify the stepwise behavior in an unbiased way, we used an automated step-finding algorithm (*9*, *19*) to determine the average FRET values and dwell times of each step (fig. S4 and Fig. 1, D and E). The histogram of FRET states obtained from the automated analysis (209 molecules that showed four steps) revealed five peaks, suggesting that well-defined FRET states are visited during unwinding (Fig. 1D). A transition density plot (TDP) (*20*), which pictorializes the two-dimensional histogram for pairs of FRET values before and after each transition (Fig. 1F), also indicates a discrete step size.

To investigate the possibility that the stepwise pattern may originate from secondary structure formation within the complementary strand liberated during unwinding, we designed a duplex construct in which the complementary strand contained only Gs and As, such that self-secondary structure is unlikely to form. Single molecule traces (fig. S5) and TDP (Fig. 1G) revealed the same stepwise pattern, indicating that the stepwise pattern is intrinsic to the unwinding reaction and is not a sequence-specific feature.

To define the physical parameters of the stepwise unwinding observed, we used RNA/DNA chimeric substrate strand where RNA degradation cannot continue beyond the first 7 (Fig. 1H) or 15 nt of the substrate strand in the duplex region (fig. S6). The two constructs gave two and four steps of unwinding, respectively, suggesting an unwinding step size of about 4 $[(15-7)/(4-2)]$ bp. The 7-nt chimeric construct showed the highest FRET value of ~0.64. If Rrp44 unwinds the dsRNA only up to the boundary between RNA and DNA segments, a FRET value of ~0.48 is expected based on a calibration construct (fig. S6B), which is much lower than the actual final FRET value of ~0.64. This indicated that the Rrp44 unwinds the duplex ahead of the degradation site, consistent with the structural data that showed that ~7 nt of ssRNA is required to reach the active site through a passage too narrow for the RNA duplex (*5*, *6*).

We then analyzed the dwell time of each step (Fig. 2A). If the unwinding itself is rapid and cleavage reactions are rate-limiting, the dwell-time histogram would follow a gamma distribution with a rising phase and a decaying phase because it would be composed of about four equivalent steps that are irreversible (Fig. 2B) (*9*). In contrast, if unwinding is rate-limiting and cleavage reactions are fast, it would follow a single exponential decay (Fig. 2C). The dwell-time histogram showed a single exponential decay

[1]Department of Physics, University of Illinois at Urbana-Champaign, 1110 West Green Street, Urbana, IL 61801, USA. [2]School of Life Sciences, Gwangju Institute of Science and Technology, Gwangju 500-712, Korea. [3]Department of Molecular Biology and Genetics, Cornell University, Ithaca, NY 14853, USA. [4]Howard Hughes Medical Institute, Urbana, IL 61801, USA.

*To whom correspondence should be addressed. E-mail: tjha@illinois.edu

with a lifetime of ~1.6 s, indicating that unwinding of ~4 bp occurs in a burst with a single rate-limiting step (Fig. 2, C and D, and fig. S7).

By combining our finding that Rrp44 unwinds dsRNA in ~4-bp steps in a burst, the available biochemical data that showed that Rrp44 digests RNA into single nucleotides, and the structural information (*5*, *6*), we propose the following mechanism (Fig. 2, E and F). When Rrp44 encounters a ss/dsRNA junction, the exonuclease activity residing in the RNB domain can continue to degrade an additional ~4 nt in single nucleotide steps while one of the RNA binding domains—for example, CSD1—maintains a contact with the duplex ahead, possibly stabilizing it (Fig. 2F and fig. S8). This would pull in the 3′ ssRNA tail without unwinding, resulting in an accumulation of elastic energy in the RNA-protein complex. Through thermal activation, Rrp44 then unwinds several base pairs in a burst, releasing the elastic energy with an accompanying movement of the CSD1 domain. Rrp44 then continues this cycle to traverse the double-stranded RNA region (Fig. 2, E and F). This model predicts that if duplex melting is prevented, the substrate strand would still be degraded until much less than 7 nt is left on the 3′ overhang of the substrate strand. A gel-based RNA degradation experiment using a substrate with the first base pair of the duplex cross-linked to each other confirmed this prediction (fig. S9).

Next, we examined how the dwell time in each step or the unwinding step size is affected by duplex stability. First, an RNA-DNA heteroduplex was used in which the substrate RNA strand remains the same but the complementary strand is DNA (fig. S10). FRET traces also showed four distinct steps at similar FRET values, suggesting that the unwinding step size remains the same (fig. S10). However, the average dwell time at each step was ~60% shorter than that of the all-RNA duplex (fig. S11). The difference cannot be attributed to a difference in degradation rate because the substrate RNA strand is identical. Therefore, the less stable heteroduplex (*21*) is unwound faster, further showing that unwinding, but not degradation, is rate-limiting. The elastic energy accumulated would be the same, but the total free energy barrier is lower for the RNA-DNA

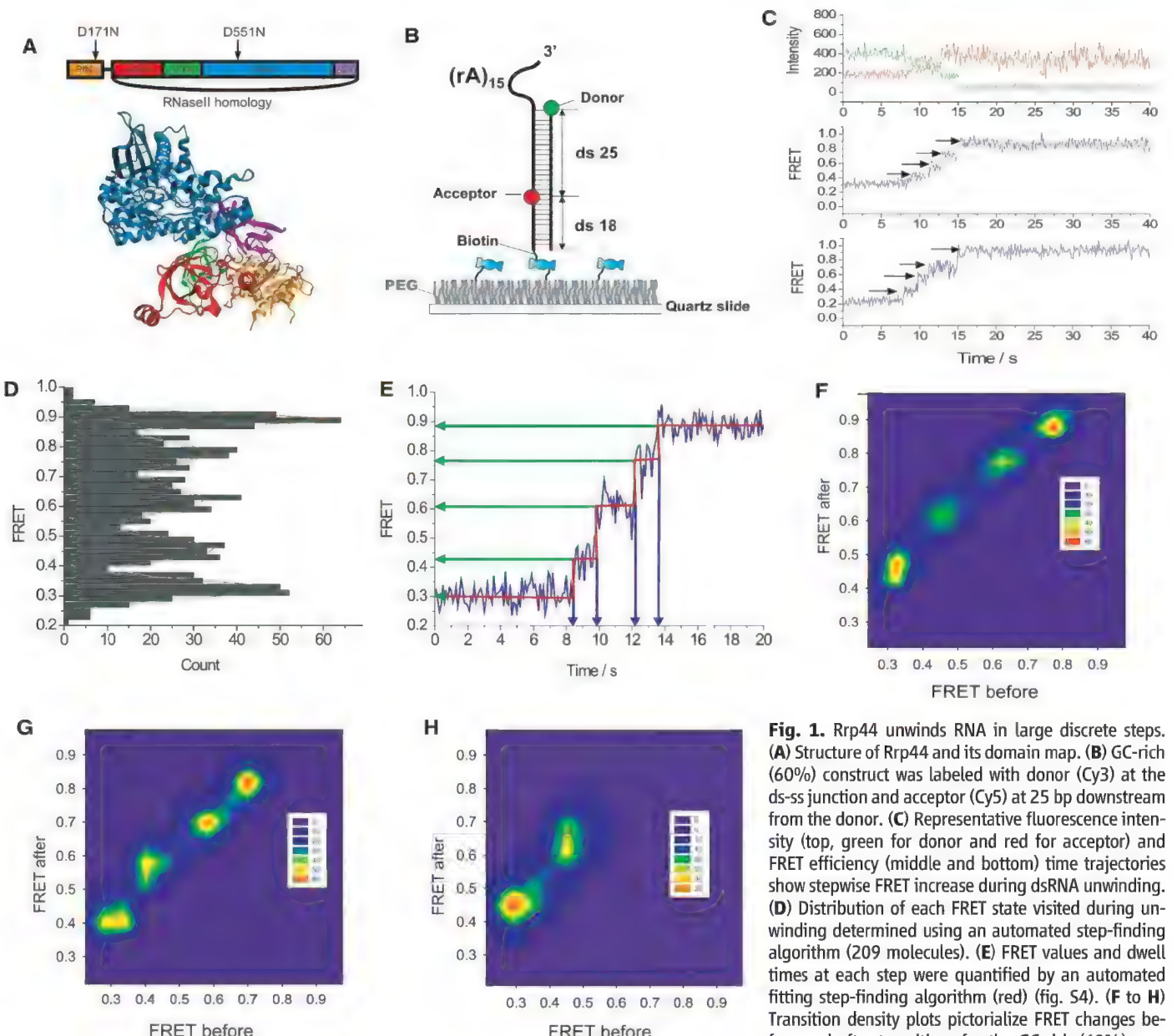

Fig. 1. Rrp44 unwinds RNA in large discrete steps. (**A**) Structure of Rrp44 and its domain map. (**B**) GC-rich (60%) construct was labeled with donor (Cy3) at the ds-ss junction and acceptor (Cy5) at 25 bp downstream from the donor. (**C**) Representative fluorescence intensity (top, green for donor and red for acceptor) and FRET efficiency (middle and bottom) time trajectories show stepwise FRET increase during dsRNA unwinding. (**D**) Distribution of each FRET state visited during unwinding determined using an automated step-finding algorithm (209 molecules). (**E**) FRET values and dwell times at each step were quantified by an automated fitting step-finding algorithm (red) (fig. S4). (**F** to **H**) Transition density plots pictorialize FRET changes before and after transitions for the GC-rich (60%) construct (F), GA-only RNA duplex (G) (see fig. S5), and Chimera1 (H) (see fig. S6).

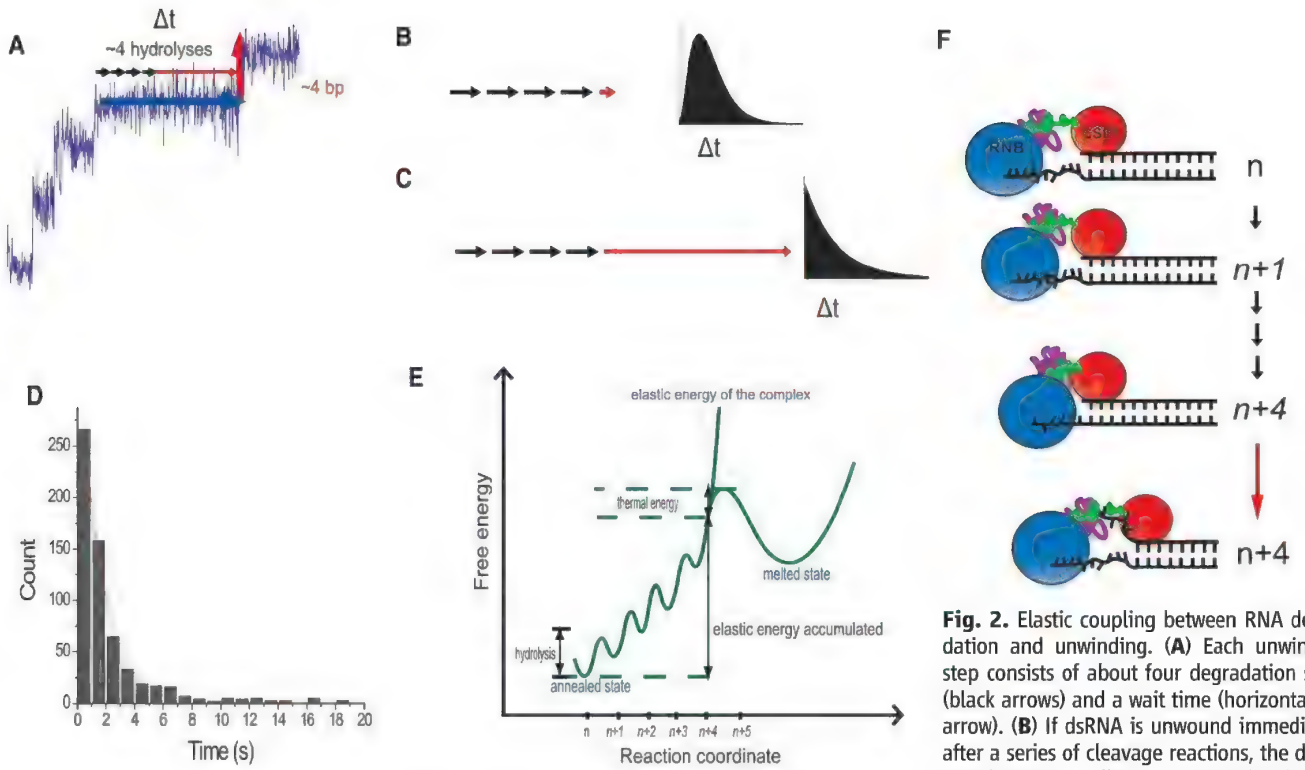

Fig. 2. Elastic coupling between RNA degradation and unwinding. (**A**) Each unwinding step consists of about four degradation steps (black arrows) and a wait time (horizontal red arrow). (**B**) If dsRNA is unwound immediately after a series of cleavage reactions, the dwell-time histogram follows a gamma distribution. (**C**) If unwinding occurs after a long delay, the histogram follows a single exponential-like decay. (**D**) Histogram of the dwell times in the second, third, and fourth steps. Exponential fit gives a 1.6-s decay time (see fig. S7 for individual histograms). (**E**) Elastic energy accumulated versus number of nucleotides digested without duplex unwinding. (**F**) Structural model on how the RNB domain that contains the exonuclease activity and the putative dsRNA binding domain (CSD1) might allow the build-up of elastic energy during about four cleavage reactions until abrupt unwinding of ~4 bp resets the system for the next cycle. In (E) and (F), the states with accumulated elastic energy are italicized.

hybrid, so it takes less time for thermal fluctuations to overcome the barrier (Fig. 2E).

We also tested a construct with 100% AU base pairs in the RNA duplex. Its unwinding at room temperature was too fast for resolving steps clearly (fig. S12B). Lowering the temperature or increasing the magnesium concentration decreased the reaction speed sufficiently to show hints of stepwise unwinding (fig. S12, C and D). We therefore performed experiments in 5 mM $MgCl_2$ at ~9°C and found that the four-step pattern is the dominant unwinding behavior for the AU-rich (100%) construct as well. We also observed an increased fraction of five-step degradation patterns (~19%) (Fig. 3, A and B), suggesting that there may exist an occasional premature unwinding event before a ~4-nt digestion is achieved if the duplex is less stable.

We determined the overall unwinding time, τ_{unwind}, defined as the time it takes for the FRET signal to increase from minimum to maximum, for different substrates and conditions (Fig. 3E). τ_{unwind} was four times as long at 9°C as at 23°C for all three constructs. τ_{unwind} increased by a factor of 2 when the NaCl concentration was increased from 10 mM to 150 mM (Fig. 3F), whereas it increased by a factor of 4 when the $MgCl_2$ concentration was increased from 0.1 mM to 5 mM (fig. S12A). Overall, reducing the duplex stability decreases the dwell time of each step without changing the step size, indicating that unwinding is rate-limiting and that the discrete steps in FRET trajectories are due to steps in unwinding rather than other effects, such as release of unwound strand from the protein surface (*11*).

How large a distortion would the RNA-protein complex accumulate before an unwinding burst? Because the A-form RNA double helix has a helical pitch of 2.5 nm and 11 bp per turn (*22*), the step size of ~4 bp is equivalent to ~0.9 nm in length. Therefore, a distortion of up to ~1 nm would need to be accommodated, either by ssRNA stretching or through protein compression (which may be achieved through reorganization of various domains of Rrp44), or a combination of both.

What determines the step size of RNA unwinding? For degradation to continue without strand separation, there must be a large kinetic barrier against duplex melting, which may originate from interactions between the RNA and one of the RNA binding domains (Fig. 2F and fig. S8). Most proteins and ssRNA are nonlinear springs (*23*, *24*); thus, the elastic energy of the complex would increase dramatically at a particular length, which might determine how many nucleotides can be degraded before the elastic energy overcomes the kinetic barrier and unwinds the duplex (Fig. 2E). If so, unwinding step size would be determined by the physical properties of the Rrp44/RNA complex.

We propose that the RNB domain acts as an engine that converts chemical energy into mechanical work by translocation along the RNA. Rrp44 functions as a chemomechanical machine that converts and combines a series of chemical energy releases from hydrolysis of the RNA chain into an elastic energy reserve through a spring-loaded mechanism until several base pairs are unwound in bursts. This mode of action may also apply to yeast Rrp44 in complex with the 9-subunit core exosome, depending on how RNA is delivered to Rrp44 (*25*, *26*), and to the human Rrp44 proteins that either interact weakly with the 9-subunit core exosome or not at all (*27*). Elastic coupling between RNA digestion and unwinding may be common in RNase II–type exonucleases, because we found similarly sized steps in RNA unwinding by *Escherichia coli* RNase R (fig. S13). Many helicases possess auxiliary domains, besides the core adenosine triphosphatase, that may display springlike behavior so that a single nucleotide step translocation can yield an unwinding step size of several base pairs, as was proposed for hepatitis C virus nonstructural protein 3 (*9*). The concept that nucleic acid motors can have a hierarchy of different-sized

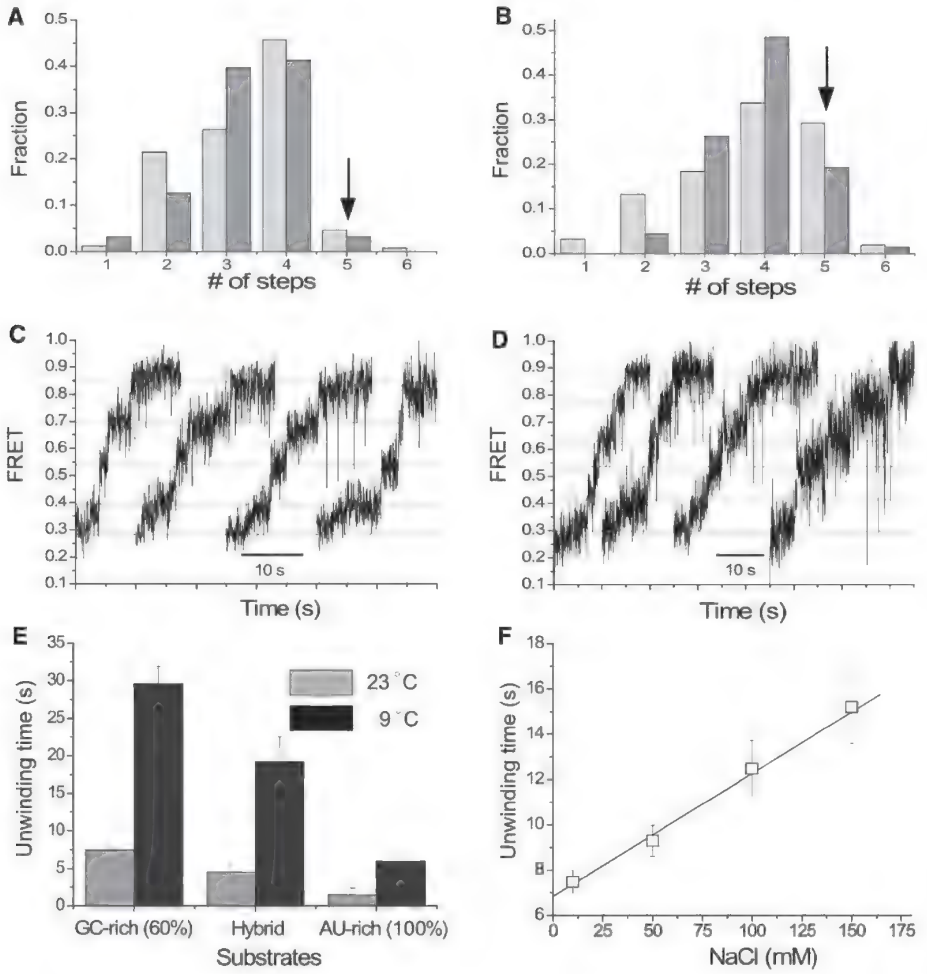

Fig. 3. Unwinding characteristics for different sequences and conditions. (**A**) Distribution of the number of steps for the standard substrate (60% GC content) (light gray, 23°C; dark gray, 9°C; both in 100 μM $MgCl_2$). (**B**) Distribution of the number of steps for the AU-rich construct (light gray, 23°C; dark gray, 9°C; both in 5 mM $MgCl_2$). (**C** and **D**) Representative four- and five-step patterns, respectively, obtained from AU-rich construct in 5 mM $MgCl_2$ at 9°C. (**E**) Unwinding for different constructs and temperatures. (**F**) Unwinding time versus NaCl concentration for the standard substrate.

steps or can accumulate elastic energy before transitioning to a subsequent phase (*8–10*, *28–30*) is further supported by our data on Rrp44.

References and Notes

1. J. Houseley, J. LaCava, D. Tollervey, *Nat. Rev. Mol. Cell Biol.* **7**, 529 (2006).
2. S. Vanacova, R. Stefl, *EMBO Rep.* **8**, 651 (2007).
3. A. Lebreton, R. Tomecki, A. Dziembowski, B. Séraphin, *Nature* **456**, 993 (2008).
4. D. Schaeffer *et al.*, *Nat. Struct. Mol. Biol.* **16**, 56 (2009).
5. C. Frazão *et al.*, *Nature* **443**, 110 (2006).
6. E. Lorentzen, J. Basquin, R. Tomecki, A. Dziembowski, E. Conti, *Mol. Cell* **29**, 717 (2008).
7. A. Dziembowski, E. Lorentzen, E. Conti, B. Séraphin, *Nat. Struct. Mol. Biol.* **14**, 15 (2007).
8. J. A. Ali, T. M. Lohman, *Science* **275**, 377 (1997).
9. S. Myong, M. M. Bruno, A. M. Pyle, T. Ha, *Science* **317**, 513 (2007).
10. A. Schwartz *et al.*, *Nat. Struct. Mol. Biol.* **16**, 1309 (2009).
11. W. Cheng, S. G. Arunajadai, J. R. Moffitt, I. Tinoco Jr., C. Bustamante, *Science* **333**, 1746 (2011).
12. J. Y. Lee, W. Yang, *Cell* **127**, 1349 (2006).
13. T. Ha *et al.*, *Proc. Natl. Acad. Sci. U.S.A.* **93**, 6264 (1996).
14. M. C. Murphy, I. Rasnik, W. Cheng, T. M. Lohman, T. J. Ha, *Biophys. J.* **86**, 2530 (2004).
15. S. Liu, E. A. Abbondanzieri, J. W. Rausch, S. F. J. Le Grice, X. W. Zhuang, *Science* **322**, 1092 (2008).
16. G. Lee, J. Yoo, B. J. Leslie, T. Ha, *Nat. Chem. Biol.* **7**, 367 (2011).
17. Among all FRET traces obtained, more than 45% show four apparent steps. The step analysis suggests that most of the remaining traces may also have four steps, but some of them are missed because they are faster than our time resolution (fig. S2).
18. G. Lee, S. Hartung, K. P. Hopfner, T. Ha, *Nano Lett.* **10**, 5123 (2010).
19. J. W. J. Kerssemakers *et al.*, *Nature* **442**, 709 (2006).
20. S. A. McKinney, C. Joo, T. Ha, *Biophys. J.* **91**, 1941 (2006).
21. E. A. Lesnik, S. M. Freier, *Biochemistry* **34**, 10807 (1995).
22. R. E. Dickerson *et al.*, *Science* **216**, 475 (1982).
23. M. S. Z. Kellermayer, S. B. Smith, H. L. Granzier, C. Bustamante, *Science* **276**, 1112 (1997).
24. Y. Seol, G. M. Skinner, K. Visscher, A. Buhot, A. Halperin, *Phys. Rev. Lett.* **98**, 158103 (2007).
25. H. W. Wang *et al.*, *Proc. Natl. Acad. Sci. U.S.A.* **104**, 16844 (2007).
26. F. Bonneau, J. Basquin, J. Ebert, E. Lorentzen, E. Conti, *Cell* **139**, 547 (2009).
27. R. Tomecki *et al.*, *EMBO J.* **29**, 2342 (2010).
28. J. R. Moffitt *et al.*, *Nature* **457**, 446 (2009).
29. A. Revyakin, C. Y. Liu, R. H. Ebright, T. R. Strick, *Science* **314**, 1139 (2006).
30. A. N. Kapanidis *et al.*, *Science* **314**, 1144 (2006).

Acknowledgments: We thank J. Park, R. Vafabakhsh, A. Jain, S. Park, R. Zhou, X. Shi, M. Comstock, and S. Syed for helpful discussions; J. Yoo, C. Maffeo, and S. Arslan for experimental help; and K. Lee for the data acquisition program. Funds were provided by grants from National Science Foundation (0646550, 0822613 to T.H.) and National Institutes of Health (GM065367 to T.H. and GM-086766 to A.K.). G.L. was supported in part by the Jane Coffin Childs Medical Institute. T.H. is an investigator with Howard Hughes Medical Institute.

Supplementary Materials

www.sciencemag.org/cgi/content/full/336/6089/1726/DC1
Materials and Methods
Figs. S1 to S13
References (*31–33*)

18 November 2011; accepted 15 May 2012
10.1126/science.1216848

New Products: Sample Prep/Handling

SEMI-MICRO BALANCES

The NewClassic MS105 converts easily from a laboratory balance with 0.01 mg readability into a standalone pipette check-station: an evaporation trap is the only external device needed if the pipetting volume is smaller than 50 µl. The trap keeps humidity levels stable during the check and thus minimizes evaporation for accurate testing. Since minute quantities cannot be measured directly, ISO8655-6 recommends distilled water for gravimetric capacity meter calibration. Distilled water is pipetted onto the balance and converted to a volumetric value. An application built-in to the balance firmware guides users through the check process. Systematic and random pipette errors are automatically calculated in absolute and relative values. Results are displayed and can be printed for traceability or for easy and quick comparison with the manufacturer's tolerances. The NewClassic MS is ideal for labs that need frequent accuracy checks in between periodic required ISO standard calibrations.

Mettler Toledo

For info: 800-638-8537 | www.mt.com

ELECTRONIC PIPETTE

The intuitive operating concept and ergonomic display of Eppendorf Xplorer plus pipettes set new standards in simplicity, precision, and reproducibility. The Xplorer is specially designed for users working with complex or long pipetting series requiring the exact setting of parameters, maximum reproducibility, and low operating force. The Xplorer plus has intelligent applications, adjustable fixed-volumes, and allows individual programming tasks to be performed much faster and easier. The Xplorer plus also includes a history function that automatically saves the last parameters for faster handling. A password can be entered to guarantee the highest degree of protection for your programming and settings. Together, these features mean no more delays due to complicated programming or inflexible processes. Instead, you get precisely adjustable parameters, reproducible results, fatigue-free work, and consistent, full control over the pipetting processes.

Eppendorf

For info: 800-645-3050 | www.eppendorfna.com

CHIRAL RESOLUTION SCREENING AND PURIFICATION KITS

Maybridge Chiral Resolution Screening and Purification Kits give organic chemists simple and rapid access to optically pure chiral compounds from their racemic mixtures. Identifying the best separation conditions under which a target compound can be isolated with optimal yield and purity can take days, or even weeks. These new, ready-to-use kits reduce development time to just one day, with as little as 0.4 mmol of racemate required. As a commonly used process to obtain optically pure chiral compounds from their racemic mixtures, diastereomeric crystallization requires careful optimization of process conditions. Maybridge Chiral Resolution Screening and Purification Kits consist of 384 different combinations of resolving agents and solvents, for both acid and amine-based resolutions, to increase the chances of finding the optimal separation conditions. Cost-effective and convenient, with resolving agents and solvents predispensed in 96-well plates, the kits provide easily identifiable results when screening and simple recovery and purification of enantiomers.

Maybridge/Thermo Fisher Scientific

For info: +44-(0)-1840-770567 | www.maybridge.com

SPECTROPHOTOMETER

The 6850 ultraviolet/visible spectrophotometer is Jenway's first double-beam instrument with a variable spectral bandwidth—of 5 nm down to 0.5 nm. This new instrument has highly stable optics and is particularly well-suited for use in laboratories where compliance with multiple regulatory agencies is required. The double beam optics and two detectors measure the sample and reference simultaneously for optimum measurement accuracy and stability over long periods of time. The 6850 has a variable spectral bandwidth of 0.5 nm, 1 nm, 2 nm, 4 nm, and 5 nm, giving flexibility while ensuring compliance with European Pharmacopeia requirements. The narrow spectral bandwidth also ensures improved peak resolution. An integrated user interface provides full control of the instrument so there is no need to buy a PC to run the spectrophotometer. However, Jenway Prism PC control software is included as standard, introducing functionality such as greater data storage, additional postmeasurement tools, and preloaded DNA and protein methods.

Bibby Scientific

For info: +44-(0)-1785-812121 | www.bibby-scientific.com

TABLETOP ULTRACENTRIFUGE

The Optima MAX-TL tabletop ultracentrifuge delivers optimum functionality and efficiency within a compact and quiet package. This entry-level instrument offers context-sensitive on-screen help and is available in multiple native languages to meet a full range of separation requirements in a user-friendly environment. Users can set multiple programs of up to five steps each using an easily navigated, full-color LCD touchscreen accessible in nine languages. Fully compatible with Beckman Coulter TL labware and fixed-angle, swinging bucket and unique near-vertical tube (NVT) rotors, the Optima MAX-TL can be used in applications including separation of subcellular particles, viruses and viral particles, rate-zonal separation of proteins in sucrose gradient, separation of lipoproteins, pelleting of RNA through a CsCl gradient, isopycnic separation of plasmid DNA, and others. With a maximum speed of 120,000 rpm and maximum rcf of 657,000 x g, the instruments control speed within ±50 rpm of set point.

Beckman Coulter

For info: 800-742-2345 | www.beckmancoulter.com

Electronically submit your new product description or product literature information! Go to **www.sciencemag.org/products/newproducts.dtl** for more information.

Newly offered instrumentation, apparatus, and laboratory materials of interest to researchers in all disciplines in academic, industrial, and governmental organizations are featured in this space. Emphasis is given to purpose, chief characteristics, and availability of products and materials. Endorsement by *Science* or AAAS of any products or materials mentioned is not implied. Additional information may be obtained from the manufacturer or supplier.

Science Careers Advertising

For full advertising details, go to ScienceCareers.org and click For Employers, or call one of our representatives.

Tracy Holmes
Worldwide Associate Director
Science Careers
Phone: +44 (0) 1223 326525

UNITED STATES & CANADA

E-mail: advertise@sciencecareers.org
Fax: 202-289-6742

Tina Burks
Midwest/West Coast/
Canada/South America
Phone: 202-326-6577

Elizabeth Early
East Coast & Corporate
Phone: 202-326-6578

Marci Gallun
Sales Administrator
Phone: 202-326-6582

Online Job Posting Questions
Phone: 202-312-6375

EUROPE & REST OF WORLD

E-mail: ads@science-int.co.uk
Fax: +44 (0) 1223 326532

Simone Jux
Phone: +44 (0)1223 326529

Lucy Nelson
Phone: +44 (0)1223 326527

Kelly Grace
Phone: +44 (0) 1223 326528

JAPAN

Yuri Kobayashi
Phone: +81-6-6627-9250
E-mail: ykobayas@aaas.org

CHINA & TAIWAN

Ruolei Wu
Phone: +86-1367-1015-294
E-mail: rwu@aaas.org

All ads submitted for publication must comply with applicable U.S. and non-U.S. laws. *Science* reserves the right to refuse any advertisement at its sole discretion for any reason, including without limitation for offensive language or inappropriate content, and all advertising is subject to publisher approval. *Science* encourages our readers to alert us to any ads that they feel may be discriminatory or offensive.

Science Careers
From the journal *Science* AAAS

NC STATE UNIVERSITY

ASSISTANT/ASSOCIATE OR FULL PROFESSOR
Global Environmental Change and Human Well-Being

As one of the leading land-grant institutions in the nation, North Carolina State University is proud to announce its Chancellor's Faculty Excellence Program, a cluster hire program that marks the first major initiative of the university's 2011-2020 strategic plan, "The Pathway to the Future." Starting in 2012, NC State will hire thirty-eight faculty in twelve research areas or "clusters" to promote interdisciplinary scholarship and the development of innovative curricula in emerging areas of strategic strength. As part of this university-wide program, the Department of Biology and the Department of Forestry and Environmental Resources are hiring a cluster of three faculty at any rank to provide leadership for a new initiative in Global Environmental Change and Human Well-Being. We seek leaders in any area of biology under this theme, and encourage applications from those who study global change as it relates to fisheries and aquatic diversity, quantitative ecology, evolutionary biology, or other areas. Successful applicants are expected to have a strong vision for their vibrant and extramurally-funded research program, a commitment to leadership in the area of Global Environmental Change, and demonstrated excellence and innovation in graduate education. This cluster will strengthen and bridge emerging initiatives at NC State including: 1) the Southeast Climate Science Center; 2) the Nature Research Center of the NC Museum of Natural Sciences; and 3) programs in Ecology and Evolutionary Biology. More information on these positions and this initiative can be found at **http://www.theglobalchangeforum.org/clusterhire/** We are targeting applicants already holding a position at the level of Assistant Professor or higher (or equivalent), but exceptional postdoctoral fellows also will be considered.

To apply for these positions, go to **http://jobs.ncsu.edu/postings/7389** and provide a cover letter, curriculum vitae, and a 1-page vision for Global Environmental Change and Human Well-being, focused on your research program and/or building this programmatic theme at NC State. Confidential inquiries and nominations should be directed to Dr. Damian Shea, Search Chair, **d_shea@ncsu.edu, 919-513-3065.**

Review of applications will begin 15 August 2012 and continue until the positions are filled. We welcome applications from groups of individuals and dual-career couples and will work with candidates to identify suitable employment opportunities for spouses or partners.

ADA Accommodations: please call **919-515-3148.**

NCSU is an AA/EO employer. All qualified applicants will receive consideration for employment without regard to race, color, national origin, religion, sex, age, veteran status or disability. In its commitment to diversity and equity, NC State University seeks applications from women, minorities, and persons with disabilities. NC State welcomes all persons without regard to sexual orientation.

HARVARD UNIVERSITY
Assistant/Associate Professors
Department of Genetics and Complex Diseases

The Department of Genetics and Complex Diseases (GCD) at the Harvard School of Public Health (HSPH) seeks candidates for the position of assistant or associate professor. This is a tenure-ladder position, with the academic rank to be determined in accordance with the successful candidate's experience and productivity.

Successful applicants will hold a PhD and/or MD degree and will have a record of outstanding productivity. Individuals are sought particularly in the following areas to complement the existing research and training goals of the department: signal transduction related to energy and nutrient sensing pathways, regulation of metabolic homeostasis, inflammatory and stress response pathways related to chronic metabolic diseases and aging, cancer metabolism, and genetic and epigenetic approaches to study metabolism. Programs that utilize mass spectroscopy platforms for high resolution approaches as well as those individuals using systems and/or computational approaches applied at a mechanistic level to problems of metabolic homeostasis and gene-environment interactions and/or adaptive responses are also encouraged to apply. The candidate should possess the ability to work collaboratively with other scientists and the scholarly qualities required to mentor doctoral students in the graduate program in the Division of Biological Sciences. Generous start-up packages and state-of-the-art research facilities are available.

Please apply to: **https://academicpositions.harvard.edu**

For questions, please contact:

Marjorie Tatum
Department of Genetics and Complex Diseases
gcddept@hsph.harvard.edu

The Harvard School of Public Health is committed to increasing the representation of women and minority members among its faculty, and encourages applications from such candidates.

中国科学院虚拟经济与数据科学研究中心
CAS Research Center On Fictitious Economy & Data Science

Professors/Associate Professors/Assistant Professor/Post-doctor Positions

Chinese Academy of Sciences Research Center on Fictitious Economy and Data Science (CASFEDS), Beijing, China (**http://www.feds.ac.cn/Pages/default.aspx**) is a newly research unit under the direct leadership of Chinese Academy of Sciences. Professor Cheng Siwei, the former Vice-Chairman of Standing Committee of the National People's Congress of the People's Republic of China, serves as the director. The objective of CASFEDS is to be a truly international leader on research, technology transfer and think tank in the fields of financial markets, data science, environment policy, social computing, and related issues. The center has 4 research labs: fictitious economy lab, data mining and optimization lab, green economy lab, and social computing and e-health science. The applicants are kindly invited to apply the open positions for Professors, Associate Professors, Assistant Professor, and Post-doctors. The research interests of applicants include but not limited to data science (data mining), intelligent knowledge, optimization-based approaches, knowledge management, bioinformatics, fictitious economy theory, finance, e-health science and social computing. The outstanding candidates will be recommended to the "1000 talents program" and/or "100 talents programs" through the Graduate University of Chinese Academy of Sciences.

Applicants for these positions should have a PhD degree, excellent academic records, and good communication and writing skills. The rank of a position will depend on the experience. The application profile must contain resume, copy of degree certificate, 3 selected publications, and 3 recommendation letters from the references. The applications can be sent via e-mail to:

Ms. Zhao Zhao
Room 203, Building 6, No.80 Zhongguancun East Road,
Research Center on Fictitious Economy and Data Science,
Graduate University of Chinese Academy of Sciences,
Chinese Academy of Sciences
Haidian District, Beijing, 100190, China.
(0): **+86-10-82680699** (F): **+86-10-82680698**
E-mail: **zhaozhao@gucas.ac.cn**

UNIVERSITY of HOUSTON

COLLEGE OF PHARMACY

Post-Doctoral Fellow Position
Department of Pharmacological and Pharmaceutical Sciences

The College of Pharmacy is accepting applications for the position of a Post-Doctoral Fellow in Pharmacology. This new position has been created in the laboratory of an NIH funded Assistant Professor, to study the biochemical mechanisms underlying anxiety and depression-like behaviors. Eligible candidates must have earned a Ph.D. degree in Neuroscience and have experience in rodent behavior assays, especially with depression and anxiety-like behaviors. Experience in stereotaxic surgery, western blotting, cell culture, PCR and fluorescent imaging techniques is also needed.

Applications will be accepted until the position is filled. Interested individuals should apply online at: **https://jobs.uh.edu/ (Posting #000185)**.

Candidates should also send a letter describing their research Interests, a curriculum vitae, and names of three references with postal and email addresses, telephone and fax numbers at the email address provided below.

University of Houston
College of Pharmacy
Department of Pharmacological and Pharmaceutical Sciences
Houston, TX 77204-5037
Email: ssalim@uh.edu

The University of Houston is an Affirmative Action/Equal Opportunity Employer. Minorities, women, veterans, and persons with disabilities are encouraged to apply.

DEPARTMENT HEAD OF PHARMACAL SCIENCES HARRISON SCHOOL OF PHARMACY AUBURN UNIVERSITY

The Auburn University Harrison School of Pharmacy seeks applications and nominations for the position of Department Head of Pharmacal Sciences. This department focuses on research and instruction of basic pharmaceutical and biomedical sciences. This individual's responsibilities include: participation as a member of the senior administrative team; guiding the department regarding research, faculty mentorship and development, and graduate and professional education.

To ensure success in addressing the School's vision and mission, applicants must possess a Ph.D. in pharmaceutical or biomedical sciences or related field, excellent interpersonal and communication skills, and demonstrated experience in leadership and management. The ideal candidate should have academic credentials sufficient to meet tenure eligibility requirements, an outstanding scientific background, an established and ongoing record of obtaining extramural funds, and the proven abilities to foster an interdisciplinary approach to research in order to assist the School towards achieving the next level of biomedical research.

Salary will be competitive and commensurate with education and experience. The candidate selected for this position must be able to meet eligibility requirements to work in the United States at the time appointment is scheduled to begin and continue working legally for the proposed term of employment.

To assure full consideration, applications must include a curriculum vitae, a letter of interest providing a summary of qualifications for the position, and the name and contact information for three references. Review of applications will begin **September 1, 2012** and will continue until the position is filled. Applications and nominations should be submitted via e-mail to **Ms. Jennifer Johnston** at **jmj0025@auburn.edu** or via mail to **Search Committee, Pharmacal Sciences Department Head, 4306 Walker Building, Auburn, AL 36849**. For further information concerning the position, applicants may also contact **Ms. Johnston** at **(334) 844-7432**.

Women and minorities are encouraged to apply. Auburn University is an Equal Opportunity/Affirmative Action Employer.

UNESCO
United Nations Educational, Scientific and Cultural Organization

REGIONAL CENTRE FOR BIOTECHNOLOGY

an institution of education, training & research

(Established by the Dept. of Biotechnology, Govt. of India under the auspices of UNESCO)

Adv. No. 5/2012

Leadership Position in Technology Platforms in Interdisciplinary Biomedical Research

Regional Centre for Biotechnology (RCB), an institution of education, training and research established by the Govt. of India under the auspices of UNESCO, is looking for dynamic, result-oriented and dedicated aspirants at leadership position at the Advanced Technology Platforms Centre, a major research resource of NCR Biotech Science Cluster of which RCB is a partner institution. Applications/nominations from/for suitable candidates are invited for a position at the level of Scientist 'H'. The candidate should have Ph. D. in any area of Natural Sciences, Medicine or Engineering and at least 15 years as Principal Investigator in interdisciplinary biomedical research using diverse technology platforms including experience of guiding research at doctoral level in Universities/Institutions/Industrial Research Laboratories. Experience of establishing and managing any of the technology platforms for innovative research in interdisciplinary biomedical areas at the leading levels will be an added advantage. Curriculum vitae containing relevant details, list of publications and the names of three potential referees along with their electronic mail addresses may be sent to the Executive Director, Regional Centre for Biotechnology, 180, Udyog Vihar, Phase-I, Gurgaon- 122016, India with an advance copy to the e-mail address: **office@rcb.res.in** latest by **August 15, 2012**. Only the short-listed candidates will be contacted for further discussions. A detailed version of the advertisement can be found on the RCB website: **http://www.rcb.res.in** and **www.rcb.ac.in**.

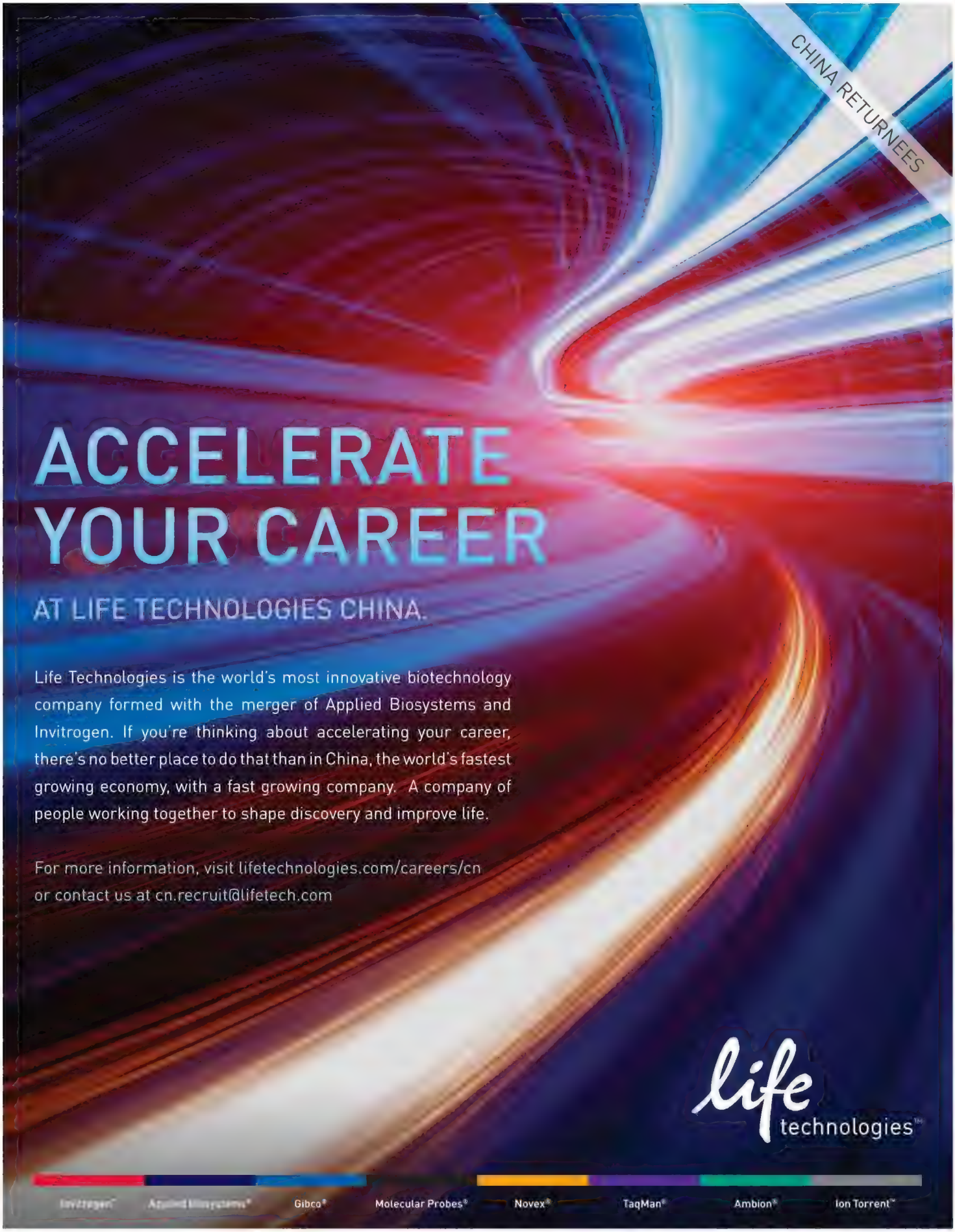

AAAS is here – helping scientists achieve career success.

Every month, over 400,000 students and scientists visit ScienceCareers.org in search of the information, advice, and opportunities they need to take the next step in their careers.

A complete career resource, free to the public, *Science* Careers offers a suite of tools and services developed specifically for scientists. With hundreds of career development articles, webinars and downloadable booklets filled with practical advice, a community forum providing answers to career questions, and thousands of job listings in academia, government, and industry, *Science* Careers has helped countless individuals prepare themselves for successful careers.

As a AAAS member, your dues help AAAS make this service freely available to the scientific community. If you're not a member, join us. Together we can make a difference.

To learn more, visit aaas.org/plusyou/sciencecareers

AAAS + U = Δ

FACTS & FICTION

Careers in Industry and Academia

Trying to figure out the next step in your career? Join us for a roundtable discussion that will look at facts and fiction surrounding academic and industry career options for PhD-level scientists. Get some nuts and bolts advice on how to research career options, what questions to ask, and how to best prepare for various careers.

- Do industry and academic careers require different skill sets?
- Do industry jobs have better compensation? Less autonomy?
- Do academic scientists have less work/life balance?

For answers view our roundtable discussion for free at:

ScienceCareers.org/webinar

Science Careers
From the journal *Science* AAAS

Produced by the *Science*/AAAS Business Office.

POSITIONS OPEN

PROFESSOR AND DIRECTOR of Stem Cell Molecular Imaging

The University of California, San Diego (UCSD) Stem Cell Program, in cooperation with Pharmacology, Chemistry/Biochemistry, Radiology and other departments seeks a senior tenure-track professor to head the molecular imaging facility in the Sanford Consortium for Regenerative Medicine, and conduct strongly interdisciplinary research in stem cell science and medicine. This tenure-track faculty position is available in Fall 2012 at the **ASSOCIATE** or **FULL PROFESSOR LEVEL.**

The molecular imaging facility in the Sanford Consortium for Regenerative Medicine already has an operational 11.7T Bruker small animal MRI, a shielded facility specifically designed for a cyclotron, and funds reserved for radiochemistry and microPET facilities. The mission is to develop preclinical and clinical molecular imaging to support stem cell therapies and regenerative medicine.

The Program seeks a candidate with independent and vigorous extramurally funded research programs in stem cell radiology or imaging, biology, biochemistry, medicine, engineering, or other fields related to stem cell science, with innovative approaches and expertise in more than one discipline. Candidates should have a track record of publications in internationally recognized journals, and a willingness to participate in university service, graduate and undergraduate teaching. UCSD is committed to academic excellence and diversity within the faculty, staff, and student body. Successful candidates will demonstrate strong contributions to diversity, equity, and inclusion, and a commitment to achieving excellence and diversity UC San Diego. Applicants must possess a Ph.D. or M.D. degree.

The UCSD Stem Cell Program is an interdisciplinary, collaborative research and teaching program focused on using stem cells to understand basic biology and the causes and treatment of human disease. The successful applicant will have appointments in one or more home departments at UC San Diego.

The Chair of the Search Committee, **Roger Y. Tsien,** Ph.D., invites you to submit your curriculum vitae, a statement of research experience and interests, the names and e-mail addresses of three references, and a separate statement summarizing past experience or potential to contribute to equity and diversity to **website: https://apol-recruit.ucsd.edu/apply.**

Please select the following open position: Professor, Stem Cell Program 10-427.

UCSD is an Affirmative Action/Equal Opportunity Employer with a strong institutional commitment to excellence through diversity.

FACULTY POSITIONS - MEDICAL SCHOOL

The Saint James School of Medicine, an international medical school (**website: http://www.sjsm.org**), invites applications from candidates with teaching and/or research experience in any of the basic medical sciences for its Caribbean campuses.

Faculty positions are currently available in Anatomy and Pathology. Applicants must be a M.D., D.O., and/or Ph.D.

Teaching experience in the U.S. system is desirable but not required. Retired persons are encouraged to apply. Attractive salary and benefits. Submit curriculum vitae electronically to **e-mail: mjansen@mail.sjsm.org** or mail to: **HRDS Inc., 1480 Renaissance Drive. Suite 300, Park Ridge, IL 60068.**

REGISTER NOW!
webinar.sciencemag.org

WEBINAR

Techniques and Methods in Live-Cell Imaging

Practical Advice for Microscopy-based Research

WEDNESDAY, JULY 18, 2012
12 noon ET, 9 a.m. PT, 4 p.m. GMT, 5 p.m. UK

Imaging technologies are ubiquitous in today's life science laboratory. From basic microscopy to high throughput modalities, most cell based research benefits from some tried and true methods for imaging. Techniques applied to imaging live cells, either in culture or in vivo, have enabled many biological questions to be addressed that were not possible with fixed samples. Advances in the technologies available, and in the different ways in which they can be applied to analyze live cells, is continuously occurring. This webinar will examine some of the cutting-edge technologies available today, through real-world examples provided by our panel of experts.

DURING THE WEBINAR, THE SPEAKERS WILL:

- Provide specific examples of imaging modalities and how they can be applied in a basic research setting
- Give practical problem-solving advice on imaging issues encountered
- Discuss specific methodologies for achieving the best imaging data
- Answer your questions live during the webinar!

SPEAKERS

Vytas Bindokas, Ph.D.
University of Chicago
Chicago, IL

Simon C. Watkins, Ph.D.
University of Pittsburgh School of Medicine
Pittsburgh, PA

Tomasz Zal, Ph.D.
MD Anderson Cancer Center
Houston, TX

Webinar sponsored by

Leica MICROSYSTEMS

Brought to you by the *Science*/AAAS Custom Publishing Office

Science AAAS